Chapter 5

Formal Synthesis of (–)-Cylindrocyclophane F[†]

5.1 INTRODUCTION

Ni-catalyzed reductive cross-coupling (RCC) reactions are powerful and mild methods of joining two electrophiles using a stoichiometric reductant.[1] These cross-couplings forge C–C bonds between partners of varying functionality (e.g., halides, redox-active esters, etc.) and carbon hybridization (i.e., Csp^3, Csp^2, and Csp) and—when performed with a chiral catalyst—can form enantioenriched products from prochiral substrates.[2,3] Owing to these advantages, Ni-catalyzed RCCs, in particular those reactions constructing Csp^2–Csp^3 bonds,[4] are useful in the enantioselective preparation of pharmaceutically relevant small molecules.[5] Indeed, the success of many RCCs is measured by their practicality in an industrial pharmaceutical setting,[6] such as compatibility with aryl bromides[7] featuring drug-like functionalization[8] or performance

[†] The research presented in this chapter was completed in collaboration with Dr. Christopher Lavoie and Stephanie Cortez, former Reisman group members, as well as Cedric Lozano, a current graduate student in the Reisman group.

on large scale.[9] In contrast to the pharmaceutical landscape, natural product synthesis remains a largely unexplored terrain in which to explore the power of reductive cross-coupling for strategic bond construction.

Figure 5.1 *Ni-catalyzed reductive ring formation*

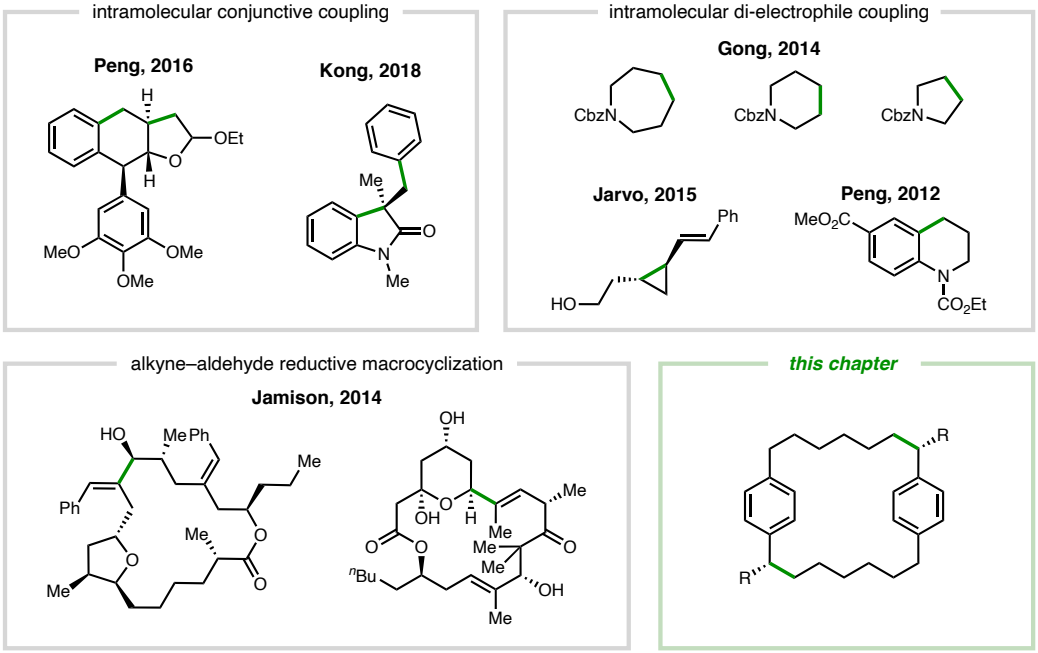

One defining feature of complex molecules, such as natural products and their derivatives, is a carbocyclic skeleton. If drawing from the rapidly expanding pool[10] of Ni-catalyzed RCCs in developing a synthetic route, the available transformations would be suitable for installation of carbon-based appendages around the skeletal periphery. Given the state-of-the-art, it is significantly more challenging to construct the carbon ring system itself using these methods. Several studies have established the feasibility of Ni-catalyzed RCCs in ring formation (Figure 5.1). In the cases where aryl halide substrates feature pendant alkenes, *n-exo*-trig cyclization can accompany cross-coupling to generate five- or six-membered rings, whether by cyclization of radical intermediates[11] or as a pathway toward three-component couplings.[12] Difunctional electrophiles can undergo

intramolecular coupling to access cyclopropanes[13] or five-, six-, or seven-membered[14] carbocyclic rings. In the generation of rings with greater than seven members, successful intramolecular coupling partners are limited to aldehydes with epoxides, alkenes, or alkynes, which restricts the oxidation pattern around the thus-generated C–C bond.[15]

Against this backdrop, we view [7.7]paracyclophane[16] as an exciting system in which to explore Ni-catalyzed reductive cross-coupling in the formation of stereochemically enriched macrocyclic carbocycles.[17] Synthesis of these macrocycles via cyclodimerization is a known proving ground for new methods.[18] The success of any transformation in this context requires high levels of efficiency and selectivity as well as the ability to impart stereochemical control across a large, flexible ring. Emblematic of the [7,7]paracyclophanes is the cylindrocyclophane family[19] of tumor cytotoxins. The following introductory sections outline our motivation for pursuing the synthesis of the cylindrocyclophane natural products via application of Ni-catalyzed RCC to macrocyclization.

5.1.1 *Natural Paracyclophanes*

Nature produces a large number of cyclophanes which serve as inspiration for biological study and chemical synthesis. The paracyclophane natural product family is found in photosynthetic cyanobacteria and has been continually expanding since 1990—when cylindrocyclophanes were isolated from *C. licheniforme* in blue-green algae[20,21]—to 2023, in which year the newest addition to the family was reported.[22] Common to members of this family is a carbon-based, 22-membered [7,7]paracyclophane core in which a seven-carbon aliphatic chain bridges two *para*-substituted arenes. Based on the

characteristic substitution pattern of the aryl moieties, these natural products are generally termed dialkylresorcinols.[19]

Figure 5.2 *[7.7]Paracyclophane natural products*

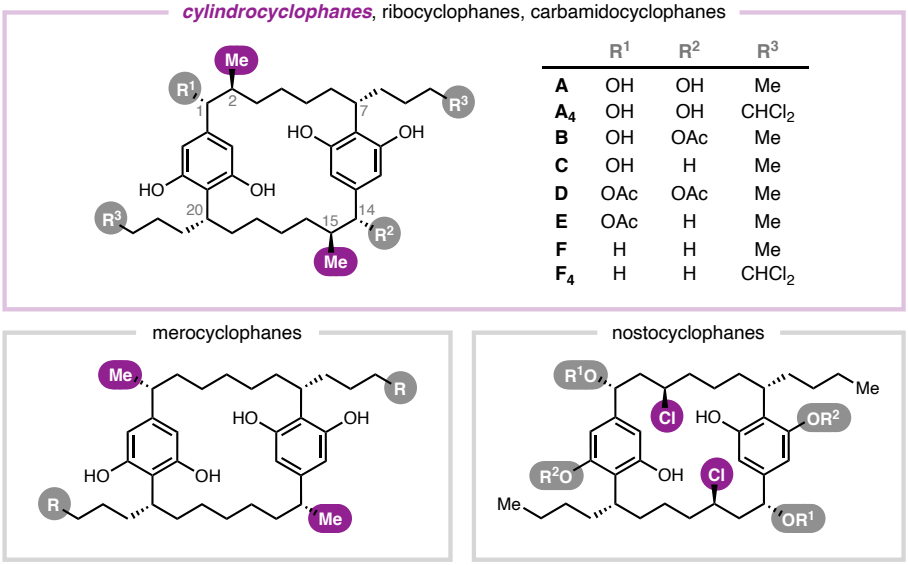

The family is divided into several structural subclasses, including the cylindrocyclophanes,[20,21,23] carbamidocyclophanes,[24,25,26,27] merocyclophanes,[28,29] and nostocyclophanes[30] (Figure 5.2). Cylindrocyclophanes A–F feature various C1/C14 oxidation (R^1 and R^2); they each share a stereodefined methyl group along the alkyl bridge but differ at the terminus of the appended *n*-butyl chain (R^3). Similarly, members of the other subclasses feature a single shared structural feature, such as the benzylic methyl group of the merocyclophanes or the aliphatic chloride substituent of the nostocyclophanes, and diverge with respect to additional peripheral decoration. Based on the solid-state structure of nostocyclophane D,[31] the benzylic substituents lie in equatorial positions with the faces of the arenes aligned in parallel—a conformation well-disposed for inclusion of small molecules (e.g., EtOH) within the macrocyclic pocket (Ar–Ar distance ca. 7.85 Å).[32]

These macrocyclic natural products are biosynthetically related, and substantial progress toward the identification and validation of key enzymes has been made by the Balskus group[33,34,35] and others.[31,36] Despite their related biogenesis, the natural paracyclophanes demonstrate wide-ranging therapeutic potential, demonstrating antibacterical[26] activity, cytotoxicity toward several cancer cell lines,[21,29,37] and proteasome inhibition,[23] just among the cylindrocyclophanes. Still other paracyclophanes are antifungal[25] and anticancer agents (against additional tumor cells)[38] and serve as possible treatments for tuberculosis.[25] The breadth of bioactivity reflects the staggering array of metabolites from related cyanobacterial genera that are making significant headway as pharmaceutical candidates across a variety of therapeutic areas.[39]

In the course of preliminary structure–activity relationship (SAR) studies, a few structural features of paracyclophanes have been implicated as important for bioactivity. Unlike most natural products, both enantiomers of cylindrocyclophane A (1) display a similar level of cytotoxicity.[40] The resorcinol warhead is critical for reactivity and is rendered more potent by arrangement in a [7.7]paracyclophane framework[40] (as opposed to a half-sized alkyl resorcinol fragment).[41] The *n*-butyl chain is also important for low micromolar activity.[42] In addition, several studies have noted a considerable improvement in potency (up to 40x)[27] due to *n*-butyl chain halogenation, particularly with Br-[27] but also Cl-substituents.[23] To facilitate these studies—and supplement recent advances in the isolation of these complex molecules from natural sources[39]—efficient methods for their chemical synthesis are required.

5.1.2 *Synthetic Efforts*

Whether captivated by the cyclophane structure or driven by the promise of their success a pharmaceuticals, chemists and biologists alike have worked to expand the pool of these cyclic compounds for several decades—since the introduction of paracyclophane[43] to the chemical community. As examples, many groups have prepared cyclophanes to probe their use as chiral ligands,[44] for host-guest chemistry,[45] and as building blocks for complex supramolecular structures.[46,47] To inform these synthetic studies, the structure and related properties (e.g., conformation, [16,32] strain,[48,49,50] dynamics,[51] electronic structure,[52] etc.) of hypothetical and physically accessible compounds have been computationally investigated. There has also been substantial synthetic work devoted to cyclophanes that are biologically relevant. Nevertheless, many interesting targets in this category feature complex functionalization and stereochemical patterns that are inaccessible via known methods of peripheral modification[53] and pose substantial challenges to direct preparation of a fully elaborated macrocycle.[54,55]

Of utmost concern to the synthesis of a paracyclophane is the ring-forming event. An early approach has been to sequentially form a thiacyclophane and then pyrolyze the sulfone linkage; in this way, a paracyclophane (of type [*n*,*n*], where *n* = even number) is initially generated which can then lead to odd- or mixed-length bridges, [*m*,*m*][56] or [*n*,*m*],[57] respectively. This method represents a commonly used general strategy for macrocycle formation, including up to ring sizes *m* = 11: use of distinct difunctional substrates that each contain the same reactive group (i.e., di-electrophile and di-nucleophile).[58] One main challenge to this approach is the difficulty of controlling head-to-head versus head-to-tail dimerization. An alternative strategy is to forge the

macrocycle from a single difunctional substrate (e.g., an ambiphilic monomer), the feasibility of which was established by early implementation of a high-dilution Friedel–Crafts reaction.[59]

Another traditional approach to paracyclophane synthesis is sequential coupling and ring closure. In this case, a linear precursor is prepared first, followed by macrocycle construction in a separate step.[60,32] One advantage of this strategy is that a higher level of control over macrocyclization is generally possible in the ring-closing step. An illustrative example is presented in Figure 5.3;[61] notably, two stereocenters are established at the same time as macrocycle closure, albeit with low levels of substrate-controlled diastereoselectivity.

Figure 5.3 *Concomitant paracyclophane ring closure and stereocenter formation*

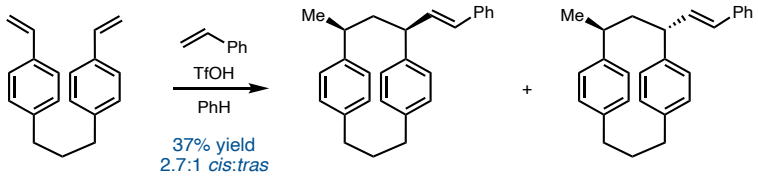

5.1.2.1 Cylindrocyclophanes: Macrocyclization

These foundational studies of cyclophane assembly have undoubtedly guided partial and complete syntheses[18] of the cylindrocyclphane natural products. The Albizati group designed a two-step approach that would access cylindrocyclophane A (**1**) via sequential radical–enone addition reactions, but they were unable to observe macrocyclization (Figure 5.4).[62] A related report from the Davies and Stoltz groups utilized a C–H functionalization reaction to prepare a linear intermediate, which underwent ring formation via subsequent C–H functionalization (*vide infra*); this strategy

which provided access to an undersubstituted model macrocycle[63] with the goal of elaborating via C–H acetoxylation to oxidized **1**.[64] Another successful approach to stepwise ring formation by Smith and coworkers hinged on reductive alkylation followed by ring-closing metathesis (RCM). RCM of **3** was selective against oligomerization, generating the desired macrocycle in 88% yield, advanced to cylindrocyclophane F (**2**) in two steps.[65]

Figure 5.4 *Prior art: stepwise macrocyclization*

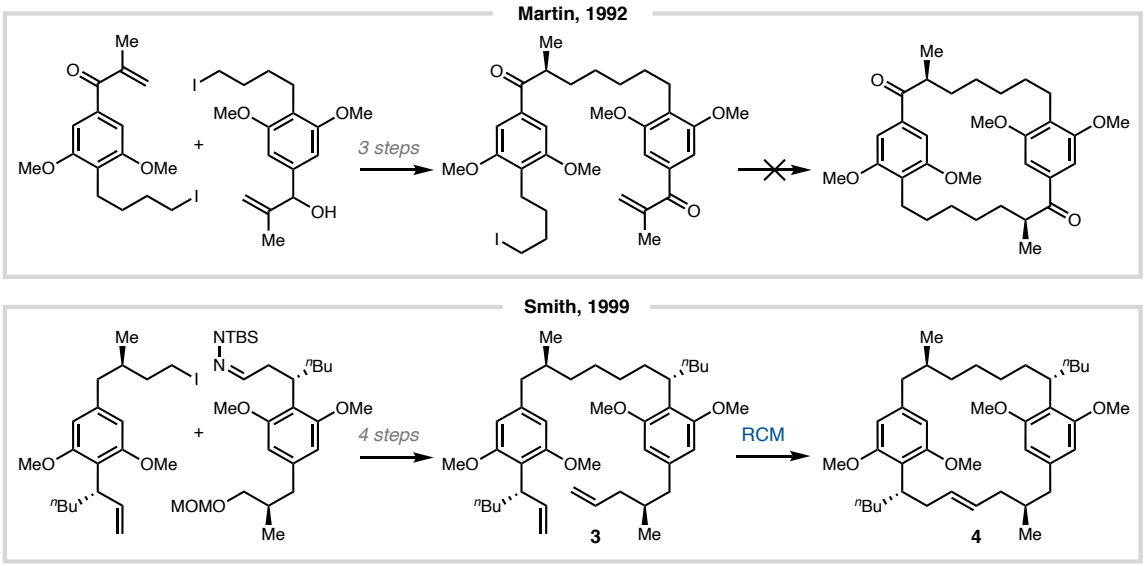

Because of their C_2 symmetry, these natural products have inspired one-step, head-to-tail cyclodimerization as the gold standard. This can be an extremely efficient strategy, as only one half of the target molecule needs to be prepared prior to macrocycle formation. However, development of an appropriately selective and high-yielding method for dimerization is not an insignificant challenge. Indeed, synthetic approaches based on Alder–ene reaction[66] or double Suzuki cross-coupling,[67] developed by the Trost and MacMillan groups, respectively, were unable to afford the [7.7]paracyclophane skeleton (Figure 5.5). The former dimerization attempt ended in unselective polymerization and

exemplifies one of the more significant challenges of reacting difunctional monomers. The latter approach illustrates another: the tactic for dimerization must be compatible with synthesis of the requisite substrate, a challenge if the molecule contains both a reactive nucleophile and electrophile (i.e., **5**).

Figure 5.5 *Challenges of single-step cyclodimerization*

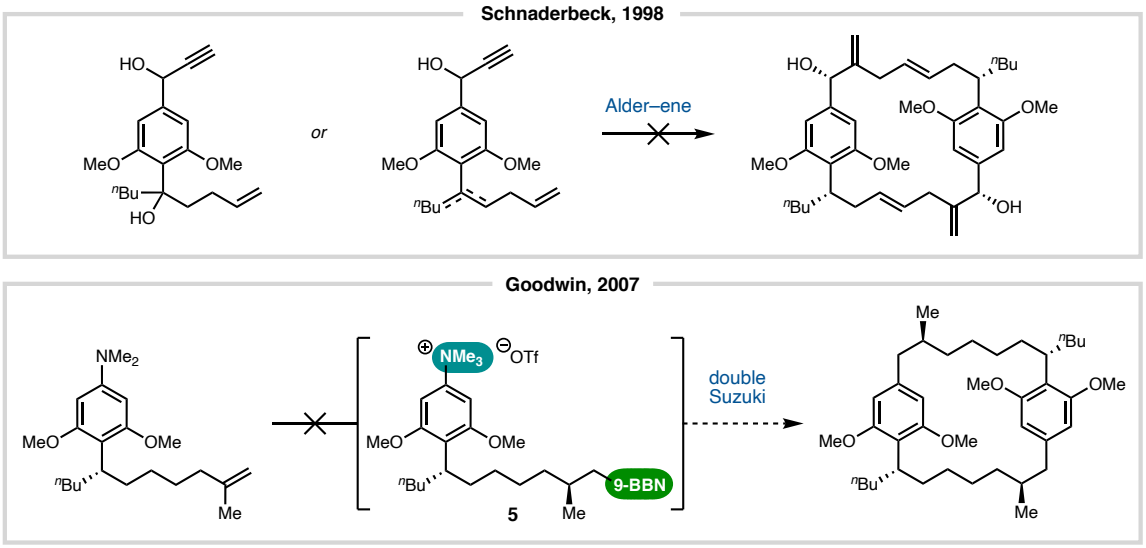

Successful methods for cyclodimerization include a Horner–Wadsworth–Emmons olefination reported by Hoye and coworkers[68] en route to natural product **1**, as well as Nicolaou's double S_N2-type displacement of mesolate-containing thioester **6**, which was followed by Ramberg–Bäcklund rearrangement and led to the total synthesis of **2** and the formal synthesis of **1** (Figure 5.6).[69] The ability of S_N2 displacement to forge the macrocycle via reaction at C1/C15 of one fragment, despite the failure of a similar reaction[70] at C4/C18 (of **7**), encapsulates another key consideration for dimerization design. The choice of which bond of the aliphatic bridge to construct during macrocyclization can profoundly impact the success of ring formation.

Figure 5.6 *Prior art: cyclodimerization*

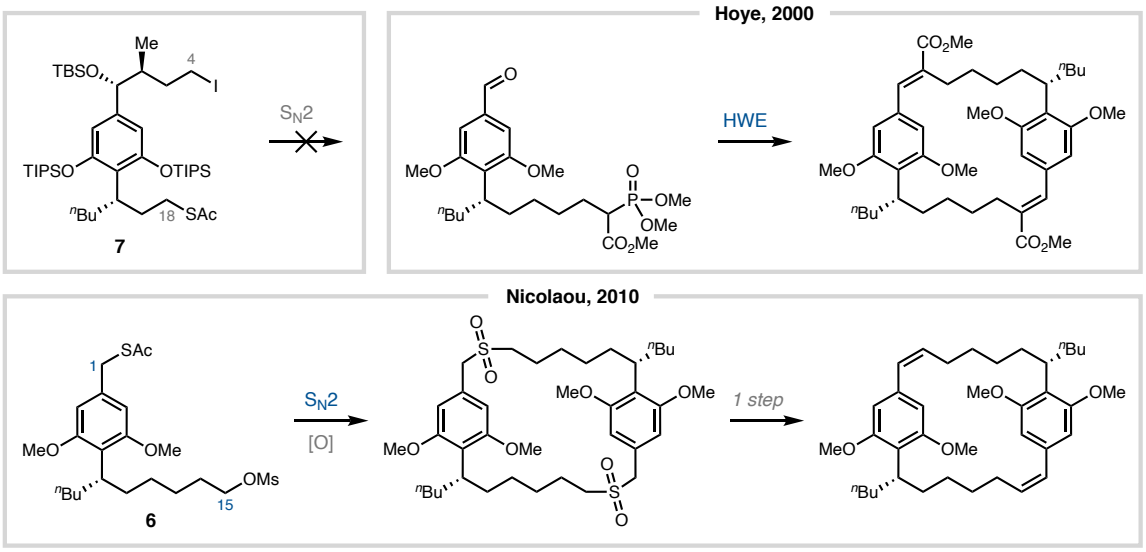

It is notable that metathesis has demonstrated surprising[71] flexibility with respect to the placement of the resultant double bond within the macrocyclic bridge. Initial application by Smith and coworkers[72,70] of cross-metathesis/ring-closing metathesis (CM/RCM) to dimerization attached the resorcinol motifs through the center of the connecting carbon chain. This approach was so successful it has since been applied to additional formal[67] and total syntheses[40] of cylindrocyclophane A (Figure 5.7). CM/RCM has also been utilized in the formation of a homobenzylic double bond, critical to the total synthesis of cylindrocyclophane F (**2**) by the Breit group[73] and to preparation of non-natural derivatives of **1**.[40]

Figure 5.7 *Cyclodimerization via CM/RCM*

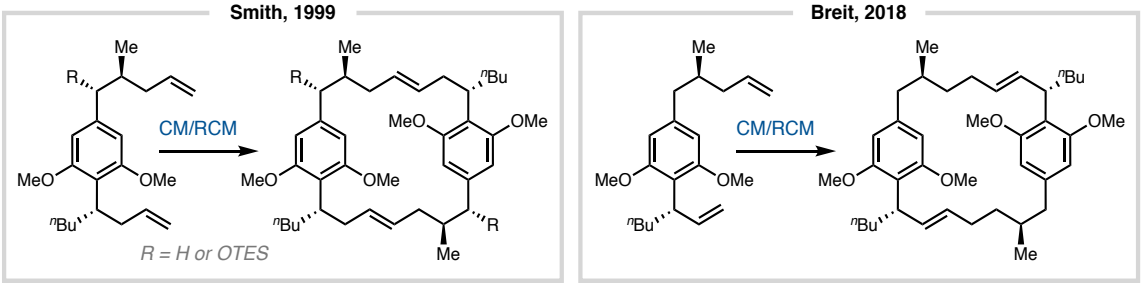

5.1.2.2 Cylindrocyclophanes: Stereocenter Installation

Synthetic access to the [7.7]paracyclophane skeleton is only part of the problem of cylindrocyclophane preparation, which also requires stereoselective installation of benzylic and homobenzylic substituents. On the one hand, this can be accomplished prior to macrocyclization. Two main challenges arise that have generally led to lengthy linear sequences. First, stereochemical information is not efficiently transmitted across the resorcinol motif, so C20 and C1/C2 must be independently established. Second, the natural products lack functionality at these sites that inherently enable stereocenter formation; instead, lateral steps are required both to install and to remove functional groups used for stereoselective transformations.

For instance, Hoye and coworkers[68] employed enzymatic resolution followed by an Ireland–Claisen rearrangement to set C20, and the Nicolaou group[69] pursued enantioselective ketone reduction then directed hydrogenation (Figure 5.8). Iwabuchi and coworkers derived the C20 stereocenter from commercial chiral material, advanced through a Johnson–Claisen rearrangement to furnish enantioenriched intermediate **8** in 12 steps; an additional eight-step sequence, involving aldol reaction using Evans' chiral auxiliary, followed to set the remaining stereogenic centers.[40]

Figure 5.8 *Addressing the benzylic stereocenter*

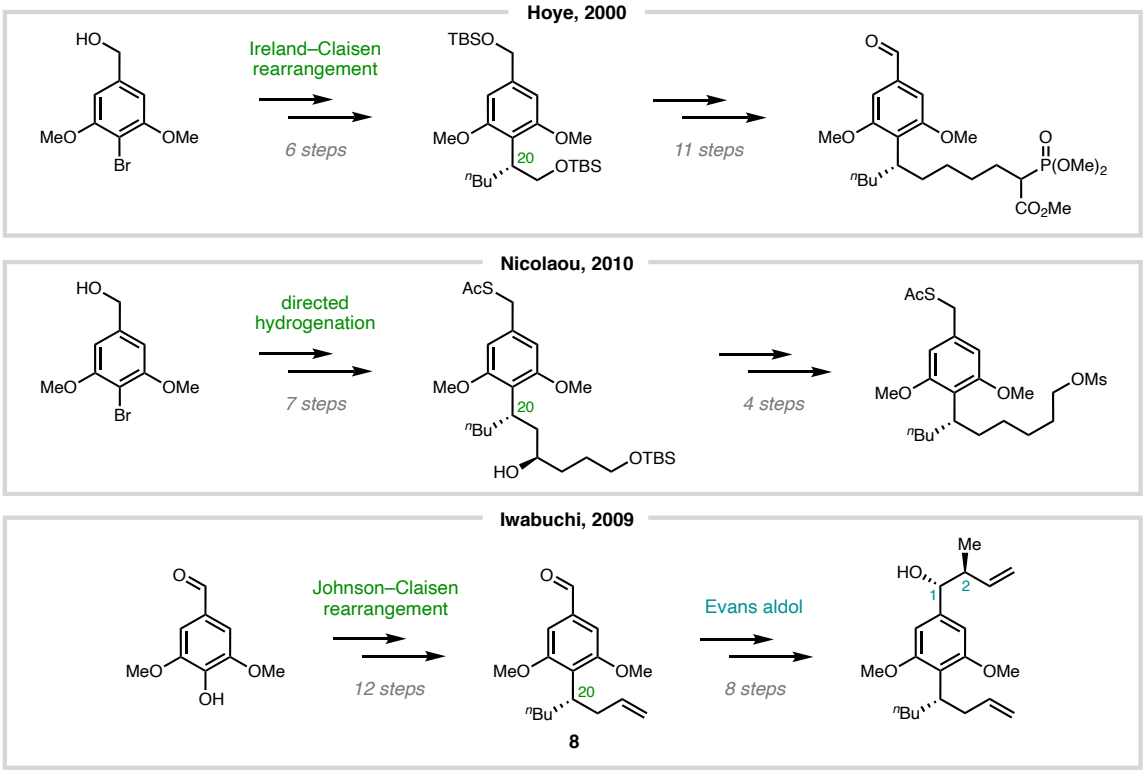

On the other hand, stereoselective substitution can occur post-cyclodimerization. Exemplified by the Hoye[68] and Nicolaou[69] syntheses, enantioselective transformations were required to give rise to the *trans*-C1/C2 hydroxymethyl motif. Hydroboration/oxidation and a sequence of dihydroxylation (and deoxygenation toward **2**) followed by methylation served this purpose (Figure 5.9).

Figure 5.9 *Stereoselective installation of hydroxymethyl motif*

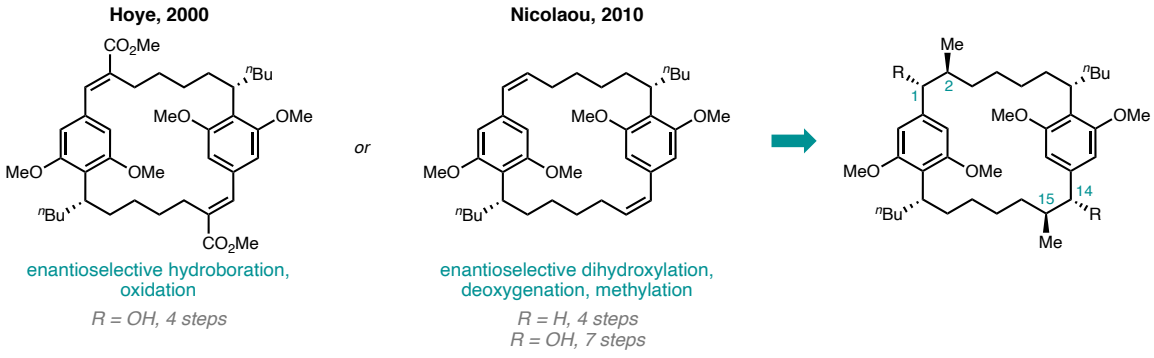

A conceptually distinct approach was pioneered by the Davies/Stoltz report (Figure 5.10).[63] A chiral dirhodium catalyst was first used to install the C1/C2 stereodiad with good enantioselectivity and excellent dr. In subsequent ring closure, the remaining C14/C15 stereocenters were forged with near-perfect ee but reduced diastereomeric ratio. Thus, existing chiral information (of macrocyclic precursor **9**) does not upset the ability of bond formation to proceed with catalyst-controlled enantioselectivity but instead amplifies enantiomeric excess as a consequence of the Horeau principle.[74] There is, however, an observable effect of ring formation on diastereoselectivity. If applied to appropriately functionalized substrates, this efficient sequence of stereoselective paracyclophane generation would need to be followed by removal or oxidative cleavage of the guiding C/C14 carboxylates to advance toward natural products **2** or **1**, respectively.

Figure 5.10 *Diastereoselective ring closure*

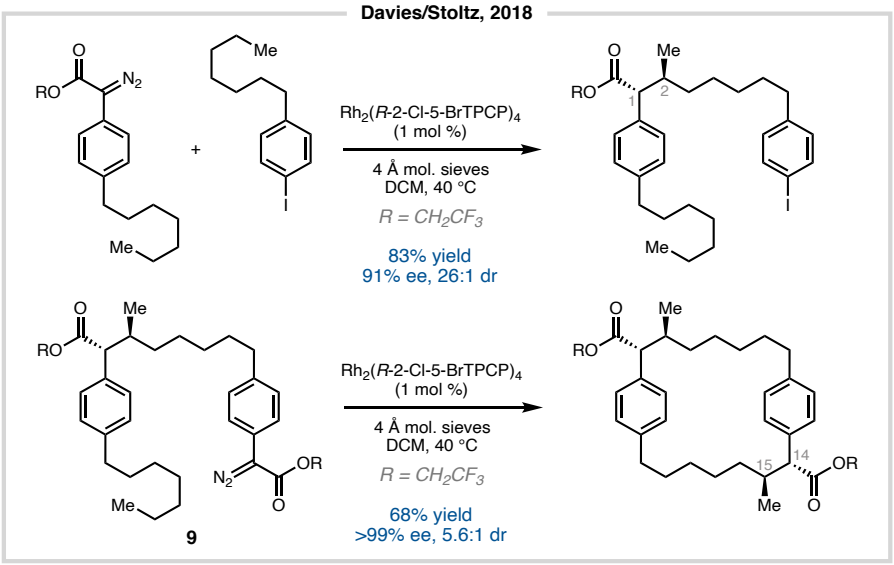

5.2 CONCEPTUAL SYNTHETIC DESIGN AND RETROSYNTHESIS

Given that cyclodimerization has been proven an efficient approach to C_2 symmetric macrocycles, we sought to apply *double* reductive cross-coupling as a key transformation for accessing, in a single step, the [7,7]paracyclophane skeleton common to all cylindrocyclophanes. We anticipated double RCC to be an advantageous dimerization tactic with respect to difunctional monomer synthesis (e.g., **11**), as reductive coupling obviates the need to install incompatible electrophiles and reactive organometallic functionalities on the same molecule. We also postulated that enantioselective RCC would be necessary to establish the stereocenters distally located on the macrocycle, via double asymmetric reaction.

Specifically, we envisioned that double reductive alkenylation of *N*-hydroxyphthalimide (NHP) esters would dimerize difunctional substrate **11** to generate macrocyclic dialkene **10**, a known intermediate from which cylindrocyclophane F (**2**) is accessible via hydrogenation and deprotection (Figure 5.11).[73] We drew inspiration from the single decarboxylative RCC reaction[75] of alkenyl bromides with NHP esters, which has been shown to proceed in high yield and excellent enantioselectivity following subjection of these coupling partners to a chiral nickel catalyst and an organic reductant, tetrakis(dimethylamino)ethylene (TDAE). These conditions seemed well-suited for application to the substrate of dimerization (alkenyl bromide/NHP ester **11**), given that (1) high yield of a single C–C bond formation event would be critical for efficient double coupling to forge the C6–C7 and C19–C20 bonds, and (2) the ability of the catalyst to effectively control enantioselectivity in this step (i.e., generation of the benzylic stereocenters at C7 and C20) would be unlikely to be affected by the distant C2 and C15

stereochemical elements.

Figure 5.11 *Retrosynthetic analysis of cylindrocyclophane F*

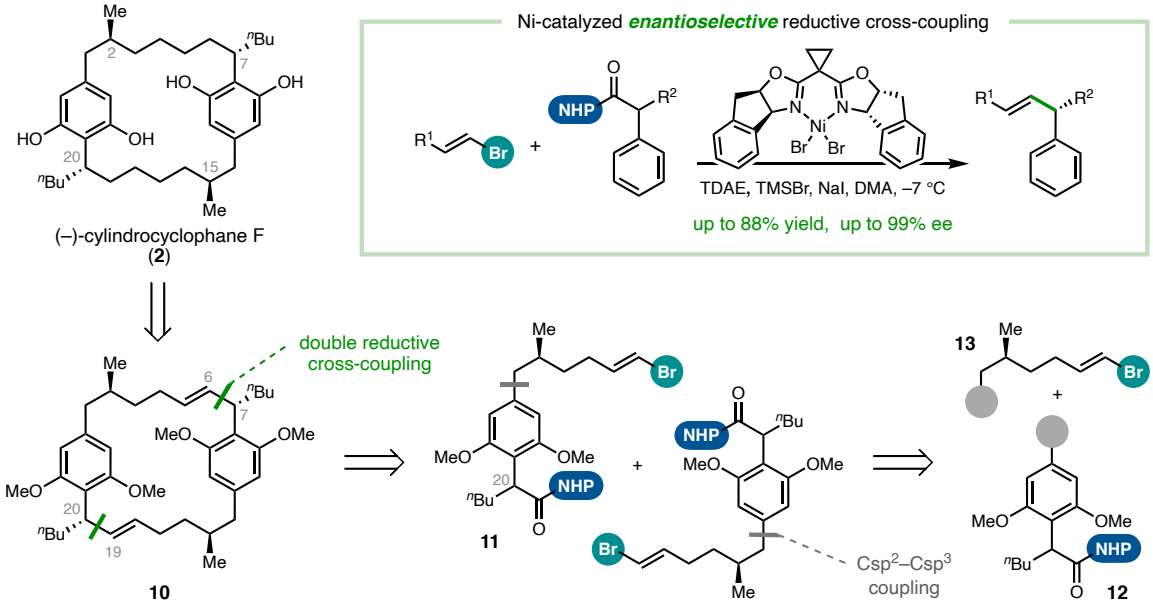

To develop double reductive cross-coupling as a cyclodimerization reaction of **11**, this key event would need to overcome known limitations of single RCCs. Electrophiles with *o*-substitution have proven to be challenging substrates in these methods,[75,5] and Ni-catalyzed cross-coupling reactions of redox-active esters have been generally documented to be capricious and substrate dependent.[76] Also, attempts concurrent to our own to apply decarboxylative RCC to the construction of C–C bonds in the context of total synthesis[77] have met with failure.[78]

Nonetheless, we recognized the strategic value of this macrocycle disconnection. As an ester, redox-active **11** could not only facilitate macrocyclization but could allow ready installation of the *n*-butyl group at the α-position (C20). In light of preliminary SAR data (*vide supra*), retrosynthetic cleavage through the C7–^{n}Bu bond via simple α-alkylation would be a boon to the preparation of cylindrocyclophane derivatives. From a

synthetic efficiency standpoint, removal of the ester functional group concomitant to establishing both the C20 stereocenter and the C19–C20 bond would be advantageous.

Retrosynthetically, the aryl–alkyl linkage of intermediate **11** keyed the convergent joining of aryl and alkyl fragments, a strategic disconnection inspired by a proposed biosynthetic route proceeding through this Csp^2–Csp^3 bond formation.[79] The ideal retrons would contain the requisite NHP ester and alkenyl bromide moieties for later dimerization (**12** and **13**, respectively); however, we anticipated that convergent fragment coupling might require these functional groups to be transiently 'masked.' Lastly, we planned to rely on well-established methods of stereoselective methylation to access enantioenriched fragment **13**.

This strategy would lead to the formal synthesis of cylindrocyclophane **2** and establish the peripheral stereocenters concurrently to the macrocycle. We expected that our synthetic design could readily lend itself to the preparation of additional cylindrocyclophane variants (e.g., **1**). As such, we pursued this conceptual synthesis via a multi-pronged approach: investigating the key RCC reaction on a model system alongside development of a synthetic route to a variety of cyclodimerization precursors.

5.3 SINGLE REDUCTIVE CROSS-COUPLING: MODEL REACTION

Figure 5.12 *Motivation for single reductive cross-coupling*

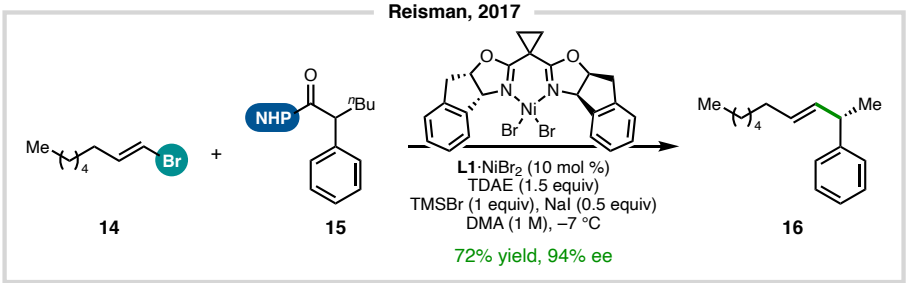

In order to apply reductive cyclodimerization to the synthesis of the cylindrocyclophanes, an NHP ester with disubstitution (i.e., intermediate **11**, see Fig. 5.11) is required. To demonstrate effective single reductive cross-coupling of an *o*,*o*-disubstituted benzylic electrophile, we studied the reaction of a 2,6-dimethoxy-substituted NHP ester with a simple alkenyl bromide as a model system. In a previous report,[75] treatment of analogous but unsubstituted NHP ester **15** and alkenyl bromide **14** to an IndaBOX-ligated Ni catalyst ($NiBr_2 \cdot$**L1**) in the presence of TDAE as a stoichiometric reductant led to cross-coupled **16** in 72% yield and 94% ee (Figure 5.12). We therefore selected these conditions as a starting point for our model RCC.

Early work suggested that this ligand and reductant combination—albeit at higher temperature, higher ligand loading, and lower concentration—failed to effect the coupling of 2,6-dimethoxy **18** (Table 5.1, entry 1).[80] These early studies pointed to the potential success of using Mn^0 instead of TDAE, as this reductant delivered 15% yield of cross-coupled **19** when bis(oxazoline) (BOX) ligand **L1** was used (entry 2).[80] Hypothesizing that increased ligand *N*–*N* distance might facilitate access to nickel for more sterically demanding coupling partners (i.e., *o*,*o*-disubstituted **18**), the bi-oxazoline (BiOX) ligand framework was investigated under otherwise identical conditions. Use of BiOX ligand **L2** with 2 equiv NHP ester **18** was reported to deliver desired product **19** in 52% yield and 73% ee (entry 3).[80] It was noted that TDAE was unsuccessful (0% yield **19**) even with BiOX **L2** (entry 4).[80]

Table 5.1 *Guiding preliminary results*

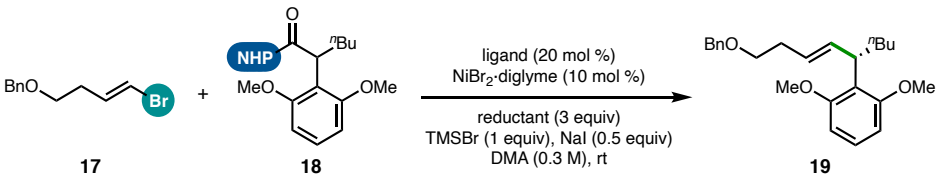

Entry	Ligand	Reductant	% Yield 19	% ee
1	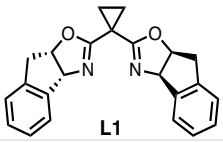 L1	TDAE	0	—
2		Mn^0	15	62
3	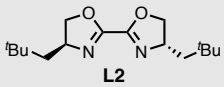 L2	Mn^0	52	73
4		TDAE	0	—

5.3.1 *Investigation Using BiOX Ligands*

We were unable to reproduce the results in Table 5.1. Instead, use of Zn^0 as an alternative reductant gave similar yield and enantioselectivity to that reported for Mn^0 (using BOX **L1**: 11% yield, 67% ee), and we selected this metal powder for our studies. We ultimately found that modification of the BiOX ligand could substantially affect the enantiomeric excess of the product but led to consistently low yields of **19** (Figure 5.13). Enantioselectivity improved with increasing ring size of carbocycle-substituted ligands (**L3**–**L5**). Addition of a methylene linker between the oxazoline and carbocyclic ring, as in **L6**, moderately decreased ee. However, a similar methylene linker was critical for reactivity with an acyclic *tert*-butyl substituent (**L2** versus **L7**), and **L2** displayed a significant improvement in ee versus cyclic variants. For ligands with alkyl chains branched adjacent to the oxazoline (**L7**–**L10**), increased chain length corresponded to an increase in ee. Although 4-heptylBiOX (**L10**) exhibited the highest level of

enantioselectivity in this screen, the highest-yielding ligand (CyBiOX, **L4**) was selected for further optimization due to its availability in large quantities.

Figure 5.13 *BiOX ligand screen*

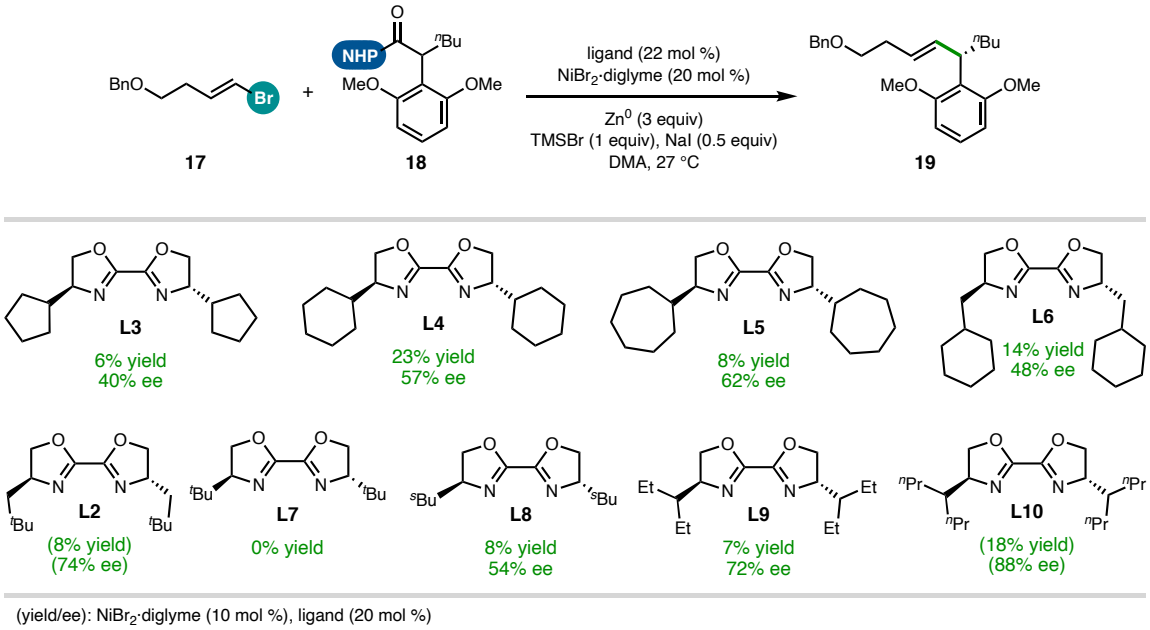

Using CyBiOX (**L4**) as ligand, in combination with a metal reductant, we did not observe significant improvement to yield across a variety of deviations to the reaction conditions (Table 5.2). As examples, changing the concentration (entries 1 and 2), relative equivalents of substrates (entries 3 and 4), and additive quantities (entries 5–7) each resulted in a yield of product **19** within a 9% range. In contrast, use of soluble reductant TDAE instead of Mn^0 led to a mild improvement in **19** yield (26%, entry 8); in addition, enantioselectivity in this case (85% ee) was comparable to that when using **L10** (88% ee, see Figure 5.13). However, in light of our long-term goal of *double* RCC, we recognized the need for much higher levels of desired reactivity when performing a *single* cross-coupling event.

Table 5.2 *Reaction optimization using CyBiOX*

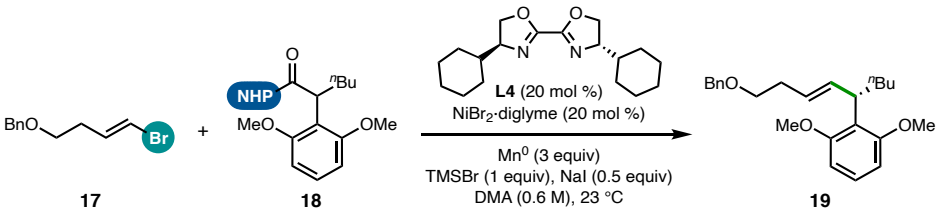

Entry	Deviation from Conditions	% Yield 19	% ee
1	—	13	71
2	0.3 M	19	70
3	NHP ester **18** (2 equiv)	18	65
4	alkenyl Br **17** (2 equiv)	20	—
5	NaI (0 equiv)	17	56
6	NaI (1 equiv)	13	56
7	NaI (2 equiv)	11	56
8	TDAE (3 equiv)	26	85

Seeking access to product **19** in yields higher than ca. 30%, we sought to better understand the pathways available to each substrate other than productive cross-coupling, as a way to guide our optimization efforts. Tracking NHP ester **18** under the reaction conditions revealed an assortment of byproducts without any reaction parameter-based trend in yield distribution (Figure 5.14). In general, styrene **20**, bibenzyl **21**, and reduced **22** were present in the most quantities (10–30% yield each), whereas carboxylic acid **23** was occasionally observed. Presumably, reductive fragmentation of the NHP ester generates an intermediate benzylic radical, which can proceed down several undesired pathways, including: benzylic olefination (**20**), possibly via a Ni-mediated β-hydride elimination process; dimerization (**21**), with no diastereoselectivity; hydrogen-atom abstraction to furnish alkane **22**; or hydrolysis to return substrate precursor **23**. Formation

of each of these byproducts would not only siphon the starting material away from desired product-forming pathways but could also lead to catalyst inhibition, as conjugated π-systems and carboxylates (i.e., **20** and **23**, respectively) readily ligate Ni.

Figure 5.14 *Byproduct distribution of NHP ester*

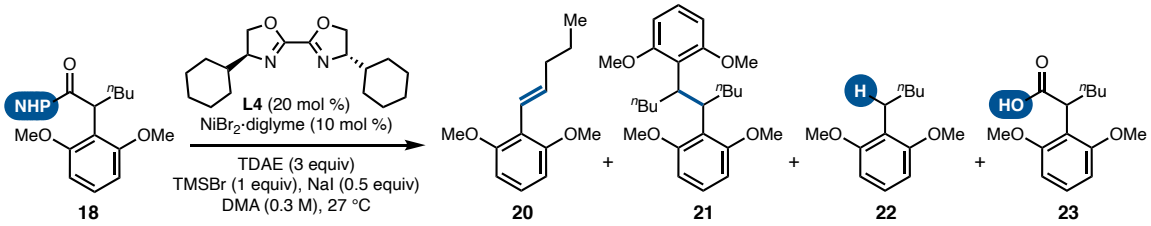

We next performed a series of control experiments to elucidate the pathways involving alkenyl bromide **17** (Table 5.3). Under standard reaction conditions in the presence of coupling partner **18**, the product of **17** homocoupling (i.e., diene **24**) was consistently observed as the major product. Accordingly, subjection of only substrate **17** to these conditions, without the TMSBr or NaI additives, led to its complete consumption; the majority of **17** was homocoupled, indicating this process is independent of the NHP ester (entry 1). Small quantities of reduced alkene **25** were also identified, but in most cases, protodebromination appeared to be insignificant (i.e., trace **25**).

Table 5.3 *Control experiments: alkenyl bromide*

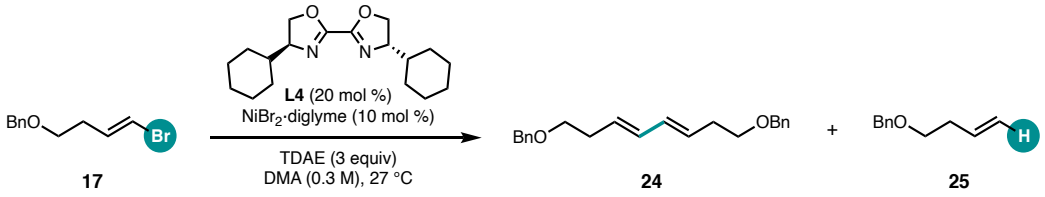

Entry	Deviation from Conditions	Result
1	—	62% homocoupled **24** trace protodebromination (**25**)
2	no TDAE	82% recovered **17**
3	no Ni/**L4**	79% recovered **17**

In the presence of the Ni^{II} precatalyst and ligand but without the reductant, substrate **17** was recovered in high yield, indicating that Ni^{II} alone was not able to engage the substrate (entry 2). Likely, reduction of Ni is required to precede oxidative addition of **17**. Alternatively, it could be possible for the alkenyl bromide to be directly reduced, initiating a homocoupling process not mediated by the metal. However, the Csp^2 substrate was effectively untouched by the reductant in the absence of nickel (entry 3).

Figure 5.15 *Working mechanistic hypothesis: single RCC*

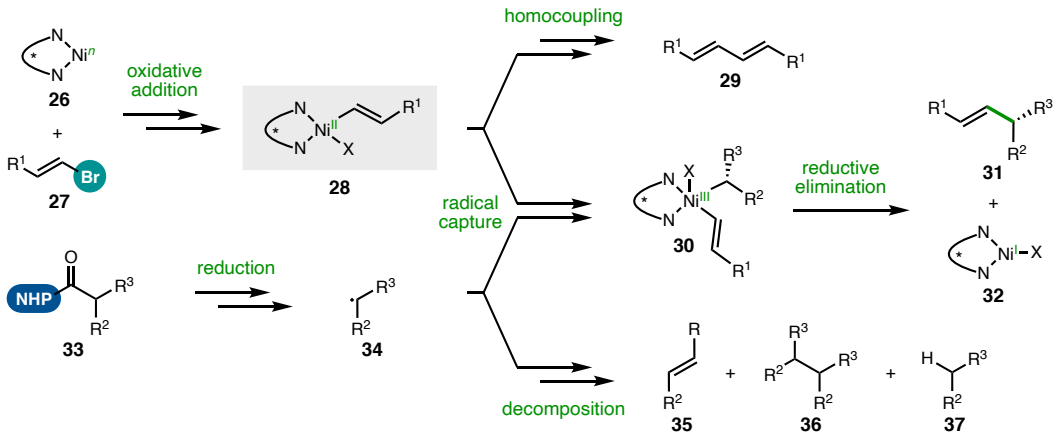

With the knowledge of the mass balance of each coupling partner, we considered a hypothetical mechanistic scenario, based on recent mechanistic investigation of a BiOX·Ni-catalyzed RCC,[81] that could explain the origin of the observed byproducts. Specifically, we hypothesized that the fate of a Ni^{II}–alkene species (**28**) would be a key determinant of reaction outcome (Figure 5.15). Organonickel complex **28** would arise following oxidative addition of an alkenyl bromide (**27**); we imagine that this intermediate would be partitioned between competing pathways. The desired pathway (en route to product **31**) would occur via capture of radical **34**, generated from the NHP ester (**33**). Thus-formed Ni^{III} complex **30** would be expected to proceed to cross-coupled **31** via

reductive elimination; concomitantly, Ni^{I} **32** would be released, available for either reduction or direct substrate interaction to turn over a catalytic cycle.

If, however, radical capture is inefficient—potentially due to steric hindrance—hen the NHP-derived intermediate (**34**) may unselectively decompose, as observed. In this case, the alkenyl Ni complex (**28**), without a distinct coupling partner, could engage another equivalent of alkenyl bromide **27** or a second organonickel species to form homocoupled **29** (*vide infra*), also consistent with experimental evidence. The same substrate decomposition products could be formed regardless of whether productive radical capture was hindered by radical **34** instability (i.e., fast decomposition) or rapid alkene–alkene homocoupling.

Figure 5.16 *Reaction time course: cross-coupling versus byproducts*

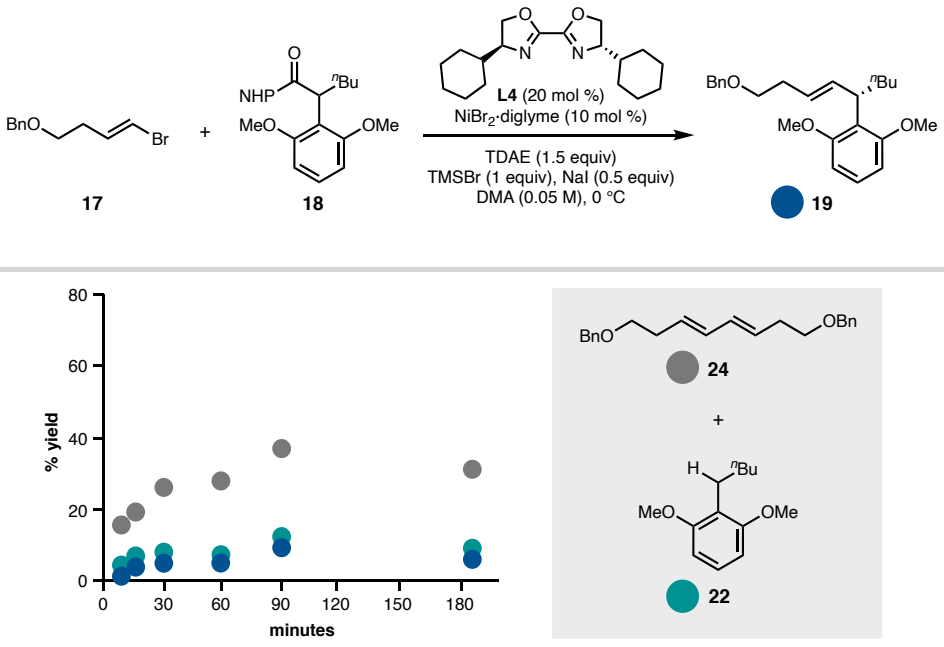

To uncover the relative rates of cross-coupling versus homocoupling, we monitored the reaction over time using CyBiOX (**L4**), at lower temperature and higher dilution than standard conditions. Following analysis of reaction aliquots by quantitative

^{1}H NMR, we discovered that the rate of alkenyl bromide homocoupling (**24**, grey; Figure 5.16) far exceeded the rate of desired product (**19**, blue) generation. Formation of one NHP decomposition product, alkane **22** (teal), was similarly slow, outpaced by the Csp^2–Csp^2 byproduct. Based on this reaction time course, we hypothesized that disfavoring the most rapid pathway (i.e., homocoupling) might render productive pathways more competitive, leading to an increase in cross-coupling.

We considered several scenarios in which homocoupling could occur (Figure 5.17). First, it is often proposed that a Csp^2–Ni complex (e.g., **28**) can undergo reduction followed by oxidative addition;[82] the resulting bisalkenyl Ni^{III} species (**39**) would be primed for reductive elimination to generated homocoupled **29**. If this were operative under the reaction conditions, then the X-type ligand of **28** could be used to electronically tune **28** to render reduction of this species more challenging. Preliminary efforts toward this end involved replacing the NaI additive with sodium salts featuring anions that could serve as stronger σ-donating ligands. However, when X = OTMS or OMe, the yield of the cross-coupled product remained low (<10%) and the homocoupling byproduct was not diminished.

Figure 5.17 *Mechanistic hypothesis: homocoupling*

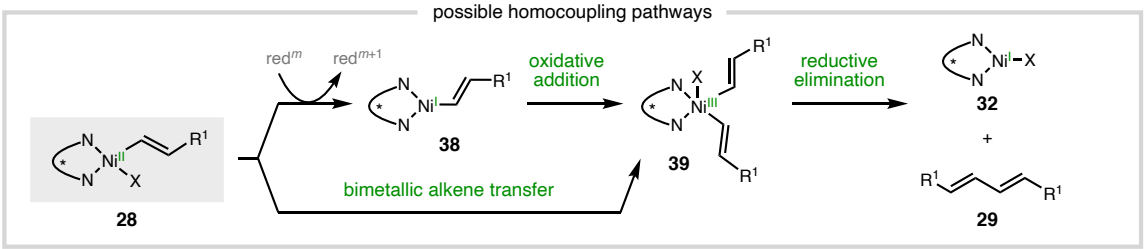

A second scenario, inspired by foundational mechanistic investigations of Ni-catalyzed biaryl formation,[83] implicates an organonickel species, in addition to **28**, in an

alkene transfer step. In effect, this bimetallic oxidative addition would generate homocoupled **29** by way of a Ni^{III} intermediate (i.e., **39**). Given the bimolecular nature of this putative pathway, we hypothesized that decreasing the loading of the Ni catalyst could serve to reduce formation of byproduct **29** in favor of the desired cross coupling.

Figure 5.18 *Catalyst loading*

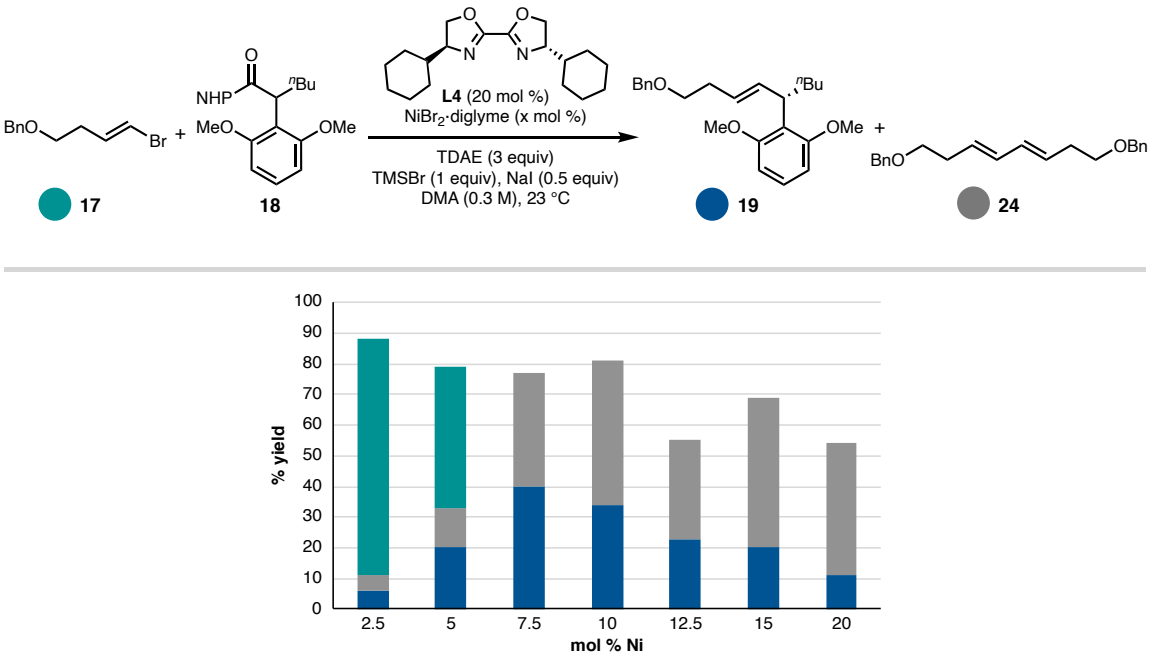

Indeed, sequential lowering of the amount of nickel from initial 20 mol % resulted in a corresponding improvement in the yield of **19** (blue), reaching a maximum at 7.5 mol % (ca. 40% yield, Figure 5.18). At sufficiently low amounts of catalyst, the beneficial effect on cross-coupling was countered by inefficient alkenyl bromide (**17**, teal) activation, indicated by significant levels of remaining starting material. We were encouraged by the empirical success of this screen and questioned whether the yield enhancement could be augmented by additional modifications to the reaction.

Pursuing an alternative strategy, we returned to our working mechanistic hypothesis (see Fig. 5.15) and postulated that instead of *disfavoring* undesired paths of intermediate **28**, we might achieve the same effect (i.e., improvement to cross-coupling) by promoting the desired pathway: *facilitating* radical capture. As it seemed likely that this step could be challenging for a sterically encumbered radical, we prepared the singly *o*-substituted NHP ester **40**. Compared to the control (dimethoxy **18**: 16% yield), this less bulky substrate offered marginal improvement (Figure 5.19). This suggests the existence of a threshold steric effect. It is possible that any *ortho* aryl substitution effects a drop-off in reactivity, which is often the case for RCCs of *o*-substituted aryl halide electrophiles;[84,5] thus, steric modulation of the substrate would not be compatible with our synthesis objectives.

Figure 5.19 *Steric modification of NHP ester*

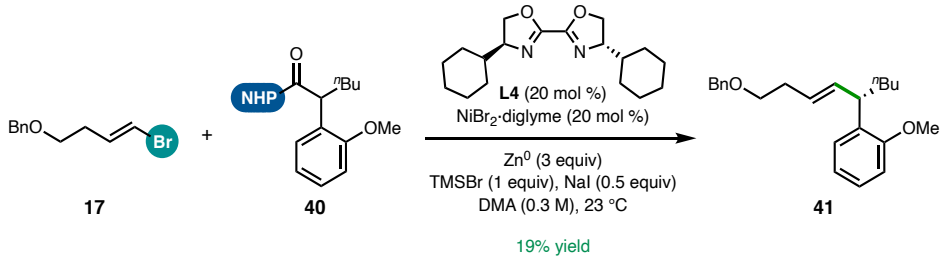

Up to this point, we had primarily targeted reaction steps occurring after the formation of key intermediates (i.e., oxidative addition toward organonickel **28** or reductive fragmentation to generate radical **34**; see Fig. 5.15), so we turned our attention upstream. Analysis of the reaction time course, with a focus on the rates of substrate conversion, proved instructive (Figure 5.20). The alkenyl bromide (**17**) was consumed at a faster rate than its counterpart, NHP ester **18**, under these conditions. An exaggerated mismatch in the rates of coupling partner activation could inhibit the desired

organonickel radical capture pathway by skewing the effective concentration of the requisite components (i.e., **28** and **34**).[85]

Figure 5.20 *Reaction time course: substrate conversion rates*

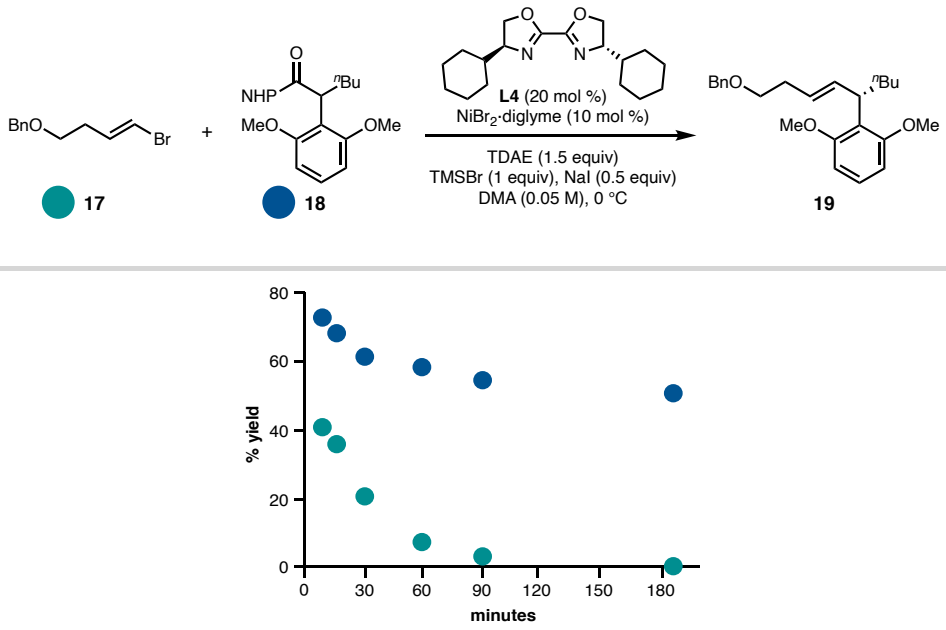

As a first approach to rectifying this possible scenario, we attempted to disfavor oxidative addition of **17** (i.e., reducing [Ni^{II}–alkene]). As such, we prepared the chloride analog of Csp^2 substrate **17**, alkenyl chloride **40**, given the challenging reaction of chloride-based electrophiles in Ni-catalyzed RCCs.[86] Treatment of this electrophile with the NHP ester and Ni/**L4** combination in the presence of TDAE failed to afford cross-coupled product (Table 5.4, entry 1). Instead, the near-quantitative recovery of **42**, even at high temperatures, was observed. It was thus unsurprising that use of NaCl in the reaction led to lower yields of product **19** (entry 2); based on related studies,[87] we presume that *in situ* halide exchange is plausible and, in this case, leads to less-reactive electrophiles. Sodium iodide—which presumably generates the more-reactive alkenyl–I

species *in situ*—led to the highest product levels observed in this study (26% yield **19**, entry 4).

Table 5.4 *Alkenyl halide alternatives*

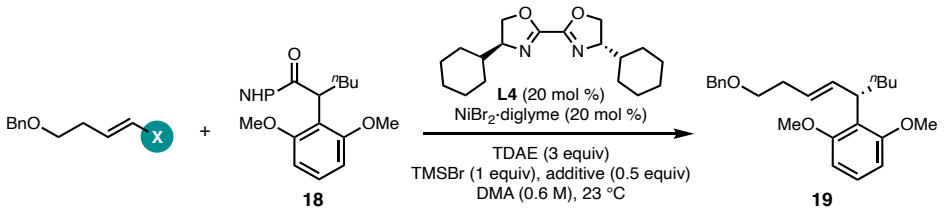

Entry	X	Additive	% Yield 19
1	BnO, Cl **42**	NaI	0
2		NaCl	9
3	BnO, Br **17**	NaBr	16
4		NaI	26

Subsequent efforts focused on promotion of NHP ester reduction to match the facile reaction of alkenyl–Br **17**. We posited that the reduction potential of the redox-active ester would correlate with the rate of radical generation via reductive fragmentation. We expected that introduction of electron-withdrawing substituents on the phthalimide moiety would serve both to anodically shift $E_{1/2}^{red}$ of the corresponding NHP ester and to increase the rate of substrate consumption—importantly, leading to an improvement in the yield of product **19**. In the event, only two of the synthesized NHP derivatives (**43** and **44**) yielded any amount of cross-coupled **19** (Table 5.5, entries 1–3). The disappointing performance of those redox-active esters with >100 mV shift in reduction potential (i.e., **45** and **46**) made it challenging to discern any trends from this survey of substrates (entries 4 and 5). A recent report has demonstrated the expected correlation of redox potential and RCC yield, albeit using NHP ester derivatives less challenging to reduce than **18**/**43**–**46**.[88]

Table 5.5 *Redox-active ester derivatives*

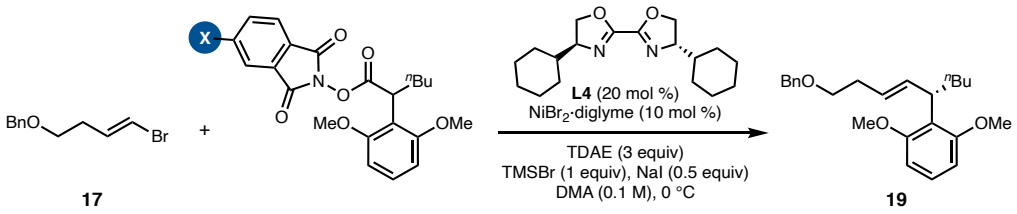

Entry	X	$E_{1/2}^{red}$ vs SCE, MeCN	% Yield XX
1	OMe (**43**)	–1.36	1
2	H (**18**)	–1.34	11
3	Cl (**44**)	–1.28	13
4	Me (**45**)	–1.18	0
5	Br (**46**)	–1.16	0

As reductive radical generation requires participation of both an NHP ester (i.e., **18**) and a reductant, we questioned whether the latter might prove more amenable to modification. The reductant mediates a fragmentation process of general NHP ester **33**, leading to intermediate **47** that is presumably initiated by single electron transfer (SET) and subsequently ejects phthalimide anion and a molecule of CO_2, in addition to radical **34** (Figure 5.21). Traditionally, in reactions of redox-active esters catalyzed by nickel, on- or off-cycle Ni species have been implicated in this SET event.[89,90,91,92] Given the multi-faceted role of organonickel intermediates in the reaction, any effort to tune the reducing power of these compounds is unlikely to be straightforward (*vide supra*).

However, in a radical chain mechanism, it is possible that a species independent of the catalyst could provide the electron necessary for NHP ester fragmentation, such as the stoichiometric reductant nominally added to turn over Ni. In the case of related alkyl halide electrophiles, this mechanistic picture has recently been proposed for reactions

involving Mn^0/BiOX·Ni.[81] In the absence of Ni or other transition metal catalysts, Zn^0 has been demonstrated to effectively reduce select NHP esters,[93,94,88] and Zn^{2+} Lewis acids—the byproducts of reduction—can have an accelerating effect on this event.[94] Should this type of terminal reductant-mediated pathway also be operative under the present Ni-containing conditions, TDAE could directly reduce NHP ester **33** without catalyst involvement. Given the tunable nature of this class of soluble, organic reductants,[95] appropriate matching of TDAE derivative with a phthalimide-substituted NHP ester could be imagined to offer a fine level of control over the rate of radical generation.[96]

Figure 5.21 *Mechanistic hypothesis: radical generation*

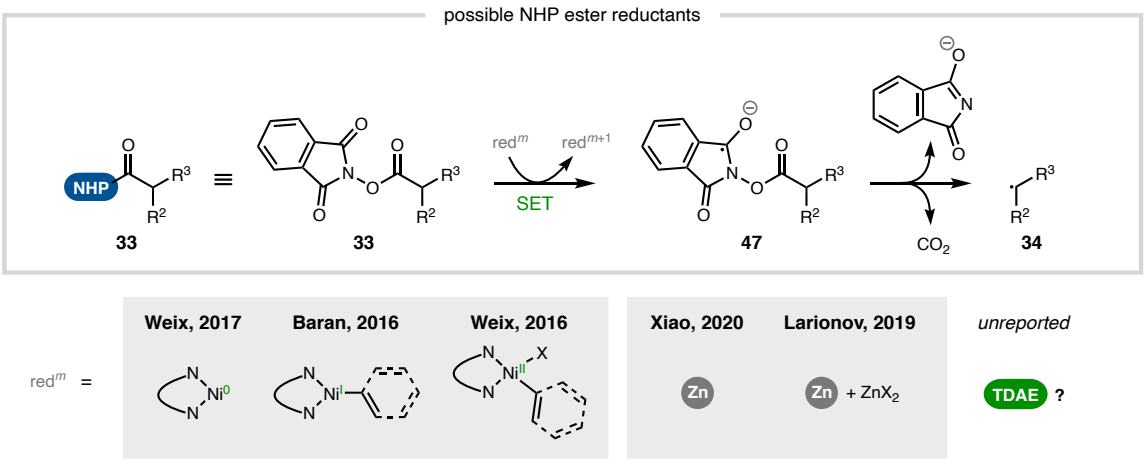

To tease out the nature of the reduction step involved in benzylic radical generation, we subjected the NHP ester (**18**) to various reductant contenders in DMA and analyzed conversion (Figure 5.22). The CyBiOX/Ni^{II} catalyst (**L4**·Ni) without exogenous reductant effected little NHP ester conversion. Metal powder Zn^0 was slightly more effective, and NHP ester **18** was recovered in ca. 60% yield. We considered that the additives critical for cross-coupling (i.e., TMSBr and NaI) might one or both function to

allow the nominally thermodynamically inaccessible reduction by Zn^0; perhaps the silyl halide could serve to activate the NHP ester, as proposed for Zn^{2+} Lewis acids.[94] However, inclusion of these additives did not significantly change consumption of **18** in the presence of Zn^0.

Figure 5.22 *NHP ester reduction*

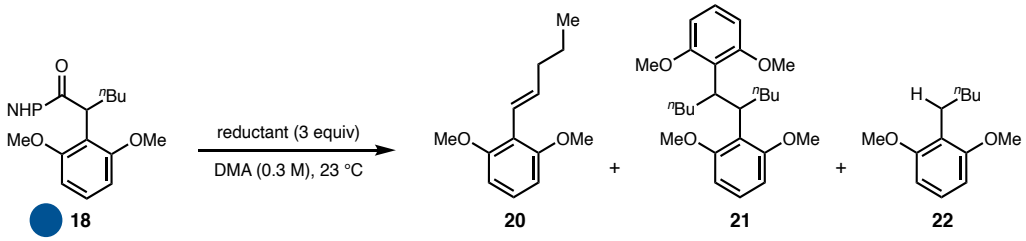

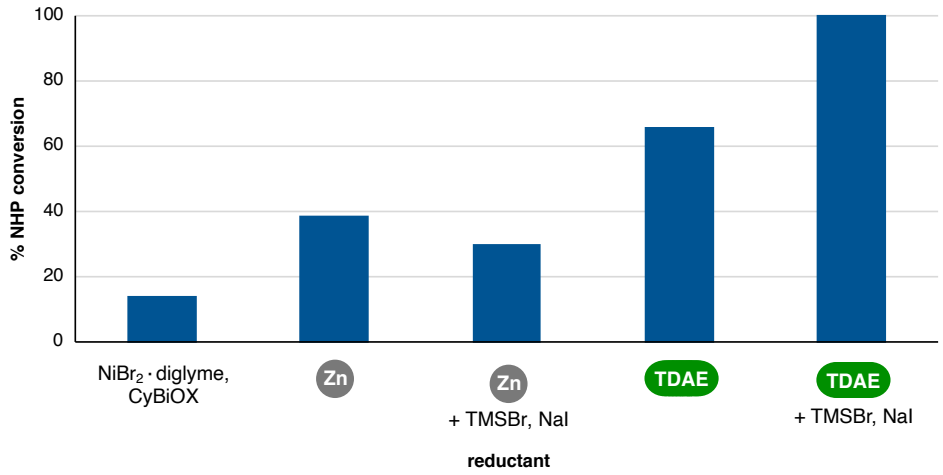

In contrast, stirring TDAE with NHP ester **18** in the absence of Ni catalyst led to over 60% conversion. Furthermore, addition of TMSBr and NaI, as well as TDAE, led to complete decomposition of **18** in a time frame consistent with standard cross-coupling reactivity at this temperature and concentration. The identification of byproducts **20**–**22** from this experiment indicates that non-Ni-mediated processes are involved in their formation. Taken together, these results suggest that intermediate radical generation could occur independent to a Ni-based catalytic cycle and that the slightly improved

performance of the RCC when TDAE is used, as opposed to metal powders, may be a result of more facile NHP ester reduction.

Such a discovery was pivotal, because it indicated that throughout our optimization campaign we had significantly underestimated the sensitivity of NHP ester **18** to TDAE. This prompted re-examination of the experimental design. We postulated that our reaction setup, in which TDAE was added *after* the NHP ester but *prior* to Ni/L and alkenyl bromide, might allow rapid reductive decomposition of the NHP ester to occur without the possibility of productive capture of any resulting benzylic radical species (Figure 5.23). To determine whether this order of addition was a plausible reason that we had consistently observed low yields of desired product, we reversed the order, adding all components (i.e., NHP ester, alkenyl bromide, Ni/L, NaI, and solvent) to the reaction vessel *before* addition of TDAE and TMSBr. When L = CyBiOX (**L4**), the impact of experimental setup was minimal with respect to cross-coupled product yield. At this stage, it appeared that this catalyst system (with a BiOX ligand scaffold) was not suitable for RCC of substrates **17** and **18** and that continued efforts to improve the overall poor performance of reaction in this manifold would lead to diminishing returns.

Figure 5.23 *Order of addition*

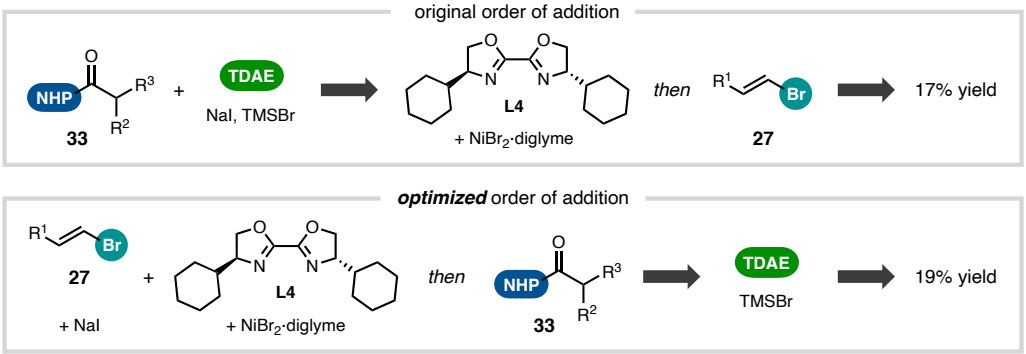

5.3.2 *Investigation Using BOX Ligands*

Given that cross-coupling had been reported to be at least minimally viable for BOX ligands (see Table. 5.1),[80] we turned our attention to this catalyst system. Although originally dissuaded from use of TDAE as reductant with **L1**·$NiBr_2$ based on initial investigations, it now seemed plausible that the reported 0% yield of **19** arose from suboptimal reaction setup, as these details were unknown.[80] Indeed, revisiting the original conditions for successful RCC of NHP esters[75] and adding TDAE/TMSBr last, we observed a remarkable turn-on of desired reactivity between **17** and **18** with **L1**·$NiBr_2$: 40% yield of cross-coupled **19** (Figure 5.24).

Figure 5.24 *Catalyst loading: optimized order of addition*

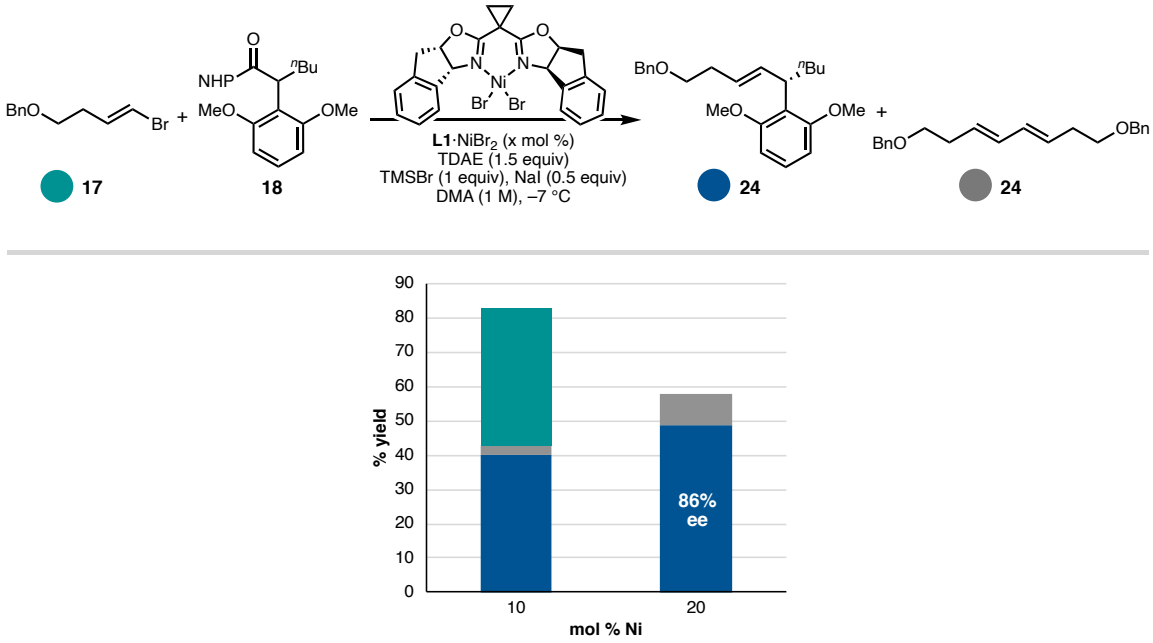

The stark change to product **19** yield elicited by the BOX versus BiOX ligand scaffold (19% yield with **L4**; 40% yield with **L1**)—following the optimized order of addition—was matched by a dramatic decrease in homocoupled **24** formation (from 47%

to 3% yield). This observation suggested that one important feature of the IndaBOX ligand (**L1**) might be to inhibit alkenyl bromide homocoupling; this effect could potentially arise via stabilization of key organonickel intermediate **28** or oxidative addition rendered challenging (see Fig. 5.15). In support of the latter, we recovered 40% of the alkenyl bromide (**17**) from the reaction. Thus, increasing the catalyst loading allowed full consumption of that substrate with a corresponding improvement in cross-coupled yield (49%).

Using chiral **L1** as ligand allowed isolation of product **19** in 86% ee. The absolute configuration of **19** was assigned by analogy to previous studies of these reaction conditions.[75] With viable reaction conditions for *single* RCC of an *o*,*o*-disubstituted NHP ester in hand, we were poised to launch investigation of *double* RCC toward paracyclophanes (see section 5.5).

5.4 SYNTHESIS OF DIMERIZATION SUBSTRATES

Together with model cross-coupling studies, we pursued the synthesis of fully elaborated systems. Our initial target was a substrate for dimerization en route to cylindrocyclophane F, and we envisioned that a route developed with this objective could be readily adjusted to enable access to additional cylindrocyclophane natural products, such as **1**. Central to our strategy (see Fig. 5.11) was use of an arene linchpin which could undergo convergent coupling with a number of alkyl units to eventually arrive at either natural product or their derivatives.

5.4.1 *Toward Cylindrocyclophane F*

We anticipated that arene **52** would be accessible via enolate arylation followed by C–H borylation/halogenation and commenced our studies with commercial resorcinol derivative **48**. Conditions from Hartwig and coworkers[97] provided an excellent starting point for effecting the desired α-arylation reaction (Figure 5.25). Likely due to the sterically bulky substitution of aryl bromide **48**, *tert*-butyl acetate (**49**) was found to be the only competent coupling partner. Irreproducibility upon scale-up required optimization of enolate generation and catalyst identity; ultimately, use of 3.3 equiv LHMDS proved to be critical for intermediate enolate stability and, when combined with the reported catalyst (i.e., $Pd(dba)_2/P^tBu_3$), provided a successful balance of high yield (79%) and ease of purification on 10-gram scale. The *n*-butyl chain was then readily installed in a subsequent step to afford arene **50** in 71% yield. Although attempts to perform one-pot arylation/alkylation to generate disubstituted ester **50** directly from starting **48** were unsuccessful, the sequential reactions could be telescoped to provide **50** (66% yield over two steps) after a single chromatographic purification step.

Figure 5.25 *Synthesis of aryl fragment*

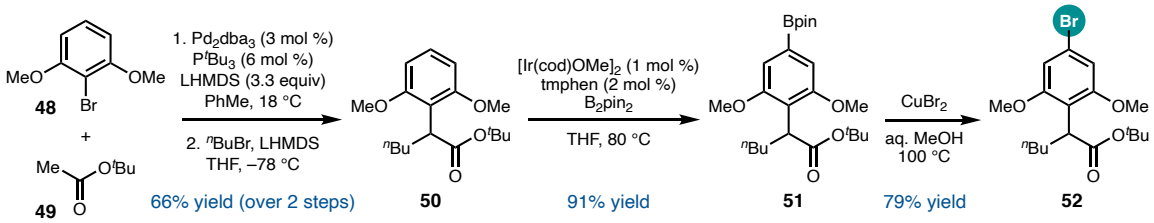

At this point, we were able to exploit the aryl substitution pattern of **50** to sterically direct C–H functionalization,[98] catalyzed by the optimized[99] combination of an Ir precatalyst and tmphen, which afforded *para*-substituted boronic ester **51** in excellent

yield (91%) and perfect regioselectivity on multi-gram scale. Subsequent treatment with cupric bromide yielded aryl bromide **52** in 79% yield. Subjection of Ar–Bpin **51** to bromination conditions on large scale (ca. 10 g) often led to mixtures of Bpin/ester **51** with its hydrolysis product; attempts to separate these compounds led to hydrolysis of the boronic ester. Instead, we found that allowing complete conversion of substrate **51** to the brominated acid (3 equiv $CuBr_2$, 83% yield) could be followed by ready esterification to afford desired ester **52**.

Having developed a scalable route to the aryl fragment, we turned to investigate coupling with an alkyl partner. We found that lithiation of the aryl bromide (**52**) followed by addition of a simple alkyl iodide (**54**) effected an S_N2-type reaction in 71% yield, forging the crucial Csp^2–Csp^3 bond (Figure 5.26). This alkyl chain served as a model for a substituted variant more closely reflecting the natural product in order to validate the use of a protected alkyne as a masking group for the alkenyl bromide, which would be unlikely to survive treatment with ^{n}BuLi required for lithiation at the aryl bromide position.[100] A short sequence involving deprotection of the alkyne followed by regioselective hydrozirconation and electrophilic attack of bromine was then used to reveal the requisite moiety (i.e., alkenyl bromide **56**) in 81% yield over two steps. Similarly, the NHP ester was unmasked via transformation of the *tert*-butyl ester to a carboxylic acid substrate of Steglich esterification, affording difunctional **57** in 63% yield over two steps.

Figure 5.26 *Fragment coupling and electrophile unmasking*

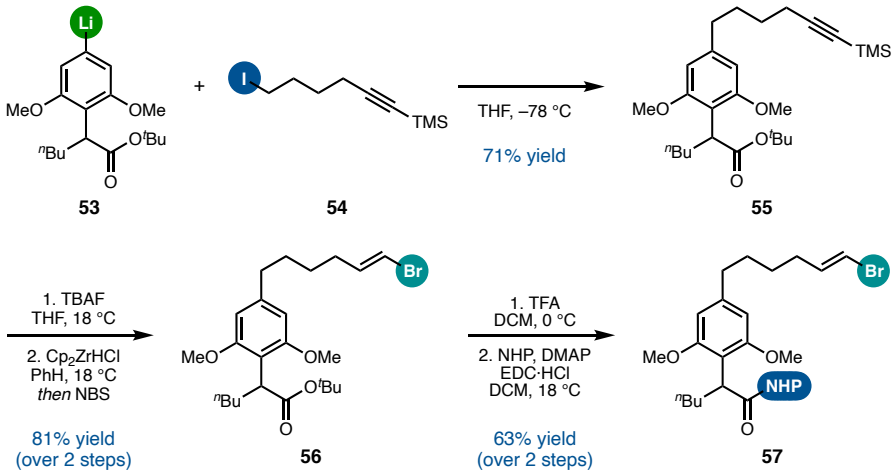

As we planned to investigate the effect of stereodefined groups on the alkyl chain (as are present in cylindrocyclophane F) in the macrocyclization reaction, we prepared β-methyl iodoalkane (+)-**60** in 92% ee over five steps (Figure 5.27).[101] Condensation of Myers' pseudoephedrine chiral auxiliary with known TMS-protected 5-hexynoic acid (**58**) produced the chiral amide in 66% yield.[102] Subsequent diastereoselective alkylation[101] proceeded in 64% yield, then redution[103] furnished the intermediate alcohol in 67% yield. Lastly, transformation to iodide **60** occurred in 59% yield to afford the enantioenriched alkyl fragment poised for coupling to aryl linchpin **52**.

Figure 5.27 *Synthesis of enantioenriched alkyl fragment*

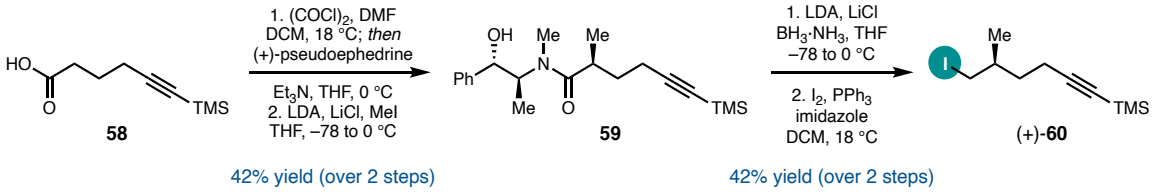

We found the developed lithiation/alkylation sequence to perform poorly with this more sterically hindered alkyl iodide (conditions in Fig. 5.26). In lieu of the desired coupled product, we observed protonated arene **50** as the major byproduct, along with

unreacted iodoalkane **60**. We considered that the introduction of the C2/15 methyl group served to slow the displacement reaction with the aryl lithium intermediate enough to render deprotonation of the acidic α-ester proton kinetically competitive, thus stymying productive reactivity.

Figure 5.28 *Deuterium quenching study: alkyl lithium base*

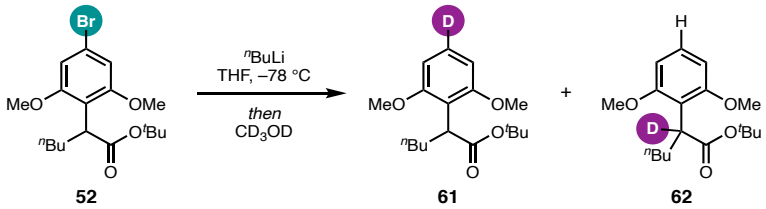

To test this hypothesis, we treated aryl bromide **52** with ^{n}BuLi then quenched with deuterated methanol. We observed the formation of deuterated byproducts **61** and **62** (Figure 5.28). Aryl deuteration (**61**) suggests that ^{n}BuLi is able to exchange with the aryl bromide and remain stable in solution, required for the desired alkylation. However, production of α-deuterated **62** provides support for the self-quenching hypothesis; an initially generated Ar–Li species can deprotonate the α-proton, leading to aryl protonation and delivering **62** upon deuterium quench of the resulting lithium enolate. In addition, prediction—or control—of whether deprotonation of an acidic proton or lithium–halogen exchange occurs first when using alkyl lithium bases has long been the subject of debate.[104,105]

Figure 5.29 *Deuterium quenching study: aryl lithium base*

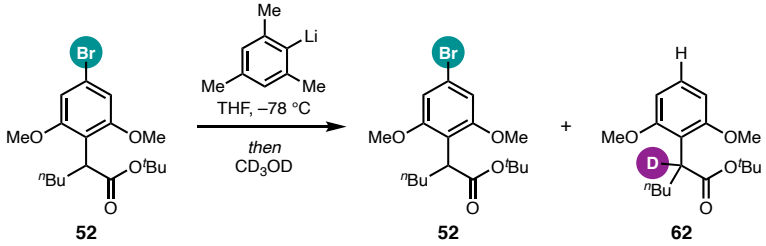

We reasoned that deprotonation with a base unable to exchange with Ar–Br could precede addition of ^{n}BuLi to address this challenge. Studies of related substrates suggested that mesityl lithium held promise to play the role of the initial base, as it has been demonstrated to be selective against aryl bromide lithiation[106] as well as unreactive toward *tert*-butyl esters.[107] In contrast to this precedent, we found reaction of aryl bromide **52** with MesLi to not be selective, evinced by the presence of α-deuterated **62** (Figure 5.29). Unfortunately, extension of this strategy to additional bases was also unsuccessful, generally due either to incomplete deprotonation (and thus self-quenching) or to decomposition of the ester enolate.

Table 5.6 *Fragment coupling attempts: Suzuki cross-coupling*

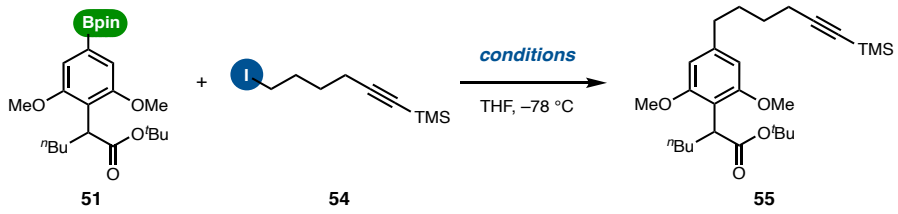

Entry	Conditions	% Yield 55
1	CuI, LiO^{t}Bu DMF, 60 °C	10
2	$NiBr_2$·dme, diamine KO^{t}Bu, 2-butanol 1,4-dioxane, 80 °C	6

As an alternative solution, we hypothesized that attenuating the basicity[108] of intervening metalated species might prove compatible with the acidic proton of aryl bromide **52**. We recognized that the aryl boronic ester precursor (**51**) was in fact a less basic organometallic reagent. Preliminary efforts to couple Ar–Bpin **51** with simple alkyl partner **54** were met with limited success; conditions for Cu-[109] or Ni-catalyzed[110] Suzuki

reactions led to cross-coupled **55** but in low yield (<10%; Table 5.6).[79] As a further extension of this logic, we considered application of a transition metal-catalyzed reaction but without organometallic reagents of any basicity and thus pursued the cross-electrophile coupling (i.e., RCC) of aryl bromide **52**.

Specifically, we anticipated that conditions for Ni-catalyzed RCC developed by Weix and coworkers[111] might be effective in our system. Although recent precedent[112] highlighted the detriment to desired reactivity posed by the stereoelectronic effects of resorcinol motifs, the reported 10% yield of a related substrate under these conditions appeared to us to be a promising foundation for optimization (Figure 5.30). However, subjection of coupling partners **52** and **54** to a Ni catalyst and metal powder reductant generated only trace quantities of product **55**. Instead, we observed low levels of conversion of each substrate. We interpreted these data as suggesting catalyst inhibition and attributed this to coordination of the terminal alkyne (i.e., the alkenyl bromide masking group). It stood to reason that an alternative functional group less likely to bind a low-valent metal would lead to successful RCC.

Figure 5.30 *Fragment coupling attempts: Ni-catalyzed reductive cross-coupling*

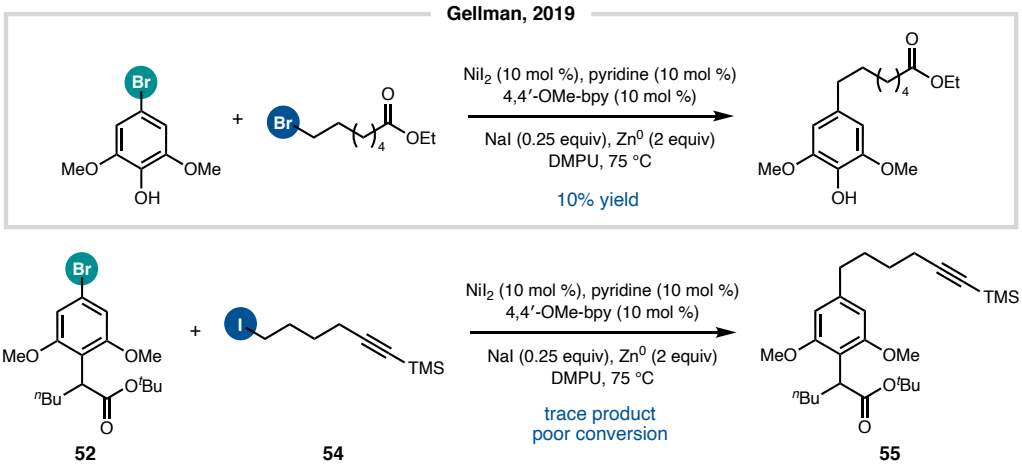

Since we did not expect α-deprotonation to be a significant issue under the mild conditions of RCC, we used commercial **63** as a model for the more-complex aryl bromide (**52**). In this case, silyl protection of the alkyne was not sufficient to effect full conversion of the starting material, and what amount did convert led predominantly to a protodebrominated arene byproduct (Table 5.7, entry 1). Using an alkenyl boronic ester in lieu of the requisite alkenyl bromide, the presumed alkyl radical intermediate (likely generated from alkyl iodide **64**) proceeded down side pathways, such as 5-*exo*-trig cyclization to form a stable α-boryl radical, instead of productive cross-coupling (entry 2). Finally, protected ether **65** yielded cross-coupled **67** in 22% yield (entry 3), which could be improved to 39% yield upon use of an alternative leaving group (mesylate **66**, entry 4). A similar level of cross-coupling was observed for a different model aryl bromide bearing a pendant ester, validating our initial assumption regarding the tolerance of acidic protons under these conditions.

Table 5.7 *RCC with various alkenyl bromide masking groups*

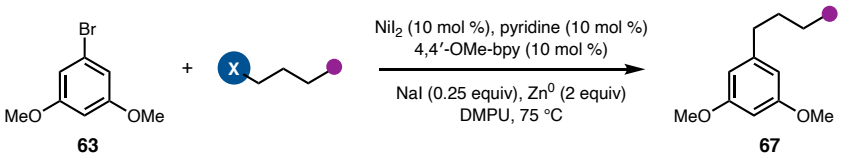

Entry	X	Masking Group	Result
1	I	TMS **54**	protodebromination
2	I	Bpin **64**	**64** decomposition
3	I	OBn **65**	22% yield **67**
4	OMs	OBn **66**	39% yield **67**

Despite the apparent success of this study, the cross-coupling yield proved to be inversely correlated to the number of subsequent steps required to reveal the alkenyl bromide. A number of such sequences could be imagined, one of which is presented in Figure 5.31. A protected alcohol used to mask a bromoalkene would need to undergo deprotection then oxidation, followed by a homologation sequence. Installation of the requisite bromide substituent on any alkene furnished by this pathway must be stereoselective, in preparation for downstream dimerization. Although a lengthy sequence, it would provide a viable point of entry for investigating the key transformation of the synthesis. As such, we continued exploration of RCC, with the goal of coupling the more complex, stereodefined alkyl electrophile.

Figure 5.31 *Alkenyl bromide unmasking from protected alcohol*

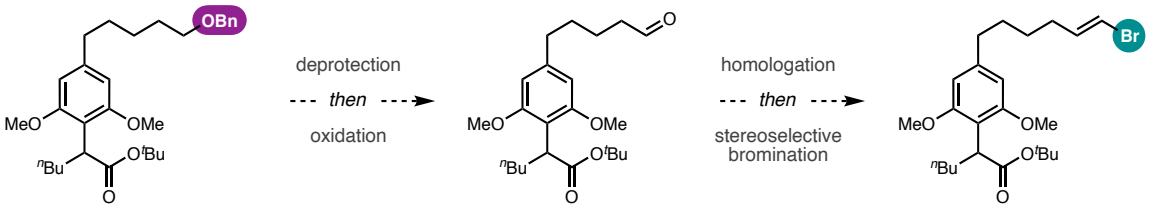

Treatment of the model aryl bromide (**63**) and chiral alkyl iodide **68** to Ni^{II}/Zn^{0} indeed led to cross-coupled **70** formation in 38% yield (Table 5.8, entry 1). Although exciting, this result was overshadowed by (1) an intractable yield with respect to material throughput and (2) the stepwise unmasking sequence required of the protected alcohol. To address the first point (i.e., improve the yield of **70**), we transitioned to use of mesylate **69** as the alkyl electrophile, given the previous success of this tactic (see Table 5.7); however, electrophile **69** led to 0% yield of cross-coupled **70** (entry 2).

Table 5.7 *RCC with functionalized alkyl fragment*

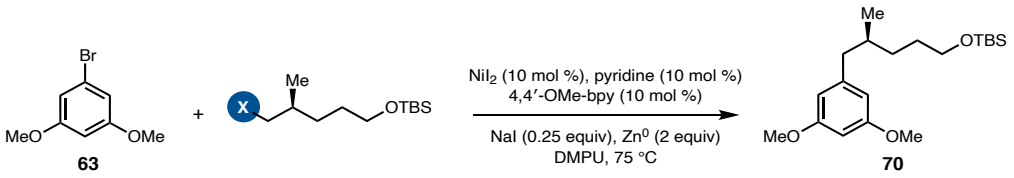

Entry	X	% Yield 70
1	I (**68**)	38
2	OMs (**69**)	0

As with the prior lithiation chemistry, it seemed likely that this failure was due to slow displacement of the mesylate leaving group—adjacent to the branched methyl group—by iodide to generate in situ an alkyl iodide required for productive coupling. We thus considered that the effective concentration of reactive iodide in solution (i.e., the rate of alkyl electrophile activation) should be matched to that of the aryl bromide (**52**) and postulated that an epoxide fit this criterion, given that ring-opening by iodide would be expected to outpace mesylate displacement. Indeed, regioselective epoxide opening/coupling[113] occurred upon subjection of epoxide **71** to reductive conditions, delivering alkyl–aryl-joined **72** in much-improved 51% yield (Figure 5.32). As epoxide **71** was prepared with near-perfect enantiopurity (99% ee) via Jacobsen hydrolytic kinetic resolution,[114] the RCC effectively installed a stereocenter at the location of the requisite methyl group (C2/15).

From homobenzylic alcohol **72**, stereospecific conversion was envisioned to proceed via nucleophilic displacement of the corresponding tosylate (**73**) with Gilman's reagent to forge the necessary C–C bond with the correct stereochemistry.[115,116] While we did observe this expected result (i.e., methylated **74**), concomitant elimination of the

tosylate led to an inseparable mixture with alkene **75**. Nevertheless, this epoxide-opening route was able to successfully improve the fragment coupling yield (aim 1, *vide supra*). However, the equally important goal (aim 2) of reducing the post-coupling step count to unmask the alkenyl bromide remained unaddressed by this workaround.

Figure 5.32 *Fragment coupling via reductive epoxide opening*

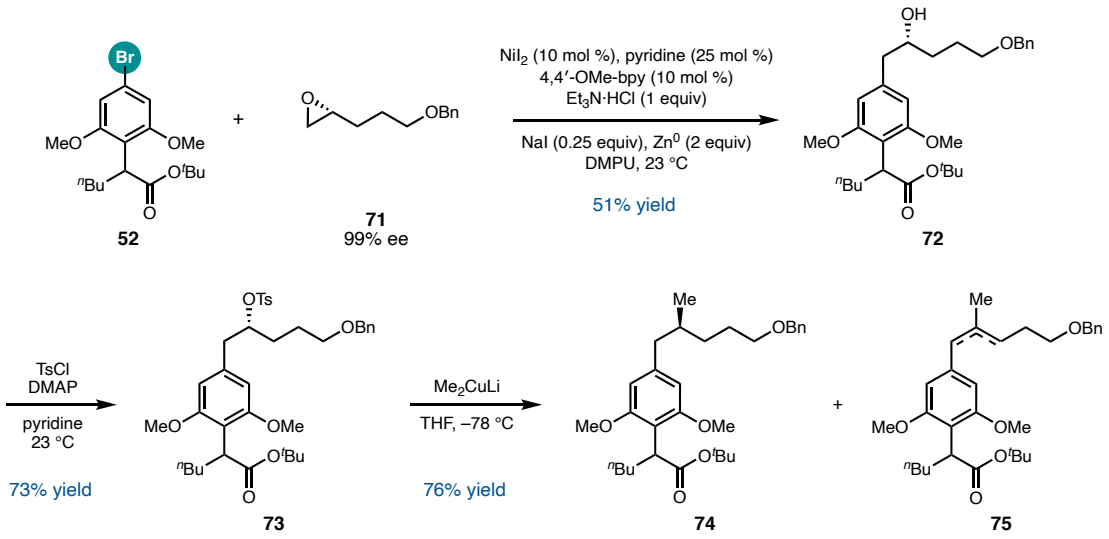

With this objective in mind, we elected to refocus our investigation on an alkyne-containing fragment and revisit our hypothesis that the incompatibility of this functional group with cross-coupling owed to catalyst inhibition. It seemed likely that a transition metal rendered electron-poor by back-bonding to an alkyne would be unable to undergo oxidative addition—particularly of a challenging, electron-rich aryl electrophile[117]—so we targeted a metal for which that catalytic step would be more favorable, either due to a change in oxidative addition mechanism[118,119] or to less favorable back-bonding. On the basis of weaker d-electron donation,[120] we selected palladium, rather than nickel, as catalyst. Given the relative dearth of Pd-mediated cross-electrophile couplings, this necessitated return to a redox-neutral manifold.

Figure 5.33 *Motivation for Pd-catalyzed Negishi cross-coupling*

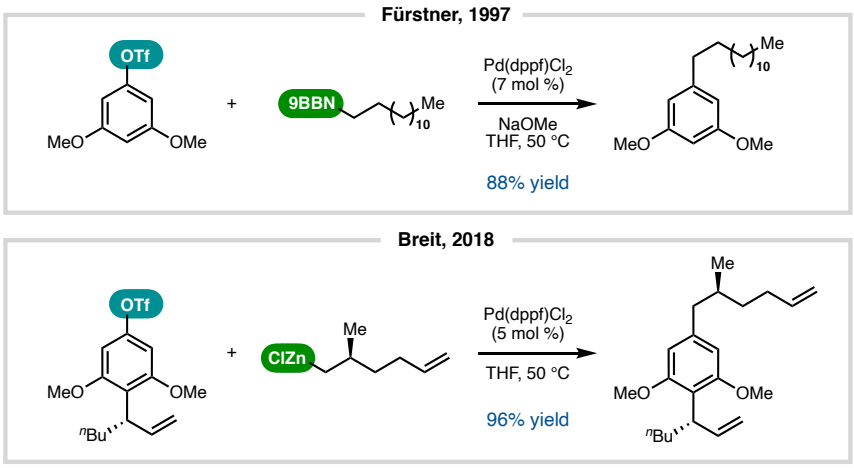

We were motivated by select examples[121,73] of high-yielding, Pd-catalyzed reactions of resorcinol-derived electrophiles with alkyl nucleophiles (Figure 5.33). Although these reports lent credence to our redesigned cross-coupling reaction, there were a few outstanding questions of importance to the current system. Namely, tolerance toward alkynes was unknown, and, notwithstanding that complication, it was unclear that aryl bromide **52**, as opposed to a triflate, would be able to be activated, as the failure of this event had been previously noted.[122] Critically, the alkyl nucleophile would need to be nucleophilic enough[123] but less basic enough[108] to allow cross-coupling to outcompete α-deprotonation; although this competition had not been explored for either organoboron or organozinc reagents, the success of a β-Me-alkyl–ZnCl partner inspired selection of the latter for our studies.

We designed a series of model reactions to interrogate these questions. First, treatment of aryl bromide **63** and organozinc **76** (from alkyl iodide **68**, see Table 5.8) with Pd(dppf)Cl_2 forged the Csp^2–Csp^3 bond of product **70** (Figure 5.34). This result provided evidence for the feasibility of oxidative addition of electron-rich aryl bromides

under these conditions. Second, expected challenges of the pendant alkyne and the α-proton were investigated in the reaction of alkynyl organometallic partner **78** with ester-containing **77** (available in one or two steps from commercial material). Cross-coupled **79** was formed in 73% yield, suggesting that neither of these functionalities were a significant detriment to this Negishi reaction.

Figure 5.34 *Fragment coupling via Negishi cross-coupling: model substrates*

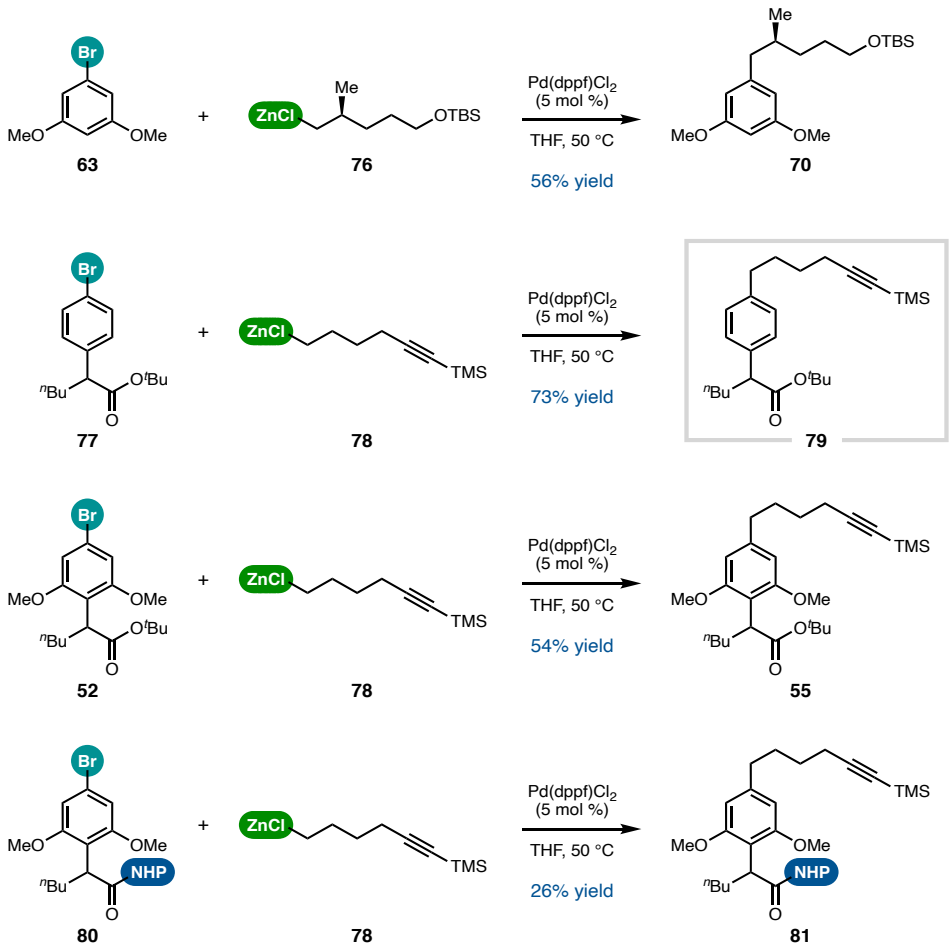

This conclusion was further supported by the successful cross-coupling of 2,6-dimethoxy **52** with alkyl iodide **54** (via alkyl–Zn **78**), which delivered intermediate **55** in 54% yield. In addition, we discovered that the NHP ester moiety of **80** was compatible with the redox-neutral cross-coupling conditions; if optimized for yield, this reaction

would expedite access to a difunctional substrate for cyclodimerization in only two steps from coupled **81**. In neither case did the presence of an alkynyl motif substantially diminish desired reactivity of simple alkyl–Zn **78**.

Figure 5.35 *Failed Negishi cross-coupling toward cylindrocyclophane F*

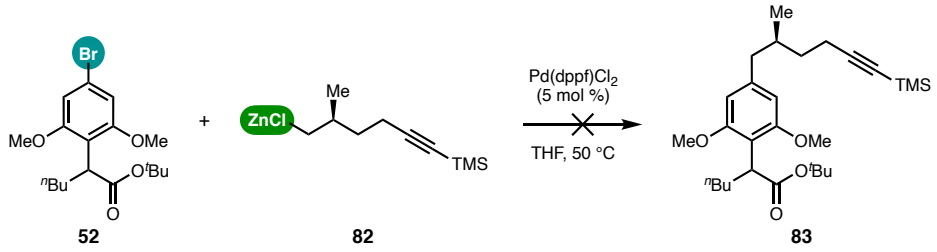

Therefore, we were surprised to find that when the alkyl coupling partner was generated from iodide **60** (i.e., alkyl–Zn **82**), no aryl halide conversion was observed (Figure 5.35). At this time, it is not clear why this specific combination of substrate functional groups prevents Negishi cross-coupling.

5.4.2 *Toward Unsubstituted Paracyclophanes*

Although we were unable to access via Negishi cross-coupling an intermedaite on path to cylindrocyclophane F (i.e., methylated **83**), this transformation was useful in furnishing unsubstituted derivatives. The convergent coupling of simplified partners **77** and **78** could be performed on >7 g scale in 49% yield (see Fig. 5.34)—provided sufficient cooling was applied to prevent radical 5-*exo*-dig cyclization of reduced **78** and coupling of the resultant α-silyl vinyl radical. Aryl/alkyl intermediate **79** was then advanced smoothly through a short sequence used to unmask the difunctional species (**85**, Figure 5.36). We expected that ready access to gram-quantities of **85** would prove useful

in optimizing the double RCC and preparing the paracyclophane skeleton, albeit simplified as compared to the natural products.

Figure 5.36 *Electrophile unmasking: model substrate*

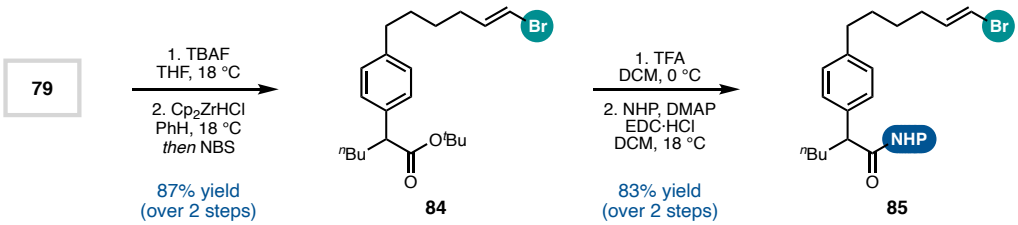

In a parallel manner, we also prepared intermediates designed to interrogate the effect of bridge length on [*n*,*n*] and [*m*,*m*]paracyclophane formation via double reductive coupling (Figure 5.37). The cyclophane structures arising from such unsubstituted monomers would be novel and could find use outside the scope of natural product synthesis (i.e., for host–guest chemistry, as subjects of computational physical organic studies, etc.). Ultimately, however, we planned to return to the system necessary to access natural product **2** (i.e., methoxy/methyl **83**) following macrocyclization proof-of-concept.

Figure 5.37 *Toward paracyclophanes with modified bridge lengths*

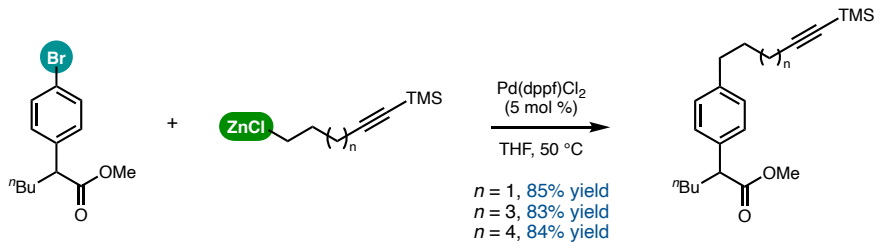

5.4.3 *Toward Cylindrocyclophane A*

We also applied the developed general synthetic strategy to an intermediate that could give rise to cylindrocyclophane A (**1**). Preparation of the requisite alkenyl iodide precursor (**88**) of fragment coupling proceeded via stereoselective methyliodination and

basic deprotection of TMS-alkyne **86** (Figure 5.38). The 38% yield of iodoalkene **87**, although moderate, was consistent on large scale. Subsequently, the alcohol was transformed to enyne **88** via a sequence of oxidation, Ohira–Bestmann[124] homologation, then protection. Available in 42% yield (over three steps), alkenyl iodide **88** was zincated and cross-coupled with aryl bromide **52** to provide intermediate **90** in excellent yield (94%).

For maximal convergency in the planned cyclodimerization step, we hoped to install the hydroxymethyl stereodiad prior to macrocyclization using enantioselective hydroboration/oxidation conditions.[125] Although this was only briefly surveyed, it appeared likely that this step would need to occur after successful generation of the [7.7]paracyclophane. Nonetheless, we were interested in exploring how the 'turn' introduced by the rigid alkene to the structure of these intermediates (e.g., conjugated **90**) would affect cyclodimerization of the corresponding alkenyl bromide/NHP ester.

Figure 5.38 *Successful Negishi cross-coupling toward cylindrocyclophane A*

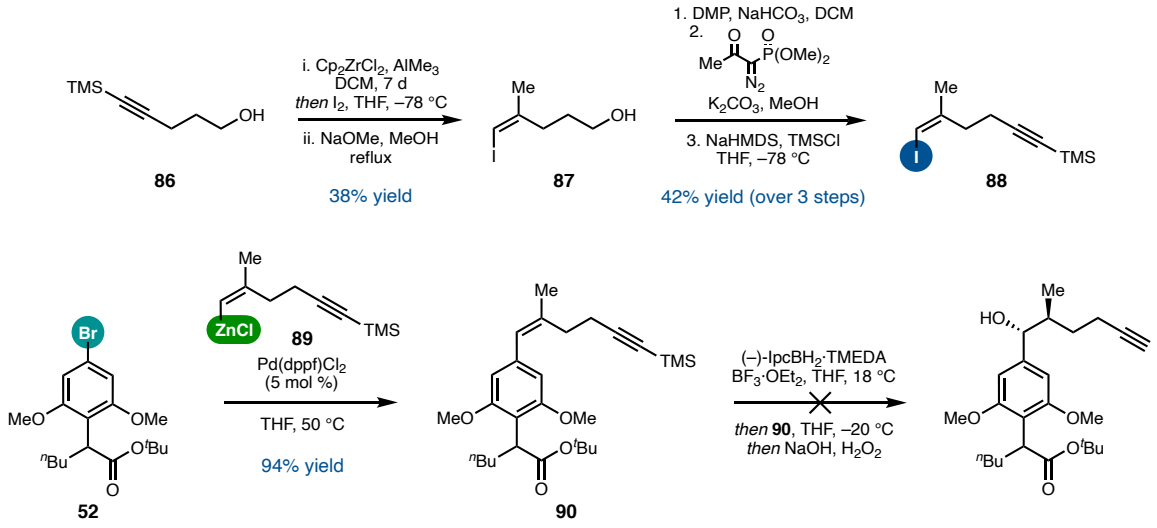

5.5 DOUBLE REDUCTIVE CROSS-COUPLING

5.5.1 *Guiding Mechanistic Design*

We initiated investigation of double RCC as a method for cyclodimerization using unsubstituted difunctional substrate **85**. Based on our initial mechanistic design, presented in Figure 5.39, Ni catalysis was deemed well-suited for cyclodimerization. Specifically, we considered the benefit to cyclization provided by formal oxidative addition of NHP esters being mediated primarily by a Ni catalyst, which at the outset of our studies, was a reigning hypothesis in the literature (*vide supra*). In the context of double RCC, following the first *intermolecular* C–C bond formation event, continued coordination of the catalyst to the π-system might allow ring closure to proceed via an *intramolecular* (and unimolecular) pathway with respect to intermediate **91** and catalyst. Electron transfer, followed by radical generation and its subsequent internal capture could occur via associated nickel; from an intermediate [8.7]paracyclophane-type nickelacycle, ring strain-releasing[16] reductive elimination would forge the second requisite C–C bond and complete the macrocyclic ring. Critically, we assumed that an operative unimolecular ring-closing process would provide a kinetic basis for cyclization to be favored over competing intermolecular pathways.

This hypothetical mechanism was grounded in catalyst-transfer polymerization (CTP), specifically polycondensation of dihaloarenes initiated by Ni^0 complexes—including Ni–diamines. In these reactions, successful polymerization is due to a strong association between the catalyst and substrate,[126] which affects several propagation steps: (1) interaction of low-valent Ni d-orbitals and substrate π-orbitals allows the catalyst to remain bound following reductive elimination;[120] (2) π-complexation[127] occurs prior to

oxidative addition[126] of a terminal Csp^2 halide; and (3) transfer of Ni across a π-system (i.e., ring-walking) enables subsequent *intramolecular* oxidative addition.[128]

Figure 5.39 *Working mechanistic hypothesis: double RCC*

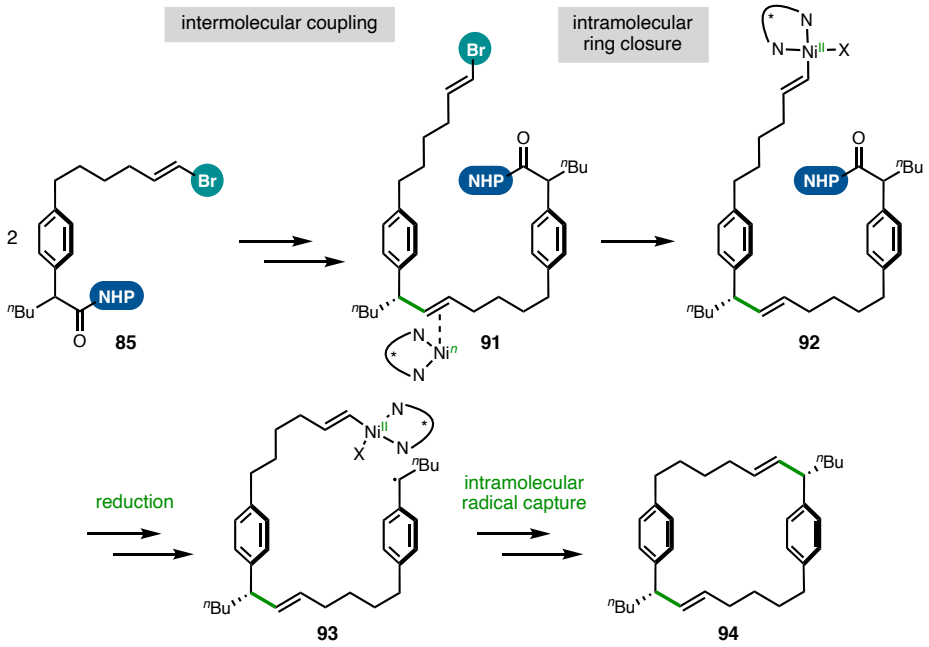

We postulated that the Ni catalyst in the present reaction could be similarly transferred across a singly-coupled intermediate (i.e., **91**) to effect the second oxidative addition step in an intramolecular fashion. Although ring-walking has largely been demonstrated in fully conjugated π-systems, over which the metal 'travels' by migrating via η^2 alkene coordination, specific mechanisms can be substrate dependent;[129] it is plausible that analogous transfer of Ni across neighboring aromatic rings or alkenes could take place even if they are not conjugated but rather appropriately arranged in space. Indeed, CTP has been demonstrated for monomers in which arenes are connected by a saturated carbon; this seminal report[130] lends credence to our hypothesis regarding adduct **92** generation.

As a consequence of putative through-space ring-walking-type metal transfer, the molecule (**92**) could be spatially arranged in a way that would facilitate electron transfer from Ni to the phthalimide moiety, thereby intramolecularly initiating reductive fragmentation and radical generation. In this case, intervening reduction would be required, potentially prior to NHP loss (e.g., $Ni^{II} \rightarrow Ni^{I}$ mediated by the terminal reductant, present in excess).[90,89] We expected that this type of process would outcompete reaction with distinct organic/organonickel species of either the Ni- or the NHP-terminus of an intermediate like **92**, and in so doing, promote cyclodimerization over polymerization.

As our understanding of NHP ester reduction was expanded throughout the course of single RCC optimization (*vide supra*), this conformational arrangement of the incipient macrocycle (ostensibly to promote intramolecular Ni transfer) also seemed crucial in a regime where NHP ester reduction occurred external to Ni involvement. The readiness of intramolecular oxidative addition could build up appreciable [**92**]; this would increase the probability that an NHP ester undergoing reduction would be Ni-adduct **92**, which is poised for immediate intramolecular radical capture (leading to ring formation). In contrast, without an attached alkenyl–Ni moiety, an NHP ester could preferentially decompose or undergo intermolecular reaction (e.g., polymerize) instead. It is also possible that preorganization resembling the macrocycle could stabilize a radical generated by initial NHP reduction in the internal pocket[131] (via hydrogen bonds, electrostatic interactions, etc.) until a Ni center suitable for radical capture could be produced.

The conformational control elements[132] installed by nature into the cylindrocyclophanes could serve to effectively promote the requisite preorganization of macrocycle precursors. Although an intuitive assumption, no systematic study of substituent effects on [7.7]paracyclophane construction has been reported; syntheses of structurally related cyclophanes offer indirect experimental support. For instance, the stereocenters along the seven-membered bridge of natural products **1** and **2** could facilitate proper arrangement of open-chain species for ring closure, viz. positioning the aliphatic 'arms' in close proximity to each other. Indeed, installation of a single methyl substituent along an aliphatic chain of one cyclophane produced a turn-on effect in its generation via RCM.[133] A benzylic hydroxyl group[134] and an alkene at the benzylic position[135] of other cyclophanes have achieved similar results. Too, the conformational effects of aryl substitution (i.e., the resorcinol motif) could be additive, as *o*,*o*-disubstitution has been noted to gear alkyl 'arms' appended at the *para*-positions out of the aryl plane (and presumably toward each other).[136,137]

For difunctional monomers bearing minimal substitution along the periphery of the carbon skeleton (e.g., **35**, see Fig. 5.39), intrinsic conformational bias would be comparatively minimal. This model system would thus provide a platform for investigating the extrinsic factors (i.e., RCC reaction conditions) that could favor an appropriately folded conformation of open-chain species en route to cyclodimer **94**. Templating is a highly successful tactic in promoting macrocyclization over competitive polymerization, and halide anions (e.g., iodide and bromide) have been demonstrated to serve as templates to preorganize intermediates in the preparation of cyclophanes.[138] The exogenous iodide additive in the RCC reaction, as well as *in situ*-generated bromide,

could play a similar role. It is also possible for the other ions in solution, such as the Ni catalyst, to engage in cation–π interactions;[139] this would be required for through-space metal transfer (*vide supra*), and metal-binding to one or both arenes of paracyclophanes is well precedented.[140]

In the same vein, we envisioned that π–π stacking with the aryl groups[141] of paracyclophane **94** could play a similar role in facilitating ring closure. This effect has been demonstrated with an electronically biased perfluoroarene covalently bound to a cyclophane precursor.[142] In that example, the arrangement of the two arenes rigidified the structure, in which the aliphatic 'arms' were hypothesized to be oriented opposite to the additional aromatic ring and thus near each other. The more synthetically efficient approach involves a distinct aryl-containing species in the macrocyclization reaction that could engage noncovalently with the intermediate undergoing cyclization; following this reasoning, cationic *N*-heterocycles have proven useful in the generation of [12]paracyclophanes.[143] In the current system, a phthalimide byproduct might be implicated in this type of interaction. Unlikely to fit inside the cavity[32] of the incipient paracyclophane, such arenes could π–π stack on the external face to properly dispose the alkyl chains.

Lastly, we reasoned that nonclassical hydrophobic effects could play a role in generating a tight apolar complexation of cyclization intermediates conducive to ring closure. This is established behavior of cyclophanes, and would likely be a factor in the DMA reaction solvent given the extremely nonpolar nature of hydrocarbon **94** (*vide infra*) and that binding strength increases with solvent polarity.[144] Having thus

rationalized the potential success of cyclodimerization via double RCC, we turned to experimental exploration.

5.5.2 *Cyclodimerization versus Polymerization*

Following the developed synthetic route to access a model difunctional substrate for study of cyclodimerization, we subjected the NHP ester/alkenyl bromide (**85**) to the optimized conditions for single reductive cross-coupling (Figure 5.40). We were pleased to find that in the crude reaction mixture, the desired macrocycle (**94**) appeared to be the major product. We identified the mass of dimer **94** by GCMS, and the ^{1}H and ^{13}C NMR spectra were consistent with a C_2 symmetric molecule containing diagnostic signals matching those predicted for **94**. By both spectroscopic methods, the reaction profile was clean, with no obvious remaining starting material or decomposition byproducts.

However, isolated macrocycle **94** was elusive, despite extensive attempts at chromatographic purification. Ultimately, preparative HPLC was successful in delivering isolable quantities of the expected product, but the amount of thus-obtained **94** was significantly less than anticipated. This work-up and purification sequence did not yield additional species, thus the mass balance of the reaction remained in question.

Figure 5.40 *Analysis of initial double RCC: challenges*

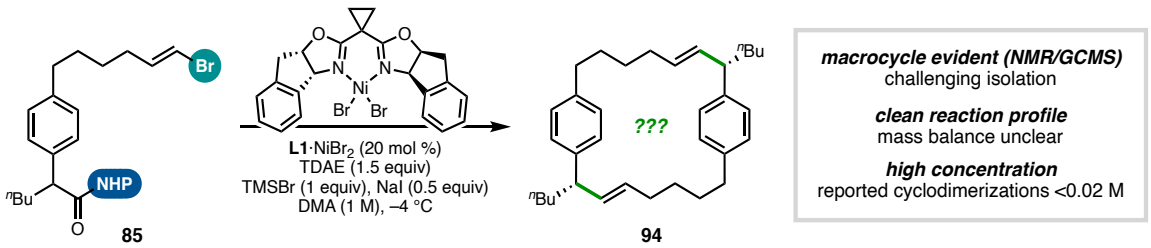

We also noted that the double RCC was run at a high concentration (1 M). Intramolecular reaction at this concentration would need to be an extremely efficient process, since intermolecular reactivity would generally be expected to dominate in this regime. In comparison, cyclodimerizations reported in syntheses of cylindrocyclophanes are orders of magnitude more dilute (ca. 0.02 M and less concentrated).[18]

To understand the outcome of treating difunctional electrophile **85** with **L1**·$NiBr_2$/TDAE in a way that accounted for these observations, we expanded the mechanistic hypothesis presented in Fig. 5.39 to include possible—albeit undesired—reaction pathways (Figure 5.41). If initial C–C bond formation (such as to generate homobenzylic alkene **85**) is not followed by the planned ring closure event, which would lead to macrocycle **94**, then remaining reactive functionalities (e.g., alkenyl bromide and NHP ester of **85**) could decompose. However, byproducts of the nature observed in the single RCC system were not identified in the crude reaction mixture.

Alternatively, subsequent intermolecular coupling events could generate larger cyclooligomers (**96**) or even much larger polymers (**97**). In these cases, the repeat unit would be spectroscopically similar to the desired cyclodimer (**94**). In addition, the higher molecular weight of species such as **96** or **97** would render them invisible to the mass spectrometers available for use. Polarity and behavior on silica distinct from cyclic **94** and unamenable to chromatography would account for the challenges of product isolation. We recognized that the large difference in molecular weight between desired dimer **94** and oligomers or polymers containing multiple equivalents of substrate might provide a useful handle for identification of the latter species.

Figure 5.41 *Alternative reaction pathways of double RCC*

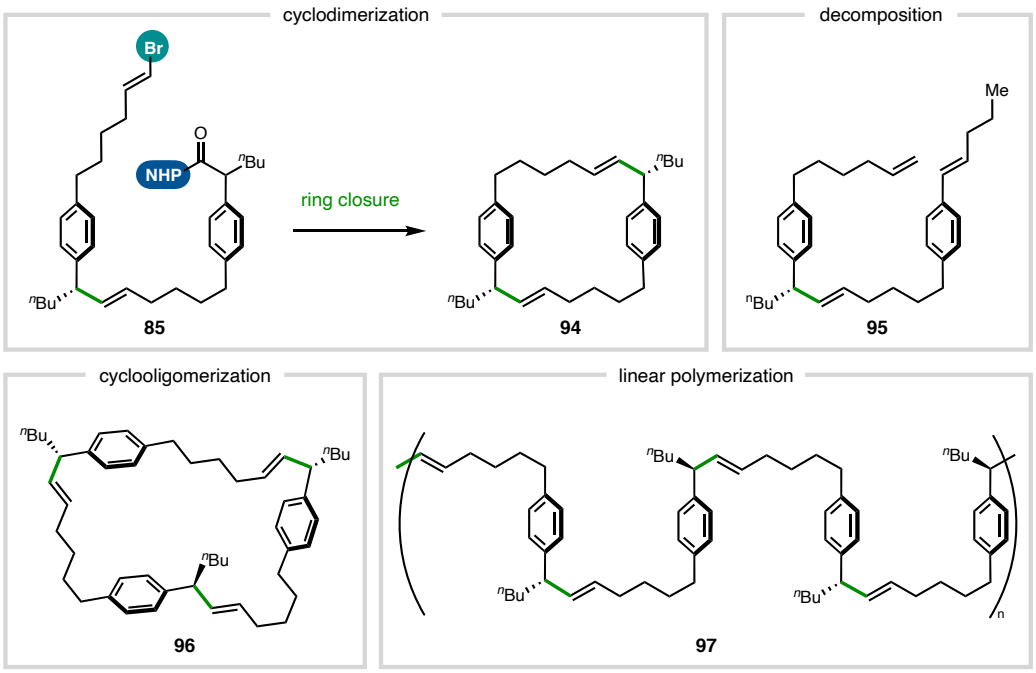

We turned first to diffusion-ordered spectroscopy (DOSY), which is an NMR technique that allows separation of compounds in a mixture based on their translational diffusion coefficients. The DOSY workflow is presented in Figure 5.42; attenuation of ^{1}H NMR signals is observed during a pulsed field gradient experiment and is a function of magnetic gradient pulse amplitude occurring at a rate proportional to the diffusion coefficient.[145] In short, the derived diffusion coefficient for each species in solution is related to its molecular weight (and shape). We found DOSY to provide excellent qualitative information regarding the distribution of differently sized species in a hard-to-separate crude reaction mixture. Specifically, analysis of the double RCC via DOSY revealed a bimodal distribution: species with near-identical ^{1}H NMR signals featured diffusion coefficients separated by an order of magnitude. This evidences oligomerization and/or polymerization under the reaction conditions.

Figure 5.42 *DOSY workflow*

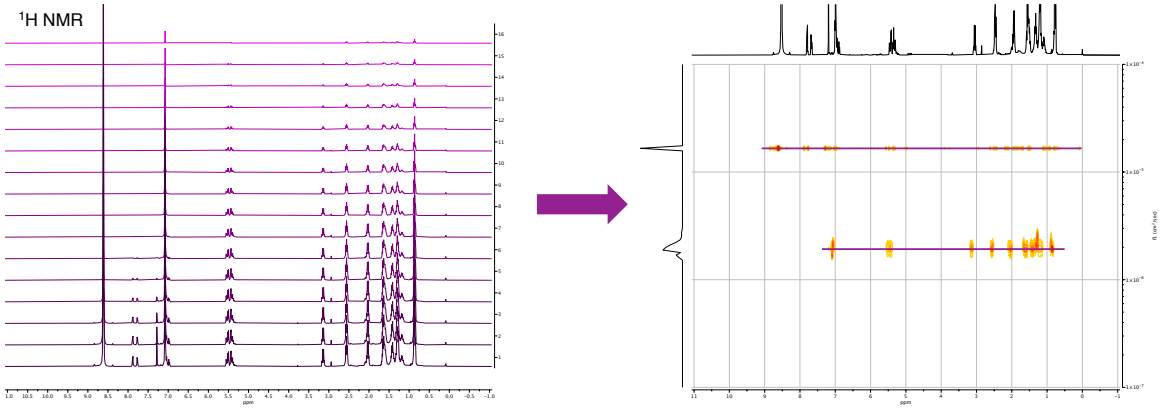

To understand in finer detail the nature of the high-molecular weight products of double RCC, we analyzed the crude reaction via gel permeation chromatography (GPC). A peak in the GPC trace with a short retention time was observed, which would correspond to a macromolecule; indeed, we estimated the molecular weight to be ca. 4–8 kDa (Figure 5.43). Due to the challenges of obtaining a completely purified sample of this polymer, the size and polydispersity (Đ ≈ 1.7) were limited to rough estimates. A peak in the small molecule regime of the GPC trace matched that of a purified sample of macrocycle **94**.

Figure 5.43 *Polymer characterization by GPC*

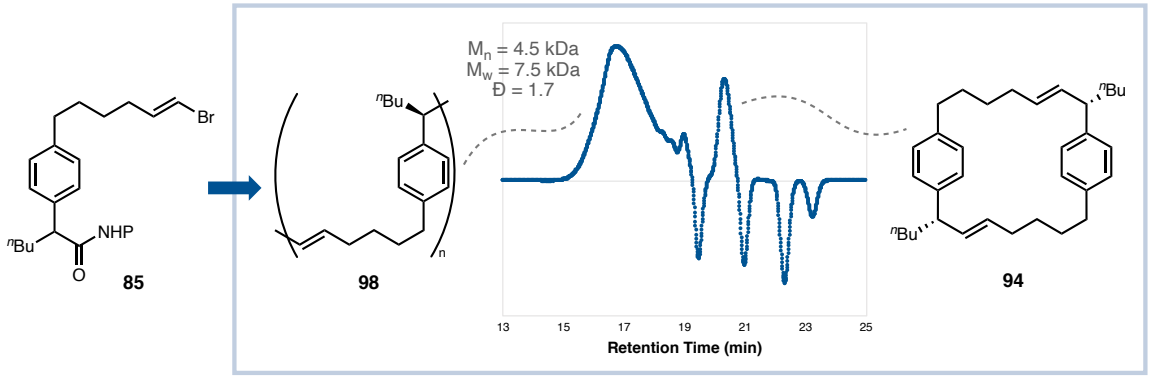

Characterization by MALDI-TOF of samples from the reaction containing high-molecular weight species, assigned by GPC, determined the the molecular weight of each repeat unit, consistent with polymer structure **98**. Connectivity was based on $^{1}H/^{13}C$ NMR spectra (*vide supra*) and established **98** as a head-to-tail polymer. Based on these characterization methods, polymerization can be terminated in different ways. The exact nature of the end groups is unclear; however, tentative evidence suggests that alkenyl bromide terminus is reduced in the reaction, generating a terminal alkene.

Efforts to determine the tacticity have been unsuccessful to date. In the single cross-coupling, we presume that catalyst **L1**·$NiBr_2$ mediates bond formation, as opposed to a radical chain mechanism involving direct addition of the benzylic radical to the alkene, based on the (1) high enantioselectivity, (2) lack of alkene isomerization, and (3) lack of byproducts arising from intervening radical species. As such, the stereocenters of polymer **98** (and **94**) are represented based on the major enantiomer expected when using **L1**·$NiBr_2$ as catalyst in the reaction of model substrates **17** and **18** (see Fig. 5.24).

Taken together, these results led us to conclude that the double RCC reaction of difunctional monomer **85** provided a mixture of cyclodimer (**94**) in addition to polymer **98** (Figure 5.44). DOSY was beneficial in identifying the ^{1}H NMR signals assigned to paracyclophane **94** in the crude reaction spectrum, allowing us to quantify the yield of desired product (3%). Unfortunately, determination of the stereochemistry of macrocycle **94** was significantly more challenging.

Figure 5.44 *Double RCC: cyclodimerization and polymerization*

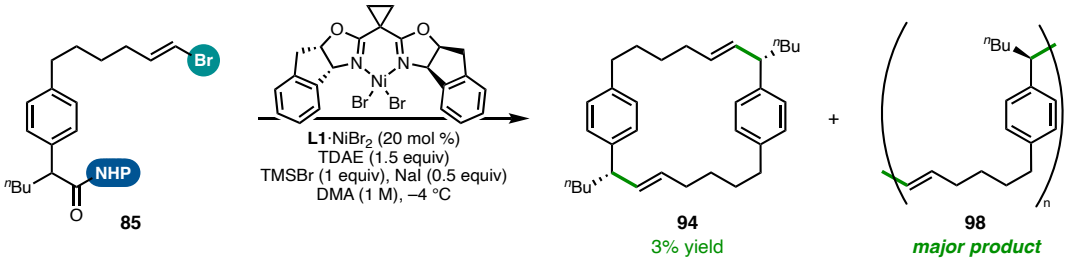

It is plausible that initial cross-coupling occurs with a similar level of enantioselectivity as that observed in the model RCC (86% ee), and our guiding hypothesis is that formation of one stereocenter will minimally affect subsequent bond construction. If these assumptions hold true, then we expect the initial ee to be amplified based on the Horeau principle such that the diastereomeric ratio of generated macrocycles would offer a greater range with which to judge the stereoselectivity of the cyclodimerization. We were unable to separate enantiomers or diastereomers of cyclophane **94** via chiral SFC or HPLC. However, we have identified a diastereomeric macrocycle by ^{1}H NMR, based on apparent splitting of the signals attributed to aryl and alkene protons. This diastereomer was only observed when a racemic mixture of **L1**·$NiBr_2$ was used to catalyze the reaction and was therefore assigned as the meso isomer of **94**. Although, lack of baseline separation of the diagnostic ^{1}H NMR signals of the diastereomeric macrocycles precluded definitive determination of dr.

With a clearer picture of the outcome of double RCC, we attempted to optimize the reaction with the goal of improving cyclodimer formation as opposed to polymerization. The reaction parameter of highest priority for study was concentration. Systematic dilution of the reductive dimerization of difunctional **85** did not result in significantly higher yields of macrocycle **94** (Table 5.9). Instead, under the least

concentrated conditions, cross-coupling completely failed; neither cyclodimer **94** nor polymer was observed at 0.01 M (entry 4). We postulate that this is due to the intermediate benzylic radical engaging the solvent preferentially to the catalyst or coupling partner (itself), evinced by species tentatively assigned as DMA adducts by mass and diagnostic ^{1}H NMR signals. That the most successful cyclodimerization occurred at an intermediate concentration (i.e., 0.5 M, entry 2) underscores the challenge of balancing the sensitivity to concentration of an intermolecular radical-based reaction with the equal but opposite concentration dependence of intermolecular coupling.

Table 5.9 *Optimization of cyclodimerization via double RCC*

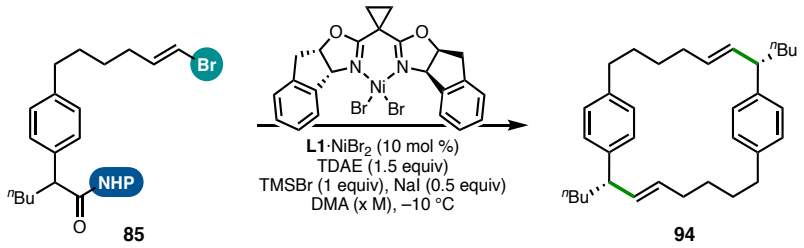

Entry	Concentration	% Yield 94
1	1 M	1
2	0.5 M	7
3	0.1 M	3
4	0.01 M	0

Where concentration had a more pronounced effect was polymer size (Table 5.10). Sequentially increasing concentration resulted in increasingly larger macromolecules. However, polydispersity also followed this trend, and, in general, the size of **98** was on the border between classification as a polymer or a few-repeat unit oligomer. Thus, RCC was equally unfit as a cyclodimerization tactic as it was a practical

method for polymerization. Regardless, reductive oligomerization/polymerization appeared to be unavoidable under these conditions, and it was not evident how we might be able to overcome this propensity in order to access the desired macrocycle and continue toward our synthetic goals.

Table 5.10 *Optimization of reductive polymerization*

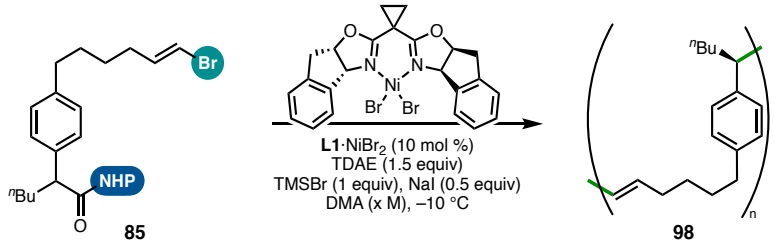

Entry	Concentration	Polymer 98 (M_n, M_w; Đ)
1	**1 M**	4.5, 8.6 kDa; 1.9
2	**0.5 M**	2.3, 3.9 kDa; 1.7
3	**0.1 M**	1.3, 1.5 kDa; 1.2
4	0.01 M	—

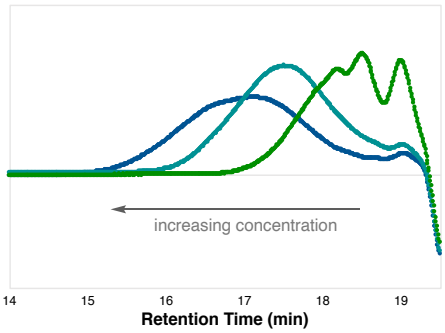

It is worth commenting that the irreversible coupling steps of cyclodimerization via Ni catalysis are under kinetic control; thus, model alkenyl bromide/NHP ester **85** is expected to be a less favorable substrate for macrocyclization than that required for advancement to cylindrocyclophane F (i.e., functionalized **11**, see Fig. 5.11). The conformational control elements inextricably part of the stereochemically enriched substituents on the substrate designed based on the natural product are absent from simplified **85**. It could be that the target difunctional monomer (**11**) demonstrates

improved cyclization under identical reductive conditions. However, the synthetic inaccessibility of **11** (*vide supra*) prevented empirical substantiation of this claim.

Nonetheless, we were able to treat semi-functionalized monomer **57** to the reductive coupling reaction (Figure 5.45). The outcome of this transformation was analyzed following the protocol established for analogous substrate **85**. The ^{1}H NMR signals of the crude mixture established the connectivity expected of head-to-tail cross-coupling, but subjecting this sample to our DOSY workflow revealed only species with mid-range diffusion constants. Consistent with the lack of molecules of the approximate size of desired product **99** (determined via DOSY), the mass of macrocycle **99** was not evident by GCMS. Based on these results, we concluded that the 2,6-dimethoxy substitution of electrophile **57** was not beneficial to cyclization—instead, likely detrimental—suggesting that any intrinsic conformational control of further-functionalized **11** would be based on aliphatic chain substitution.

Figure 5.45 *Double RCC using 2,6-dimethoxy substrate: oligomerization*

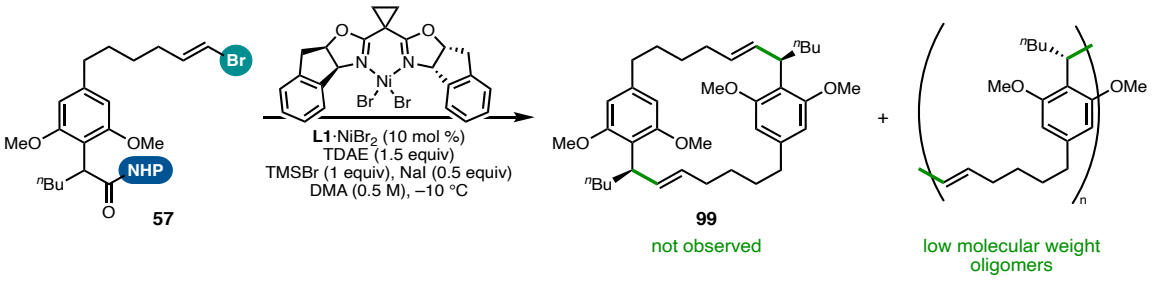

5.5.3 *Macrocyclization via Depolymerization*

Determined to progress toward the synthesis of the cylindrocyclophanes, we questioned whether the polymer formed via reductive cross-coupling was not a dead end but could serve as an intermediate en route to the paracyclophane skeleton. In reframing

the central challenge to macrocyclization in this way, we realized that while the cross-coupling reaction forges a benzylic C–C single bond, the polymer could instead be viewed as a string of alkenes. Therefore, reaction with a metathesis catalyst could, in principle, break down the polymer at each double bond and then reassemble the fragments into the desired macrocycle (Figure 5.46).

Figure 5.46 *New approach to the challenge of macrocyclization*

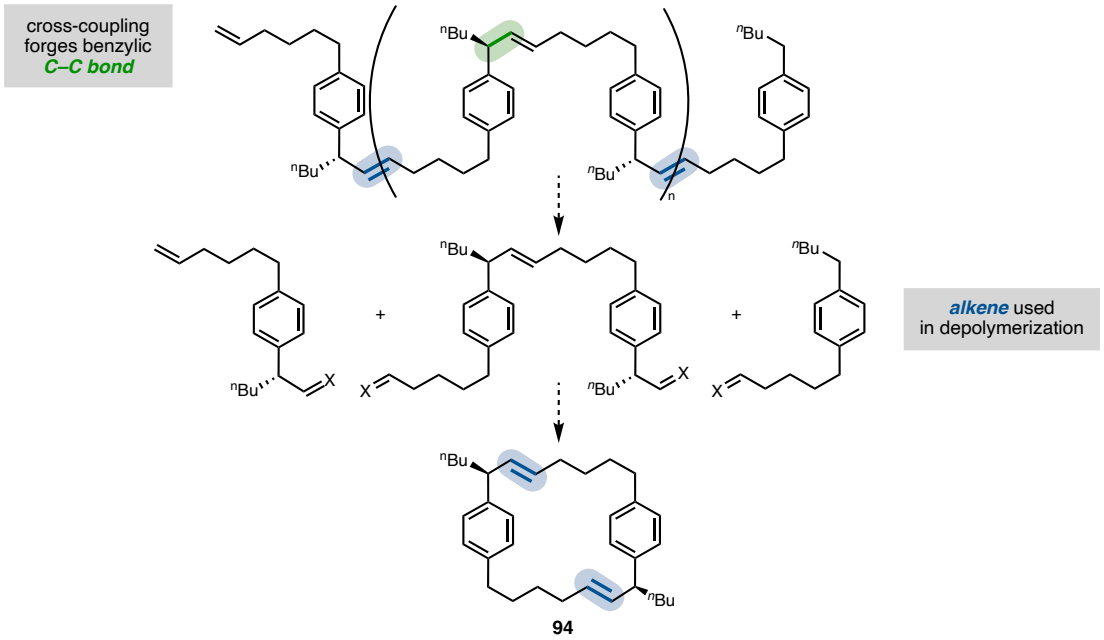

This approach is not dissimilar to that of Smith and coworkers, who were the first to implement CM/RCM in the synthesis of a cylindrocyclophane (Figure 5.47).[72] The Smith reports hinged on the reversible nature of metathesis to effect cyclodimerization of monomer **100**; as well, products of a single metathesis reaction (i.e., **101** and **102**) poised for formation of alternative, undesired macrocyclic products were successfully funneled to a single paracyclophane (**103**) in high yield.[70] Molecular mechanics calculations were performed to determine relative energies of the low-energy conformers of all possible

CM/RCM products, attributing metathesis selectivity (i.e., high yield of **103**) to a thermodynamic preference for **103**, the lowest energy macrocycle.[72,70]

Figure 5.47 *Motivation for depolymerization via reversible metathesis*

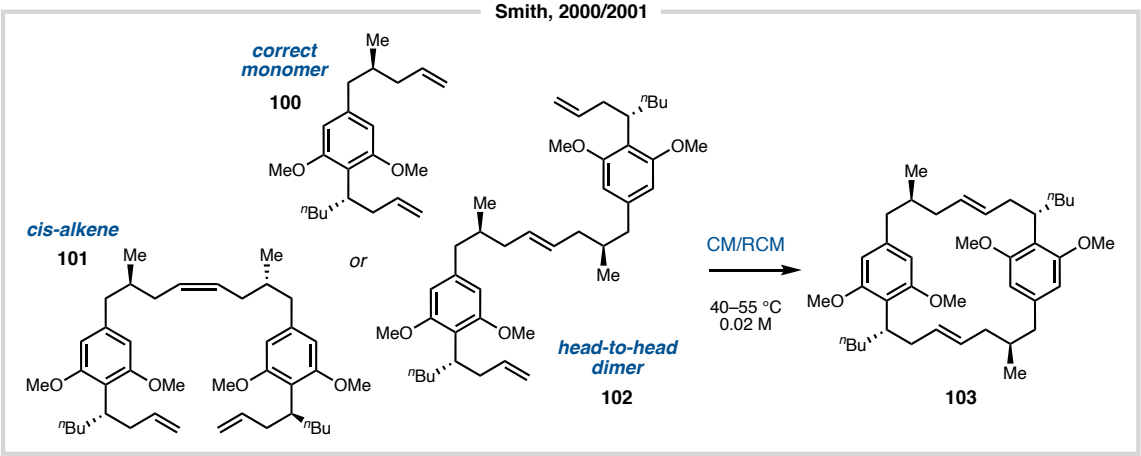

We attempted to use DFT calculations to similarly assess the thermodynamic driving force for depolymerization/RCM to afford head-to-tail dimer **94**. These efforts were stymied by the many conformers available to unsubstituted macrocycle **94** and related metathesis products. We developed a computational workflow to include entropy correction via conformer ensemble generation (GFN-FF, CREST) with DFT sorting (B3LYP/6-31G**, CENSO);[146] however, the supercomputing time required was prohibitive.

Nevertheless, we anticipated that cyclized **94** would be accessible in this thermodynamically controlled process given that macrocyclic ring strain of **94** should be minimal.[147] As a corollary, we did not expect significant enthalpy gain of cyclization, owing to the flexible nature of both the linear precursor and the cyclic product (**94**). Thus, depolymerization would be an entropically driven process, whereby reducing

concentration and increasing temperature could be used to push the ring–chain equilibrium toward the macrocycle.

Indeed, a two-step sequence consisting of cross-coupling then ring formation delivered the paracyclophane (**94**) in 34% yield relative to the intermediate polymeric mixture (Figure 5.48). Specifically, subjection of monomer **85** to **L1**·$NiBr_2$ under reductive conditions furnished a mixture of minimal macrocycle and polymer as the major product, which could be purified away from RCC byproducts, such as phthalimide, by a series of triturations. This was followed by treatment of the mixture with 35 mol % Grubbs second generation catalyst at high dilution (PhH, 0.02 M) and 50 °C. We did not observe the diastereomeric meso macrocycle to form in the two-step procedure, indicating that—notwithstanding the limitations to dr measurement (*vide supra*)—polymerization occurred with high stereoselectivity, since the stereochemistry would be unaffected by metathesis.

Figure 5.48 *Two-step macrocyclization: depolymerization/RCM*

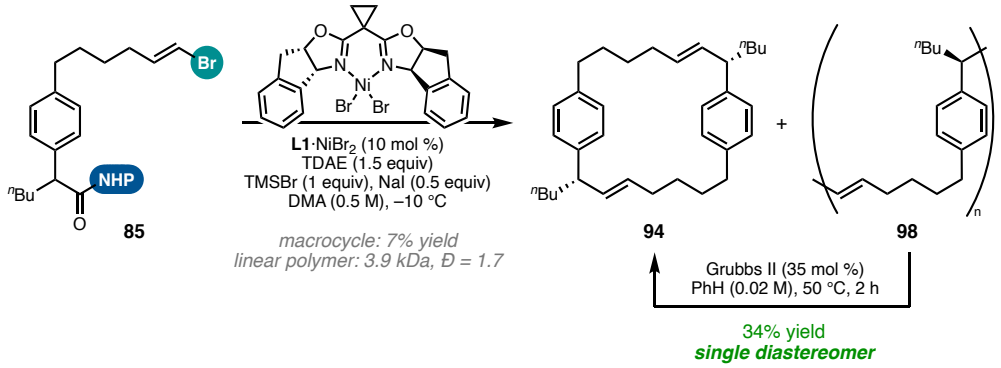

Tracking over time the relative amounts of polymer and macrocycle in aliquots of the metathesis reaction by GPC and NMR provided evidence that depolymerization was responsible for the increase in macrocycle **94** yield following initial cyclodimerization via double RCC. It was clear that high-molecular weight macromolecules were

disassembled upon addition of metathesis catalyst. These analytical methods also provided evidence for the presence of intermediate-weight oligomers, although quantitation of these molecules was elusive. We presume that ca. 34% yield of cyclized **94** represents the thermodynamic ring–chain equilibrium under these conditions. A brief survey of metathesis reaction parameters (e.g., reaction time, catalyst, temperature, solvent, concentration, etc.) did not qualitatively perturb the equilibrium to effect a significant increase in macrocycle **94** yield relative to the putative oligomeric species.

Figure 5.49 *One-step macrocyclization: depolymerization/RCM*

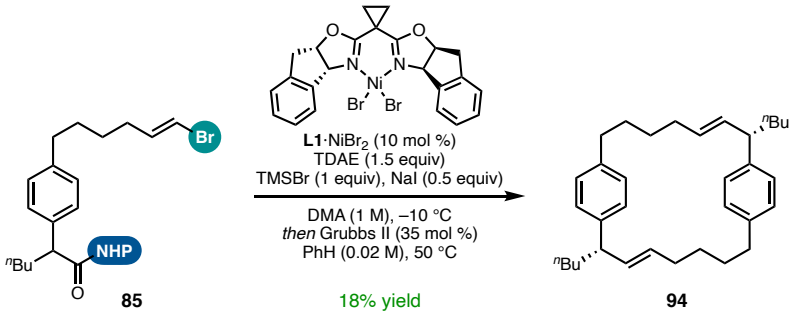

The sequence could be accomplished in one pot (Figure 5.49). Following reductive coupling, a solution of metathesis catalyst in benzene was added directly to the mixture in DMA then heated. In this reaction, macrocycle **94** was formed in 18% yield from difunctional monomer **85**. While this one-pot approach advantageously avoided intervening purification steps—in which a nonzero amount of macrocycle and/or polymer was lost—we observed that the polymer was reticent to convert to macrocycle in the DMA/PhH solution. This effect could arise from inhibition or degradation of the Ru catalyst by the Lewis basic co-solvent.[148] Given the preference of the decarboxylative reductive coupling for amide-based solvents,[75] we did not attempt to reoptimize this

component of the overall transformation to perform under conditions more compatible with metathesis.

Theoretically, the yield of cyclodimer **94** arising via this sequence was capped by the molecular weight and polydispersity of the polymer. It is only possible for the internal olefinic units of polymer **98** to be regenerated into diene **94**; the exception is if protodebromination leads to one polymeric end group being an alkene, which renders this unit a potential macrocycle precursor. Therefore, a smaller ratio of repeat units to terminal units (i.e., reduced molecular weight of **98**) limits cyclophane **94** formation.

Figure 5.50 *Effect of polymer molecular weight on macrocyclization: GPC analysis*

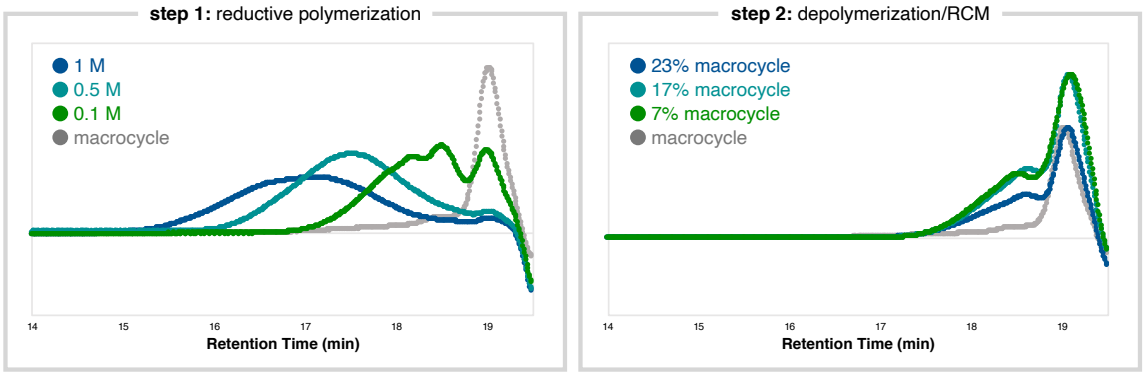

This concept was observed across a range of polymer sizes (Figure 5.50). Running the first (reductive coupling) step at concentrations of 0.1, 0.5, and 1 M, a series of smaller, medium, and larger macromolecules were obtained, respectively. Subsequent subjection of these mixtures to depolymerization conditions afforded desired product **94** in increasing yields: 7%, 17%, and 23%. However, further concentration of the first reaction in the sequence presented practical challenges to reaction setup, so extrapolation of the observed concentration dependence to >1 M was not pursued as a means to achieving higher yields of cyclic **94**.

In sum, this investigation established a novel synthetic approach to paracyclophanes. By viewing the polymer as a viable intermediate toward the desired macrocycle, we were able to harness the high level of selectivity for head-to-tail cross-coupling, as well as the stereoselectivity, of Ni-catalyzed decarboxylative reductive coupling in a manner that significantly outperformed direct cyclodimerization via double RCC. Yet, at the current level of development, both methods for accessing a macrocycle from a difunctional monomer were not maximally efficient. To advance further toward the synthesis of the cylindrocyclophanes, we regarded the metathesis depolymerization as a conceptual springboard.

5.6 REVISED APPROACH AND FORMAL SYNTHESIS

Having discovered the power of metathesis for assembly of a paracyclophane structure *from a polymer*, we questioned the value of proceeding through this intermediate. Of the key advantages, being (1) head-to-tail connectivity and (2) stereoselective aliphatic bridge substitution, only the latter could not also be addressed via metathesis (see Fig. 5.7). As such, we aimed to simplify the system—and reduce the step count—by limiting our demands of the RCC reaction to generation of a single stereocenter (Figure 5.51). Accordingly, the *single* alkene established by Ni catalysis would be poised for cyclodimerization via CM/RCM.

Figure 5.51 *Revised conceptual synthetic design*

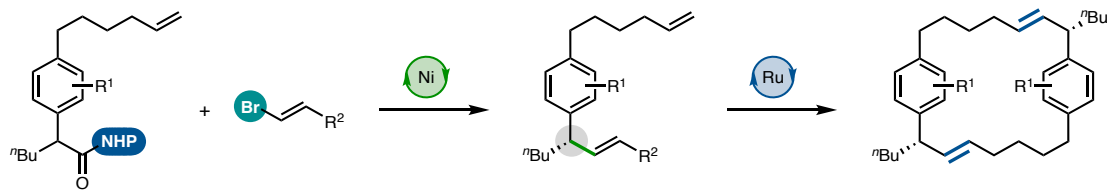

In our initial investigation of this modified synthetic design plan, we continued to make use of the readily accessible, unsubstituted substrate class. Intercepting the deprotected product of fragment coupling (**104**), alkyne hydrogenation delivered terminal alkene **105** in 82% yield (Figure 5.52). As our immediate goal was to test the planned macrocyclization, this step allowed rapid preparation of the requisite substrate (i.e., **106**), but a more convergent pathway was envisioned in which the alkyl fragment precursor to **106** would contain the alkene functionality prior to coupling. The NHP ester of **106** was then revealed following deprotection and esterification (86% yield over two steps).

Figure 5.52 *Preparation of NHP ester for single RCC*

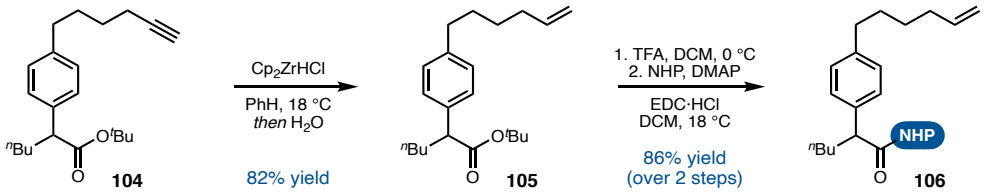

In the context of our redesigned approach, the most atom-economical coupling partner would feature R^2 = H (see Fig. 5.51). For practical reasons, we selected commercial 1-bromopropene (**107**) as a surrogate for gaseous vinyl bromide. Reductive cross-coupling of NHP ester **106** with alkenyl bromide partner **107** furnished diene **108** in 79% yield (97:3 *E*:*Z*), with the major (*E*)-alkene isomer generated in 92% ee (Figure 5.53). We assigned the absolute configuration of product **108** by analogy to previous studies.[75]

To test the feasibility of subsequent cross-metathesis, we subjected monomer **108** to Grubbs second generation catalyst in C_6D_6 (0.02 M) at 50 °C and monitored the course of the reaction by quantitative ^{1}H NMR. After 30 minutes, target cyclophane **94** was observed to form in 44% yield without evidence of the diastereomeric meso compound.

Given this result, two-step cyclodimerization via single RCC and CM/RCM occurred in 35% overall yield from the monomeric substrate to deliver a single observable diastereomer of paracyclophane.

Figure 5.53 *Two-step macrocyclization: sequential single RCC and CM/RCM*

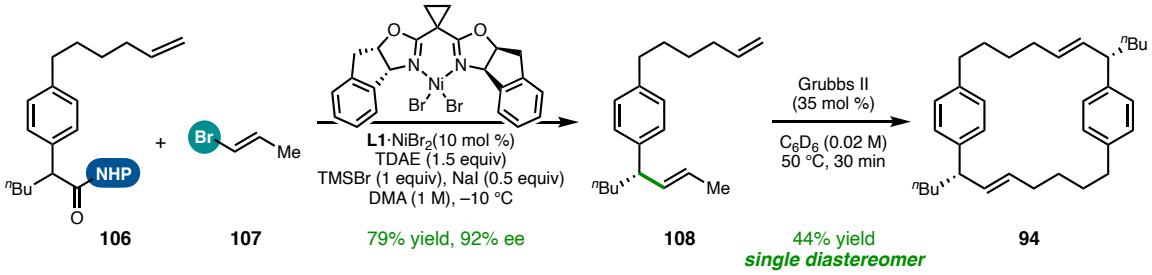

Continuing to track the metathesis reaction over longer periods of time, we found the macrocycle yield to diminish, approaching the equilibrium concentration of **94**. After 2 hours, macrocycle **94** was present in 34% yield, which is consistent with the yield of depolymerization/RCM—run under identical, albeit non-deuterated, conditions for the same length of time (see Fig. 5.48). Likewise, the mass balance of monomer **108** was qualitatively found in oliogomeric/polymeric species. As previously noted, the predominance of macromolecules rendered purification of the macrocycle challenging; cyclized **94** was isolated in 18% yield following silica gel chromatography.

With this exciting precedent for sequential single RCC and CM/RCM to deliver the paracyclophane skeleton, we endeavored to apply this approach to a substrate that could be advanced to cylindrocyclophane F (**2**) upon successful execution of this two-step cyclodimerization. To this end, we prepared an alkene-containing alkyl fragment from the corresponding protected alkyne (**60**, see Fig. 5.27; 78% yield over two steps) then subjected this compound to Negishi cross-coupling with 2,6-dimethoxy aryl bromide **52** (Figure 5.54). In stark contrast to the alkyne congener, branched organozinc reagent

109 was coupled in 80% yield. From alkene **110**, the NHP ester (**111**) was accessed in short order (85% yield over two steps).

Figure 5.54 *Fragment coupling toward cylindrocyclophane F via single RCC*

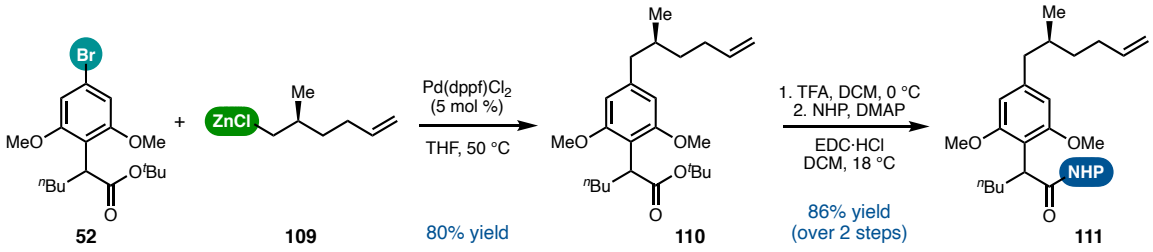

Treatment of fully substituted electrophile **111** and simple alkenyl bromide **107** with **L1**·$NiBr_2$ and TDAE afforded cross-coupled product **112** in 47% yield (Figure 5.55). This moderate yield is fully consistent with the performance of the truncated NHP ester bearing identical aryl *o*,*o*-disubstitution in the single RCC model reaction; accordingly, we expect the high ee of related product **19** to translate to excellent dr of homobenzylic alkene **112** (see Fig. 5.24). In the case of elaborated **112**, no separation of diastereomers (epimeric at the benzylic position) was attained via chiral SFC or HPLC. The diastereomeric cross-coupled product was also unidentifiable by NMR when substrate **111** was subjected to a racemic mixture of Ni catalyst. Although the dr of cross-coupled **112** remained unknown, we expected that determination of the diastereomeric ratio of the downstream macrocycle could be used as a readout for RCC stereoselectivity.

Figure 5.55 *Successful single RCC toward cylindrocyclophane F*

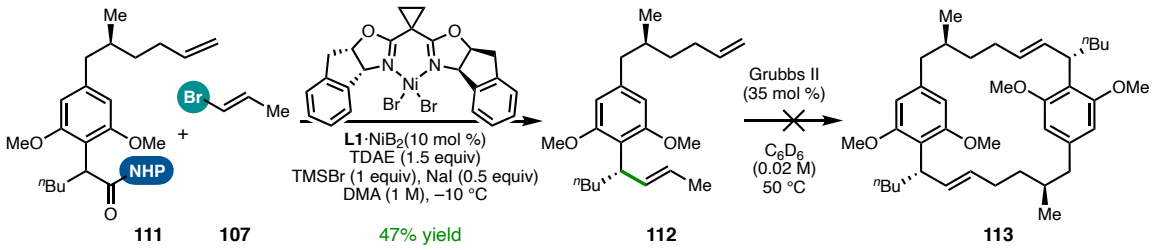

With diene **112** in hand, we were poised to achieve the formal synthesis of cylindrocyclophane F following CM/RCM. Unfortunately, attempts to cyclodimerize **112** were not met with success. To parse the obstacles to productive reactivity, we monitored the course of this reaction by quantitative ^{1}H NMR. Using the solvent of choice for formation of the model paracyclophane (i.e., C_6D_6), we observed gradual loss of signals assigned to substrate **112** but without corresponding increase in other signals; we attributed this to oligomerization and/or polymerization.

We recognized that use of $CDCl_3$ instead could allow ready identification of macrocyclic signals, as characterization data for **113** have been reported in this solvent.[73] However, we were unable to detect paracyclophane **113** upon reaction of monomer **112** with the metathesis catalyst in chlorinated solvent (Figure 5.56). Analysis of the reaction mixture by mass spectrometry allowed us to tentatively assign one of the several resulting species as **114**. Compound **114** exemplifies as a possible challenge in this system the inertness of intervening metathesis products toward eventual assembly of desired macrocycle **113**. We were surprised by this result, given the resemblance of diene **112** to a successful cyclophane precursor, a des-methyl homolog of **112** (see Fig. 5.7).

Figure 5.56 *Failure of CM/RCM to afford cyclodimer*

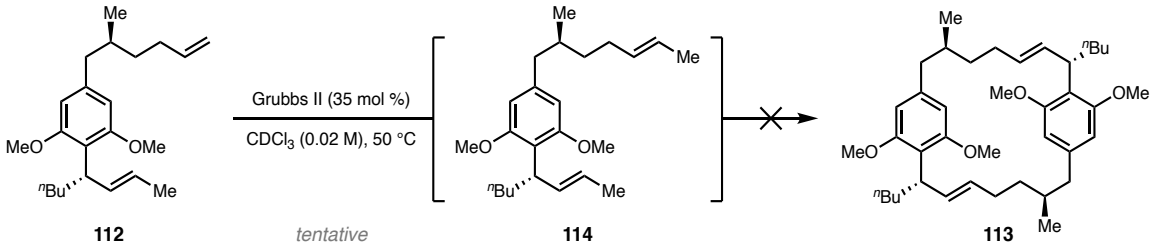

112 *tentative* **114** **113**

Three observations led us to hypothesize that the aryl substitution pattern of **112**, in combination with the position of internal alkenes (along the bridge of the intended

paracyclophane), preclude efficient reversibility of the various metathesis reactions required to funnel to head-to-tail dimer **113**. (1) Exchanging the simple arene of difunctional monomer **85** with a resorcinol motif (i.e., 2,6-dimethyoxy **57**) prevented macrocyclization in the reductive coupling protocol (see Fig. 5.45). (2) For a polymer without aryl substitution that featured internal alkenes at the same positions as monomer **112** (and unreactive **113**), RCM—following depolymerization—was successful in generating a paracyclophane (see Fig. 5.48). (3) Smith and coworkers[70] demonstrated that resorcinol derivatives (i.e., **101** and **102**) could be disassembled at an internal alkene to deliver a single macrocyclic product (see Fig. 5.47). Although presumed that *any* of the possible metathesis reactions would be reversible, and thus lead to the head-to-tail cyclodimer, only an internal alkene positioned furthest away from the dimethoxy substituents was empirically tested.

Figure 5.57 *Related failure of CM/RCM toward cylindrocyclophane A*

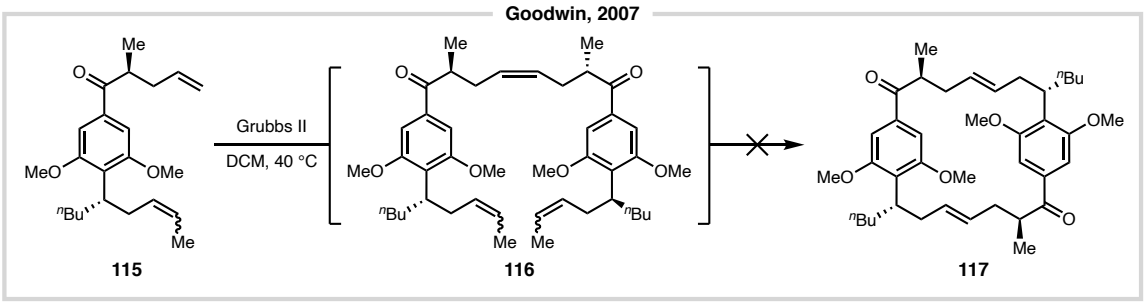

A related synthetic approach to the cylindrocyclophanes via CM/RCM lends credence to this hypothesis (Figure 5.57). MacMillan and coworkers[67] applied Grubbs second generation catalyst to terminal alkene/internal alkene **115**—bearing a methoxy-substituted arene—in dichloroethane. In lieu of macrocyclization, they obtained only

head-to-head dimer **116**, in which the terminal alkene of monomer **115** dimerized but the internal alkene (positioned adjacent to the OMe groups) was inert.

In line with this hypothesis, a feasible solution could be to remove the alkenyl methyl substituent and attempt cyclodimerization of the di-(terminal)alkene. We first attempted this workaround using the unsubstituted model system. The requisite terminal alkene could be indirectly appended via Ni-catalyzed RCC by use of alkenyl silane **118**, a readily handled liquid alternative to vinyl bromide hypothesis (Figure 5.58). Reductive cross-coupling of silyl **118** with the simplified NHP ester (**106**) proceeded in good yield (83%) and ee. Desilylation was then smoothly effected by treatment of the cross-coupled product with TsOH (91% yield), and the enantiomeric excess of the resulting diene (**119**) was determined to be 96%. Following the NMR-scale protocol previously established for CM/RCM of the methylated variant (**108**, see Fig. 5.53), paracyclophane **94** was generated in 49% yield after 30 minutes of reaction time. The improvement to macrocyclization afforded by the lack of alkene substitution—albeit slight—bodes well for the more complex system.

Figure 5.58 *Two-step macrocyclization of dienyl monomer*

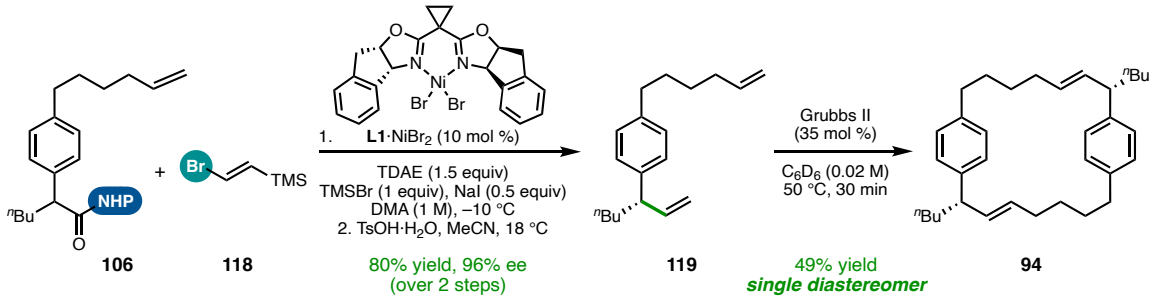

In an analogous RCC/desilylation sequence, 2,6-dimethoxy-containing diene **120** was prepared in 59% yield over two steps (Figure 5.59). With alkenyl silane **118**, the cross-coupling yield (66%) from NHP ester **111** was noticeably improved relative to prior

RCC using this substrate (*cf.* 47%; see Fig. 5.55). It stood to reason that the enantioselectivity could also be higher for reaction of this coupling partner combination. Consistent with our inability to measure dr for methylated **112**, any minor diastereomers of cross-coupled product **111** formed in the RCC did not yield to separation via chiral SFC or HPLC. As well, the benzyl epimer was not observed by NMR when racemic **L1**·$NiBr_2$ was the catalyst employed.

Figure 5.59 *Completion of the formal synthesis of (–)-cylindrocyclophane F*

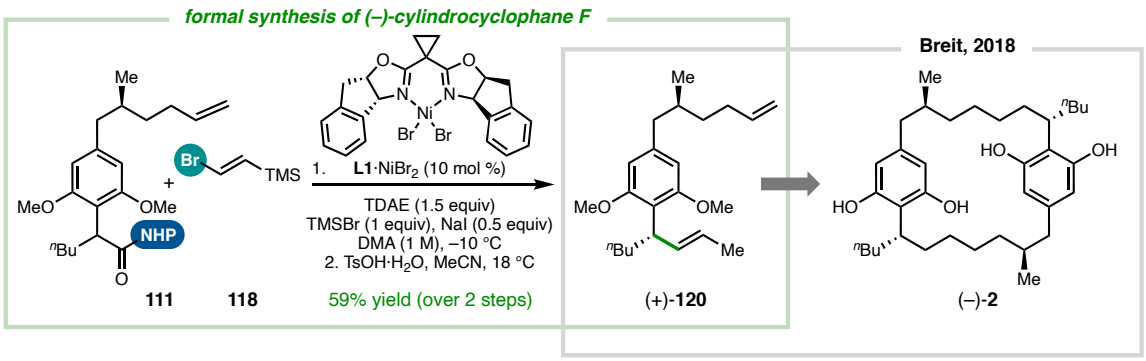

To confirm the presumed configuration of the benzylic stereocenter of **120**, we compared our synthesized compound to that reported by the Breit group.[73] Note that the absolute configuration of the methyl group appended to the aliphatic chain of **120** had been confirmed by Mosher ester analysis[149] of an intermediate prior to aryl–alkyl fragment coupling, and this position was expected to be stable against epimerization throughout the remaining steps of the route; thus, only the relative configuration at the benzylic position was in question. Spectroscopic data for **120** were consistent with those reported, as well as the enantiomeric series (i.e., (+)-**120**), measured by optical rotation. When we prepared an identical diene using the opposite enantiomer of **L1**·$NiBr_2$ as that presented in Figure 5.59, this compound was found to be in the opposite enantiomeric series compared to both synthesized **120** and reported **120**.

Taken together, these data constitute compelling evidence for the structural and stereochemical assignment of **120**. As such, macrocyclic precursor **120** represents the completion of a formal synthesis of (–)-cylindrocyclophane F (**2**).

5.7 CONCLUDING REMARKS

This chapter details efforts aimed at addressing the synthetic challenges posed by dialkylresorcinol natural products, which led to several key discoveries. In the context of Ni-catalyzed reductive alkenylation of NHP esters, use of TDAE as the terminal reductant (with silyl halide additives) led to non-Ni-mediated reductive fragmentation of resorcinol-derived NHP esters. This study coincides with an ongoing mechanistic investigation in our lab that suggests this phenomenon is general to other benzylic NHP ester substrates of Ni-catalyzed RCCs. We expect these findings to be of use in the application of reductive cross-coupling reactions which use soluble organic reductants to the synthesis of additional complex molecules or natural products. Of note, we demonstrated the orthogonal reactivity of redox-active esters in redox-neutral cross-coupling (i.e., Pd-catalyzed Negishi reaction), important for synthetic efficiency.

Streamlined access to the [7.7]paracyclophane skeleton was accomplished by development of a convergent synthetic route. Modular assembly of the *n*-butyl substituent, aliphatic bridge, and substituted arene components of the cylindrocyclophanes allowed rapid preparation of a natural product-like macrocycle from simple building blocks and would be advantageous for future SAR studies. The ability of **L1**·Ni-catalyzed RCC to forge an *o*,*o*-disubstituted benzylic stereocenter in high yield and enantioselectivity was critical to this success of this route.

Reductive cyclodimerization via Ni catalysis was demonstrated in three distinct approaches of varying synthetic utility. Direct application of asymmetric reductive cross-coupling conditions to an NHP ester/alkenyl bromide afforded the corresponding head-to-tail cyclodimer as a single observable diastereomer, albeit in less than 10% yield. The proclivity for di-electrophile polymerization under these conditions inspired development of an unprecedented sequence of reductive polymerization and depolymerization/RCM to deliver the same macrocycle in increased yield with a high level of stereoselectivity. This discovery contributes [7.7]paracyclophanes as new macrocyclic monomers of reversible polymerization and is an exciting entry into the burgeoning field of chemical polymer recycling to monomers.[150]

Ultimately, use of Ni-catalyzed reductive Csp^3–Csp^2 cross-coupling to generate an enantioenriched diene monomer followed by CM/RCM furnished a paracyclophane in good yield. This approach led to the formal synthesis of (–)-cylindrocyclophane F (Figure 5.60). Key CM/RCM precursor **120** was synthesized in ten steps in the longest linear sequence from commercial or known materials and could be advanced to the natural product in two steps.

Figure 5.60 *Formal synthesis of (–)-cylindrocyclophane F via stereoselective RCC*

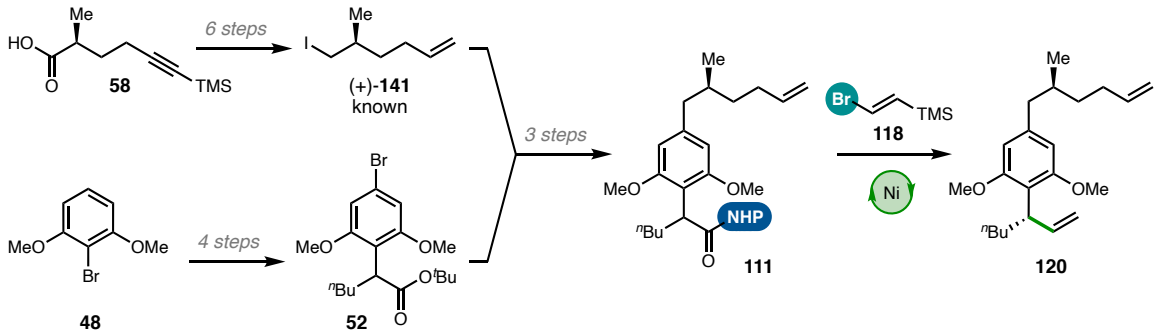

5.8 EXPERIMENTAL SECTION

5.8.1 *Materials and Methods*

Unless otherwise stated, reactions were performed under a N_2 atmosphere with freshly dried solvents. Glassware was oven-dried at 120 °C for a minimum of four hours or flame-dried utilizing a Bunsen burner under high vacuum. Tetrahydrofuran (THF), methylene chloride (DCM), acetonitrile (MeCN), benzene (PhH), and toluene (PhMe) were dried by passing through activated alumina columns. Diisopropylamine ($^{i}Pr_2NH$), was distilled from calcium hydride prior to use and stored under N_2. Unless otherwise stated, chemicals and reagents were used as received. Anhydrous tetrabutylammonium iodide, $TBAPF_6$, sodium iodide (NaI), TDAE, trimethylsilyl bromide (TMSBr), trimethylsilyl chloride (TMSCl), lithium chloride (LiCl), tetrabutylammonium fluoride, *N*,*N*-dimethylacetamide (DMA), and triethylamine (Et_3N) were purchased from Sigma-Aldrich. Manganese and zinc were purchased from Strem. All metal complexes, including Cp_2ZrHCl, $Pd(dppf)Cl_2$, $NiBr_2$·diglyme, $Ni(cod)_2$, Pd_2dba_3, $[Ir(cod)(OMe)]_2$, and $CuBr_2$, were purchased from Strem or Sigma-Aldrich and stored under N_2. Reactions were monitored by liquid chromatography mass spectroscopy (LCMS) or by thin layer chromatography (TLC) using EMD/Merck silica gel 60 F254 pre-coated plates (0.25 mm), visualized by UV (254 nm) and $KMnO_4$, *p*-anisaldehyde, iodine, or CAM staining. Flash column chromatography was performed using silica gel (SiliaFlash® P60, particle size 40–63 microns [230 to 400 mesh] ('silica') or 20–45 microns ('extra-fine silica')) purchased from Silicycle. ^{1}H and ^{13}C NMR spectra were recorded on a Bruker Advance III HD with Prodigy Cryoprobe (at 400 MHz and 101 MHz, respectively) or Varian Inova 500 (at 500 MHz and 126 MHz, respectively) and are reported relative to internal

$CDCl_3$ (^1H, δ = 7.26; ^{13}C, δ = 77.16) or C_6D_6 (^1H, δ = 7.16; ^{13}C, δ = 128.06). Data for ^1H NMR spectra are reported as follows: chemical shift (δ ppm) (multiplicity, coupling constant (Hz), integration). Multiplicity abbreviations are as follows: s = singlet, d = doublet, t = triplet, q = quartet, and m = multiplet. IR spectra were recorded on a Perkin Elmer Paragon 1000 spectrometer and are reported in frequency of absorption (cm^{-1}); alternatively, a Thermo Scientific Nicolet iS5 FTIR Spectrometer FTIR-ATR was used to obtain FTIR-ATR spectra. Analytical chiral SFC was performed with a Mettler SFC supercritical CO_2 analytical chromatography system (CO_2 = 1450 psi, column temperature = 40 °C) with a Chiralcel OB–H column (4.6 mm x 25 cm). Analytical chiral GC was performed with a RESTEK Rt-bDEXse column (30 m, 0.32 mm/D, 0.25 um). HRMS data were acquired using an Agilent 6230 Series time-of-flight (TOF) mass spectrometer with an Agilent G1978A Multimode source in electrospray ionization (ESI) mode, by LC-MS using a Waters LCT Premier XE Electrospray TOF mass spectrometer interfaced with Waters UPLC chromatography, by GC-MS interfaced with a JEOL JMS-T2000 GC AccuTOF GC-Alpha with Field Ionization, or with Bruker Autoflex MALDI-(TOF/TOF)-MS. Molecular formulas of the observed ion fragment of compounds are given (e.g., $[M + H]^+$). Optical rotations were measured on a Jasco P-2000 polarimeter using a 100 mm path-length cell at 589 nm. Gel permeation chromatography (GPC) was performed using an Agilent 1260 series pump equipped with two Agilent PLgel MIXED-B columns (7.5 x 300 mm), an Agilent 1200 series diode array detector, a Wyatt 18-angle DAWN HELEOS light scattering detector, and an Optilab rEX differential refractive index detector. The mobile phase was THF at a flow rate of 1 mL/min. Molecular weight and dispersity data are reported relative to polystyrene standards.

5.8.2 *Single Reductive Cross-Coupling*

(*E*)-(((4-bromobut-3-en-1-yl)oxy)methyl)benzene (17)

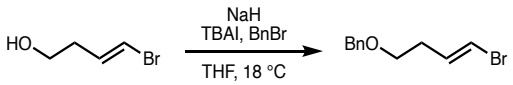

To a flame-dried round bottom flask with a stir bar was added sodium hydride (361 mg, 14.3 mmol, 1.5 equiv), tetrabutylammonium iodide (35 mg, 0.1 mmol, 0.01 equiv), and THF (19.0 mL, 0.5 M). The mixture was stirred for 5 min, then (*E*)-4-bromobut-3-en-1-ol[151] (1.44 g, 9.5 mmol, 1 equiv) was added dropwise. After 5 min of stirring, benzyl bromide (1.3 mL, 10.9 mmol, 1.15 equiv) was added dropwise. After 16 h, the reaction was quenched with sat. aq. NH_4Cl and was diluted with water and Et_2O. The organic layer was separated, and the aqueous layer was extracted with Et_2O thrice. Combined organics were dried over Na_2SO_4, filtered, and concentrated. The crude residue was purified by column chromatography (silica, 5% EtOAc/hexanes) to afford **17** (1.95 g, 85% yield) as a yellow oil.

^{1}H NMR ($CDCl_3$, 500 MHz): δ 7.44 – 7.28 (m, 5H), 6.23 (dt, *J* = 14.0, 7.1 Hz, 1H), 6.13 (dt, *J* = 13.6, 1.5 Hz, 1H), 4.52 (s, 2H), 3.52 (t, *J* = 6.5 Hz, 2H), 2.36 (qd, *J* = 6.7, 1.3 Hz, 2H).

^{13}C{^{1}H} NMR ($CDCl_3$, 101 MHz): δ 138.3, 134.8, 128.6, 127.8, 106.2, 73.2, 68.8, 33.5.

FTIR (NaCl, thin film, cm^{-1}): 2908, 2857, 1621, 1453, 1362, 1103, 937, 736, 698.

HRMS (FI, *m/z*): $[M]^+$ calcd for $C_{11}H_{13}OBr$: 240.0150; found: 240.0157.

2-(2,6-dimethoxyphenyl)hexanoic acid (23)

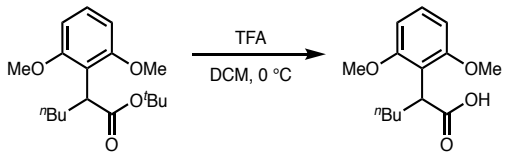

To a round bottom flask with a stir bar was added ester **50** (3.2 g, 10 mmol, 1 equiv) and DCM (86 mL, 0.12 M). The solution was cooled to 0 °C in an ice/water bath then TFA (86 mL, 0.12 M) was added dropwise. The red solution was warmed to ambient temperature over 18 h and then concentrated. The crude residue was azeotroped with PhMe to afford **23** (2.52 g, 96% yield) as a white amorphous solid.

^{1}H NMR ($CDCl_3$, 400 MHz): δ 7.19 (t, *J* = 8.3 Hz, 1H), 6.56 (d, *J* = 8.4 Hz, 2H), 4.19 (dd, *J* = 8.9, 5.5 Hz, 1H), 3.79 (s, 6H), 2.09 (ddt, *J* = 13.3, 10.5, 5.2 Hz, 1H), 1.79 – 1.65 (m, 1H), 1.26 (ddddd, *J* = 12.6, 10.4, 5.5, 3.4, 1.8 Hz, 2H), 1.20 – 1.01 (m, 1H), 0.91 – 0.77 (m, 3H).

^{13}C{^{1}H} NMR ($CDCl_3$, 101 MHz): δ 158.1, 128.3, 117.0, 104.3, 55.9, 39.8, 29.7, 29.6, 22.8, 14.1.

FTIR (NaCl, thin film, cm^{-1}): 2955, 2935, 1702, 1594, 1474, 1250, 1115, 1100, 725.

HRMS (FI-MS, *m/z*): $[M]^+$ calcd for $C_{14}H_{20}O_4$: 252.1356; found: 252.1249.

1,3-dioxoisoindolin-2-yl 2-(2,6-dimethoxyphenyl)hexanoate (18)

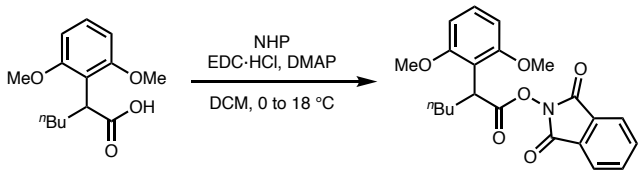

To a round bottom flask with a stir bar was added acid **23** (1.0 g, 4 mmol, 1 equiv), *N*-hydroxyphthalimide (646 mg, 4 mmol, 1 equiv), DMAP (73 mg, 0.6 mmol, 0.15 equiv),

then DCM (40 mL, 0.1 M). The solution was cooled to 0 °C in an ice/water bath then EDC·HCl (836 mg, 4.4 mmol, 1.1 equiv) was added in portions. The reaction was stirred at 0 °C for 30 min and then concentrated. The crude residue was purified by column chromatography (silica, 20% EtOAc/hexanes) to afford **18** (1.25 g, 79% yield) as a white amorphous solid.

^{1}H NMR ($CDCl_3$, 400 MHz): δ 7.84 (s,2), 7.75 (dd, *J* = 5.5, 3.1 Hz, 2H), 7.24 (t, *J* = 8.3 Hz, 1H), 6.59 (d, *J* = 8.4 Hz, 2H), 3.87 (s, 6H), 2.28 – 2.13 (m, 1H), 1.92 – 1.78 (m, 1H), 1.42 – 1.11 (m, 6H), 0.85 (t, *J* = 7.1 Hz, 3H).

^{13}C{^{1}H} NMR ($CDCl_3$, 101 MHz): δ 171.3, 158.0, 134.6, 128.9, 123.8, 114.7, 103.8, 55.9, 37.9, 29.7, 29.2, 22.7, 14.1.

FTIR (NaCl, thin film, cm^{-1}): 3422, 2956, 2934, 1814, 1788, 1746, 1596, 1476, 1253, 1110, 966, 698.

HRMS (FD, *m/z*): $[M]^+$ calcd for $C_{22}H_{23}NO_6$: 397.1525; found: 397.1522.

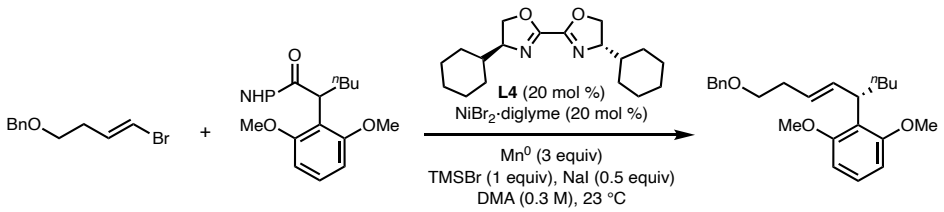

General Procedure A (original order of addition): On the bench, a flame-dried ½-dram vial with a stir bar and Teflon cap was sequentially charged with metal powder reductant (if applicable) (Zn^0: 9.8 mg, 0.15 mmol, 3 equiv *or* Mn^0: 8.2 mg, 0.15 mmol, 3 equiv), NaI (3.8 mg, 0.025 mmol, 0.5 equiv), ligand (CyBiOX (**L4**): 3.0 mg, 0.01 mmol, 0.2 equiv), and NHP ester **18** (19.9 mg, 0.05 mmol, 1 equiv). In a N_2-filled glovebox, this vial was sequentially charged with DMA (84 μL), TDAE (if applicable) (35 μL, 0.15 mmol, 3 equiv), and TMSBr (7 μL, 0.05 mmol, 1 equiv) (fumed slightly), each via syringe. A solution of $NiBr_2$·diglyme (3.5 mg, 0.01 mmol, 0.2 equiv) in DMA (84 μL, total 0.3 M) was added, followed by vinyl bromide **17** (12.1 mg, 0.05 mmol, 1 equiv), each by via syringe. The vial was sealed and then stirred at 1000 rpm outside the glovebox at ambient temperature. After 16 h, the reaction mixture was diluted with 20% EtOAc/hexanes and filtered over a plug of silica, eluting with 20% EtOAc/hexanes. The filtrate was concentrated and assayed by quantitative ^1H NMR. This sample was concentrated and purified by preparative thin layer chromatography (silica, 15% Et_2O/hexanes) to afford **19**, which was assayed by chiral SFC.

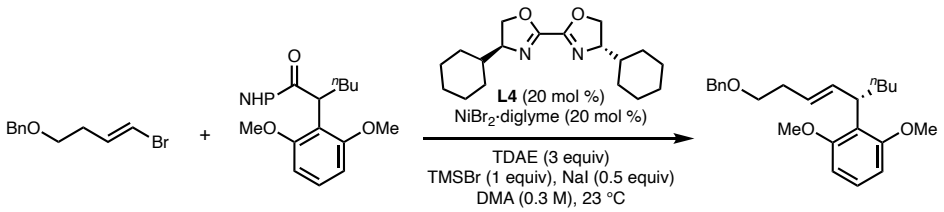

General Procedure B (optimized order of addition): In a N_2-filled glovebox, a flame-dried ½-dram vial with a stir bar and Teflon cap was sequentially charged with NaI (3.8 mg, 0.025 mmol, 0.5 equiv) and vinyl bromide **17** (12.1 mg, 0.05 mmol, 1 equiv). A solution of $NiBr_2$·diglyme (3.5 mg, 0.01 mmol, 0.2 equiv) and ligand (CyBiOX (**L4**): 3.0 mg, 0.01 mmol, 0.2 equiv) in DMA (167 µL, 0.3 M) was added via syringe and the reaction stirred for 5 min. Then, NHP ester **18** (19.9 mg, 0.05 mmol, 1 equiv) was added, followed by sequential addition of TDAE (35 µL, 0.15 mmol, 3 equiv) and TMSBr (7 µL, 0.05 mmol, 1 equiv) (fumed slightly), each via syringe. The vial was sealed and then stirred at 1000 rpm outside the glovebox at ambient temperature. After 16 h, the reaction mixture was diluted with 20% EtOAc/hexanes and filtered over a plug of silica, eluting with 20% EtOAc/hexanes. The filtrate was concentrated and assayed by quantitative ^{1}H NMR. This sample was concentrated and purified by preparative thin layer chromatography (silica, 15% Et_2O/hexanes) to afford **19**, which was assayed by chiral SFC.

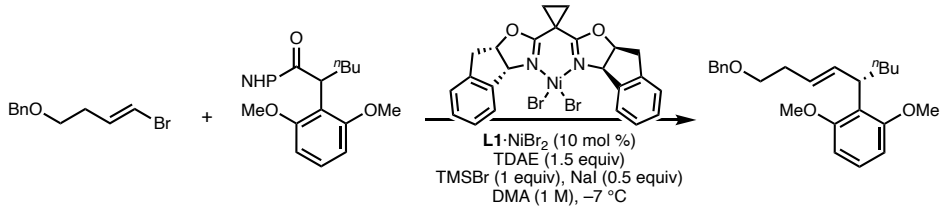

General Procedure C: On the bench, a flame-dried ½-dram vial with a stir bar and Teflon cap was sequentially charged with NaI (3.8 mg, 0.025 mmol, 0.5 equiv) and NHP ester **18** (19.9 mg, 0.05 mmol, 1 equiv). In a N_2-filled glovebox, the vial was charged sequentially with **L1**·$NiBr_2$[75] (2.9 mg, 0.005 mmol, 0.1 equiv) then DMA (50 μL, 1 M) and vinyl bromide **17** (12.1 mg, 0.05 mmol, 1 equiv), each via syringe. The vial was placed in a temperature-controlled well plate in the glovebox and then cooled to –7 °C. The mixture was stirred at 250 rpm until all reagents fully dissolved. (Note: the recirculating Julabo LH45 chiller was set to –7 °C but an external thermometer in the glovebox read the temperature as –1 °C.) Then, TDAE (17 μL, 0.075 mmol, 1.5 equiv) was added and the solution stirred for 10 min before TMSBr (7 μL, 0.05 mmol, 1 equiv) (fumed slightly) was added, each via syringe. The reaction was stirred at the chilled temperature in the glovebox. After 16 h, the reaction mixture was diluted with 20% EtOAc/hexanes and filtered over a plug of silica, eluting with 20% EtOAc/hexanes. The filtrate was concentrated and assayed by quantitative ^{1}H NMR. This sample was concentrated and purified by preparative thin layer chromatography (silica, 15% Et_2O/hexanes) to afford **19**, which was assayed by chiral SFC.

(*S*,*E*)-2-(1-(benzyloxy)non-3-en-5-yl)-1,3-dimethoxybenzene (19)

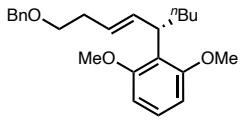

^{1}H NMR ($CDCl_3$, 400 MHz): δ 7.39 – 7.21 (m, 5H), 7.10 (t, *J* = 8.3 Hz, 1H), 6.53 (d, *J* = 8.3 Hz, 2H), 5.97 (ddt, *J* = 15.3, 8.4, 1.4 Hz, 1H), 5.43 (dtd, *J* = 15.1, 6.9, 1.0 Hz, 1H), 4.49 (s, 2H), 3.94 (q, *J* = 7.9 Hz, 1H), 3.78 (s, 6H), 3.47 (t, *J* = 7.1 Hz, 2H), 2.31 (qt, *J* = 7.1, 1.3 Hz, 2H), 1.74 (q, *J* = 7.6 Hz, 2H), 1.38 – 1.14 (m, 3H), 1.14 – 1.01 (m, 1H), 0.84 (t, *J* = 7.2 Hz, 3H).

^{13}C{^{1}H} NMR ($CDCl_3$, 101 MHz): δ 158.5, 138.8, 135.5, 128.5, 127.8, 127.6, 126.9, 125.5, 121.8, 104.8, 72.9, 70.6, 56.0, 39.0, 33.3, 33.3, 30.5, 22.8, 14.3.

FTIR (NaCl, thin film, cm^{-1}): 2953, 2927, 2855, 1591, 1471, 1248, 1097, 972, 727, 696.

HRMS (TOF-MS, *m/z*): $[M + H]^+$ calcd for $C_{24}H_{33}O_3$: 369.2424; found: 369.2431.

$[\alpha]_D^{22} =$ –1 (c = 1.5, $CHCl_3$).

Chiral SFC: (OB–H, 2.5 mL/min, 3% IPA/CO_2, λ = 210 nm); t_R (major) = 9.8 min, t_R (minor) = 14.0 min.

19: racemic

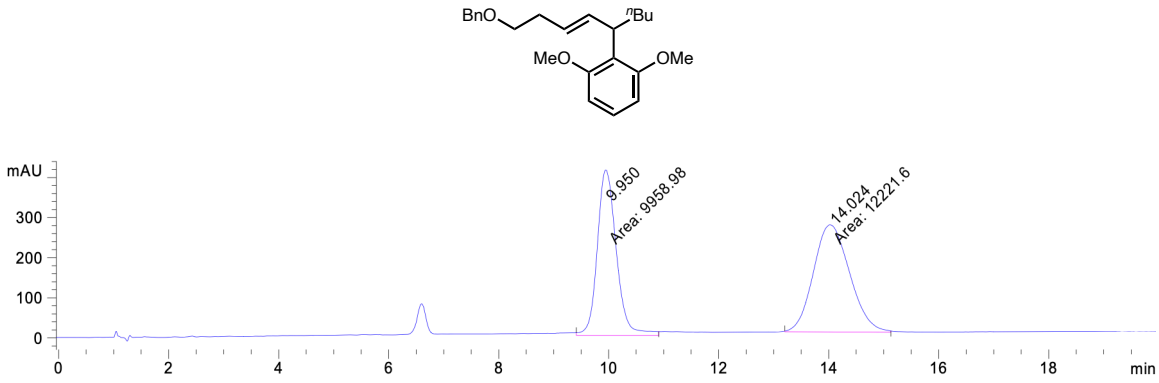

Signal 1: DAD1 A, Sig=210,16 Ref=370,60

Peak #	RetTime [min]	Type	Width [min]	Area [mAU*s]	Height [mAU]	Area %
1	9.950	MM	0.4019	9958.97852	412.94992	44.8996
2	14.024	MM	0.7623	1.22216e4	267.19855	55.1004

(–)-19: enantioenriched (84% ee)

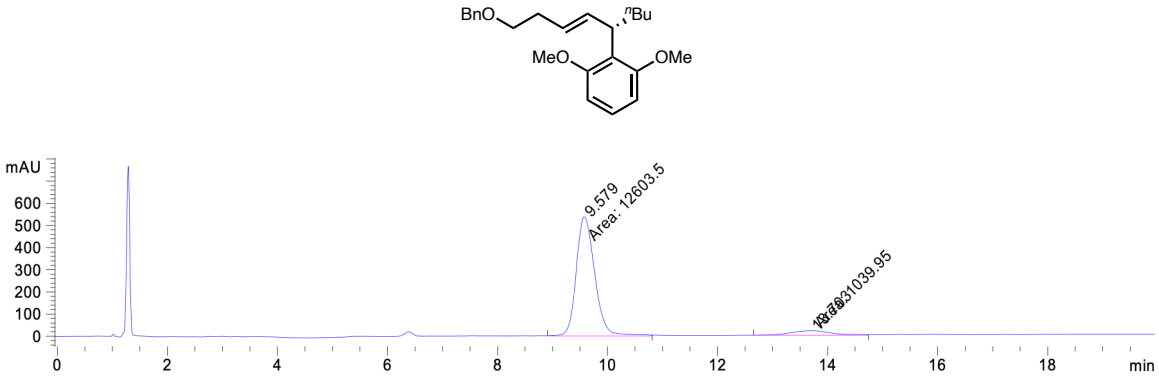

Signal 1: DAD1 A, Sig=210,16 Ref=370,60

Peak #	RetTime [min]	Type	Width [min]	Area [mAU*s]	Height [mAU]	Area %
1	9.579	MM	0.3909	1.26035e4	537.38092	92.3777
2	13.703	MM	0.8372	1039.94507	20.70299	7.6223

(*E*)-1,3-dimethoxy-2-(pent-1-en-1-yl)benzene (20)

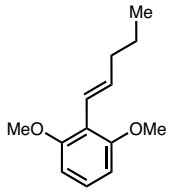

^{1}H NMR ($CDCl_3$, 500 MHz): δ 7.10 (t, *J* = 8.3 Hz, 1H), 6.64 – 6.56 (m, 2H), 6.55 (d, *J* = 8.3 Hz, 2H), 3.84 (d, *J* = 0.7 Hz, 6H), 2.28 – 2.19 (m, 2H), 1.51 (h, *J* = 7.4 Hz, 2H), 0.97 (t, *J* = 7.3 Hz, 3H).

^{13}C{^{1}H} NMR ($CDCl_3$, 101 MHz): δ 158.3, 135.8, 127.2, 121.3, 120.1, 104.2, 55.9, 37.0, 23.0, 14.0.

2,2'-(decane-5,6-diyl)bis(1,3-dimethoxybenzene) (21)

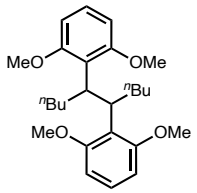

Diastereomer 21a

^{1}H NMR ($CDCl_3$, 400 MHz): δ 6.85 (t, *J* = 8.2 Hz, 1H), 6.26 – 6.18 (m, 2H), 3.85 – 3.78 (m, 1H), 3.63 (s, 3H), 3.53 (s, 3H), 1.94 (dtd, *J* = 13.1, 10.8, 5.2 Hz, 1H), 1.81 – 1.69 (m, 1H), 1.40 – 1.14 (m, 3H), 1.14 – 0.91 (m, 1H), 0.82 (t, *J* = 7.3 Hz, 3H).

^{13}C{^{1}H} NMR ($CDCl_3$, 101 MHz): δ 159.5, 158.9, 125.7, 121.8, 103.1, 102.8, 55.6, 54.8, 51.5, 38.8, 31.9, 30.9, 23.3, 14.4.

Diastereomer 21b

^{1}H NMR ($CDCl_3$, 400 MHz): δ 7.12 (t, *J* = 8.2 Hz, 1H), 6.56 (ddd, *J* = 9.5, 8.2, 1.0 Hz,

2H), 4.07 (dt, *J* = 8.2, 2.7 Hz, 1H), 3.83 (d, *J* = 2.5 Hz, 6H), 1.85 – 1.67 (m, 1H), 1.19 – 0.90 (m, 3H), 0.91 – 0.75 (m, 2H), 0.64 (t, *J* = 7.3 Hz, 3H).

$^{13}C\{^{1}H\}$ NMR ($CDCl_3$, 101 MHz): δ 160.1, 160.0, 126.4, 122.8, 104.9, 104.9, 56.7, 55.6, 37.4, 30.9, 30.6, 22.7, 14.2.

1,3-dimethoxy-2-pentylbenzene (22)

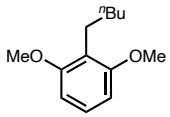

^{1}H NMR ($CDCl_3$, 500 MHz): δ 7.10 (t, *J* = 8.3 Hz, 1H), 6.53 (d, *J* = 8.3 Hz, 2H), 3.80 (s, 6H), 2.66 – 2.58 (m, 2H), 1.51 – 1.41 (m, 2H), 1.32 (q, *J* = 3.6 Hz, 4H), 0.88 (t, *J* = 7.1 Hz, 3H).

(3*E*,5*E*)-1,8-bis(benzyloxy)octa-3,5-diene (24)

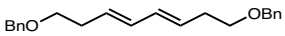

^{1}H NMR ($CDCl_3$, 400 MHz): δ 7.39 – 7.23 (m, 5H), 6.14 – 6.02 (m, 1H), 5.66 – 5.55 (m, 1H), 4.51 (s, 2H), 3.50 (t, *J* = 6.8 Hz, 2H), 2.39 (q, *J* = 6.8 Hz, 2H).

$^{13}C\{^{1}H\}$ NMR ($CDCl_3$, 101 MHz): δ 132.1, 129.0, 127.8, 127.7, 73.1, 70.0, 33.2.

((but-3-en-1-yloxy)methyl)benzene (25)

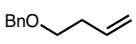

^{1}H NMR ($CDCl_3$, 500 MHz): δ 7.40 – 7.23 (m, 5H), 5.85 (td, *J* = 17.1, 7.0 Hz, 1H), 5.11 (d, *J* = 17.1 Hz, 1H), 5.05 (d, *J* = 10.3 Hz, 1H), 4.53 (s, 2H), 3.57 – 3.50 (m, 2H), 2.39 (q, *J* = 6.8 Hz, 2H).

(*E*)-(((4-chlorobut-3-en-1-yl)oxy)methyl)benzene (42)

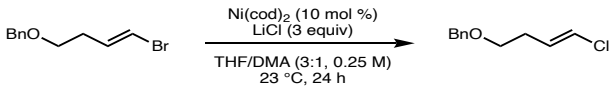

Prepared following a modified procedure:[87] In a N_2-filled glovebox, a 2-dram vial with a stir bar and Teflon cap was sequentially charged with $Ni(cod)_2$ (14.2 mg, 0.051 mmol, 0.1 equiv), LiCl (64.4 mg, 1.52 mmol, 5 equiv.), THF (1.5 mL), and DMA (0.5 mL). The mixture was stirred for a short stir period (ca. 1 min), then alkenyl bromide **17** (72.3 mg, 0.3 mmol, 1 equiv) was added dropwise via syringe. Outside of the glovebox, the reaction was stirred at 800 rpm at 23 °C. A baby blue reaction color appeared after ca. 30 min. After 23 h, the crude mixture was directly filtered over a plug of silica, eluting with 20% EtOAc/hexanes. The crude residue was purified by column chromatography (silica, 5% EtOAc/hexanes) to afford **42** as a pale yellow oil with 10% of unreacted **17**, which was inseparable.

^{1}H NMR ($CDCl_3$, 500 MHz): δ 7.40 (m, 4H), 7.35 (td, *J* = 6.4, 2.0 Hz, 1H), 6.10 (dt, *J* = 13.3, 1.4 Hz, 1H), 4.58 (s, 2H), 3.57 (t, *J* = 6.5 Hz, 2H), 2.43 (qd, *J* = 6.6, 1.3 Hz, 2H).

General Procedure D:

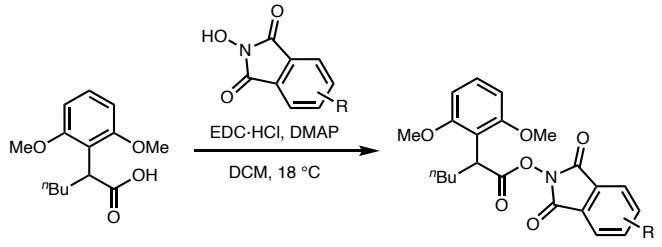

To a round bottom flask with a stir bar was added acid **23** (93.4 mg, 0.37 mmol, 1 equiv), commercial NHP derivative (0.37 mmol, 1 equiv), DMAP (6.7 mg, 0.055 mmol, 0.15 equiv), then DCM (3.7 mL, 0.1 M). To this solution was added EDC·HCl (78.0 mg,

0.407 mmol, 1.1 equiv) in portions. The reaction was stirred at ambient temperature. After 24 h, the reaction was concentrated. The crude residue was purified by column chromatography (silica, 20% EtOAc/hexanes) to afford **43**– **46** as amorphous solids.

5-methyl-1,3-dioxoisoindolin-2-yl 2-(2,6-dimethoxyphenyl)hexanoate (45)

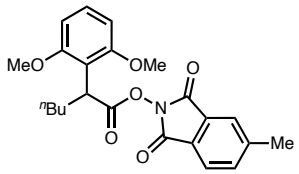

Prepared following General Procedure D in 91% yield.

^{1}H NMR ($CDCl_3$, 500 MHz): δ 7.77 (br. s, 1H), 7.69 (d, *J* = 11.3 Hz, 1H), 7.58 (d, *J* = 7.6 Hz, 1H), 6.65 (d, *J* = 8.3 Hz, 2H), 4.58 (dd, *J* = 8.9, 5.3 Hz), 3.92 (s, 6H), 2.56 (s, 3H), 2.25 (ddt, *J* =13.4, 10.6, 5.3 Hz, 1H), 1.91 (dtd, *J* = 14.1, 9.3, 5.2 Hz, 1H), 1.36 (m, 2H), 1.23 (tdd, *J* = 12.5, 5.9, 3.5 Hz, 1H), 0.92 (t, *J* = 6.9 Hz, 3H).

^{13}C{^{1}H} NMR ($CDCl_3$, 101 MHz): δ 171.3, 157.9, 145.9, 134.9, 128.8, 124.2, 123.6, 114.6, 103.6, 55.7, 37.8, 29.6, 29.1, 22.6, 22.1, 14.0.

5-methoxy-1,3-dioxoisoindolin-2-yl 2-(2,6-dimethoxyphenyl)hexanoate (43)

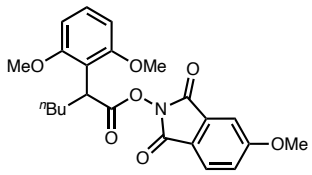

Prepared following General Procedure D in 94% yield.

^{1}H NMR ($CDCl_3$, 500 MHz): δ 7.80 (br. s, 1H), 7.37 (d, *J* = 8.1Hz, 1H), 7.30 (m, 1H), 7.23 (dd, *J* = 8.3, 2.3 Hz, 1H), 6.64 (d, *J* = 8.3 Hz, 2H), 4.57 (dd, *J* = 8.9, 5.3 Hz, 1H), 3.97 (s, 3H), 3.92 (s, 6H), 2.25 (ddt, *J* = 13.4, 10.6, 5.2 Hz, 1H), 1.91 (dtd, *J* = 13.9, 9.2,

5.0 Hz, 1H), 1.37 (m, 2H), 1.23 (m, 1H), 0.92 (t, *J* = 6.9 Hz).

$^{13}C\{^{1}H\}$ NMR ($CDCl_3$, 126 MHz): δ 171.3, 164.9, 157.9, 128.7, 120.0, 114.6, 108.6, 103.6, 56.1, 37.7, 29.6, 29.1, 22.6, 14.0.

5-chloro-1,3-dioxoisoindolin-2-yl 2-(2,6-dimethoxyphenyl)hexanoate (44)

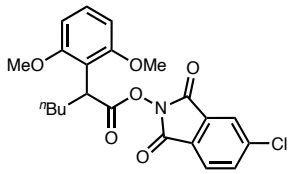

Prepared following General Procedure D in 97% yield.

^{1}H NMR ($CDCl_3$, 500 MHz): δ 7.85 (q, *J* = 9.9, 8.1 Hz, 2H), 7.77 (dd, *J* = 7.94, 1.84 Hz, 1H), 7.31 (m, 1H), 6.65 (d, *J* = 8.3 Hz, 2H), 4.58 (dd, *J* = 8.9, 5.3 Hz, 1H), 3.92 (s, 6H), 2.24 (ddt, *J* = 13.4, 10.5, 5.2 Hz, 1H), 1.91 (dtd, *J* = 14.0, 9.1, 5.1 Hz, 1H), 1.37 (m, 2H), 1.23 (dddd, *J* = 14.5, 12.0, 5.9, 3.5 Hz, 1H), 0.92 (t, *J* = 7.1 Hz, 3H).

$^{13}C\{^{1}H\}$ NMR ($CDCl_3$, 101 MHz): δ 171.1, 157.9, 141.2, 134.5, 128.8, 125.0, 124.2, 114.4, 103.6, 55.7, 37.7, 29.6, 29.1, 22.6, 13.9.

5-bromo-1,3-dioxoisoindolin-2-yl 2-(2,6-dimethoxyphenyl)hexanoate (46)

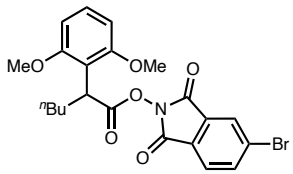

Prepared following General Procedure D in 89% yield.

^{1}H NMR ($CDCl_3$, 500 MHz): δ 8.03 (d, *J* = 10.0 Hz, 1H), 7.94 (dd, *J* = 7.9, 1.7 Hz, 1H), 7.76 (s, 1H), 7.31 (d, *J* = 7.9 Hz, 1H), 6.65 (d, *J* = 8.3 Hz, 2H), 4.57 (dd, *J* = 8.9, 5.3 Hz), 3.92 (s, 6H), 2.24 (ddt, *J* = 13.4, 10.6, 5.3 Hz, 1H), 1.91 (dtd, *J* = 14.0, 9.2, 5.1 Hz, 1H),

1.36 (m, 2H), 1.23 (dddd, J = 11.7, 9.6, 8.4, 6.4 Hz, 1H), 0.92 (td, J = 7.1, 2.3 Hz, 3H).

$^{13}C\{^{1}H\}$ NMR ($CDCl_3$, 101 MHz): δ 171.1, 157.9, 137.5, 128.8, 127.0, 125.1, 114.4, 103.6, 55.7, 37.7, 29.6, 29.1, 22.6, 14.0.

Determination of NHP ester derivative reduction potential

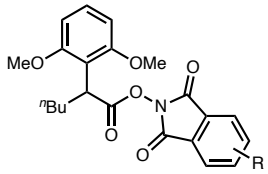

Cyclic voltammograms (CV) were obtained at an analyte concentration of 10 mM and a supporting electrolyte concentration of 0.1 M $TBAPF_6$ in electrochemical grade DMA (Sigma-Aldrich). A glassy carbon working electrode, graphite counter electrode, and silver wire pseudo-reference electrode were employed, and data was collected using a Biologic SP-300 potentiostat. All cyclic voltammograms were normalized by adding 1 equivalent of sublimed ferrocene (relative to analyte) and collecting new CV. The ½-wave potential of the Fc/Fc^+ peak was identified and set to 0.0 V.

R = H (18), 100 mV scan rate

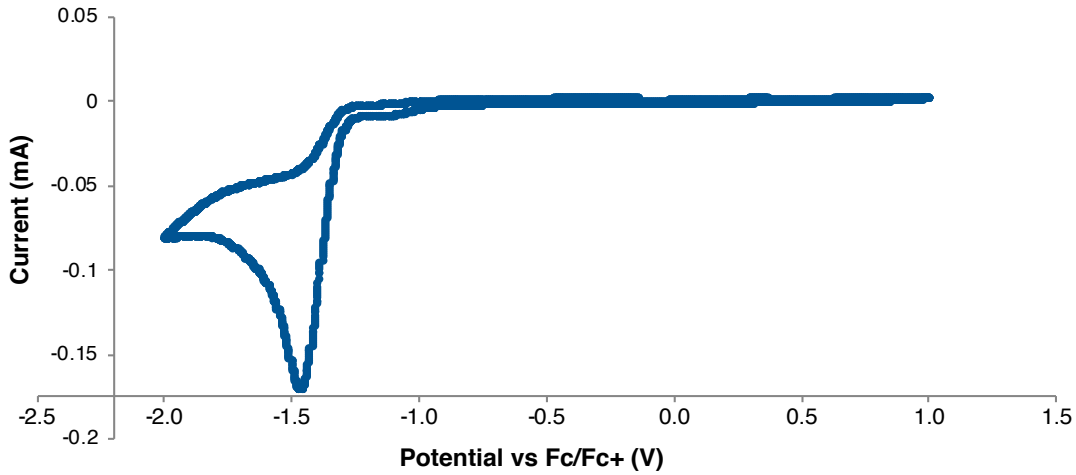

R = Me (45), 100 mV scan rate

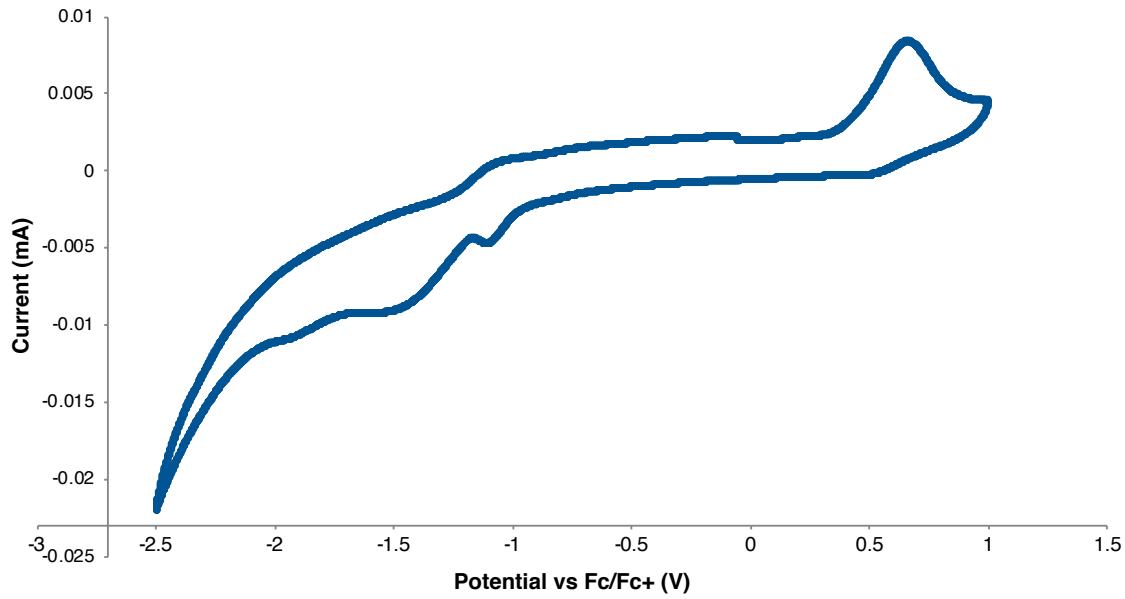

R = OMe (43), 150 mV scan rate

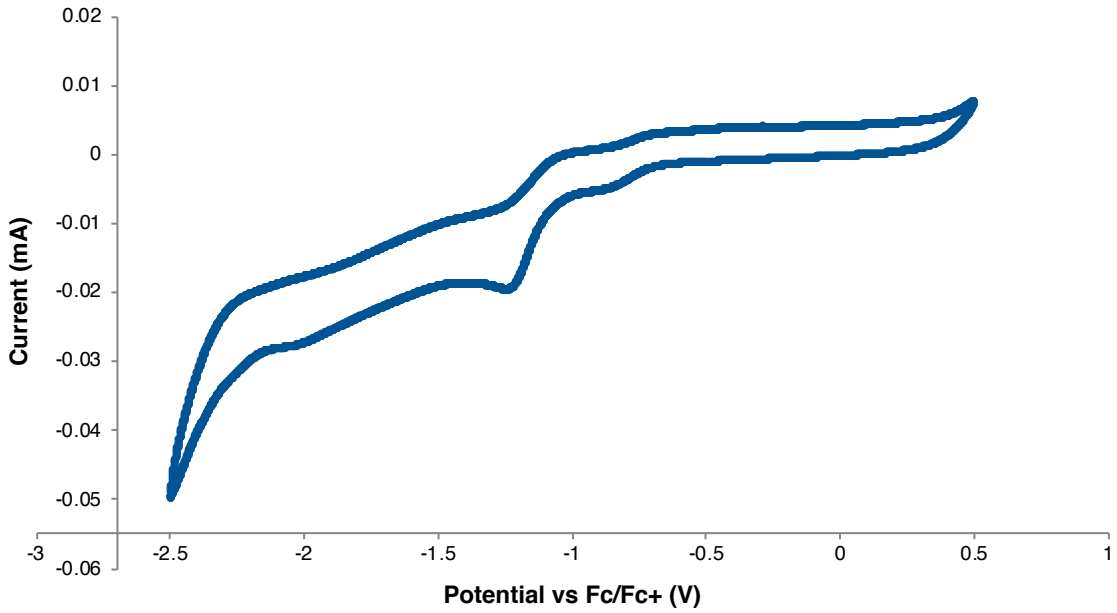

R = Br (46), 100 mV scan rate

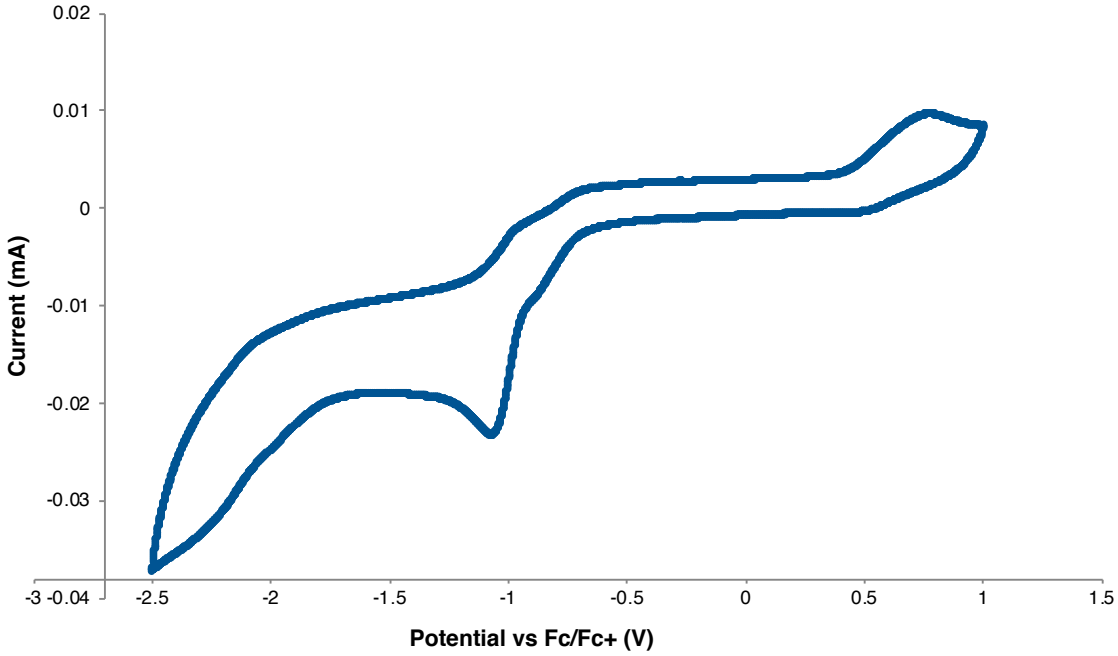

R = Cl (44), 150 mV scan rate

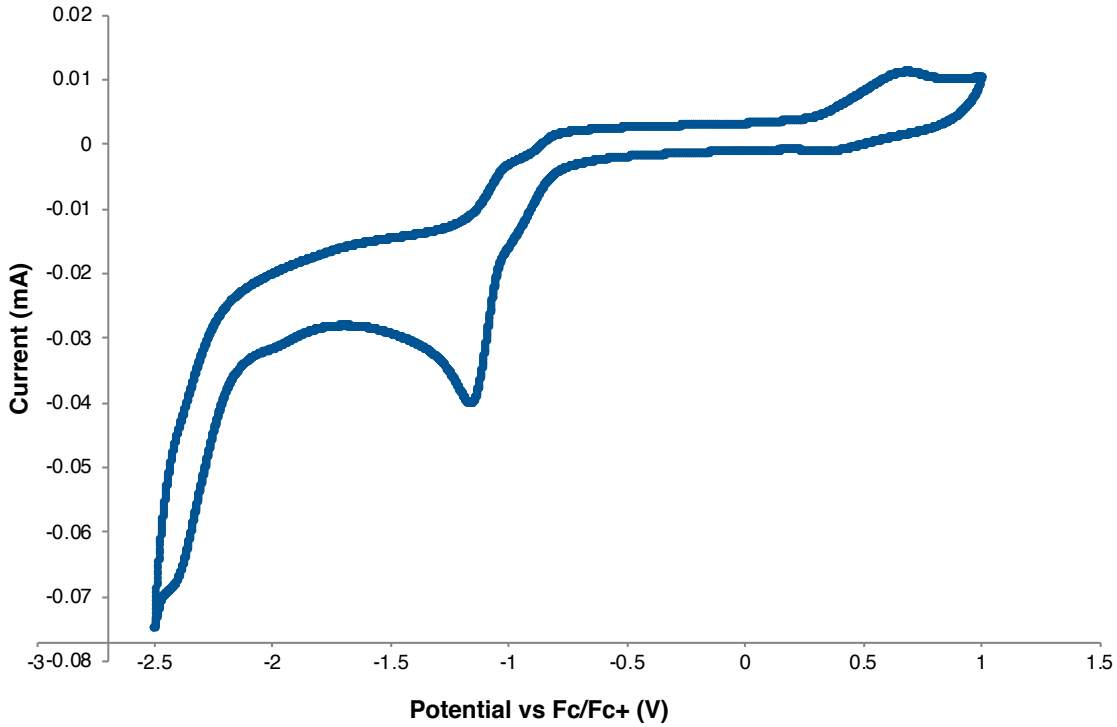

5.8.3 *Synthesis of Dimerization Substrates*

tert-butyl 2-(2,6-dimethoxyphenyl)acetate (121)

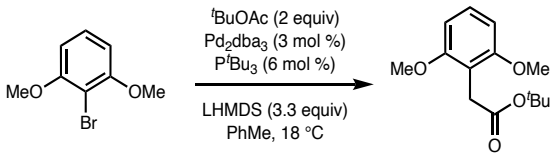

Prepared following a modified procedure:[97] In a N_2-filled glovebox, Pd_2dba_3 (1.37 g, 1.5 mmol, 0.03 equiv), tri-*tert*-butylphosphine (606 mg, 3 mmol, 0.06 equiv), and 2-bromo-1,3-dimethoxybenzene (10.8 g, 50 mmol, 1 equiv) were added to a flame-dried round bottom flask with a stir bar. Also in the glovebox, LiHMDS (27.6 g, 165 mmol, 3.3 equiv) was added to a separate flame-dried round bottom flask with a stir bar. Both flasks were sealed and removed from the glovebox. To the first flask was added PhMe (125 mL,

0.2 M total); the solution was stirred at ambient temperature for 20 min. To the second flask was added PhMe (125 mL, 0.2 M total); the solution was cooled to 0 °C in an ice/water bath, then *tert*-butyl acetate (13.4 mL, 100 mmol, 2 equiv) was added dropwise. This solution was stirred for 20 min at 0 °C and then transferred to the first flask via cannula. The reaction was stirred at ambient temperature for 24 h. Upon complete consumption of the aryl bromide, the reaction was quenched with sat. aq. NH_4Cl (200 mL). The organic layer was separated, and the aqueous layer was extracted with EtOAc twice. Combined organics were washed with brine, dried over Na_2SO_4, filtered, and concentrated. The crude residue was purified by column chromatography (silica, 7% EtOAc/hexanes) to afford **121** (9.96 g, 79% yield) as an amorphous white solid.

^{1}H NMR ($CDCl_3$, 400 MHz): δ 7.18 (t, *J* = 8.3 Hz, 1H), 6.54 (d, *J* = 8.4 Hz, 2H), 3.80 (s, 6H), 3.60 (s, 2H), 1.44 (s, 9H).

^{13}C{^{1}H} NMR ($CDCl_3$, 101 MHz): δ 171.8, 158.5, 128.1, 112.4, 103.8, 80.1, 55.9, 30.2, 28.2.

FTIR (NaCl, thin film, cm^{-1}): 2979, 2968, 2839, 1736, 1599, 1475, 1339, 1142, 1104, 784.

HRMS (FI-MS, *m/z*): $[M]^+$ calcd for $C_{14}H_{20}O_4$: 252.13561; found: 252.1345.

tert-butyl 2-(2,6-dimethoxyphenyl)hexanoate (50)

Procedure 1:

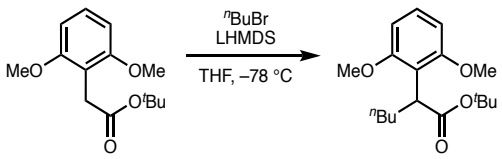

To a flame-dried round bottom flask with a stir bar was added ester **121** (2.46 g, 9.8

mmol, 1 equiv) and THF (101 mL, 0.1 M). The solution was cooled to –78 °C in a dry ice/acetone bath, and LiHMDS (1 M in THF, 17.8 mL, 17.8 mmol, 1.8 equiv) was added dropwise. The reaction was stirred for 1.5 h and then warmed to 0 °C followed by dropwise addition of 1-bromobutane (1.92 mL, 17.8 mmol, 1.8 equiv). The reaction was stirred while warming to ambient temperature and monitored by TLC. Upon complete consumption of the ester, the reaction was quenched with slow addition of water then the layers separated. The aqueous layer was extracted with EtOAc thrice. Combined organics were washed with brine, dried over Na_2SO_4, filtered, and concentrated. The crude residue was purified by column chromatography (silica, 7% EtOAc/hexanes) to afford **50** (2.31 g, 77% yield) as a yellow oil.

Procedure 2:

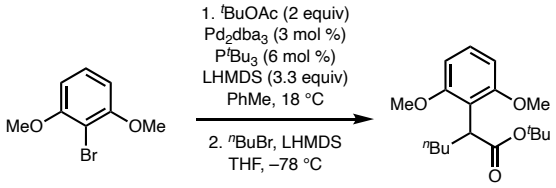

Step 1: Prepared following a modified procedure:[97] In a N_2-filled glovebox, Pd_2dba_3 (1.37 g, 1.5 mmol, 0.03 equiv), tri-*tert*-butylphosphine (606 mg, 3 mmol, 0.06 equiv), and 2-bromo-1,3-dimethoxybenzene (10.8 g, 50 mmol, 1 equiv) were added to a flame-dried round bottom flask with a stir bar. Also in the glovebox, LiHMDS (27.6 g, 165 mmol, 3.3 equiv) was added to a separate flame-dried round bottom flask with a stir bar. Both flasks were sealed and removed from the glovebox. To the first flask was added PhMe (125 mL, 0.2 M total); the solution was stirred at ambient temperature for 20 min. To the second flask was added PhMe (125 mL, 0.2 M total); the solution was cooled to 0 °C in an ice/water bath, then *tert*-butyl acetate (13.4 mL, 100 mmol, 2 equiv) was added

dropwise. This solution was stirred for 20 min at 0 °C and then transferred to the first flask via cannula. The reaction was stirred at ambient temperature for 24 h. Upon complete consumption of the aryl bromide, the reaction was quenched with sat. aq. NH_4Cl (200 mL). The organic layer was separated, and the aqueous layer was extracted with EtOAc twice. Combined organics were washed with brine, dried over Na_2SO_4, filtered, and concentrated. The crude residue was used directly in the next step without purification.

Step 2: To a flame-dried round bottom flask with a stir bar was added the crude residue (1 equiv) as a solution in THF (250 mL, 0.2 M). The solution was cooled to –78 °C in a dry ice/acetone bath, and LiHMDS (1 M in THF, 75.0 mL, 75 mmol, 1.5 equiv) was added slowly. The reaction was stirred for 1 h and then warmed to 0 °C followed by dropwise addition of 1-bromobutane (8.0 mL, 75 mmol, 1.5 equiv). The reaction was allowed to warm to ambient temperature. After 17 h, the reaction was quenched with slow addition of sat. aq. NH_4Cl, diluted with Et_2O, then the layers separated. The aqueous layer was extracted with Et2O. Combined organics were washed with brine, dried over Na_2SO_4, filtered, and concentrated. The crude residue was purified by column chromatography (silica, 1 to 20% EtOAc/hexanes) to afford **50** (10.2 g, 66% yield over 2 steps) as a yellow oil.

^{1}H NMR ($CDCl_3$, 500 MHz): δ 7.15 (t, *J* = 8.3 Hz, 1H), 6.52 (d, *J* = 8.3 Hz, 2H), 4.02 (dd, *J* = 9.1, 5.3 Hz, 1H), 3.78 (s, 6H), 2.07 (ddt, *J* = 13.5, 10.6, 5.4 Hz, 1H), 1.66 (dddd, *J* = 13.2, 9.7, 9.0, 5.2 Hz, 1H), 1.37 (s, 9H), 1.36 – 1.16 (m, 2H), 1.12 – 1.00 (m, 1H), 0.84 (t, *J* = 7.2 Hz, 3H).

^{13}C{^{1}H} NMR ($CDCl_3$, 101 MHz): δ 174.4, 158.1, 127.5, 118.5, 103.9, 79.5, 55.7, 41.0,

29.9, 29.8, 28.14, 22.9, 14.2.

FTIR (NaCl, thin film, cm^{-1}): 2953, 2870, 2837, 1731, 1594, 1455, 1249, 1163, 1119, 853, 724.

HRMS (FI-MS, *m/z*): $[M]^+$ calcd for $C_{18}H_{28}O_4$: 308.1982; found: 308.1978.

tert-butyl 2-(2,6-dimethoxy-4-(4,4,5,5-tetramethyl-1,3,2-dioxaborolan-2-yl)phenyl)hexanoate (51)

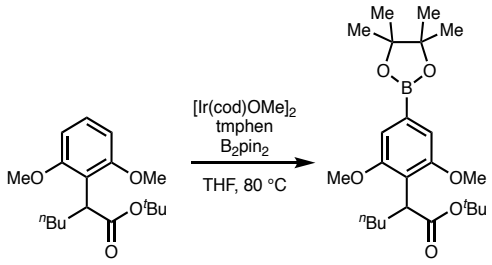

Prepared following a modified procedure:[98] In a N_2-filled glovebox, $[Ir(cod)(OMe)]_2$ (50 mg, 0.08 mmol, 0.01 equiv) and 3,4,7,8-tetramethyl-1,10-phenanthroline (35 mg, 0.15 mmol, 0.02 equiv) were added to a flame-dried round bottom flask with a stir bar. THF (10.0 mL, 0.67 M total) was then added and the dark green mixture was stirred for 1 h. To this mixture was added a solution of ester **50** (2.31 g, 7.5 mmol, 1 equiv) in THF (1.0 mL, 0.67 M total) followed by B_2pin_2 (3.8 g, 15 mmol, 2 equiv). The flask was sealed, removed from the glovebox, and stirred while heating to 80 °C in an oil bath. Upon complete consumption of the ester, as judged by TLC, the reaction was allowed to reach ambient temperature and then concentrated. The crude residue was purified by column chromatography (silica, 5 to 7% EtOAc/hexanes) to afford **51** (2.94 g, 91% yield) as a white amorphous solid.

^{1}H NMR ($CDCl_3$, 400 MHz): δ 6.95 (s, 2H), 4.03 (dd, J = 9.2, 5.2 Hz, 1H), 3.82 (s, 6H),

2.06 (ddt, *J* = 14.7, 10.4, 5.2 Hz, 1H), 1.65 (dh, *J* = 14.4, 5.2 Hz, 1H), 1.36 (d, *J* = 2.0 Hz, 14H), 1.35 (s, 8H), 1.33 – 1.14 (m, 2H), 1.04 (td, *J* = 12.1, 10.8, 5.1 Hz, 1H), 0.82 (t, *J* = 7.1 Hz, 3H).

$^{13}C\{^{1}H\}$ NMR ($CDCl_3$, 101 MHz): δ 174.2, 157.6, 121.9, 109.8, 84.0, 79.5, 55.8, 41.1, 29.78, 29.7, 28.1, 25.1, 25.0, 22.9, 14.2.

^{11}B NMR ($CDCl_3$, 128 MHz): δ 30.6.

FTIR (NaCl, thin film, cm^{-1}): 2976, 2936, 1731, 1406, 1366, 1146, 1128, 968.

HRMS (FI-MS, *m/z*): $[M]^+$ calcd for $C_{24}H_{39}BO_6$: 434.2834; found: 434.2825.

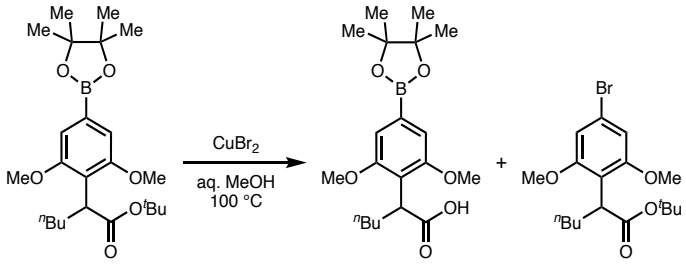

Prepared from boronic ester **51** (950 mg, 2.2 mmol, 1 equiv), $CuBr_2$ (488 mg, 2.2 mmol, 1 equiv), and MeOH/water (1:1, 0.04 M) following a published procedure.[98] The crude mixture in a minimum amount of EtOAc was triturated with cold hexanes to afford acid **122** as a white solid. The supernatant was concentrated and purified by column chromatography (silica, 2% EtOAc/hexanes) to afford ester **52** (673 mg, 79% yield) as a pale yellow amorphous solid.

2-(2,6-dimethoxy-4-(4,4,5,5-tetramethyl-1,3,2-dioxaborolan-2-yl)phenyl)hexanoic acid (122)

^{1}H NMR (DMSO-d_6, 400 MHz): δ 11.74 (s, 1H), 6.87 (s, 2H), 6.86 – 6.81 (m, 0H), 3.92

(dd, *J* = 9.2, 5.3 Hz, 1H), 3.74 (s, 6H), 1.97 (ddt, *J* = 13.2, 10.3, 5.4 Hz, 1H), 1.58 (dtd, *J* = 14.2, 9.3, 5.2 Hz, 1H), 1.30 (s, 13H), 1.27 – 1.20 (m, 0H), 1.20 – 1.05 (m, 3H), 0.95 (tdd, *J* = 12.1, 9.5, 4.7 Hz, 1H), 0.78 (t, *J* = 7.1 Hz, 3H).

$^{13}C\{^{1}H\}$ NMR (DMSO-d_6, 101 MHz): δ 174.8, 157.3, 121.0, 109.6, 83.8, 55.8, 29.2, 24.7, 24.6, 22.1, 13.9.

FTIR (ATR, cm^{-1}): 2932, 2360, 1704, 1405, 11364, 1127.

HRMS (TOF-ESI, *m/z*): $[M + H]^+$ calcd for $C_{20}H_{31}BO_6$: 378.2323; found: 378.2337.

***tert*-butyl 2-(4-bromo-2,6-dimethoxyphenyl)hexanoate (52)**

^{1}H NMR ($CDCl_3$, 400 MHz): δ 6.67 (s, 2H), 3.95 (dd, *J* = 9.3, 5.2 Hz, 1H), 3.76 (s, 6H), 2.03 (ddt, *J* = 13.3, 10.3, 5.3 Hz, 1H), 1.69 – 1.55 (m, 1H), 1.36 (s, 9H), 1.33 – 1.10 (m, 2H), 1.02 (dddd, *J* = 16.5, 12.8, 8.9, 5.3 Hz, 1H), 0.82 (t, *J* = 7.1 Hz, 3H).

$^{13}C\{^{1}H\}$ NMR ($CDCl_3$, 101 MHz): δ 173.8, 158.5, 120.6, 117.5, 107.8, 79.7, 55.9, 40.8, 29.8, 29.5, 28.1, 22.8, 14.2.

FTIR (NaCl, thin film, cm^{-1}): 2959, 2936, 1731, 1584, 1405, 1166, 1157, 1127, 816.

HRMS (FI-MS, *m/z*): $[M]^+$ calcd for $C_{18}H_{27}BrO_4$: 386.1087; found: 386.1074.

2-(4-bromo-2,6-dimethoxyphenyl)hexanoic acid (123)

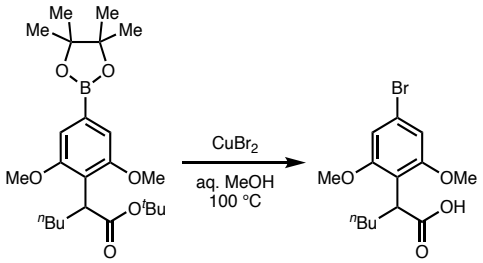

Prepared following a modified procedure:[98] To a three-neck flask with reflux condenser

and stir bar was added $CuBr_2$ (9.02 g, 40.4 mmol, 3 equiv) and water (135 mL, 0.05 M). To this mixture was added boronic ester **51** (5.85 g, 13.5 mmol, 1 equiv) as a solution in MeOH (135 mL, 0.05 M), then the reaction was stirred while heating to 100 °C in an oil bath and monitored by LCMS. Upon complete conversion to acid **123**, the reaction was allowed to reach ambient temperature and diluted with excess sat. aq. NH_4Cl (until all solids dissolved). Following extraction thrice with Et_2O, the combined organics were washed with brine, dried over Na_2SO_4, filtered, and concentrated. The crude residue was purified by column chromatography (silica, 50% EtOAc/hexanes) to afford **123** (3.68 g, 83% yield) as a white amorphous solid.

^{1}H NMR ($CDCl_3$, 400 MHz): δ 6.73 (s, 2H), 4.13 (dd, *J* = 9.1, 5.3 Hz, 1H), 3.81 (s, 6H), 2.09 (ddt, *J* = 13.3, 10.3, 5.3 Hz, 1H), 1.78 – 1.64 (m, 1H), 1.44 – 1.16 (m, 3H), 1.16 – 0.98 (m, 1H), 0.85 (t, *J* = 7.1 Hz, 3H).

^{13}C{^{1}H} NMR ($CDCl_3$, 101 MHz): δ 178.8, 158.6, 121.5, 116.2, 108.2, 56.2, 39.6, 29.7, 29.5, 22.8, 14.2.

FTIR (ATR, cm^{-1}): 3215, 2646, 1700, 1582, 1453, 1404, 1220, 1124, 1099, 843, 811. 5-012-c2

HRMS (FD-MS, *m/z*): $[M]^+$ calcd for $C_{14}H_{19}BrO_4$: 330.0461; found: 330.0471.

(6-iodohex-1-yn-1-yl)trimethylsilane (54)

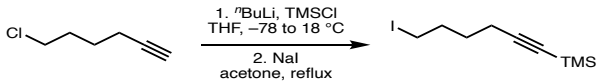

Step 1: Prepared from 6-chlorohex-1-yne (22.0 mL, 182 mmol, 1 equiv), TMSCl (25.3 mL, 200 mmol, 1.1 equiv), ^{n}BuLi (2.0 M in hexanes, 100 mL, 200 mmol, 1.1 equiv), and THF (363 mL, 0.5 M) following a published procedure[152] to afford the alkyne

intermediate. Spectra matched those reported in the literature.[153,154]

Step 2: Prepared from the protected alkyne intermediate (14.1 g, 74.6 mmol, 1 equiv), sodium iodide (67.1 g, 448 mmol, 6 equiv), and acetone (186 mL, 0.4 M) following a published procedure[155] to afford **54** (19.6 g, 93% yield over 2 steps) as a colorless oil. Spectra matched those reported in the literature.[155]

^{1}H NMR ($CDCl_3$, 400 MHz): δ 3.22 (t, J = 6.9 Hz, 2H), 2.26 (t, J = 7.0 Hz, 2H), 1.94 (p, J = 7.0 Hz, 2H), 1.63 (p, J = 7.1 Hz, 2H), 0.15 (s, 9H).

^{13}C{^{1}H} NMR ($CDCl_3$, 101 MHz): δ 106.6, 85.4, 32.5, 29.3, 19.0, 6.4, 0.3.

***tert*-butyl 2-(2,6-dimethoxy-4-(6-(trimethylsilyl)hex-5-yn-1-yl)phenyl)hexanoate (55)**

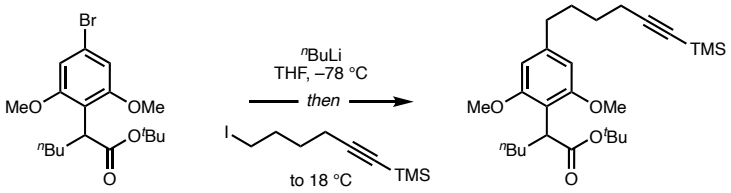

To a flame-dried round bottom flask with a stir bar was added aryl bromide **52** (60 mg, 0.16 mmol, 1 equiv) and THF (0.78 mL, 0.2 M). The solution was cooled to –78 °C in a dry ice/acetone bath, then ^{n}BuLi (2.5 M in hexanes, 0.075 mL, 0.19 mmol, 1.2 equiv) was added dropwise. The reaction was stirred at –78 °C for 30 min, then alkyl iodide **54** (87 mg, 0.31 mmol, 2 equiv) was added via syringe, and the reaction was allowed to warm to ambient temperature and then stir for 5 h before being quenched with sat. aq. NH_4Cl. The layers were separated, and the aqueous layer was extracted with EtOAc thrice. Combined organics were washed with brine, dried over Na_2SO_4, filtered, and concentrated. The crude residue was purified by column chromatography (silica, 2% Et_2O/hexanes) to afford **55** (51 mg, 71% yield) as a colorless oil.

^{1}H NMR ($CDCl_3$, 400 MHz): δ 6.34 (s, 2H), 3.96 (dd, *J* = 8.9, 5.4 Hz, 1H), 3.75 (s, 6H), 2.63 – 2.55 (m, 2H), 2.26 (t, *J* = 7.1 Hz, 2H), 2.11 – 1.98 (m, 1H), 1.74 (tt, *J* = 9.0, 6.7 Hz, 2H), 1.69 – 1.49 (m, 6H), 1.33 – 1.14 (m, 3H), 1.06 (qd, *J* = 11.9, 10.8, 7.2 Hz, 1H), 0.83 (t, *J* = 7.0 Hz, 3H), 0.15 (s, 8H).

^{13}C{^{1}H} NMR ($CDCl_3$, 101 MHz): δ 174.5, 157. 9, 142.1, 115.8, 104.1, 79.4, 55.7, 40.9, 36.1, 30.5, 30.0, 28.4, 28.2, 22.9, 19.9, 14.2, 0.3.

FTIR (ATR, cm^{-1}): 3000, 2171, 1726, 1455, 1248, 1157, 1122, 841.

HRMS (FI-MS, *m/z*): $[M]^+$ calcd for $C_{27}H_{44}O_4Si$: 460.3003; found: 460.2989.

***tert*-butyl 2-(4-(hex-5-yn-1-yl)-2,6-dimethoxyphenyl)hexanoate (124)**

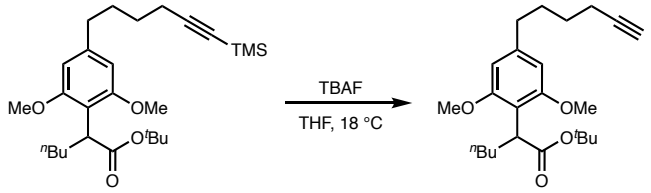

To a flame-dried round bottom flask with a stir bar was added protected alkyne **55** (60 mg, 0.09 mmol, 1 equiv) followed by THF (4.3 mL, 0.02 M) then tetrabutylammonium fluoride (0.048 mL, 0.17 mmol, 2 equiv). The reaction was stirred at ambient temperature for 5 min and then quenched with sat. aq. Na_2HCO_3. The layers were separated, and combined organics were washed with water thrice, dried over Na_2SO_4, filtered, and concentrated to afford **124** (33 mg, 99% yield) as a colorless oil.

^{1}H NMR ($CDCl_3$, 400 MHz): δ 6.34 (s, 2H), 3.95 (dt, *J* = 8.6, 4.3 Hz, 1H), 3.75 (s, 6H), 2.64 – 2.55 (m, 2H), 2.23 (td, *J* = 7.1, 2.7 Hz, 2H), 2.04 (ddt, *J* = 13.4, 10.5, 5.4 Hz, 1H), 1.95 (t, *J* = 2.6 Hz, 1H), 1.82 – 1.69 (m, 2H), 1.69 – 1.56 (m, 6H), 1.36 (s, 9H), 1.34 – 1.15 (m, 3H), 1.11 – 1.00 (m, 1H), 0.83 (t, *J* = 7.0 Hz, 3H).

$^{13}C\{^{1}H\}$ NMR ($CDCl_3$, 101 MHz): δ 174.5, 157.9, 141.9, 115.9, 104.1, 84.6, 79.4, 68.5, 66.0, 55.7, 40.9, 36.1, 30.4, 29.9, 29.9, 28.3, 28.2, 22.9, 18.5, 15.4, 14.2.

FTIR (ATR, cm^{-1}): 2962, 2875, 2359, 2323, 1574, 1462, 1401, 1250, 1156, 1123, 1010, 735.

HRMS (FD, m/z): $[M]^+$ calcd for $C_{24}H_{36}O_4$: 388.2614; found: 388.2618

***tert*-butyl (*E*)-2-(4-(6-bromohex-5-en-1-yl)-2,6-dimethoxyphenyl)hexanoate (56)**

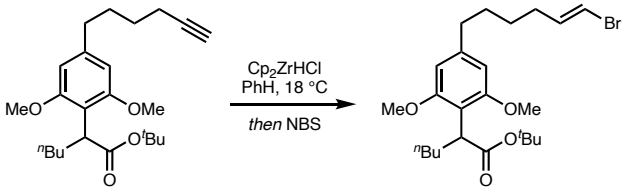

Prepared from alkyne **124** (34 mg, 0.09 mmol, 1 equiv), Cp_2ZrHCl (28 mg, 0.1 mmol, 1.25 equiv), *N*-bromosuccinimide (19 mg, 0.1 mmol, 1.25 equiv), and PhH (0.87 mL, 0.1 M) following a published procedure[156] to afford **56** (41 mg, 82% yield) as a colorless oil.

^{1}H NMR ($CDCl_3$, 400 MHz): δ 6.32 (s, 2H), 6.17 (dt, *J* = 14.2, 7.2 Hz, 1H), 6.05 – 5.98 (m, 1H), 3.96 (dd, *J* = 9.0, 5.3 Hz, 1H), 3.76 (d, *J* = 0.6 Hz, 6H), 2.61 – 2.54 (m, 2H), 2.13 – 2.00 (m, 2H), 1.64 (p, *J* = 7.7 Hz, 3H), 1.51 – 1.42 (m, 2H), 1.37 (d, *J* = 0.7 Hz, 9H), 1.34 – 1.17 (m, 1H), 1.12 – 1.02 (m, 1H), 0.84 (t, *J* = 7.1 Hz, 3H).

$^{13}C\{^{1}H\}$ NMR ($CDCl_3$, 101 MHz): δ 174.5, 157.9, 142.0, 138.1, 115.9, 104.4, 104.1, 79.4, 55.7, 40.9, 36.4, 32.9, 30.7, 30.0, 29.9, 28.4, 28.2, 28.0, 22.9, 14.2.

1,3-dioxoisoindolin-2-yl (*E*)-2-(4-(6-bromohex-5-en-1-yl)-2,6-dimethoxyphenyl)hexanoate (57)

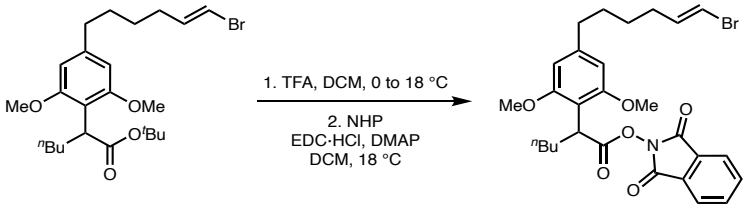

Step 1: To a round bottom flask with a stir bar was added ester **56** (33 mg, 0.07 mmol, 1 equiv) and DCM (0.7 mL, 0.1 M). The solution was cooled to 0 °C in an ice/water bath, then trifluoroacetic acid (0.054 mL, 10 equiv) was added dropwise. The solution was warmed to 18 °C over 1 hour and then concentrated. The crude residue was azeotroped with PhMe to afford the acid intermediate (29 mg).

Step 2: To a round bottom flask with a stir bar was added the acid intermediate (29 mg, 0.07 mmol, 1 equiv), *N*-hydroxyphthalimide (12 mg, 0.07 mmol, 1 equiv), DMAP (1.7 mg, 0.01 mmol, 0.2 equiv), then DCM (0.35 mL, 0.2 M). Then EDC·HCl (15 mg, 0.08 mmol, 1.1 equiv) was added in one portion. The reaction was stirred at 18 °C overnight and then concentrated. The crude residue was purified by preparative thin layer chromatography (silica, 40% Et_2O/hexanes) to afford **57** (25 mg, 63% yield over 2 steps) as a white amorphous solid.

^{1}H NMR ($CDCl_3$, 400 MHz): δ 7.84 (t, *J* = 4.3 Hz, 2H), 7.74 (dd, *J* = 5.5, 3.1 Hz, 2H), 6.18 (dt, *J* = 14.1, 7.2 Hz, 1H), 6.07 – 5.98 (m, 1H), 4.47 (dd, *J* = 8.8, 5.4 Hz, 1H), 3.85 (s, 6H), 2.60 (t, *J* = 7.8 Hz, 2H), 2.17 (ddt, *J* = 13.4, 10.5, 5.3 Hz, 1H), 2.09 (qd, *J* = 7.3, 1.3 Hz, 2H), 1.83 (ddp, *J* = 13.7, 9.0, 4.9, 4.4 Hz, 1H), 1.72 – 1.61 (m, 2H), 1.47 (dq, *J* = 13.1, 6.7, 5.8 Hz, 2H), 1.41 – 1.21 (m, 3H), 0.86 (t, *J* = 6.9 Hz, 3H).

^{13}C{^{1}H} NMR ($CDCl_3$, 101 MHz): δ 171.5, 157.8, 143.6, 138.1, 134.6, 129.2, 123.8,

112.1, 104.5, 103.9, 55.8, 37.8, 36.6, 33.0, 30.7, 29.9, 29.3, 28.5, 22.7, 14.1.

FTIR (ATR, cm^{-1}): 2933, 2857, 1788, 1745, 1587, 1462, 1119, 697.

HRMS (FD, *m/z*): $[M]^+$ calcd for $C_{28}H_{32}NO_6Br$: 557.1413; found: 557.1392.

6-(trimethylsilyl)hex-5-ynoic acid (58)

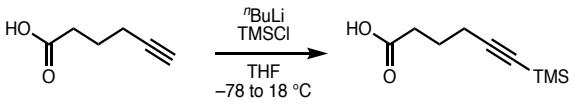

Prepared from 5-hexynoic acid (1.1 mL, 10 mmol, 1 equiv), ^{n}BuLi (2.5 M in hexanes, 8.4 mL, 21 mmol, 2.1 equiv), TMSCl (2.9 mL, 22.8 mmol, 2.28 equiv), and THF (100 mL, 0.1 M) following a published procedure[102] to afford **58** (1.42 g, 77% yield) as a yellow oil. Spectra matched those reported in the literature.[102]

^{1}H NMR ($CDCl_3$, 300 MHz): δ 2.50 (td, *J* = 7.5, 0.9 Hz, 2H), 2.37 – 2.26 (m, 2H), 1.92 – 1.76 (m, 2H), 0.23 – 0.05 (m, 9H).

^{13}C{^{1}H} NMR ($CDCl_3$, 101 MHz): δ 178.4, 105.6, 85.6, 32.4, 32.4, 23.3, 19.1, 0.0.

***N*-((1*S*,2*S*)-1-hydroxy-1-phenylpropan-2-yl)-*N*-methyl-6-(trimethylsilyl)hex-5-ynamide (125)**

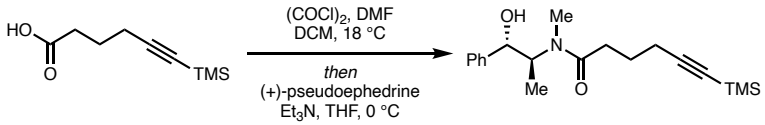

To a flame-dried round bottom flask with a stir bar and vent needle was added acid **58** (500 mg, 2.7 mmol, 1 equiv) and DCM (27 mL, 0.1 M). Oxalyl chloride (0.25 mL, 3.0 mmol, 1.1 equiv) was added dropwise, followed by a single drop of DMF; gas evolution immediately occurred. The reaction was allowed to stir at ambient temperature overnight

before being concentrated to afford a yellow oil. To a separate flame-dried round bottom flask with a stir bar was added (1*S*,2*S*)-(+)-pseudoephedrine (448 mg, 2.7 mmol, 1 equiv) and THF (7 mL). This solution was treated with triethylamine (0.49 mL, 3.5 mmol, 1.3 equiv) then cooled to 0 °C in an ice/water bath. To this flask was added a solution of the recently prepared acid chloride in THF (7 mL, total 0.2 M). The reaction mixture was allowed to stir at 0 °C for 1 h before being quenched with brine and extracted with EtOAc thrice. Combined organic layers were dried over Na_2SO_4, filtered, and concentrated. The crude residue was purified by column chromatography (silica, 30 to 60% EtOAc/hexanes) to afford **125** (593 mg, 66% yield) as a pale yellow oil.

^{1}H NMR ($CDCl_3$, 400 MHz; 3:1 rotamer ratio, asterisk denotes minor rotamer): δ 7.42 – 7.23 (m, 5H), 4.61 (d, J = 6.8 Hz, 1H), 4.58* (d, J = 9.7 Hz, 1H), 4.46 (s, 1H), 4.05* (p, J = 6.9 Hz, 1H), 2.93* (s, 1H), 2.85 (s, 3H), 2.64* (dt, J = 15.2, 7.4 Hz, 1H), 2.52* (t, J = 7.7 Hz, 1H), 2.49 – 2.36 (m, 2H), 2.36 – 2.22 (m, 3H), 1.89* (p, J = 7.0 Hz, 1H), 1.88 – 1.76 (m, 2H), 1.13 (d, J = 7.0 Hz, 3H), 1.00* (d, J = 6.8 Hz, 1H), 0.15 (s, 9H), 0.14* (s, 3H).

^{13}C{^{1}H} NMR ($CDCl_3$, 101 MHz; 3:1 rotamer ratio, asterisk denotes minor rotamer): δ 175.0, 173.7*, 142.6, 141.2*, 128.9, 128.7*, 128.6*, 127.9, 127.1*, 126.5, 106.7, 85.5, 75.7, 58.4, 32.9*, 32.3, 24.2*, 24.0, 19.6*, 19.4, 15.4*, 14.6, 0.3.

FTIR (NaCl, thin film, cm^{-1}): 3388, 2961, 2899, 2173, 1633, 1453, 1250, 1121, 1041, 840, 758.

HRMS (TOF-ESI, *m/z*): $[M - H_2O + H]^+$ calcd for $C_{19}H_{28}NOSi$: 314.1935; found: 314.1926.

$\boxed{[\alpha]_D^{22} =}$ +73 (c = 1.0, $CHCl_3$).

(*S*)-*N*-((1*S*,2*S*)-1-hydroxy-1-phenylpropan-2-yl)-*N*,2-dimethyl-6-(trimethylsilyl)hex-5-ynamide (59)

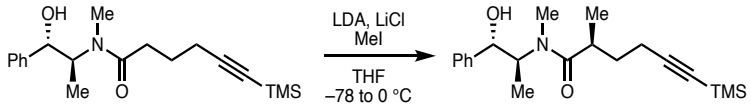

Prepared from lithium chloride (283 mg, 6.7 mmol, 6 equiv), $^{i}Pr_2NH$ (0.36 mL, 2.6 mmol, 2.3 equiv), ^{n}BuLi (2.5 M in hexanes, 0.94 mL, 2.3 mmol, 2.1 equiv), amide **125** (369 mg, 1.1 mmol, 1 equiv), methyl iodide (0.10 mL, 1.7 mmol, 1.5 equiv), and THF (6.0 mL, 0.2 M) following a published procedure.[101] The crude residue was purified by column chromatography (silica, 40 to 50% EtOAc/hexanes) to afford **59** (248 mg, 64% yield) as an orange oil.

^{1}H NMR ($CDCl_3$, 400 MHz; 3:1 rotamer ratio, asterisk denotes minor rotamer): δ 7.42 – 7.20 (m, 6H), 4.64 (t, *J* = 6.4 Hz, 1H), 4.60* (d, *J* = 8.6 Hz, 1H), 4.34 (s, 1H), 4.23* (p, *J* = 6.9 Hz, 1H), 3.13 – 3.01* (m, 1H), 2.94* (s, 3H), 2.93 – 2.87 (m, 1H), 2.86 (s, 3H), 2.33 – 2.02 (m, 2H), 1.95 – 1.81 (m, 1H), 1.59 – 1.45 (m, 1H), 1.18 (dd, *J* = 8.8, 6.9 Hz, 3H), 1.04 (t, *J* = 6.6 Hz, 3H), 0.13 (s, 9H), 0.05* (s, 3H).

^{13}C{^{1}H} NMR ($CDCl_3$, 101 MHz; 3:1 rotamer ratio, asterisk denotes minor rotamer): δ 177.4, 176.5*, 141.6, 140.2*, 127.9*, 127.6*, 127.5, 126.7, 126.0*, 125.4, 106.0, 84.4, 75.6, 74.7, 57.3, 34.1, 33.3*, 32.5*, 31.6, 17.0*, 17.0*, 16.8, 16.3, 14.9*, 13.6, –0.7.

FTIR (NaCl, thin film, cm^{-1}): 3378, 2963, 2933, 2172, 1618, 1249, 841, 756.

HRMS (TOF-ESI, *m/z*): $[M + H]^+$ calcd for $C_{20}H_{32}NO_2Si$: 346.2197; found: 346.2206.

$\boxed{[\alpha]_D^{22} =}$ +149 (c = 0.4, $CHCl_3$).

(*S*)-2-methyl-6-(trimethylsilyl)hex-5-yn-1-ol (126)

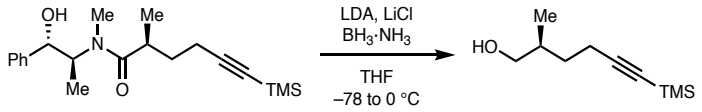

Prepared from $^{i}Pr_2NH$ (0.15 mL, 1.1 mmol, 4 equiv), ^{n}BuLi (2.5 M in hexanes, 0.43 mL, 1.1 mmol, 4 equiv), borane·ammonia complex (33 mg, 1.1 mmol, 4 equiv), amide **59** (94 mg, 0.27 mmol, 1 equiv), and THF (3.5 mL, 0.1 M) following a published procedure.[103] The crude residue was purified by column chromatography (silica, 30% EtOAc/hexanes) to afford **126** (36 mg, 72% yield) as a colorless oil.

^{1}H NMR ($CDCl_3$, 400 MHz): δ 3.57 – 3.44 (m, 2H), 2.38 – 2.17 (m, 2H), 1.83 – 1.60 (m, 1H), 1.46 – 1.32 (m, 2H), 0.94 (d, J = 6.7 Hz, 3H), 0.14 (s, 9H).

^{13}C{^{1}H} NMR ($CDCl_3$, 101 MHz): δ 106.6, 83.7, 66.8, 34.7, 31.1, 16.7, 15.4, –0.7.

FTIR (NaCl, thin film, cm^{-1}): 3340, 2957, 2929, 2174, 1249, 1039, 843, 759.

HRMS (TOF-ESI, *m/z*): $[M + H]^+$ calcd for $C_{10}H_{21}OSi$: 185.1356; found: 185.1361.

$\boxed{[\alpha]_D^{22} =}$ –4 (c = 0.2, $CHCl_3$).

To determine the absolute configuration and enantiomeric excess of alcohol **126**, both Mosher acids were prepared and analyzed: configuration as drawn and 92% ee.

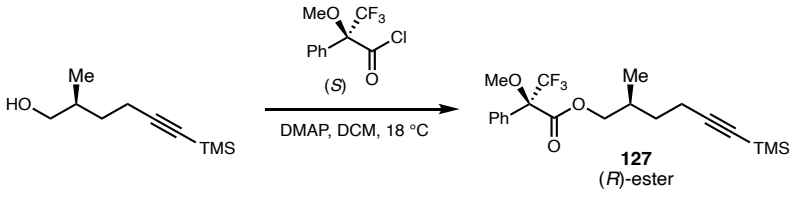

Prepared from (*S*)-(–)-α-methoxy-α-(trifluoromethyl)phenylacetyl chloride (31 μL, 0.16 mmol, 3 equiv), DMAP (26.5 mg, 0.22 mmol, 4 equiv), alcohol **126** (10.0 mg, 0.054

mmol, 1 equiv), and DCM (1 mL, 0.054 M) following a published procedure.[149] Crude **127** was analyzed by ^{1}H NMR.

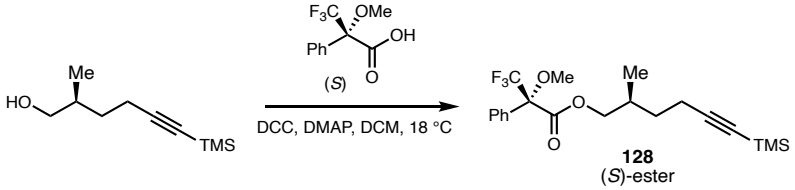

Prepared from (*S*)-(–)-α-methoxy-α-(trifluoromethyl)phenylacetic acid (39.4 mg, 0.168 mmol, 3.1 equiv), DMAP (20.5 mg, 0.168 mmol, 3.1 equiv), DCC (39 μL, 0.168 mmol, 3.1 equiv), alcohol **126** (10.0 mg, 0.054 mmol, 1 equiv), and DCM (1 mL, 0.054 M) following a published procedure.[149] Crude **128** was analyzed by ^{1}H NMR.

(*S*)-(6-iodo-5-methylhex-1-yn-1-yl)trimethylsilane (60)

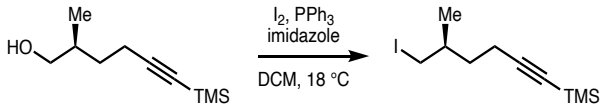

Prepared from alcohol **126** (36 mg, 0.2 mmol, 1 equiv), iodine (50 mg, 0.2 mmol, 1 equiv), imidazole (40 mg, 0.6 mmol, 3 equiv), triphenylphosphine (52 mg, 0.2 mmol, 1 equiv), and DCM (2 mL, 0.1 M) following a published procedure.[103] The crude residue was purified by column chromatography (silica, 0 to 20% EtOAc/hexanes) to afford **60** (34 mg, 59% yield) as a colorless oil.

^{1}H NMR ($CDCl_3$, 400 MHz): δ 3.26 (dd, *J* = 9.8, 4.3 Hz, 1H), 3.20 (dd, *J* = 9.8, 5.3 Hz, 1H), 2.34 – 2.17 (m, 2H), 1.68 – 1.55 (m, 1H), 1.53 – 1.38 (m, 1H), 1.33 – 1.23 (m, 1H), 1.02 – 0.97 (m, 3H), 0.15 (s, 9H).

^{13}C{^{1}H} NMR ($CDCl_3$, 101 MHz): δ 105.58, 84.27, 34.05, 32.65, 19.45, 16.64, 16.25, -

0.73.

FTIR (NaCl, thin film, cm^{-1}): 2959, 2934, 2174, 1248, 837, 758.

HRMS (FI-MS, *m/z*): $[M]^+$ calcd for $C_{10}H_{19}SiI$: 294.0295; found: 294.0268.

$\boxed{[\alpha]_D^{22} =}$ +9 (c = 0.2, $CHCl_3$).

***tert*-butyl 2-(4-bromophenyl)hexanoate (77)**

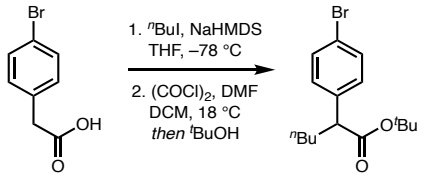

Step 1: To a flame-dried round bottom flask with a stir bar was added 4-bromophenylacetic acid (10.4 g, 48.3 mmol, 1 equiv) and THF (97 mL, 0.5 M). Then, NaHMDS (1 M in THF, 100 mL, 100 mmol, 2.07 equiv) was added via cannula. The mixture was stirred vigorously, slowly turning into a red homogenous solution, at which point 1-iodobutane (5.77 mL, 50.7 mmol, 1.05 equiv) was added. The reaction was stirred at ambient temperature for 20 h, then water was added. The mixture was washed with Et_2O twice. The aqueous layer was acidified with 1 M HCl to pH = 1 and then extracted with Et_2O. The organic layer was washed with brine, dried over Na_2SO_4, filtered, and concentrated. The crude oil was used in the next step without further purification.

Step 2: To a flame-dried round bottom flask with a stir bar was added the intermediate acid and DCM (39 mL, 1.2 M). Then, $(COCl)_2$ (4.7 mL, 55.6 mmol, 1.15 equiv) and DMF (0.78 mL, 10 mmol, 0.2 equiv) were added sequentially, and the reaction was stirred at ambient temperature for 2 h. The reaction was concentrated, then

the residue was diluted in DCM (23 mL, 2.1 M) and ^{t}BuOH (23.4 mL, 244 mmol, 5.1 equiv) was added. The reaction was stirred overnight and then diluted with DCM and washed with sat. aq. $NaHCO_3$. The aqueous layer was extracted once with DCM. Combined organics were washed with sat. aq. $Na_2S_2O_3$ to remove any remaining color, dried over Na_2SO_4, filtered, and concentrated to afford **77** (10.2 g, 64% yield over 2 steps) as a red oil.

^{1}H NMR ($CDCl_3$, 400 MHz): δ 7.45 – 7.40 (m, 2H), 7.19 – 7.14 (m, 2H), 3.37 (t, *J* = 7.7 Hz, 1H), 1.99 (dddd, *J* = 13.2, 9.8, 8.0, 5.5 Hz, 1H), 1.67 (dddd, *J* = 13.3, 9.5, 7.4, 5.7 Hz, 1H), 1.39 (s, 9H), 1.36 – 1.25 (m, 2H), 0.87 (t, *J* = 7.2 Hz, 3H).

^{13}C{^{1}H} NMR ($CDCl_3$, 101 MHz): δ 173.1, 139.1, 131.6, 129.8, 120.9, 80.9, 52.3, 33.3, 29.8, 28.1, 22.6, 14.0.

FTIR (ATR, cm^{-1}): 1725, 1614, 1487, 1367, 1254, 1144, 1073, 1011.

HRMS (FD-MS, *m/z*): $[M]^+$ calcd for $C_{16}H_{23}O_2Br$: 326.0876; found: 326.0876.

***tert*-butyl 2-(4-(6-(trimethylsilyl)hex-5-yn-1-yl)phenyl)hexanoate (79)**

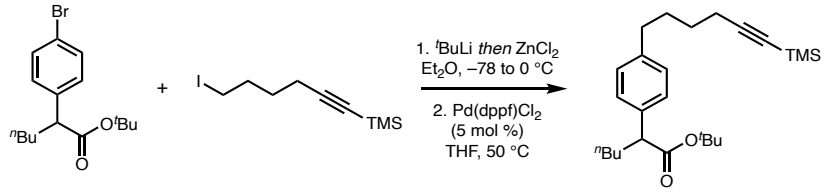

Small Scale:

Prepared from aryl bromide **77** (34 mg, 0.1 mmol, 1 equiv), alkyl iodide **54** (61 mg, 0.21 mmol, 2 equiv), ^{t}BuLi (1.7 M in pentane, 0.32 mL, 0.54 mmol, 5.17 equiv), $ZnCl_2$ (0.5 M in THF, 0.42 mL, 0.21 mmol, 2 equiv), and $Pd(dppf)Cl_2$ (3.9 mg, 0.005 mmol, 0.05 equiv) following a published procedure.[73] The crude residue was purified by preparative

thin layer chromatography (silica, 5% EtOAc/hexanes) to afford **79** (31 mg, 73% yield) as a colorless oil.

Large Scale:

To a flame-dried round bottom flask with a stir bar containing Et_2O (82 mL) and cooled to –78 °C in a dry ice/acetone bath was slowly added ^{t}BuLi (1.7 M in pentane, 41 mL, 69.0 mmol, 3.15 equiv). Alkyl iodide **54** (9.21 g, 32.8 mmol, 1.5 equiv) was added dropwise via syringe at a rate such that the internal reaction temperature remained below –70 °C; this solution was stirred at –78 °C for 30 minutes. (Note: allowing the reaction to warm above –70 °C often resulted in alkyl iodide degradation.) Then, $ZnCl_2$ (0.5 M in THF, 4.4 mL, 32.8 mmol, 1.5 equiv) was added slowly such that the internal reaction temperature remained below –70 °C; this solution was stirred at –78 °C for 1 h. To a separate flame-dried 3-neck flask with a stir bar and a reflux condenser was added $Pd(dppf)Cl_2$ (801 mg, 1.09 mmol, 0.05 equiv) and THF (22 mL, 1 M), followed by aryl bromide **77** (7.17 g, 21.9 mmol, 1 equiv); this suspension was cooled to 0 °C in an ice/water bath. The original solution was warmed to 0 °C then immediately transferred via cannula to the 3-neck flask. The resulting mixture was heated in an oil bath set to 50 °C overnight. (Note: over the course of the reaction, the color generally changed from yellow to green to red.) Upon complete consumption of the aryl bromide, as judged by TLC, the reaction was allowed to reach room temperature then quenched with water. The organic layer was separated, and the aqueous layer was extracted with Et_2O twice. Combined organics were washed with brine, dried over Na_2SO_4, filtered, and concentrated. The crude residue was purified by column chromatography (silica, 2% Et_2O/hexanes) to afford **79** (4.3 g, 49% yield) as a pale yellow oil.

^{1}H NMR ($CDCl_3$, 400 MHz): δ 7.23 – 7.17 (m, 2H), 7.14 – 7.08 (m, 2H), 3.38 (dd, *J* = 8.4, 7.0 Hz, 1H), 2.60 (t, *J* = 7.7 Hz, 2H), 2.24 (t, *J* = 7.1 Hz, 2H), 2.00 (dddd, *J* = 13.3, 9.5, 8.3, 5.3 Hz, 1H), 1.79 – 1.61 (m, 3H), 1.61 – 1.50 (m, 3H), 1.40 (s, 9H), 1.37 – 1.28 (m, 2H), 1.28 – 1.16 (m, 1H), 0.87 (t, *J* = 7.1 Hz, 3H), 0.14 (s, 9H).

^{13}C{^{1}H} NMR ($CDCl_3$, 101 MHz): δ 173.8, 140.9, 137.4, 128.5, 127.8, 107.5, 84.7, 80.5, 52.5, 35.1, 33.6, 30.5, 30.0, 28.3, 28.1, 22.7, 19.9, 14.1, 0.3.

FTIR (ATR, cm^{-1}): 2174, 1727, 1367, 1248, 1145, 1020, 840, 758.

HRMS (FD-MS, *m/z*): $[M]^+$ calcd for $C_{25}H_{40}O_2Si$: 400.2792; found: 400.2792.

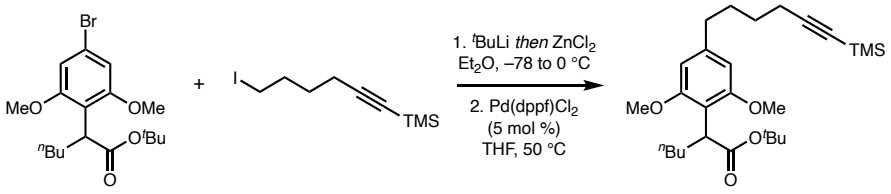

Prepared from aryl bromide **52** (250 m, 0.65 mmol, 1 equiv), alkyl iodide **54** (362 mg, 1.3 mmol, 2 equiv), ^{t}BuLi (1.7 M in pentane, 1.6 mL, 2.7 mmol, 4.2 equiv), $ZnCl_2$ (0.5 M in THF, 2.6 mL, 1.3 mmol, 2 equiv), and $Pd(dppf)Cl_2$ (24 mg, 0.32 mmol, 0.05 equiv) following a published procedure.[73] The crude residue was purified by column chromatography (silica, 80% PhMe/hexanes) to afford **55** (160 mg, 54% yield) as a colorless oil.

1,3-dioxoisoindolin-2-yl 2-(4-bromophenyl)hexanoate (80)

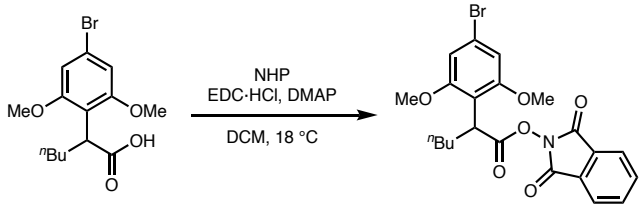

To a round bottom flask with a stir bar was added acid **23** (100 mg, 0.30 mmol, 1 equiv), *N*-hydroxyphthalimide (54.2 mg, 0.33 mmol, 1.1 equiv), DMAP (3.7 mg, 0.03 mmol, 0.1 equiv), then DCM (1.5 mL, 0.2 M). To this solution was added DIC (51 μL, 0.33 mmol, 1.1 equiv) dropwise. The reaction was stirred at ambient temperature and monitored by LCMS. Upon complete consumption of the acid, the reaction was concentrated. The crude residue was purified by column chromatography (silica, 5 to 20% EtOAc/hexanes) to afford **80** (134 mg, 93% yield) as a colorless oil.

^{1}H NMR ($CDCl_3$, 400 MHz): δ 7.84 (s, 2H), 7.76 (dd, *J* = 5.5, 3.1 Hz, 2H), 6.74 (s, 2H), 4.45 (dd, *J* = 9.1, 5.3 Hz, 1H), 3.86 (s, 6H), 2.16 (ddt, *J* = 13.3, 10.4, 5.2 Hz, 1H), 1.82 (dtd, *J* = 14.3, 9.3, 5.2 Hz, 1H), 1.44 – 1.20 (m, 3H), 1.20 – 1.01 (m, 1H), 0.85 (t, *J* = 7.0 Hz, 3H).

^{13}C{^{1}H} NMR ($CDCl_3$, 101 MHz): δ 170.9, 158.5, 134.8, 129.3, 124.0, 122.3, 113.9, 107.8, 56.3, 37.9, 29.6, 29.3, 22.8, 14.2.

FTIR (ATR, cm^{-1}): 1787, 1740, 1582, 1456, 1406, 1224, 1117, 964, 877, 695.

HRMS (FD-MS, *m/z*): $[M]^+$ calcd for $C_{22}H_{22}NO_6Br$: 475.0639; found: 475.0625.

1,3-dioxoisoindolin-2-yl 2-(2,6-dimethoxy-4-(6-(trimethylsilyl)hex-5-yn-1-yl)phenyl)hexanoate (81)

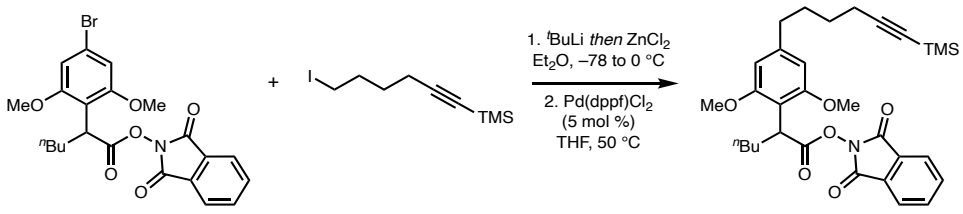

Prepared from aryl bromide **80** (40 mg, 0.084 mmol, 1 equiv), alkyl iodide **54** (24.6 mg, 0.088 mmol, 1.05 equiv), ^{t}BuLi (1.7 M in pentane, 0.13 mL, 0.23 mmol, 2.7 equiv),

$ZnCl_2$ (0.5 M in THF, 0.18 mL, 0.088 mmol, 1.05 equiv), and $Pd(dppf)Cl_2$ (3.1 mg, 0.0042 mmol, 0.05 equiv) following a modified procedure.[73] The crude residue was purified by preparative thin layer chromatography (silica, 25% EtOAc/hexanes) to afford **81** (12 mg, 26% yield) as a colorless oil.

^{1}H NMR ($CDCl_3$, 400 MHz): δ 7.73 (d, *J* = 4.7 Hz, 2H), 7.64 (dd, *J* = 5.5, 3.1 Hz, 2H), 6.31 (s, 2H), 4.37 (dd, *J* = 8.8, 5.4 Hz, 1H), 3.75 (s, 6H), 2.57 – 2.48 (m, 2H), 2.18 (t, *J* = 7.1 Hz, 2H), 2.07 (ddt, *J* = 13.3, 10.5, 5.3 Hz, 1H), 1.79 – 1.71 (m, 1H), 1.66 (tdd, *J* = 7.6, 6.0, 4.8 Hz, 2H), 1.56 – 1.43 (m, 2H), 1.34 – 1.12 (m, 3H), 1.14 – 1.01 (m, 1H), 0.82 – 0.70 (m, 3H), 0.05 (s, 9H).

^{13}C{^{1}H} NMR ($CDCl_3$, 101 MHz): δ 170.6, 156.9, 142.7, 133.7, 128.3, 122.9, 111.2, 106.6, 103.0, 83.9, 54.9, 36.9, 35.3, 29.5, 29.0, 28.4, 27.5, 21.8, 19.0, 13.2, -0.6.

FTIR (ATR, cm^{-1}): 2170, 1787, 1743, 1587, 1458, 1364, 1118, 1079, 841, 696.

HRMS (FD-MS, *m/z*): $[M]^+$ calcd for $C_{31}H_{39}NO_6Si$: 549.2541; found: 549.2538.

***tert*-butyl 2-(4-(hex-5-yn-1-yl)phenyl)hexanoate (104)**

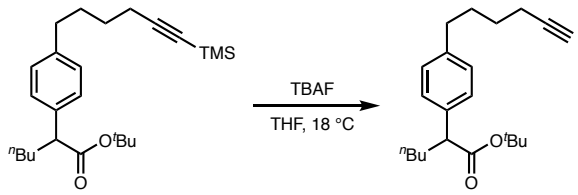

To a flame-dried round bottom flask with a stir bar was added protected alkyne **79** (2.2 g, 5.0 mmol, 1 equiv) followed by THF (25 mL, 0.2 M) then tetrabutylammonium fluoride (10 mL, 10.0 mmol, 2 equiv). The reaction was stirred at room temperature for 5 min and then quenched with sat. aq. $NaHCO_3$. The layers were separated, and combined organics were washed with water thrice, dried over Na_2SO_4, filtered, and concentrated to afford

104 (1.65 mg, quantitative yield) as a colorless oil.

^{1}H NMR ($CDCl_3$, 400 MHz): δ 7.22 – 7.17 (m, 2H), 7.11 (d, *J* = 8.0 Hz, 2H), 3.38 (dd, *J* = 8.3, 7.1 Hz, 1H), 2.60 (t, *J* = 7.7 Hz, 2H), 2.21 (td, *J* = 7.0, 2.6 Hz, 2H), 2.00 (dddd, *J* = 13.4, 9.7, 8.4, 5.4 Hz, 1H), 1.78 – 1.62 (m, 2H), 1.62 – 1.49 (m, 4H), 1.39 (d, *J* = 1.0 Hz, 9H), 1.36 – 1.13 (m, 3H), 0.87 (dd, *J* = 7.6, 6.6 Hz, 3H).

^{13}C{^{1}H} NMR ($CDCl_3$, 101 MHz): δ 173.8, 140.8, 137.5, 128.5, 127.9, 84.6, 80.5, 68.4, 52.5, 35.1, 33.6, 30.5, 30.0, 28.2, 28.1, 22.7, 18.4, 14.1.

FTIR (ATR, cm^{-1}): 2931, 2860, 1725, 1367, 1265, 1147, 844, 739.

HRMS (FD, *m/z*): $[M]^+$ calcd for $C_{22}H_{32}O_2$: 328.2402; found: 328.2421.

***tert*-butyl (*E*)-2-(4-(6-bromohex-5-en-1-yl)phenyl)hexanoate (84)**

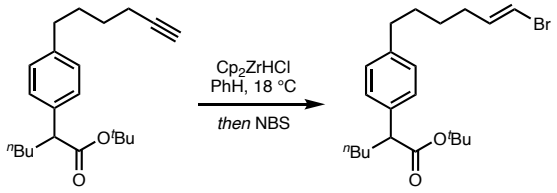

Prepared from alkyne **104** (1.64 g, 5.0 mmol, 1 equiv), Cp_2ZrHCl (1.64 g, 6.4 mmol, 1.3 equiv), *N*-bromosuccinimide (1.13 g, 6.4 mmol, 1.3 equiv equiv), and PhH (50 mL, 0.1 M) following a published procedure[156] to afford **84** (1.77 g, 87% yield) as a colorless oil.

^{1}H NMR ($CDCl_3$, 500 MHz): δ 7.23 – 7.17 (m, 2H), 7.13 – 7.06 (m, 2H), 6.16 (dt, *J* = 13.4, 7.3 Hz, 1H), 6.00 (dt, *J* = 13.4, 1.4 Hz, 1H), 3.39 (dd, *J* = 8.4, 7.0 Hz, 1H), 2.58 (t, *J* = 7.7 Hz, 2H), 2.07 (qd, *J* = 7.3, 1.3 Hz, 2H), 2.03 – 1.94 (m, 1H), 1.75 – 1.64 (m, 1H), 1.61 (td, *J* = 9.3, 8.5, 6.6 Hz, 2H), 1.43 (s, 1H), 1.40 (s, 9H), 1.38 – 1.15 (m, 4H), 0.88 (t, *J* = 7.1 Hz, 4H).

^{13}C{^{1}H} NMR ($CDCl_3$, 101 MHz): δ 173.8, 140.9, 138.1, 137.5, 128.5, 127.9, 104.4,

80.5, 52.5, 35.4, 33.6, 32.9, 30.8, 30.0, 28.4, 28.1, 22.7, 14.1.

FTIR (ATR, cm^{-1}): 3089, 1725, 1621, 1557, 1455, 1144, 1057.

HRMS (FD, *m/z*): $[M]^+$ calcd for $C_{22}H_{33}BrO_2$: 408.1664; found: 408.1665.

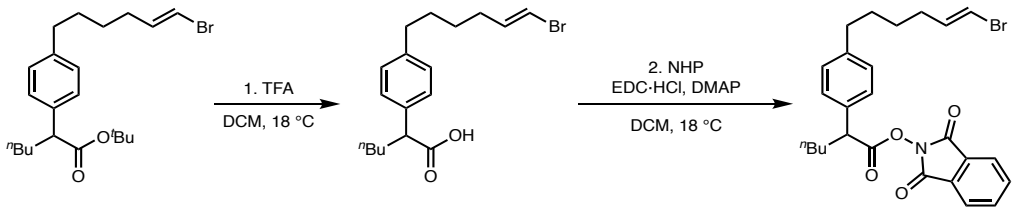

Step 1: To a round bottom flask with a stir bar was added ester **84** (1.77 g, 4.3 mmol, 1 equiv) then trifluoroacetic acid/DCM (1:1, 0.2 M). The solution was stirred at 18 °C for 30 min then concentrated. The crude residue was azeotroped with PhMe to afford acid intermediate **129** as a red oil.

Step 2: To a round bottom flask with a stir bar was added acid intermediate **129** (1.53 g, 4.3 mmol, 1 equiv), *N*-hydroxyphthalimide (777 mg, 4.8 mmol, 1.1 equiv), DMAP (106 mg, 0.9 mmol, 0.2 equiv), then DCM (22 mL, 0.2 M). Then EDC·HCl (913 mg, 4.8 mmol, 1.1 equiv) was added in one portion. The reaction was stirred at 18 °C overnight and then concentrated. The crude residue was filtered through a plug of silica, eluting with EtOAc. The filtrate was concentrated then purified by column chromatography (silica, 5 to 7% EtOAc/hexanes) to afford **85** (1.79 g, 83% yield over 2 steps) as a colorless oil.

(*E*)-2-(4-(6-bromohex-5-en-1-yl)phenyl)hexanoic acid (129)

^{1}H NMR ($CDCl_3$, 400 MHz): δ 7.26 – 7.17 (m, 2H), 7.17 – 7.06 (m, 2H), 6.15 (dt, *J* = 13.5, 7.2 Hz, 1H), 6.00 (dt, *J* = 13.5, 1.4 Hz, 1H), 3.51 (t, *J* = 7.7 Hz, 1H), 2.58 (t, *J* = 7.7

Hz, 2H), 2.14 – 1.99 (m, 2H), 1.82 – 1.68 (m, 1H), 1.61 (tdd, *J* = 9.2, 7.4, 6.1 Hz, 2H), 1.53 – 1.35 (m, 2H), 1.39 – 1.13 (m, 5H), 0.88 – 0.84 (m, 3H).

$^{13}C\{^1H\}$ NMR ($CDCl_3$, 101 MHz): δ 179.4, 141.6, 138.1, 136.1, 128.8, 128.1, 104.4, 51.1, 35.4, 33.0, 32.9, 30.8, 29.8, 28.4, 22.6, 14.0.

FTIR (ATR, cm^{-1}): 2930, 1704, 1512, 1290, 939, 739.

HRMS (TOF-ESI, *m/z*): $[M - H]^-$ calcd for $C_{18}H_{24}BrO_2$: 351.0965; found: 351.0955.

1,3-dioxoisoindolin-2-yl (*E*)-2-(4-(6-bromohex-5-en-1-yl)phenyl)hexanoate (85)

^1H NMR ($CDCl_3$, 500 MHz): δ 7.86 (dd, *J* = 5.6, 3.1 Hz, 2H), 7.77 (dd, *J* = 5.5, 3.1 Hz, 2H), 7.32 – 7.28 (m, 2H), 7.21 – 7.14 (m, 2H), 6.17 (dt, *J* = 13.7, 7.2 Hz, 1H), 6.01 (dt, *J* = 13.5, 1.4 Hz, 1H), 3.90 (t, *J* = 7.6 Hz, 1H), 2.61 (t, *J* = 7.7 Hz, 2H), 2.29 – 2.12 (m, 1H), 2.07 (qd, *J* = 7.3, 1.4 Hz, 2H), 1.97 – 1.82 (m, 1H), 1.63 (p, *J* = 7.5 Hz, 2H), 1.52 – 1.25 (m, 6H), 0.95 – 0.87 (m, 3H).

$^{13}C\{^1H\}$ NMR ($CDCl_3$, 101 MHz): δ 170.7, 162.1, 142.0, 138.1, 134.9, 134.6, 129.1, 129.0, 128.1, 124.1, 104.4, 48.5, 35.4, 33.8, 33.0, 30.7, 29.5, 28.4, 22.5, 14.0.

FTIR (ATR, cm^{-1}): 1810, 1784, 1742, 1618, 1466, 1359, 1185, 1126, 1058, 966, 877, 695.

HRMS (FD-MS, *m/z*): $[M]^+$ calcd for $C_{26}H_{28}NBrO_4$: 497.1196; found: 497.1189.

methyl 2-(4-bromophenyl)hexanoate (130)

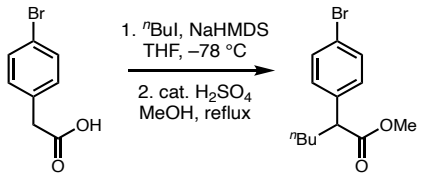

Step 1: To a flame-dried round bottom flask with a stir bar was added 4-bromophenylacetic acid (9.68 g, 45 mmol, 1 equiv) and THF (90 mL, 0.5 M). The solution was cooled to –78 °C in a dry ice/acetone bath, then NaHMDS (1 M in THF, 93.1 mL, 93.1 mmol, 2.07 equiv) was added dropwise. The mixture was allowed to reach ambient temperature with vigorous stirring; the mixture slowly turned into a red homogenous solution, at which point 1-iodobutane (5.38 mL, 47.3 mmol, 1.05 equiv) was added. The reaction was stirred at room temperature for 20 h, until the solution turned a golden color, at which point water was added. The mixture was washed with Et_2O twice. The aqueous layer was acidified with 1 M HCl to pH = 1 and then extracted with Et_2O. The organic layer was washed with brine, dried over Na_2SO_4, filtered, and concentrated. The crude oil was used in the next step without further purification.

Step 2: To a flame-dried 3-neck round bottom flask with a stir bar and reflux condenser was added the intermediate acid and MeOH (25 mL, 1.8 M). Then, H_2SO_4 (240 μL, 4.5 mmol, 0.1 equiv) was added and the reaction was stirred while heating to 65 °C in an oil bath. After 4 h of stirring at that temperature, the reaction was allowed to reach ambient temperature then diluted in 20% EtOAc/hexanes and washed with 1 M Na_2CO_3. The aqueous layer was extracted once with 20% EtOAc/hexanes. Combined organics were washed with twice with sat. aq. $Na_2S_2O_3$ to remove any remaining color, dried over Na_2SO_4, filtered, and concentrated to afford **130** (11.2 g, 87% yield over 2 steps) as a pale yellow oil.

^{1}H NMR ($CDCl_3$, 400 MHz): δ 7.44 (d, *J* = 8.5 Hz, 2H), 7.18 (d, *J* = 8.4 Hz, 2H), 3.65 (s, 4H), 3.49 (t, *J* = 7.7 Hz, 1H), 2.11 – 1.97 (m, 1H), 1.73 (dddd, *J* = 13.4, 9.3, 7.6, 5.8 Hz, 1H), 1.40 – 1.11 (m, 6H), 0.86 (t, *J* = 7.2 Hz, 5H).

$^{13}C\{^{1}H\}$ NMR ($CDCl_3$, 101 MHz): δ 174.3, 138.4, 131.8, 129.8, 121.3, 52.2, 51.2, 33.3, 29.8, 22.5, 14.0.

FTIR (ATR, cm^{-1}): 2955, 2359, 2323, 1733, 1616, 1574, 1487, 1434, 1159, 1010, 820.

HRMS (FI-MS, *m/z*): $[M]^+$ calcd for $C_{13}H_{17}O_2Br$: 284.0406; found: 284.0397.

(5-iodopent-1-yn-1-yl)trimethylsilane (131)

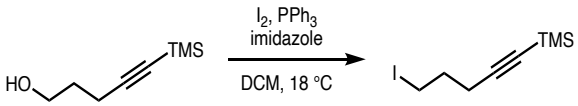

Prepared from 5-(trimethylsilyl)pent-4-yn-1-ol (5.0 mL, 27.5 mmol, 1.05 equiv), iodine (10.5 g, 41.3 mmol, 1.58 equiv), imidazole (2.81 g, 41.3 mmol, 1.58 equiv), triphenylphosphine (6.86 g, 26.2 mmol, 1 equiv), and DCM (110 mL, 0.24 M) following a modified procedure[157] to afford **131** (5.17 g, 74% yield) as a colorless oil. Spectra matched those reported in the literature.[157]

^{1}H NMR ($CDCl_3$, 500 MHz): δ 3.33 (t, J = 6.8 Hz, 2H), 2.40 (t, J = 6.8 Hz, 2H), 2.04 (p, J = 6.8 Hz, 2H), 0.19 (s, 9H).

$^{13}C\{^{1}H\}$ NMR ($CDCl_3$, 101 MHz): δ 104.8, 85.8, 32.0, 20.8, 5.1, 0. 0.

(7-iodohept-1-yn-1-yl)trimethylsilane (132)

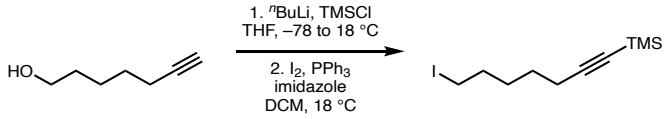

Prepared following a published procedure.[158]

Step 1: Prepared from 6-heptyn-1-ol (5.66 mL, 45 mmol, 1 equiv), ^{n}BuLi (2.5 M in hexanes, 39.6 mL, 80.6 mmol, 2.2 equiv), TMSCl (17.1 mL, 135 mmol, 3 equiv), and

THF (12 mL, 3 M) to afford the alkyne intermediate.

Step 2: Prepared from the intermediate alkyne (1.05 equiv), iodine (17.1 g, 67.5 mmol, 1.58 equiv), imidazole (4.6 g, 67.5 mmol, 1.58 equiv), triphenylphosphine (11.2 g, 42.8 mmol, 1 equiv), and DCM (180 mL, 0.24 M) to afford **132** (8.08 g, 56% yield over 2 steps) as a colorless oil. Spectra matched those reported in the literature and references therein.[158]

^{1}H NMR ($CDCl_3$, 400 MHz): δ 3.20 (t, *J* = 7.0 Hz, 2H), 2.24 (t, *J* = 6.6 Hz, 2H), 1.89 – 1.80 (m, 2H), 1.62 – 1.45 (m, 4H), 0.15 (d, *J* = 0.7 Hz, 9H).

^{13}C{^{1}H} NMR ($CDCl_3$, 101 MHz): δ 107.1, 85.0, 33.1, 29.8, 27.6, 19.8, 6.9, 0.3.

(8-iodooct-1-yn-1-yl)trimethylsilane (133)

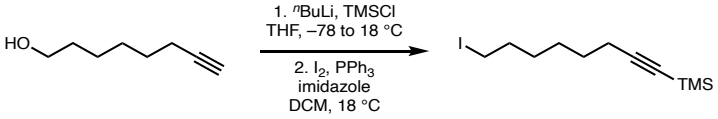

Prepared following a published procedure.[158]

Step 1: Prepared from 7-octyn-1-ol (5.2 g, 36.6 mmol, 1 equiv), ^{n}BuLi (2.5 M in hexanes, 32.2 mL, 80.6 mmol, 3 equiv), TMSCl (13.9 mL, 110 mmol, 3 equiv), and THF (12 mL, 3 M) to afford alkyne intermediate.

Step 2: Prepared from the intermediate alkyne (1.05 equiv), iodine (13.9 g, 54.9 mmol, 1.58 equiv), imidazole (3.74 g, 54.9 mmol, 1.58 equiv), triphenylphosphine (9.12 g, 34.8 mmol, 1 equiv), and DCM (146 mL, 0.24 M) to afford **133** (7.84 g, 73% yield over 2 steps) as a colorless oil. Spectra matched those reported in the literature.[158]

^{1}H NMR ($CDCl_3$, 400 MHz): δ 3.19 (t, *J* = 7.0 Hz, 2H), 2.22 (t, *J* = 7.0 Hz, 2H), 1.89 – 1.77 (m, 2H), 1.59 – 1.46 (m, 2H), 1.46 – 1.34 (m, 4H), 0.14 (s, 9H).

$^{13}C\{^{1}H\}$ NMR ($CDCl_3$, 101 MHz): δ 107.5, 84.7, 33.5, 30.1, 28.5, 27.8, 19.9, 7.2, 0.3.

methyl 2-(4-(5-(trimethylsilyl)pent-4-yn-1-yl)phenyl)hexanoate (134)

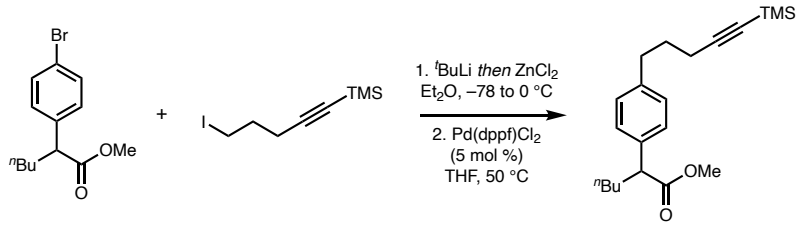

Prepared from aryl bromide **130** (500 mg, 1.75 mmol, 1 equiv), alkyl iodide **131** (933 mg, 3.51 mmol, 2 equiv), ^{t}BuLi (1.7 M in pentane, 5.33 mL, 9.06 mmol, 5.17 equiv), $ZnCl_2$ (0.5 M in THF, 7.0 mL, 3.51 mmol, 2 equiv), and $Pd(dppf)Cl_2$ (64 mg, 0.088 mmol, 0.05 equiv) following a published procedure.[73] The crude residue was purified by column chromatography (silica, 1 to 2% EtOAc/hexanes) to afford **134** (511 mg, 85% yield) as a colorless oil.

^{1}H NMR ($CDCl_3$, 400 MHz): δ 7.24 – 7.18 (m, 2H), 7.16 – 7.09 (m, 2H), 3.65 (s, 3H), 3.50 (t, J = 7.7 Hz, 1H), 2.78 – 2.66 (m, 2H), 2.23 (t, J = 7.1 Hz, 2H), 2.05 (dddd, J = 13.4, 9.6, 8.0, 5.7 Hz, 1H), 1.83 (dt, J = 8.5, 7.1 Hz, 2H), 1.79 – 1.69 (m, 1H), 1.38 – 1.15 (m, 3H), 0.87 (t, J = 7.2 Hz, 3H), 0.16 (s, 8H).

$^{13}C\{^{1}H\}$ NMR ($CDCl_3$, 101 MHz): δ 174.9, 140.6, 137.0, 128.9, 128.0, 107.2, 85.2, 52.0, 51.4, 34.4, 33.5, 30.2, 29.9, 22.6, 19.4, 14.0, 0.3.

FTIR (ATR, cm^{-1}): 2956, 1175, 1736, 1606, 1582, 1456, 1248, 1160, 911, 839, 759, 732.

HRMS (FI-MS, *m/z*): $[M]^+$ calcd for $C_{21}H_{32}O_2Si$: 344.2166; found: 344.2159.

methyl 2-(4-(7-(trimethylsilyl)hept-6-yn-1-yl)phenyl)hexanoate (135)

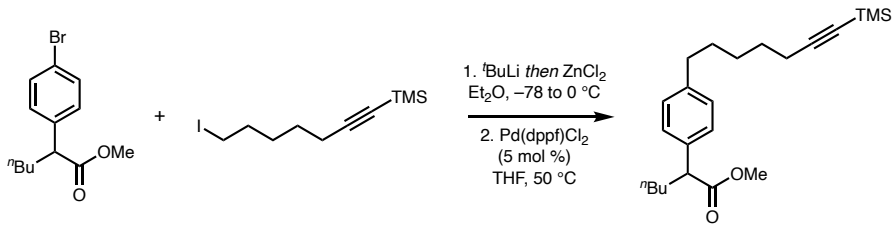

Prepared from aryl bromide **130** (1.46 g, 5.13 mmol, 1 equiv), alkyl iodide **132** (3.02 g, 10.3 mmol, 2 equiv), ^{t}BuLi (1.7 M in pentane, 15.6 mL, 26.5 mmol, 5.17 equiv), $ZnCl_2$ (0.5 M in THF, 20.5 mL, 10.3 mmol, 2 equiv), and $Pd(dppf)Cl_2$ (188 mg, 0.26 mmol, 0.05 equiv) following a published procedure.[73] The crude residue was purified by column chromatography (silica, 3% EtOAc/hexanes) to afford **135** (1.58 g, 83% yield) as a colorless oil.

^{1}H NMR ($CDCl_3$, 500 MHz): δ 7.24 – 7.17 (m, 2H), 7.15 – 7.09 (m, 2H), 3.65 (s, 3H), 3.50 (t, *J* = 7.7 Hz, 1H), 2.62 – 2.56 (m, 2H), 2.22 (t, *J* = 7.1 Hz, 2H), 2.06 (dddd, *J* = 13.4, 10.0, 8.1, 5.5 Hz, 1H), 1.75 (dddd, *J* = 13.2, 9.5, 7.3, 5.7 Hz, 1H), 1.66 – 1.58 (m, 2H), 1.55 (q, *J* = 7.3 Hz, 2H), 1.48 – 1.37 (m, 2H), 1.37 – 1.14 (m, 3H), 0.88 (t, *J* = 7.2 Hz, 3H), 0.15 (s, 6H).

^{13}C{^{1}H} NMR ($CDCl_3$, 101 MHz): δ 174.0, 140.6, 135.7, 127.7, 126.9, 106.7, 83.5, 51.0, 50.4, 34.5, 32.5, 30.0, 28.9, 27.7, 27.6, 21.6, 19.0, 13.3, 13.1, –0.7.

FTIR (ATR, cm^{-1}): 2956, 2858, 2173, 1736, 1457, 1248, 1159, 992, 839, 758.

HRMS (FI-MS, *m/z*): $[M]^+$ calcd for $C_{23}H_{36}O_2Si$: 372.2479; found: 372.2479.

methyl 2-(4-(8-(trimethylsilyl)oct-7-yn-1-yl)phenyl)hexanoate (136)

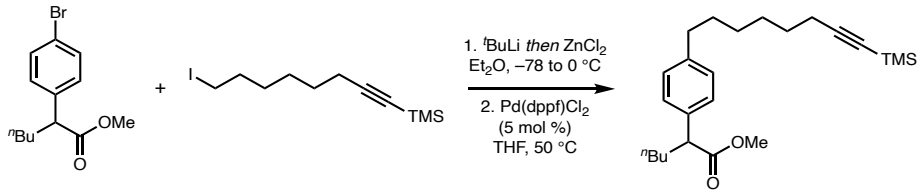

Prepared from aryl bromide **130** (1.75 g, 6.14 mmol, 1 equiv), alkyl iodide **133** (3.78 g, 12.3 mmol, 2 equiv), ^{t}BuLi (1.7 M in pentane, 18.7 mL, 31.7 mmol, 5.17 equiv), $ZnCl_2$ (0.5 M in THF, 24.5 mL, 12.3 mmol, 2 equiv), and $Pd(dppf)Cl_2$ (225 mg, 0.31 mmol, 0.05 equiv) following a published procedure.[73] The crude residue was purified by column chromatography (silica, 3% EtOAc/hexanes) to afford **136** (2.37 g, 84% yield) as a colorless oil.

^{1}H NMR ($CDCl_3$, 500 MHz): δ 7.23 (d, *J* = 8.1 Hz, 2H), 7.18 – 7.06 (m, 2H), 3.68 (s, 3H), 3.54 (t, *J* = 7.7 Hz, 1H), 2.65 – 2.58 (m, 2H), 2.25 (t, *J* = 7.1 Hz, 2H), 1.85 – 1.72 (m, 1H), 1.64 (p, *J* = 7.6 Hz, 2H), 1.55 (q, *J* = 7.2 Hz, 1H), 1.45 (dq, *J* = 9.5, 6.5 Hz, 2H), 1.36 (dtd, *J* = 16.0, 9.1, 8.4, 5.5 Hz, 2H), 1.31 – 1.18 (m, 1H), 0.91 (t, *J* = 7.2 Hz, 3H), 0.19 (s, 6H).

^{13}C{^{1}H} NMR ($CDCl_3$, 101 MHz): δ 174.0, 140.8, 135.7, 130.9, 127.7, 126.9, 106.8, 83.5, 51.0, 50.4, 34.6, 32.5, 30.4, 28.9, 27.9, 27.8, 27.7, 21.6, 19.0, 13.1, –0.7.

FTIR (ATR, cm^{-1}): 2856, 2175, 1736, 1615, 1570, 1434, 1248, 1159, 1051, 839, 732.

HRMS (FI-MS, *m/z*): $[M]^+$ calcd for $C_{24}H_{38}O_2Si$: 386.2636; found: 386.2641.

(*Z*)-5-iodo-4-methylpent-4-en-1-ol (87)

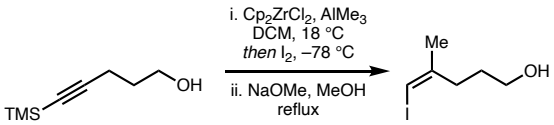

Prepared from 5-(trimethylsilyl)pent-4-yn-1-ol (4.48 g, 27.5 mmol, 1 equiv), Cp_2ZrCl_2 (8.88 g, 27.5 mmol, 1 equiv), trimethylaluminum (2 M in toluene, 41.3 mL, 84.6 mmol, 3 equiv), iodine (8.24 g, 32.5 mmol, 1.18 equiv), and sodium methoxide (25% in methanol, 25.8 mL, 113 mmol, 4.1 equiv) following a published procedure[159] to afford **87** (2.37 g, 38% yield) as a pale yellow oil. Spectra matched those reported in the literature.[159]

^{1}H NMR ($CDCl_3$, 400 MHz): δ 5.87 (d, *J* = 1.5 Hz, 1H), 3.67 (t, *J* = 6.4 Hz, 2H), 2.52 – 2.22 (m, 2H), 1.90 (d, *J* = 1.5 Hz, 3H), 1.78 – 1.63 (m, 2H).

^{13}C{^{1}H} NMR ($CDCl_3$, 101 MHz): δ 147.2, 74.8, 62.4, 35.2, 30.0, 23.4.

HRMS (FI-MS, *m/z*): $[M]^+$ calcd for $C_6H_{11}OI$: 225.9849; found: 225.9847.

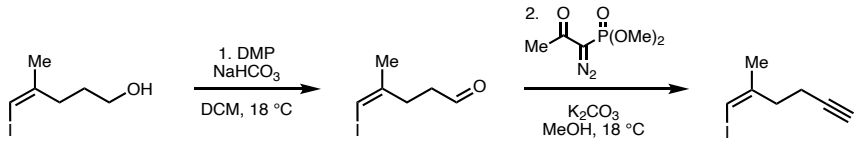

Step 1: To a round bottom flask with a stir bar was added alcohol **87** (2.32 g, 10.3 mmol, 1 equiv) and $NaHCO_3$ (2.59 g, 30.8 mmol, 3 equiv), and wet DCM (34 mL, 0.3 M), followed by Dess–Martin periodinane (5.22 g, 12.3 mmol, 1.2 equiv). The reaction mixture was stirred at ambient temperature and monitored by TLC. Upon complete consumption of the alcohol, the reaction was quenched with sat. aq. $NaHCO_3$, sat. aq. $Na_2S_2O_3$, and H_2O (1:1:1, 36 mL total); the resulting mixture was stirred for 2 h. The organic layer was separated, and the aqueous layer was extracted with DCM thrice. Combined organics were washed with brine, dried over Na_2SO_4, filtered, and

concentrated. The crude pale yellow oil (enal **137**) was immediately used.

Step 2: To a round bottom flask with a stir bar was added K_2CO_3 (276 mg, 2.0 mmol, 2 equiv) and MeOH (6.7 mL, 0.15 M), followed by intermediate aldehyde **137** (224 mg, 1.0 mmol, 1 equiv) and Ohira–Bestmann reagent[124] (30 wt% in PhMe, 768 mg, 1.2 mmol, 1.2 equiv). The mixture was allowed to stir at ambient temperature for 4 h, at which point the mixture was extracted with hexanes thrice. Combined organics were washed with water, dried over Na_2SO_4, and concentrated. The crude residue was purified by column chromatography (silica, 5% EtOAc/hexanes) to afford alkyne **138** (110 mg, 50% yield over 2 steps) as a colorless oil.

(*Z*)-5-iodo-4-methylpent-4-enal (137)

^{1}H NMR ($CDCl_3$, 400 MHz): δ 9.82 (s, 1H), 5.94 (q, *J* = 1.5 Hz, 1H), 2.60 – 2.49 (m, 5H), 1.90 (d, *J* = 1.5 Hz, 3H).

^{13}C{^{1}H} NMR ($CDCl_3$, 101 MHz): δ 201.3, 145.7, 75.8, 41.2, 31.5, 23.5.

FTIR (ATR, cm^{-1}): 3052, 2909, 2819, 2723, 2358, 1820, 1722, 1437, 1269, 1185, 1131, 1002, 765.

HRMS (FI-MS, *m/z*): $[M]^+$ calcd for C_6H_9IO: 223.9693; found: 223.9691.

(*Z*)-1-iodo-2-methylhex-1-en-5-yne (138)

^{1}H NMR ($CDCl_3$, 400 MHz): δ 5.95 (q, *J* = 1.5 Hz, 1H), 2.46 (ddd, *J* = 7.7, 7.1, 1.1 Hz, 2H), 2.37 – 2.30 (m, 2H), 1.98 (t, *J* = 2.6 Hz, 1H), 1.94 (d, *J* = 1.5 Hz, 3H).

^{13}C{^{1}H} NMR ($CDCl_3$, 101 MHz): δ 145.9, 83.4, 75.8, 69.0, 37.6, 23.7, 16.4.

HRMS (FI-MS, *m/z*): $[M]^+$ calcd for C_7H_9I: 219.9743; found: 219.9739.

(*Z*)-(6-iodo-5-methylhex-5-en-1-yn-1-yl)trimethylsilane (88)

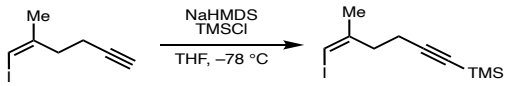

To a flame-dried round bottom flask with a stir bar was added alkyne **138** (365 mg, 1.66 mmol, 1 equiv) and THF (5.5 mL, 0.3 M). The reaction was cooled to –78 °C in a dry ice/acetone bath, then NaHMDS (1 M in THF, 2.16 mL, 2.16 mmol, 1.3 equiv) was added slowly. The mixture was stirred at –78 °C for 1 h, then TMSCl (0.32 mL, 2.49 mmol, 1.5 equiv) was added. The reaction was allowed to slowly warm to ambient temperature and stir for 20 h. Water was added, and the resulting mixture was extracted with Et_2O. Combined organics were washed with brine, dried over Na_2SO_4, filtered, and concentrated. The crude residue was purified by column chromatography (silica, 1% Et_2O/hexanes) to afford **88** (408 mg, 84% yield) as a colorless oil.

^{1}H NMR ($CDCl_3$, 400 MHz): δ 5.93 (q, *J* = 1.5 Hz, 1H), 2.48 – 2.40 (m, 2H), 2.40 – 2.31 (m, 2H), 1.94 (d, *J* = 1.4 Hz, 3H), 0.15 (s, 9H).

^{13}C{^{1}H} NMR ($CDCl_3$, 101 MHz): δ 146.1, 106.2, 85.4, 75.7, 37.7, 23.8, 17.9, 0.2.

FTIR (ATR, cm^{-1}): 2960, 2909, 2175, 1439, 1249, 1054, 908, 841, 733.

HRMS (FI-MS, *m/z*): $[M]^+$ calcd for $C_{10}H_7SiI$: 292.0139; found: 292.0122.

tert-butyl (_Z_)-2-(2,6-dimethoxy-4-(2-methyl-6-(trimethylsilyl)hex-1-en-5-yn-1-yl)phenyl)hexanoate (90)

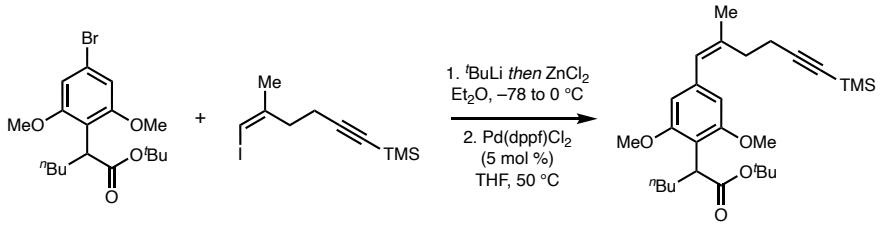

Prepared from aryl bromide **52** (186 mg, 0.48 mmol, 1 equiv), alkenyl iodide **88** (280 mg, 0.56 mmol, 2 equiv), ^{t}BuLi (1.7 M in pentane, 1.18 mL, 2.0 mmol, 4.2 equiv), $ZnCl_2$ (0.5 M in THF, 1.9 mL, 0.96 mmol, 2 equiv), and $Pd(dppf)Cl_2$ (17.5 mg, 0.024 mmol, 0.05 equiv) following a published procedure.[73] The crude residue was purified by column chromatography (silica, 0 to 5% EtOAc/hexanes) to afford **90** (214 mg, 94% yield) as a colorless oil.

^{1}H NMR ($CDCl_3$, 400 MHz): δ 6.41 (s, 2H), 6.30 (d, *J* = 1.7 Hz, 1H), 3.98 (dd, *J* = 9.0, 5.4 Hz, 1H), 3.77 (s, 6H), 2.59 – 2.49 (m, 2H), 2.48 – 2.38 (m, 2H), 2.13 – 1.99 (m, 1H), 1.89 (d, *J* = 1.5 Hz, 3H), 1.71 – 1.47 (m, 2H), 1.37 (s, 9H), 1.35 – 1.15 (m, 2H), 1.15 – 0.99 (m, 1H), 0.83 (t, *J* = 7.1 Hz, 3H), 0.11 (s, 9H).

^{13}C{^{1}H} NMR ($CDCl_3$, 101 MHz): δ 174.5, 157.8, 137.6, 137.5, 127.4, 116.7, 106.8, 104.6, 85.4, 79.6, 55.8, 41.0, 32.2, 30.0, 30.0, 28.2, 24.1, 23.0, 19.1, 14.3, 0.3.

FTIR (ATR, cm^{-1}): 2168, 1725, 1605, 1575, 1453, 1248, 1159, 1123, 841, 736.

HRMS (FD-MS, *m/z*): $[M]^+$ calcd for $C_{28}H_{44}O_4Si$: 472.3003; found: 472.3004.

5.8.4 *Double Reductive Cross-Coupling*

General Procedure E:

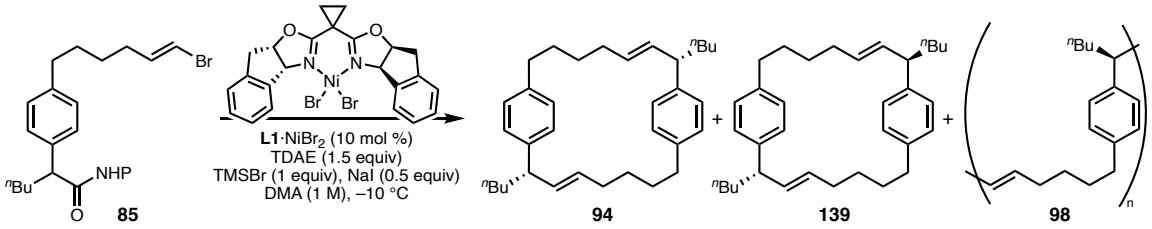

First, a stock solution of the catalyst was prepared. To a ½-dram vial with a stir bar and Teflon cap was added **L1**·$NiBr_2$[75] (3.5 mg, 0.006 mmol, 0.1 equiv). In a N_2-filled glovebox, the vial was charged with DMA (60 μL) the stirred while heating to 80 °C. The mixture was stirred at that temperature until all solids were completely dissolved and a maroon solution was obtained (ca. 5–10 min). Then the vial was allowed to completely cool to ambient temperature. Second, a separate ½-dram vial with a stir bar and Teflon cap was sequentially charged with NaI (4.5 mg, 0.03 mmol, 0.5 equiv) and electrophile **85** (30.0 mg, 0.06 mmol, 1 equiv). In a N_2-filled glovebox, this vial was charged with DMA (60 μL).

Then, both vials were transferred into a N_2-filled glovebox fitted with a temperature-controlled well plate. The catalyst stock solution was transferred to the second vial via syringe, then the reaction was stirred at ambient temperature at 250 rpm to ensure complete dissolution of **85** and appropriate mixing of all reagents (the catalyst may not be fully dissolved at this temperature). Then, the vial was placed in a well plate pre-cooled to –10 °C (cooled for 30 min). (Note: the recirculating Julabo LH45 chiller was set to –10 °C but an external thermometer in the glovebox read the temperature as –1 to –4 °C.) At this temperature, TDAE (21 μL, 0.09 mmol, 1.5 equiv) was added and the

solution stirred for 10 min before TMSBr (8 μL, 0.06 mmol, 1 equiv) (fumed slightly) was added, each via syringe. The reaction was stirred at 800 rpm at the chilled temperature in the glovebox. After 16 h, the reaction mixture was diluted with 20% EtOAc/hexanes and filtered over a plug of silica, eluting with 20% EtOAc/hexanes; the filtrate was concentrated.

The crude residue was assayed by quantitative ^{1}H NMR and DOSY. The sample was concentrated and diluted in THF (2 mg/mL), filtered through a syringe filter, then assayed by GPC and GCMS (50 to 300 °C). The sample was concentrated, diluted in 250 μL PhMe, filtered through a syringe filter, then purified by preparative HPLC (C8, 8 mL/min, 95 to 100% ACN/H_2O, 230 nm) to afford **94** (t_R = 10.6 min).

(Note: for runs employing a racemic mixture of **L1**·$NiBr_2$, an equimolar amount of each enantiomer was weighed into the vial prior to solvent addition when preparing the catalyst stock solution. Yellow precipitate formed upon cooling this mixture to ambient temperature following heat-induced dissolution; this heterogeneous mixture was added to the second vial using a needle with a sufficiently large gauge.)

(2*S*,3*E*,10*S*,11*E*)-2,10-dibutyl-1,9(1,4)-dibenzenacyclohexadecaphane-3,11-diene (94)

^{1}H NMR ($CDCl_3$, 400 MHz): δ 7.09 – 7.00 (m, 2H), 6.98 – 6.91 (m, 2H), 5.50 – 5.40 (m, 1H), 5.37 – 5.25 (m, 1H), 3.12 (q, *J* = 7.4 Hz, 1H), 2.54 (dt, *J* = 14.8, 7.4 Hz, 1H), 2.42 (dt, *J* = 14.1, 7.6 Hz, 1H), 2.13 – 1.94 (m, 2H), 1.66 (q, *J* = 7.3 Hz, 2H), 1.50 – 1.40 (m, 2H), 1.34 – 1.22 (m, 5H), 1.22 – 1.09 (m, 1H), 0.86 (td, *J* = 7.1, 1.1 Hz, 3H).

^{13}C{^{1}H} NMR ($CDCl_3$, 101 MHz): δ 142.7, 140.4, 135.8, 128.8, 128.3, 127.5, 48.3,

35.3, 34.9, 32.1, 30.6, 30.1, 28.4, 22.9, 14.2.

FTIR (NaCl, thin film, cm^{-1}): 2926, 2855, 1743, 1510, 1456, 1377, 1259, 1103, 1020, 972, 808, 621.

HRMS (FD, *m/z*): $[M]^+$ calcd for $C_{34}H_{48}$: 456.3756; found: 456.3744.

$\boxed{[\alpha]_D^{22} =}$ +1 (c = 0.1, $CHCl_3$).

Analysis of Crude ^{1}H NMR

Connectivity of repeat unit:

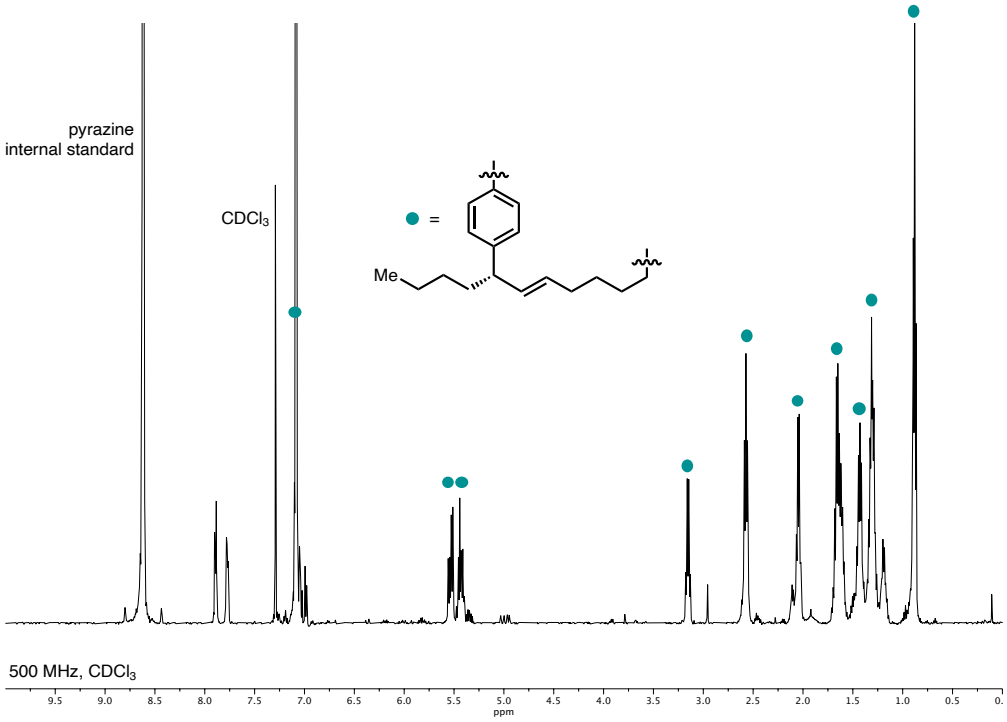

End group analysis:

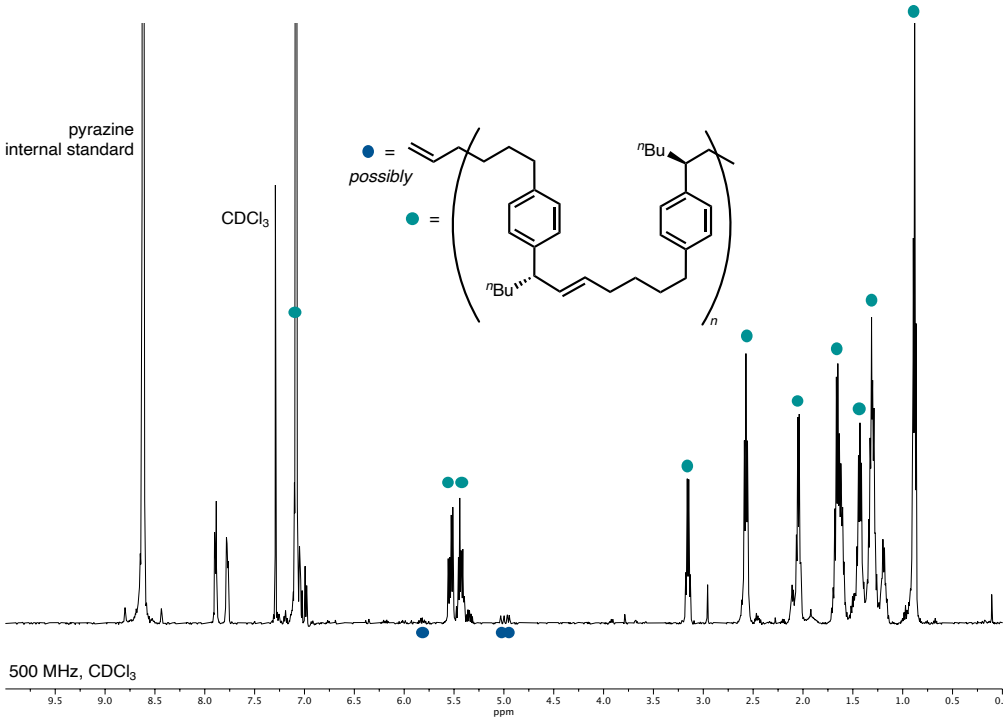

Analysis of Crude via DOSY

Bimodal distribution of species size:

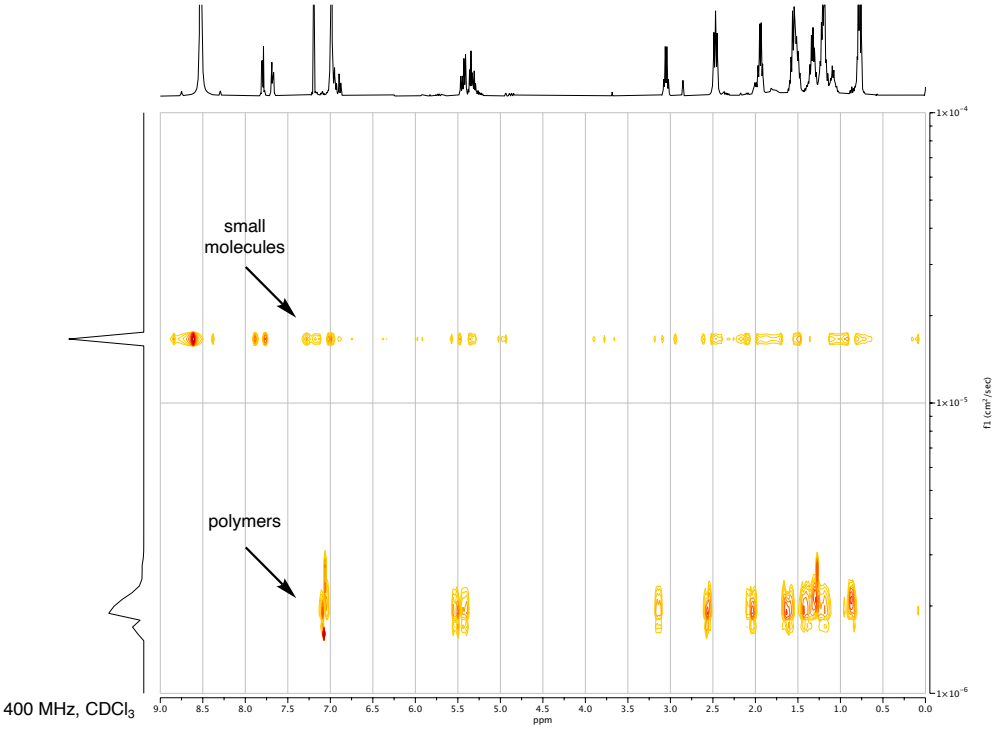

Close-up of olefinic region:

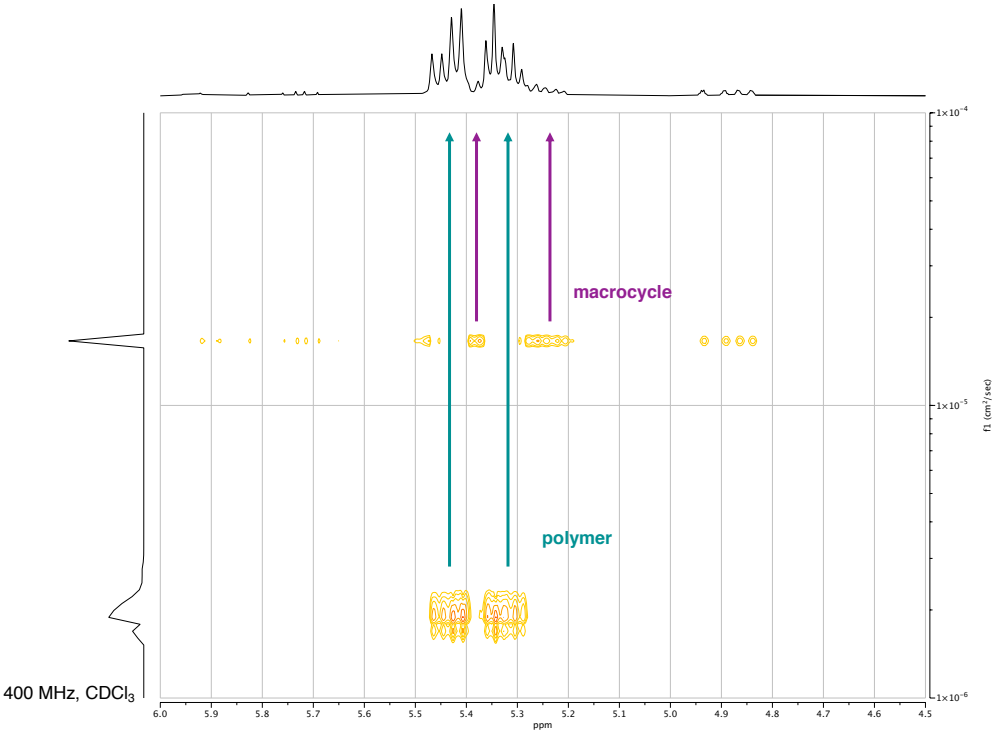

Analysis of Crude ^{1}H NMR for Quantitation of 94 Yield

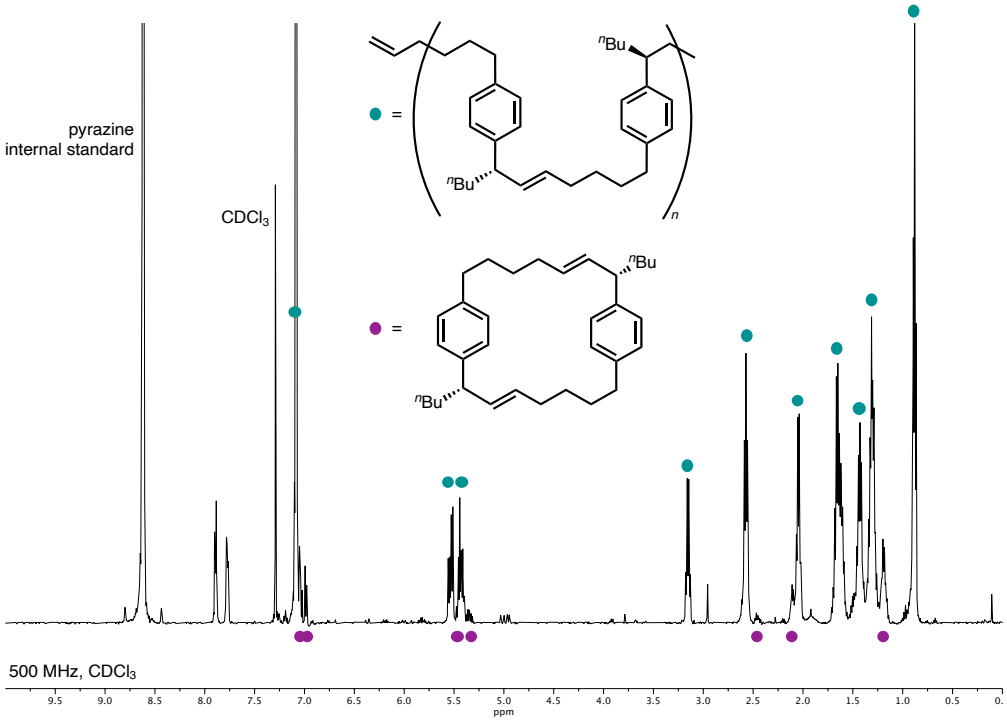

Diastereomeric Ratio Determination via ^{1}H NMR of Macrocycles 94 and 139

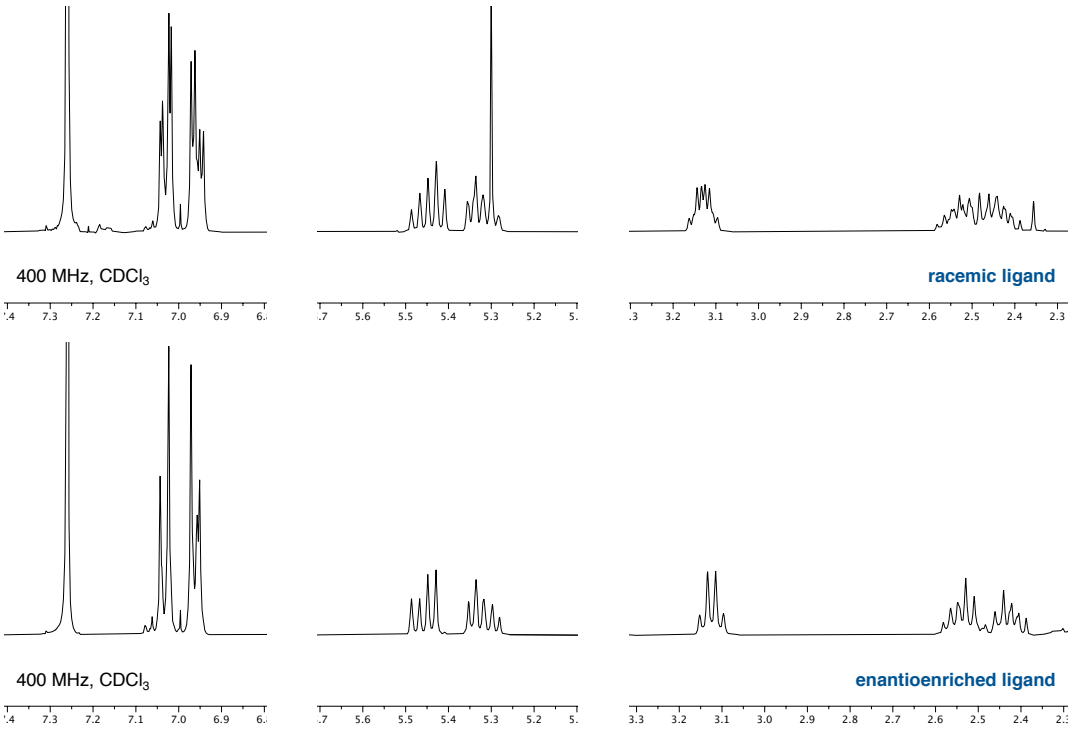

Structural Assignment of Purified Macrocycle 94

^{1}H NMR:

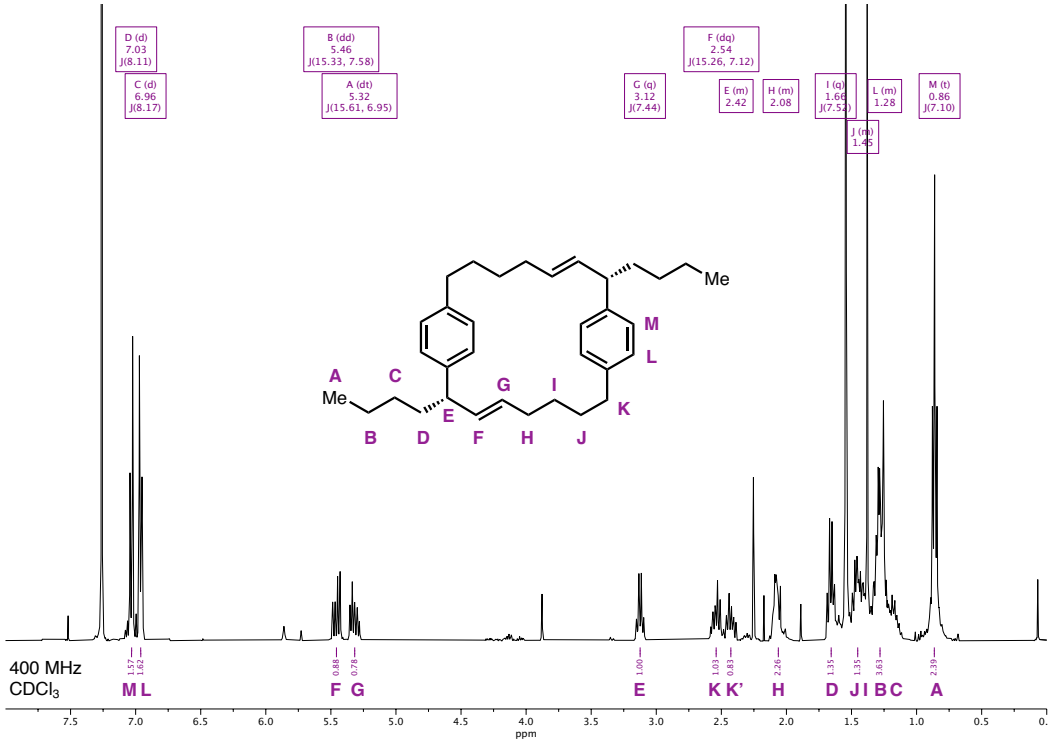

^{13}C NMR:

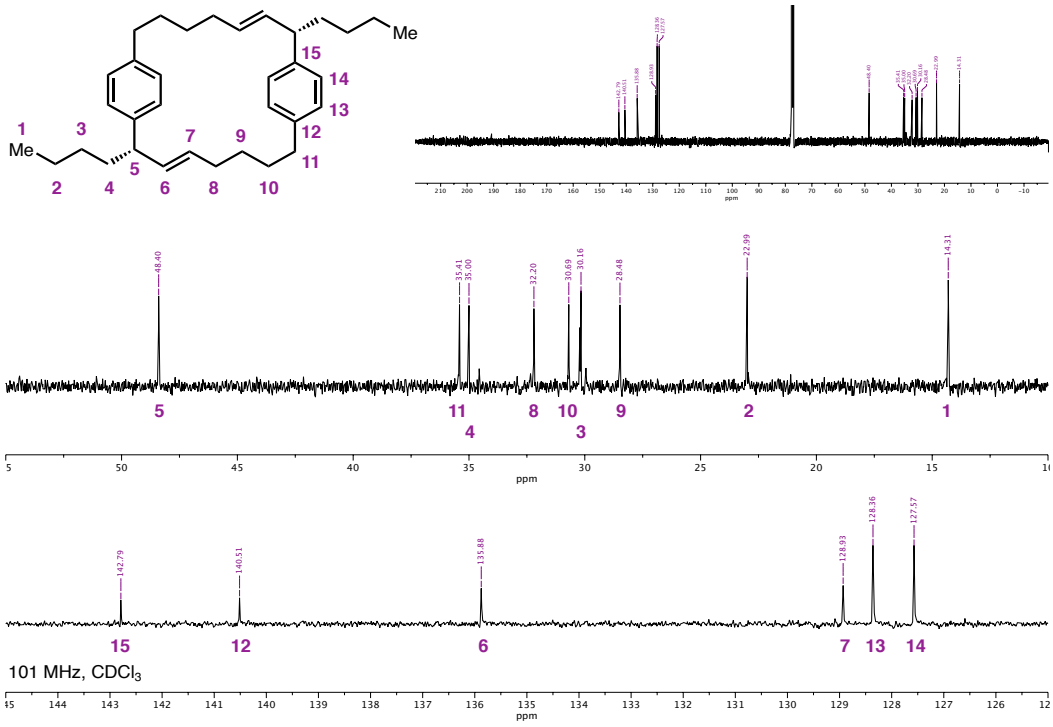

Identification of Polymer 98 by GPC

^{1}H NMR of samples following chromatographic separation (silica, 2.5% Et_2O/hexanes):

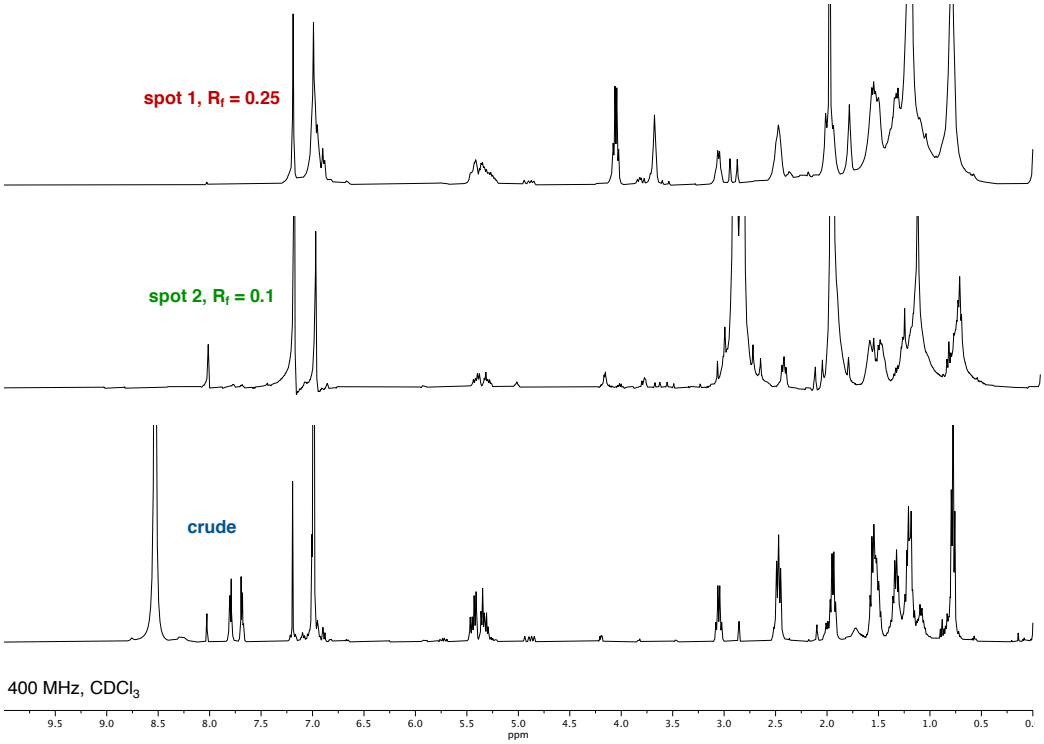

GPC trace of samples:

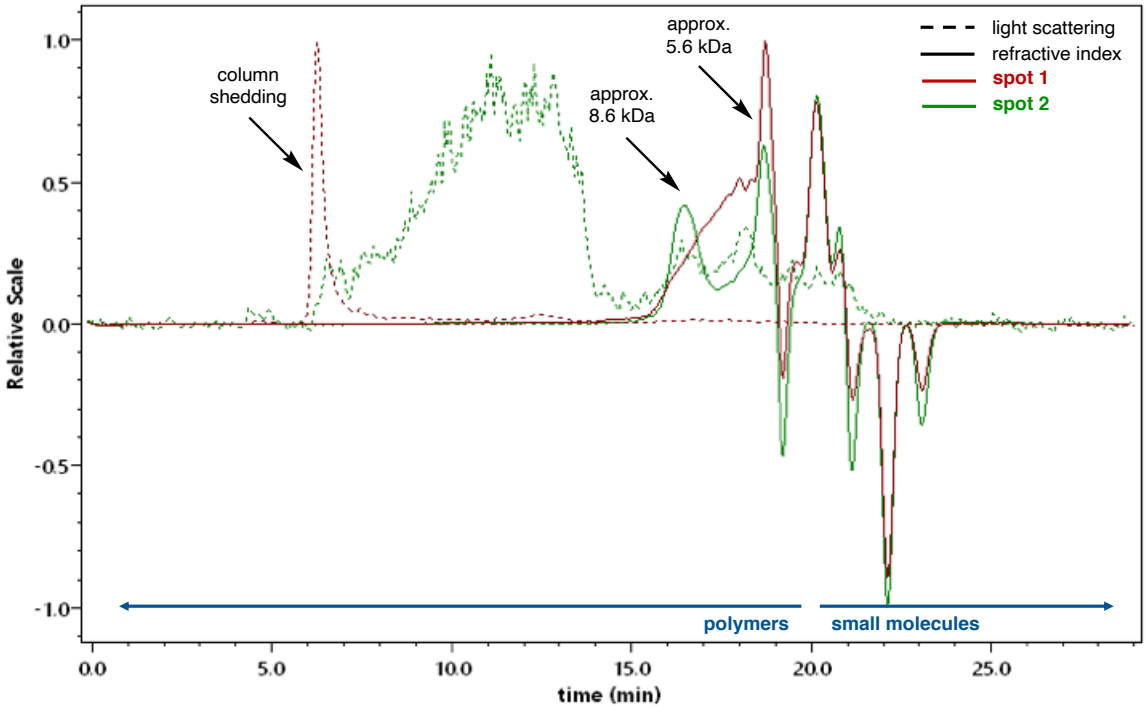

Identification of Polymer 98 by MALDI-TOF MS

GPC trace of polymer samples from reaction at 0.1 M concentration:

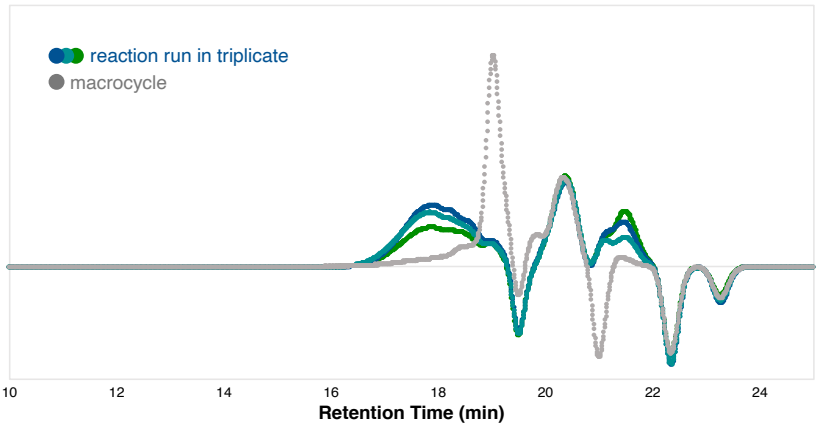

MALDI-TOF MS data for samples (different end groups, same repeat unit):

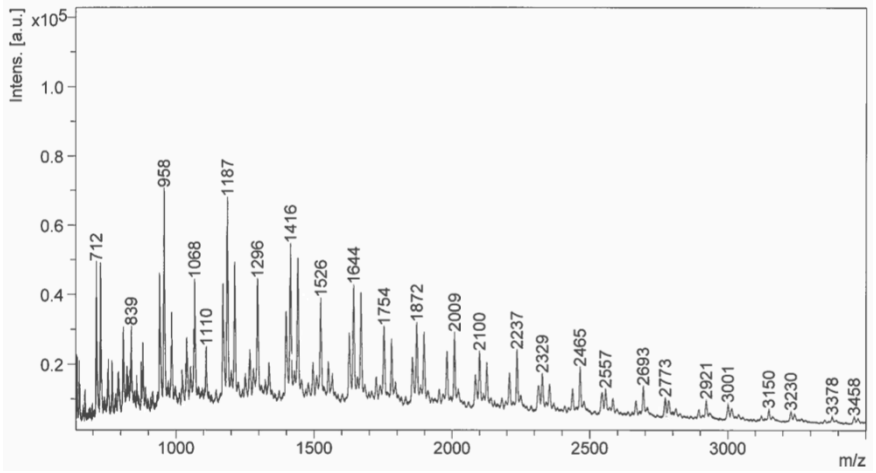

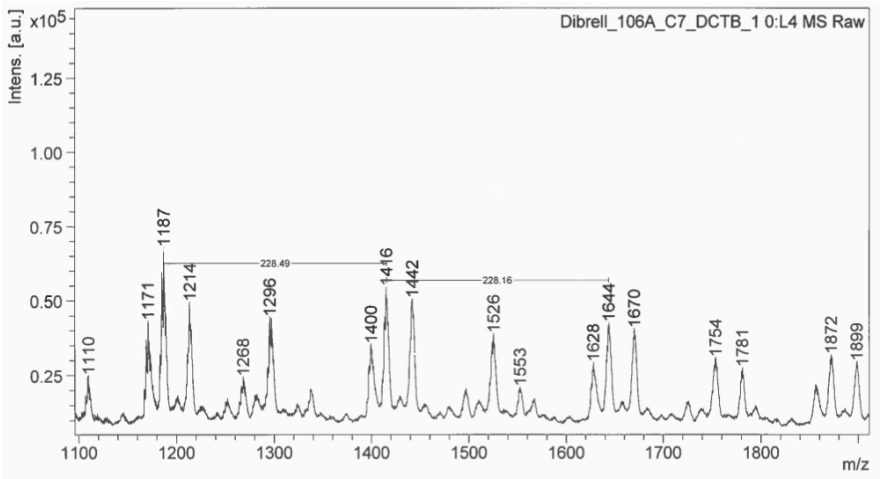

General Procedure F:

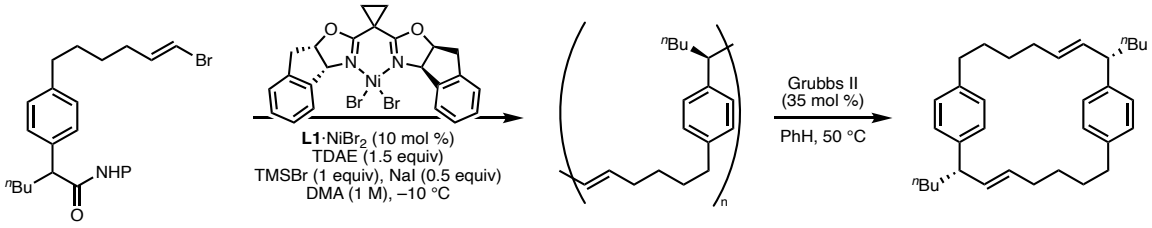

Step 1: General Procedure E was followed, with substrate **85** (35.0 mg, 0.07 mmol, 1 equiv), TDAE (25 μL, 0.11 mmol, 1.5 equiv), TMSBr (9 μL, 0.07 mmol, 1 equiv), NaI (5.3 mg, 0.035 mmol, 0.5 equiv), **L1**·$NiBr_2$ (4.0 mg, 0.007 mmol, 0.1 equiv), and DMA (140 μL, 0.5 M) at –3 °C for 16 h. After the silica filtration, the crude residue was diluted in minimal PhMe then sonicated; the white solids (NHP-containing byproducts) were filtered from the pale yellow supernatant over celite, rinsing with PhMe. The filtrate was concentrated and then diluted in minimal MeCN; the precipitate was collected by filtration, rinsing with MeCN, and concentrated to afford a translucent gel (crude polymer) that was used in the next step.

Step 2: In a N_2-filled glovebox, a 1-dram vial with a stir bar and Teflon cap was charged with the crude polymer (2.2 mg, 0.0096 mmol, 1 equiv). (Note: mmol of polymeric starting material for Step 2 was calculated based on the molecular weight of the repeat unit (228 g/mol).) Then, PhH (0.5 mL, 0.02 M) and Grubbs second generation catalyst (2.9 mg, 0.0034 mmol, 0.35 equiv) were sequentially added. Outside of the glovebox, the mixture was stirred until all solids were dissolved then heated to 50 °C in metal reaction block. After 2 h at that temperature, the reaction was concentrated and assayed by quantitative ^{1}H NMR and DOSY. The sample was concentrated and diluted in THF (2 mg/mL), filtered through a syringe filter, then assayed by GPC and by GCMS-FID (50 to 300 °C) with dodecane as standard, which determined the yield of macrocycle

94 to be 34% with respect to Step 2. (Note: the yield determined by ^{1}H NMR was in good agreement.)

Depolymerization Time Course

^{1}H NMR:

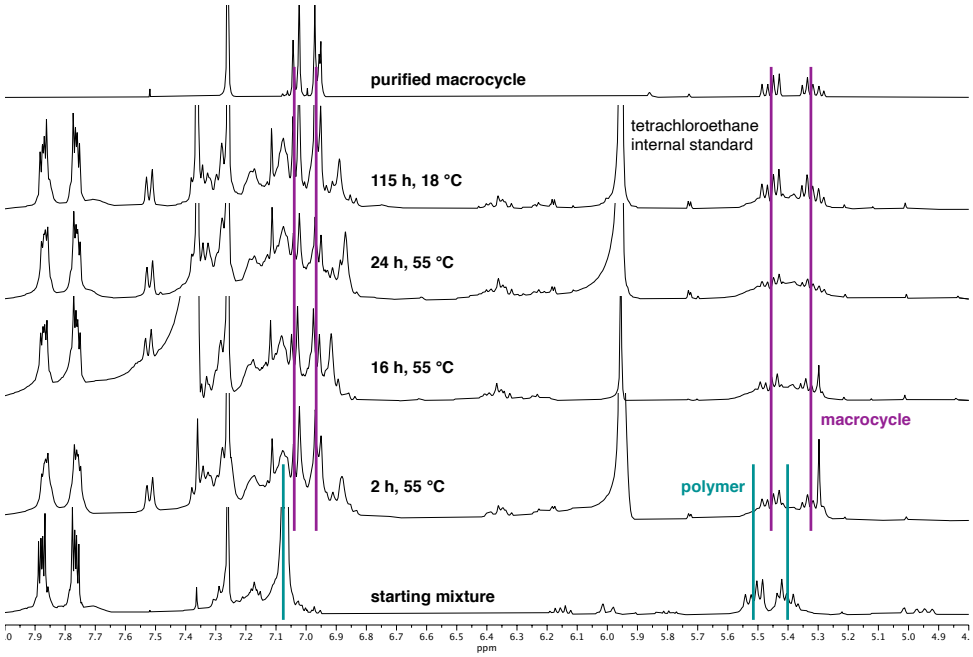

Reaction: G2 (35 mol %), C_6H_6 (0.02 M), **temp**, **time**; Sample: $CDCl_3$ (0.025 M), 400 MHz

DOSY (0.0275 M each):

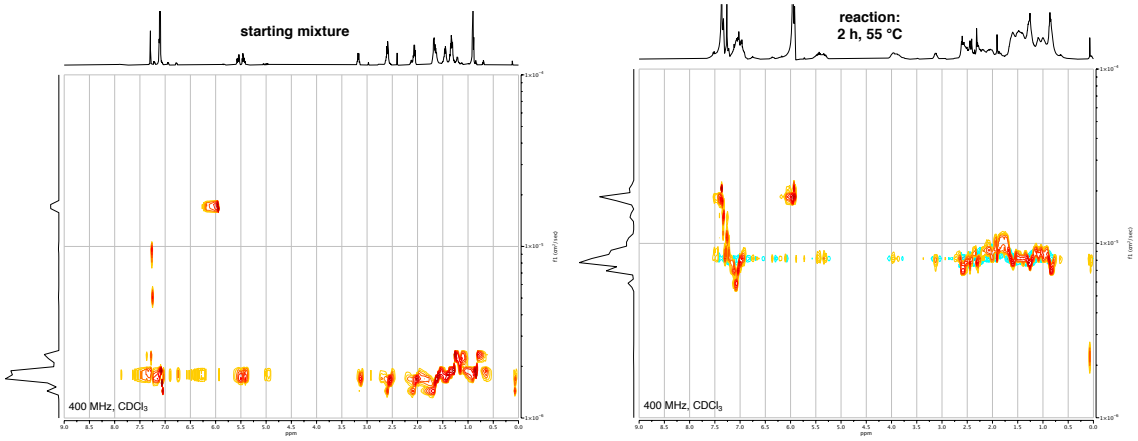

GPC:

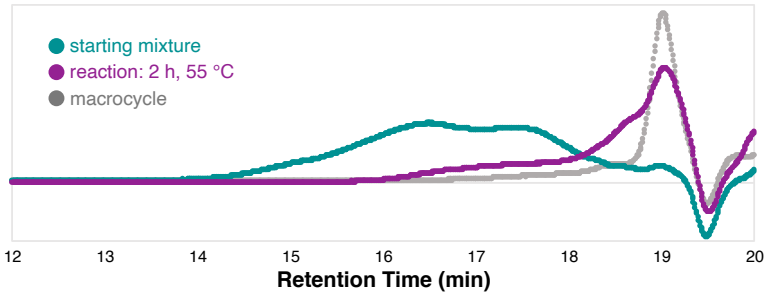

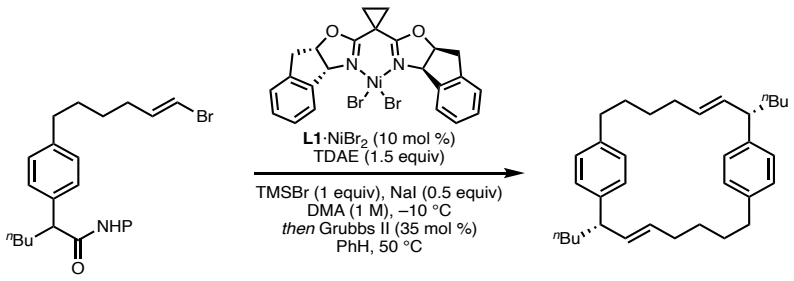

First, General Procedure E was followed with substrate **85** (24.9 mg, 0.05 mmol, 1 equiv), TDAE (17 μL, 0.075 mmol, 1.5 equiv), TMSBr (7 μL, 0.05 mmol, 1 equiv), NaI (3.8 mg, 0.025 mmol, 0.5 equiv), **L1**·$NiBr_2$ (2.9 mg, 0.005 mmol, 0.1 equiv), and DMA (50 μL, 1 M) at –10 °C for 16 h.

Second, in lieu of silica filtration, the reaction was diluted with PhH (1.0 mL) in the glovebox then transferred via pipette to a 2-dram vial with a stir bar and Teflon cap, rinsing with PhH (1.5 mL). To this mixture was added Grubbs second generation catalyst (14.9 mg, 0.0175 mmol, 0.35 equiv). Outside of the glovebox, the mixture was stirred until all solids were dissolved then heated to 50 °C in metal reaction block. After 2 h at that temperature, the reaction mixture was cooled to ambient temperature and then diluted with 20% EtOAc/hexanes and filtered over a plug of silica, eluting with 20% EtOAc/hexanes; the filtrate was concentrated and assayed by quantitative ^{1}H NMR to determine formation of **94** occurred in 18% yield.

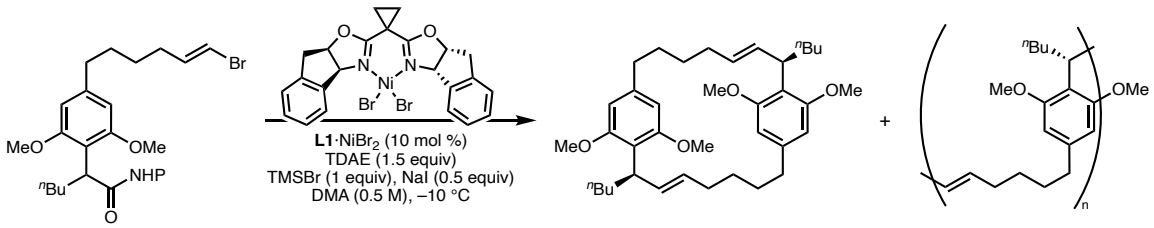

General Procedure E was followed with substrate **57** (35.0 mg, 0.063 mmol, 1 equiv), TDAE (22 μL, 0.094 mmol, 1.5 equiv), TMSBr (8 μL, 0.063 mmol, 1 equiv), NaI (4.7 mg, 0.031 mmol, 0.5 equiv), **L1**·$NiBr_2$ (3.6 mg, 0.0063 mmol, 0.1 equiv), and DMA (126 μL, 1 M) at –10 °C for 16 h. The crude residue was analyzed by quantitative ^1H NMR, DOSY, and GCMS.

Analysis of Crude ^{1}H NMR

Connectivity of repeat unit:

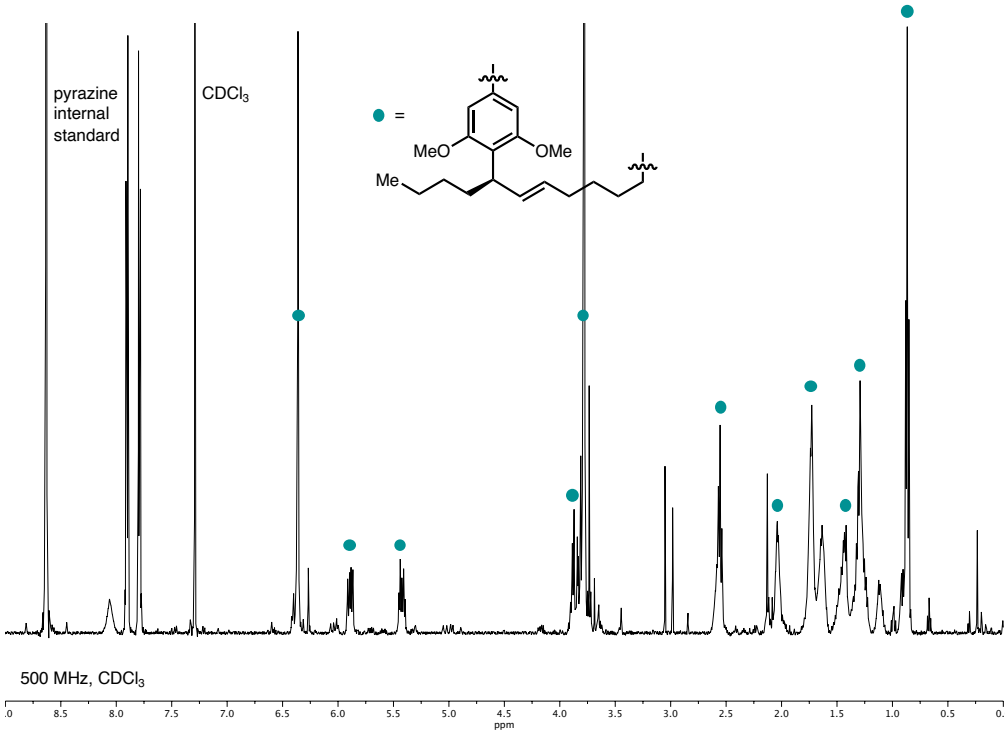

Analysis via DOSY:

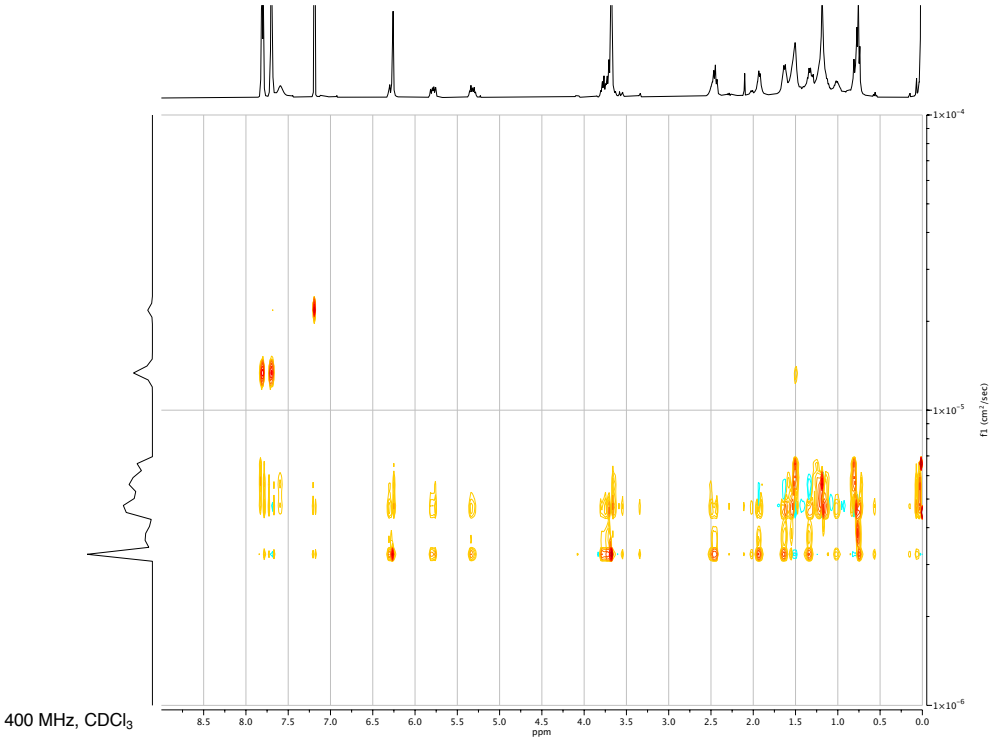

5.8.5 *Revised Approach and Formal Synthesis*

tert-butyl 2-(4-(hex-5-en-1-yl)phenyl)hexanoate (105)

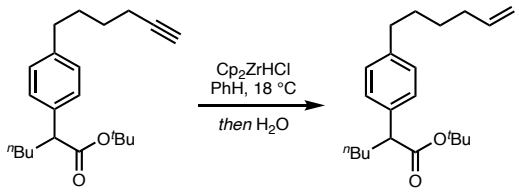

In a N_2-filled glovebox, a flame-dried round-bottom flask was wrapped in foil then charged with Cp_2ZrHCl (1.64 g, 6.4 mmol, 1.3 equiv) and PhH (50 mL, 0.1 M). Outside of the glovebox, alkyne **104** (1.64 g, 5.0 mmol, 1 equiv) was added and the reaction stirred at 18 °C in a darkened fume hood. Upon complete consumption of alkyne, as judged by TLC, water was slowly added. The mixture was extracted with Et_2O. Combined organics were dried over Na_2SO_4, filtered, and concentrated. The crude residue was filtered through a plug of silica, eluting with 5% Et_2O/hexanes. The filtrate was concentrated to afford **105** (1.36 g, 82% yield) as a colorless oil.

^{1}H NMR ($CDCl_3$, 400 MHz): δ 7.22 – 7.16 (m, 2H), 7.14 – 7.07 (m, 2H), 5.80 (ddt, J = 16.9, 10.1, 6.7 Hz, 1H), 4.99 (ddt, J = 17.1, 2.1, 1.6 Hz, 1H), 4.93 (ddt, J = 10.2, 2.3, 1.2 Hz, 1H), 3.42 – 3.34 (m, 1H), 2.62 – 2.54 (m, 2H), 2.11 – 2.04 (m, 2H), 2.04 – 1.93 (m, 1H), 1.74 – 1.57 (m, 3H), 1.48 – 1.41 (m, 2H), 1.39 (s, 9H), 1.36 – 1.13 (m, 4H), 0.87 (t, J = 7.1 Hz, 3H).

^{13}C{^{1}H} NMR ($CDCl_3$, 101 MHz): δ 173.8, 141.3, 139.1, 137.3, 128.5, 127.8, 114.5, 80.5, 52.5, 35.6, 33.8, 33.6, 31.0, 30.0, 28.7, 28.1, 22.7, 14.1.

FTIR (ATR, cm^{-1}): 1727, 1619, 1568, 1455, 1366, 1253, 1144, 1056.

HRMS (FD, *m/z*): $[M]^+$ calcd for $C_{22}H_{34}O_2$: 330.2559; found: 330.2560.

2-(4-(hex-5-en-1-yl)phenyl)hexanoic acid (140)

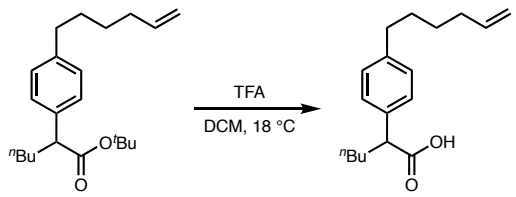

To a round-bottom flask with a stir bar was added ester **105** (1.36 g, 4.1 mmol, 1 equiv) then trifluoroacetic acid/DCM (1:1, 0.2 M). The solution was stirred at 18 °C for 30 minutes and then concentrated. The crude residue was azeotroped with PhMe to afford **140** (1.17 g, quantitative yield) as a yellow oil.

^{1}H NMR ($CDCl_3$, 400 MHz): δ 7.24 – 7.19 (m, 2H), 7.15 – 7.09 (m, 2H), 5.80 (ddt, *J* = 17.0, 10.2, 6.7 Hz, 1H), 4.99 (dq, *J* = 17.1, 1.7 Hz, 1H), 4.94 (ddt, *J* = 10.2, 2.3, 1.2 Hz, 1H), 3.50 (t, *J* = 7.7 Hz, 1H), 2.65 – 2.54 (m, 2H), 2.13 – 1.96 (m, 3H), 1.76 (dddd, *J* = 13.3, 9.4, 7.4, 5.6 Hz, 1H), 1.68 – 1.54 (m, 2H), 1.50 – 1.39 (m, 2H), 1.39 – 1.15 (m, 4H), 0.86 (t, *J* = 7.1 Hz, 6H).

^{13}C{^{1}H} NMR ($CDCl_3$, 101 MHz): δ 180.0, 142.0, 139.0, 136.0, 128.8, 128.0, 114.6, 51.2, 35.6, 33.8, 33.0, 31.0, 29.8, 28.7, 22.6, 14.0.

FTIR (ATR, cm^{-1}): 3080, 2929, 2360, 1703, 1456, 1412, 1264, 1188, 909, 737.

HRMS (TOF-ESI, *m/z*): $[M - H]^-$ calcd for $C_{18}H_{25}O_2$: 274.1933; found: 273.1860.

1,3-dioxoisoindolin-2-yl 2-(4-(hex-5-en-1-yl)phenyl)hexanoate (106)

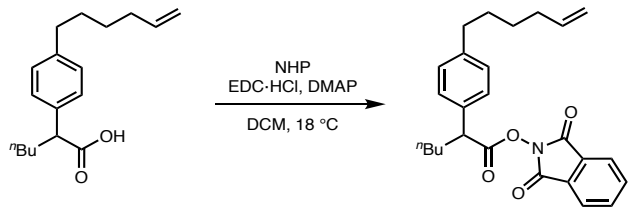

To a round-bottom flask with a stir bar was added acid **140** (1.13 g, 4.1 mmol, 1 equiv), *N*-hydroxyphthalimide (738 mg, 4.5 mmol, 1.1 equiv), DMAP (100 mg, 0.8 mmol, 0.2 equiv), then DCM (21 mL, 0.2 M). Then EDC·HCl (15 mg, 0.08 mmol, 1.1 equiv) was added in one portion. The reaction was stirred at 18 °C for 12 h and then concentrated. The crude residue was filtered through a plug of silica, eluting with EtOAc. The filtrate was concentrated and then purified by column chromatography (silica, 7 to 10% EtOAc/hexanes) to afford **106** (1.48 g, 86% yield) as a white amorphous solid.

^{1}H NMR ($CDCl_3$, 400 MHz): δ 7.85 (dt, *J* = 7.6, 3.8 Hz, 2H), 7.77 (dd, *J* = 5.5, 3.1 Hz, 2H), 7.29 (d, *J* = 8.1 Hz, 2H), 7.23 – 7.15 (m, 2H), 5.81 (ddt, *J* = 16.9, 10.1, 6.7 Hz, 1H), 5.00 (dq, *J* = 17.1, 1.7 Hz, 1H), 4.94 (ddt, *J* = 10.1, 2.2, 1.2 Hz, 1H), 3.89 (t, *J* = 7.6 Hz, 1H), 2.70 – 2.57 (m, 2H), 2.25 – 2.13 (m, 1H), 2.12 – 2.04 (m, 2H), 1.90 (ddt, *J* = 13.3, 9.9, 6.3 Hz, 1H), 1.64 (dtd, *J* = 9.4, 7.7, 6.0 Hz, 2H), 1.45 (pd, *J* = 7.4, 6.9, 3.7 Hz, 2H), 1.40 – 1.30 (m, 4H), 0.91 (t, *J* = 7.0 Hz, 3H).

^{13}C{^{1}H} NMR ($CDCl_3$, 101 MHz): δ 170.7, 142.4, 139.0, 134.8, 134.4, 129.1, 129.0, 128.0, 124.0, 114.6, 48.5, 35.6, 33.8, 33.8, 30.9, 29.5, 28.7, 22.5, 14.0.

FTIR (ATR, cm^{-1}): 3248, 3087, 2934, 2359, 1724, 1633, 1549, 1353, 1057, 877, 695.

HRMS (TOF-ESI, *m/z*): $[M + NH_4]^+$ calcd for $C_{26}H_{34}N_2O_4$: 437.2435; found: 437.2432.

General Procedure G:

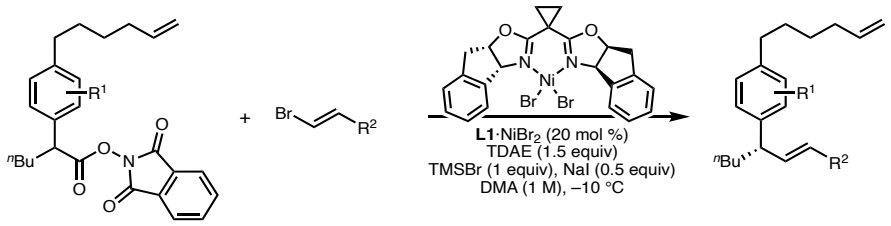

First, a stock solution of the catalyst was prepared. To a ½-dram vial with a stir bar and Teflon cap was added **L1**·$NiBr_2$[75] (5.8 mg, 0.01 mmol, 0.1 equiv). In a N_2-filled glovebox, the vial was charged with DMA (50 μL) the stirred while heating to 80 °C. The mixture was stirred at that temperature until all solids were completely dissolved and a maroon solution was obtained (ca. 5–10 min). Then the vial was allowed to completely cool to ambient temperature. Second, a separate ½-dram vial with a stir bar and Teflon cap was sequentially charged with NaI (7.5 mg, 0.05 mmol, 0.5 equiv) and NHP ester (0.1 mmol, 1 equiv). In a N_2-filled glovebox, this vial was charged with DMA (50 μL).

Then, both vials were transferred into a N_2-filled glovebox fitted with a temperature-controlled well plate. The catalyst stock solution was transferred to the second vial via syringe, followed by alkenyl bromide (0.1 mmol, 1 equiv), then the reaction was stirred at ambient temperature at 250 rpm to ensure complete dissolution of the NHP ester and appropriate mixing of all reagents (the catalyst may not be fully dissolved at this temperature). Then, the vial was placed in a well plate pre-cooled to –10 °C. (Note: the recirculating Julabo LH45 chiller was set to –10 °C but an external thermometer in the glovebox read the temperature as –1 to –4 °C.) At this temperature, TDAE (35 μL, 0.15 mmol, 1.5 equiv) was added and the solution stirred for 10 min before TMSBr (13 μL, 0.1 mmol, 1 equiv) (fumed slightly) was added, each via syringe. The reaction was stirred at 800 rpm at the chilled temperature in the glovebox. After 16 h,

the reaction mixture was diluted with 20% EtOAc/hexanes and filtered over a plug of silica, eluting with 20% EtOAc/hexanes. The filtrate was concentrated, assayed by quantitative ^{1}H NMR, then purified to afford the cross-coupled product, which was assayed by chiral SFC.

(*S*,*E*)-1-(hex-5-en-1-yl)-4-(oct-2-en-4-yl)benzene (108)

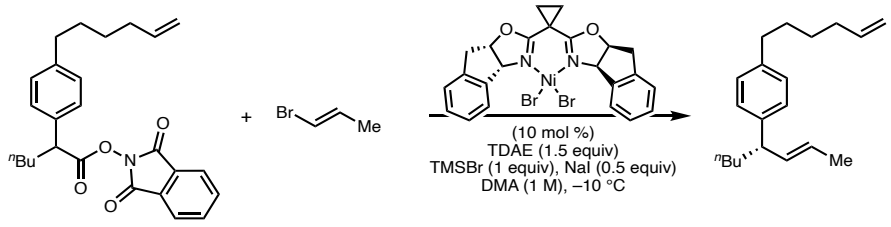

Prepared from NHP ester **106** (44 mg, 0.1 mmol, 1 equiv), 1-bromoprop-1-ene (9:1 *E*/*Z*, 9 μL, 0.1 mmol, 1 equiv), TDAE (35 μL, 0.15 mmol, 1.5 equiv), TMSBr (13 μL, 0.1 mmol, 1 equiv), NaI (7.5 mg, 0.05 mmol, 0.5 equiv), **L1**·$NiBr_2$ (5.8 mg, 0.01 mmol, 0.1 equiv), and DMA (0.1 mL, 1 M) at –10 °C for 16 h following General Procedure G. The crude residue was purified by preparative thin layer chromatography (silica, hexanes) to afford **108** (21 mg, 79% yield, 97:3 *E*/*Z*) as a colorless oil.

^{1}H NMR ($CDCl_3$, 400 MHz): δ 7.13 – 7.04 (m, 4H), 5.81 (ddt, *J* = 17.0, 10.2, 6.7 Hz, 1H), 5.54 (ddq, *J* = 15.1, 7.7, 1.4 Hz, 1H), 5.42 (dqd, *J* = 15.2, 6.2, 0.8 Hz, 1H), 5.00 (dq, *J* = 17.1, 1.7 Hz, 1H), 4.93 (ddt, *J* = 10.1, 2.2, 1.2 Hz, 1H), 3.13 (q, *J* = 7.6 Hz, 1H), 2.64 – 2.49 (m, 2H), 2.15 – 2.03 (m, 2H), 1.70 – 1.56 (m, 8H), 1.49 – 1.38 (m, 2H), 1.36 – 1.21 (m, 3H), 1.21 – 1.08 (m, 1H), 0.86 (t, *J* = 7.1 Hz, 3H).

^{13}C{^{1}H} NMR ($CDCl_3$, 101 MHz): δ 143.1, 140.3, 139.1, 135.7, 128.5, 127.4, 124.3, 114.5, 48.7, 36.0, 35.5, 33.8, 31.1, 30.0, 28.8, 22.8, 18.1, 14.2.

FTIR (ATR, cm^{-1}): 2928, 2856, 2361, 2342, 1640, 1510, 1456, 1377, 965, 910.

HRMS (FI, *m/z*): $[M]^+$ calcd for $C_{20}H_{30}$: 270.2348; found: 270.2365.

$\boxed{[\alpha]_D^{23} =}$ +10 (c = 0.5, $CHCl_3$).

Chiral SFC: (OJ-H, 2.5 mL/min, 100% CO_2, λ = 210 nm); t_R ((*E*)-major) = 4.1 min, t_R ((*E*)-minor) = 4.4 min; t_R ((*Z*)-major) = 4.8 min, t_R ((*Z*)-minor) = 4.6 min.

108: racemic

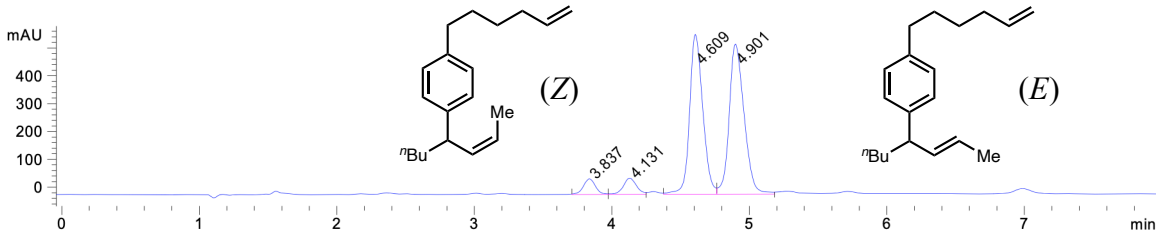

Signal 1: DAD1 A, Sig=210,16 Ref=370,60

Peak #	RetTime [min]	Type	Width [min]	Area [mAU*s]	Height [mAU]	Area %
1	3.837	BV	0.0955	340.55624	55.58408	3.9527
2	4.131	VV	0.1058	389.54742	58.41022	4.5214
3	4.609	VV	0.1061	3824.89404	571.49078	44.3946
4	4.901	VB	0.1163	4060.68286	536.50116	47.1313

(+)-(*E*)-108: enantioenriched (92% ee)

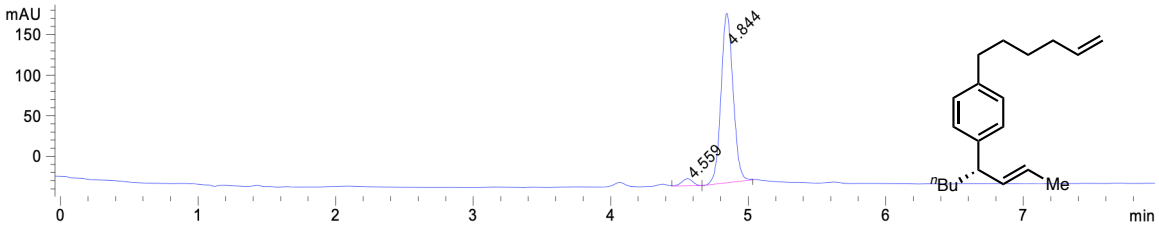

Signal 1: DAD1 A, Sig=210,16 Ref=370,60

Peak #	RetTime [min]	Type	Width [min]	Area [mAU*s]	Height [mAU]	Area %
1	4.559	VV	0.0863	48.95547	8.88725	3.7146
2	4.844	VB	0.0928	1268.97791	209.10361	96.2854

(*Z*)-108: enantioenriched (44% ee)

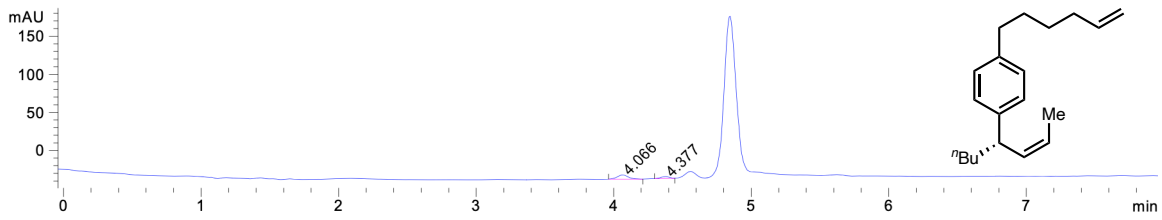

Signal 1: DAD1 A, Sig=210,16 Ref=370,60

Peak #	RetTime [min]	Type	Width [min]	Area [mAU*s]	Height [mAU]	Area %
1	4.066	BB	0.0846	29.20012	5.43954	72.3430
2	4.377	BV	0.0722	11.16334	2.49266	27.6570

General Procedure H:

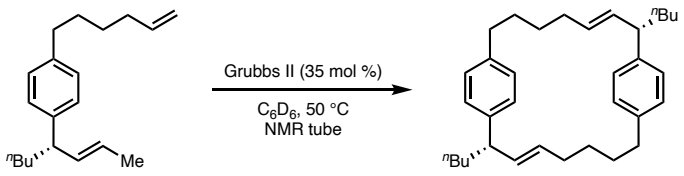

In a N_2-filled glovebox, a 1-dram vial with a stir bar was sequentially charged with an NMR tube was sequentially charged with **108** (4.3 mg, 0.016 mmol, 1 equiv), C_6D_6 (0.7 mL, 0.023 M), Grubbs second generation catalyst (4.7 mg, 0.0056 mmol, 0.35 equiv), and 2,3,4,5-tetrachloronitrobenzene (6.4 mg, 0.025 mmol, 1.54 equiv) as internal standard. The reaction was stirred at ambient temperature until all reagents dissolved (ca. 1 min) and then transferred via syringe into an NMR tube, which was capped and sealed with electrical tape. Outside the glovebox, the NMR tube was heated to 50 °C in an oil bath. At varying time points, the reaction was allowed to cool to ambient temperature, assayed by quantitative ^{1}H NMR to determine the yield of **94**, then returned to the heated oil bath.

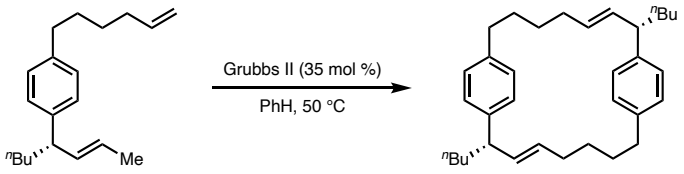

Prepared following a modified procedure:[73] In a N_2-filled glovebox, a 1-dram vial with a stir bar and Teflon cap was sequentially charged with **108** (4.7 mg, 0.017 mmol, 1 equiv), PhH (0.87 mL, 0.02 M), and Grubbs second generation catalyst (5.2 mg, 0.006 mmol, 0.35 equiv). Outside of the glovebox, the mixture was stirred until all solids were dissolved and then heated to 50 °C in an oil bath. After 2 h at that temperature, the reaction was concentrated, assayed by quantitative ^{1}H NMR, then purified by sequential preparative thin layer chromatography (silica, hexanes; then, silica, hexanes) to afford **94** (1.4 mg, 18% yield) as a colorless oil.

$\boxed{[\alpha]_D^{23} =}$ +66 (c = 0.01, $CHCl_3$).

(*S*)-6-iodo-5-methylhex-1-ene (141)

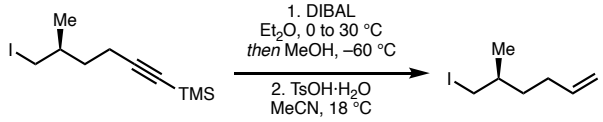

Step 1: Prepared from alkyne **60** (1.18 g, 4 mmol, 1 equiv), diisobutylaluminum hydride (1.0 M in hexanes, 4.1 mL, 4.1 mmol, 1.02 equiv), and Et_2O (4.2 mL, 0.95 M) following a published procedure[160] to afford the alkene intermediate as a clear oil.

Step 2: Prepared from the intermediate alkene (1 equiv), *p*-toluenesulfonic acid monohydrate (1.5 g, 8 mmol, 2 equiv), and MeCN (3.3 mL, 1.2 M) following a published procedure.[160] The crude residue was purified by column chromatography (silica, 0 to 1% Et_2O/hexanes) to afford **141** (764 mg, 78% yield over 2 steps) as a colorless oil. Spectra

matched those reported in the literature.[73]

^{1}H NMR ($CDCl_3$, 500 MHz): δ 5.79 (ddt, *J* = 16.9, 10.2, 6.6 Hz, 1H), 5.03 (dq, *J* = 17.1, 1.7 Hz, 1H), 4.97 (ddd, *J* = 10.2, 2.1, 1.1 Hz, 1H), 3.24 (dd, *J* = 9.6, 4.4 Hz, 1H), 3.18 (dd, *J* = 9.6, 5.7 Hz, 1H), 2.07 (dddq, *J* = 9.8, 6.4, 4.8, 1.6 Hz, 2H), 1.54 – 1.45 (m, 2H), 1.40 – 1.26 (m, 1H), 1.00 (d, *J* = 6.3 Hz, 3H).

$\boxed{[\alpha]_D^{23} =}$ +2 (c = 0.3, $CHCl_3$).

tert-butyl 2-(2,6-dimethoxy-4-((*S*)-2-methylhex-5-en-1-yl)phenyl)hexanoate (110)

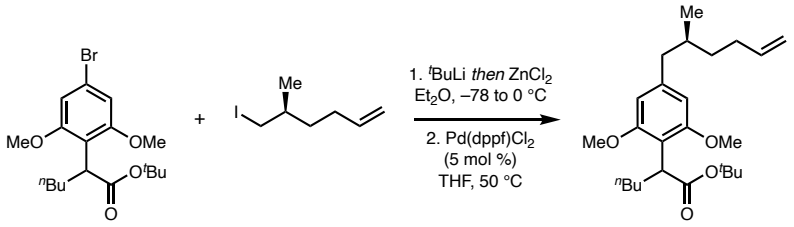

Prepared from aryl bromide **52** (200 mg, 0.52 mmol, 1 equiv), alkyl iodide **141** (297 mg, 1.03 mmol, 2 equiv), ^{t}BuLi (1.7 M in pentane, 1.3 mL, 2.17 mmol, 4.2 equiv), $ZnCl_2$ (0.5 M in THF, 2.1 mL, 1.03 mmol, 2 equiv), and Pd(dppf)Cl_2 (18.9 mg, 0.026 mmol, 0.05 equiv) following a modified procedure.[73] The crude residue was purified by preparative thin layer chromatography (silica, 2.5% EtOAc/7.5% DCM/hexanes) to afford **110** (167 mg, 80% yield) as a colorless oil.

^{1}H NMR ($CDCl_3$, 500 MHz): δ 6.30 (s, 2H), 5.80 (ddt, *J* = 17.3, 10.1, 6.6 Hz, 1H), 5.00 (dd, *J* = 17.1, 1.9 Hz, 1H), 4.97 – 4.87 (m, 1H), 3.96 (dd, *J* = 9.0, 5.4 Hz, 1H), 3.75 (s, 6H), 2.65 – 2.55 (m, 1H), 2.38 – 2.26 (m, 1H), 2.15 (td, *J* = 14.4, 6.3 Hz, 1H), 2.05 (ddt, *J* = 15.5, 10.3, 5.3 Hz, 2H), 1.77 (q, *J* = 6.8 Hz, 1H), 1.65 (dtd, *J* = 14.2, 9.4, 5.1 Hz, 1H), 1.52 – 1.42 (m, 1H), 1.36 (t, *J* = 1.3 Hz, 8H), 1.34 – 1.13 (m, 4H), 1.08 (q, *J* = 4.2, 3.4

Hz, 1H), 0.88 (dd, *J* = 6.6, 1.4 Hz, 3H), 0.84 (t, *J* = 7.1 Hz, 3H).

$^{13}C\{^{1}H\}$ NMR ($CDCl_3$, 101 MHz): δ 174.6, 157.8, 141.2, 139.3, 115.8, 114.3, 104.9, 79.3, 55.7, 44.4, 40.9, 36.0, 34.5, 31.5, 29.9, 29.6, 28.1, 22.9, 19.6, 14.2.

FTIR (ATR, cm^{-1}): 2955, 2929, 1729, 1585, 1455, 1247, 1159, 1125.

HRMS (FD, *m/z*): $[M]^+$ calcd for $C_{25}H_{40}O_4$: 404.2927; found: 404.2943.

$\boxed{[\alpha]_D^{23} =}$ –6 (c = 0.3, $CHCl_3$).

2-(2,6-dimethoxy-4-((*S*)-2-methylhex-5-en-1-yl)phenyl)hexanoic acid (142)

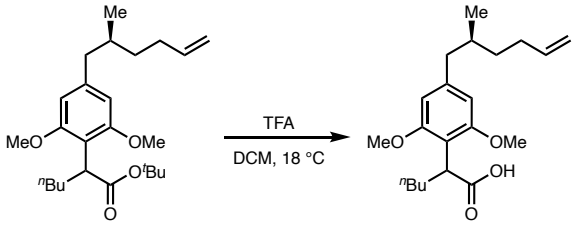

To a round-bottom flask with a stir bar was added ester **110** (154 mg, 0.38 mmol, 1 equiv) then trifluoroacetic acid/DCM (1:1, 0.2 M). The solution was stirred at 18 °C for 30 minutes and then concentrated. The crude residue was azeotroped with PhMe to afford **142** (136 mg, 97% yield) as a pale yellow oil.

^{1}H NMR ($CDCl_3$, 400 MHz): δ 6.33 (s, 2H), 5.81 (ddt, *J* = 16.9, 10.2, 6.6 Hz, 1H), 5.01 (dt, *J* = 17.1, 1.8 Hz, 1H), 4.94 (ddt, *J* = 10.3, 2.4, 1.2 Hz, 1H), 4.13 (dd, *J* = 8.9, 5.6 Hz, 1H), 3.77 (s, 6H), 2.71 – 2.50 (m, 1H), 2.32 (ddd, *J* = 13.4, 8.2, 1.1 Hz, 1H), 2.25 – 1.98 (m, 3H), 1.84 – 1.62 (m, 2H), 1.48 (ddt, *J* = 13.3, 9.7, 5.8 Hz, 1H), 1.42 – 1.15 (m, 4H), 1.16 – 1.01 (m, 1H), 0.88 (d, *J* = 6.6 Hz, 3H), 0.83 (t, *J* = 7.1 Hz, 3H).

$^{13}C\{^{1}H\}$ NMR ($CDCl_3$, 101 MHz): δ 180.0, 157.8, 142.1, 139.2, 114.4, 114.3, 105.3, 55.8, 44.4, 39.8, 36.0, 34.5, 31.5, 29.7, 29.7, 22.8, 19.6, 14.2.

FTIR (ATR, cm^{-1}): 2955, 2930, 1703, 1585, 1455, 1125.

HRMS (TOF-ESI, *m/z*): $[M - H]^-$ calcd for $C_{21}H_{32}O_4$: 347.2228; found: 347.2225.

$\boxed{[\alpha]_D^{23} =}$ –8 (c = 0.4, $CHCl_3$).

1,3-dioxoisoindolin-2-yl 2-(2,6-dimethoxy-4-((*S*)-2-methylhex-5-en-1-yl)phenyl)hexanoate (111)

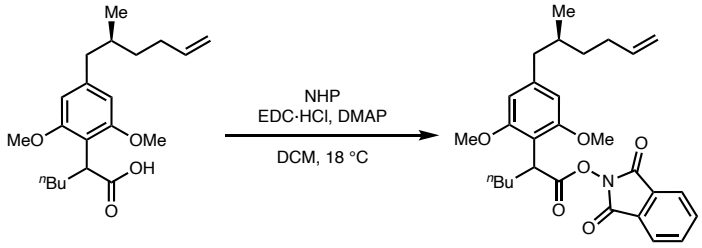

To a round-bottom flask with a stir bar was added acid **142** (240 mg, 0.69 mmol, 1 equiv), *N*-hydroxyphthalimide (112 mg, 0.69 mmol, 1 equiv), DMAP (17 mg, 0.14 mmol, 0.2 equiv), then DCM (3.4 mL, 0.2 M). Then EDC·HCl (132 mg, 0.69 mmol, 1 equiv) was added in one portion. The reaction was stirred at 18 °C overnight and then concentrated. The crude residue was purified by preparative thin layer chromatography (silica, 70% DCM/hexanes) to afford **111** (300 mg, 88% yield) as a thick, colorless oil.

^{1}H NMR ($CDCl_3$, 400 MHz): δ 7.84 (d, *J* = 5.2 Hz, 2H), 7.74 (dd, *J* = 5.5, 3.1 Hz, 2H), 6.36 (s, 2H), 5.89 – 5.74 (m, 1H), 5.01 (dt, *J* = 17.1, 1.8 Hz, 1H), 4.94 (dd, *J* = 10.4, 1.9 Hz, 1H), 4.47 (dd, *J* = 8.8, 5.4 Hz, 1H), 3.85 (s, 6H), 2.65 (ddd, *J* = 13.4, 6.0, 1.8 Hz, 1H), 2.35 (ddd, *J* = 13.0, 8.3, 3.7 Hz, 1H), 2.17 (dtd, *J* = 12.7, 6.6, 5.0, 3.2 Hz, 2H), 2.11 – 2.00 (m, 0H), 1.82 (dtd, *J* = 21.4, 12.2, 10.7, 6.9 Hz, 2H), 1.62 – 1.41 (m, 1H), 1.41 – 1.22 (m, 4H), 1.18 (ddp, *J* = 10.0, 7.8, 2.7 Hz, 1H), 0.90 (d, *J* = 6.6 Hz, 3H), 0.85 (t, *J* = 6.9 Hz, 3H).

$^{13}C\{^{1}H\}$ NMR ($CDCl_3$, 101 MHz): δ 171.5, 157.7, 142.7, 142.7, 139.3, 134.6, 129.3, 123.8, 114.4, 112.1, 104.7, 104.7, 55.8, 44.5, 37.8, 36.1, 34.5, 34.4, 31.5, 29.9, 29.6, 29.3, 22.7, 19.6, 14.1.

FTIR (ATR, cm^{-1}): 1742, 1456, 1117, 965, 695.

HRMS (FD, *m/z*): $[M]^+$ calcd for $C_{29}H_{35}NO_6$: 493.2464; found: 493.2453.

$\boxed{[\alpha]_D^{23} =}$ –6 (c = 1.3, $CHCl_3$).

1,3-dimethoxy-5-((*S*)-2-methylhex-5-en-1-yl)-2-((*S*,*E*)-oct-2-en-4-yl)benzene (112)

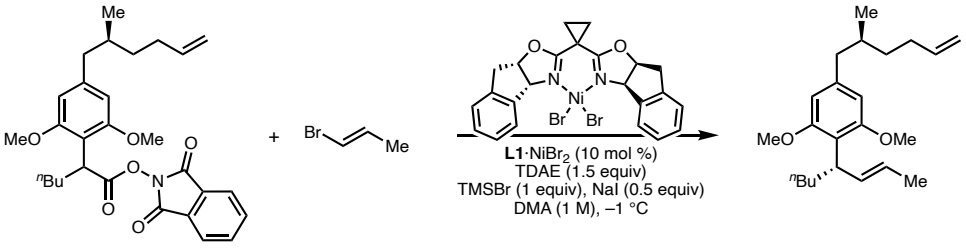

Prepared from NHP ester **111** (49 mg, 0.1 mmol, 1 equiv), 1-bromoprop-1-ene (9:1 *E*/*Z*, 9 μL, 0.1 mmol, 1 equiv), TDAE (35 μL, 0.15 mmol, 1.5 equiv), TMSBr (13 μL, 0.1 mmol, 1 equiv), NaI (7.5 mg, 0.05 mmol, 0.5 equiv), **L1**·$NiBr_2$ (5.8 mg, 0.01 mmol, 0.1 equiv), and DMA (0.1 mL, 1 M) at –10 °C for 16 h following General Procedure G. The crude residue was purified by column chromatography (silica, 20% PhMe/hexanes) to afford **112** (16 mg, 47% yield) as a colorless oil.

^{1}H NMR ($CDCl_3$, 400 MHz): δ 6.32 (s, 3H), 5.90 (ddq, *J* = 15.2, 8.6, 1.6 Hz, 1H), 5.81 (ddt, *J* = 16.9, 10.1, 6.6 Hz, 1H), 5.43 (dqd, *J* = 15.2, 6.4, 1.0 Hz, 2H), 5.01 (dq, *J* = 17.2, 1.7 Hz, 1H), 4.94 (ddt, *J* = 10.2, 2.3, 1.2 Hz, 1H), 3.86 (q, *J* = 8.0 Hz, 1H), 3.78 (s, 8H), 2.58 (dd, *J* = 13.4, 6.1 Hz, 1H), 2.31 (dd, *J* = 13.3, 8.2 Hz, 1H), 2.23 – 2.10 (m, 1H), 2.10 – 1.99 (m, 1H), 1.84 – 1.64 (m, 3H), 1.63 (dd, *J* = 6.1, 1.6 Hz, 4H), 1.48 (dddd, *J* = 13.3,

9.7, 6.2, 5.2 Hz, 1H), 1.40 – 1.14 (m, 4H), 1.14 – 1.01 (m, 1H), 0.88 (d, *J* = 6.7 Hz, 3H), 0.84 (t, *J* = 7.2 Hz, 4H).

$^{13}C\{^{1}H\}$ NMR ($CDCl_3$, 101 MHz): δ 158.1, 140.4, 139.3, 134.7, 124.0, 119.3, 114.3, 105.9, 56.0, 44.2, 39.0, 36.0, 34.5, 33.6, 31.6, 30.6, 22.9, 19.6, 18.1, 14.3.

FTIR (ATR, cm^{-1}): 2954, 2927, 1579, 1233, 1138, 1118, 970.

HRMS (FD, *m/z*): $[M]^+$ calcd for $C_{23}H_{36}O_2$: 344.2715; found: 344.2739.

$\boxed{[\alpha]_D^{23} =}$ +8 (c = 0.5, $CHCl_3$).

1,3-dimethoxy-5-((*S*)-2-methylhex-5-en-1-yl)-2-((*E*)-oct-2-en-4-yl)benzene (143)

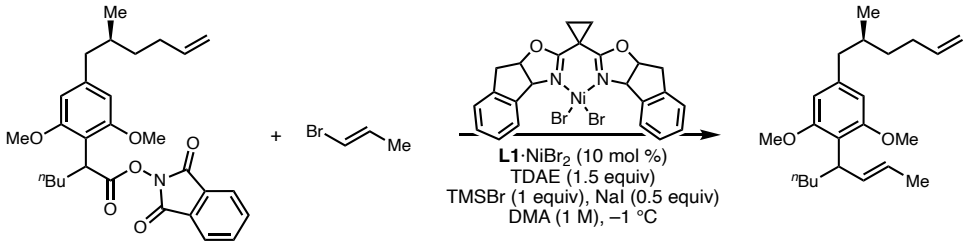

Prepared from NHP ester **111** (49 mg, 0.1 mmol, 1 equiv), 1-bromoprop-1-ene (9:1 *E*/*Z*, 9 μL, 0.1 mmol, 1 equiv), TDAE (35 μL, 0.15 mmol, 1.5 equiv), TMSBr (13 μL, 0.1 mmol, 1 equiv), NaI (7.5 mg, 0.05 mmol, 0.5 equiv), racemic **L1**·$NiBr_2$ (5.8 mg, 0.01 mmol, 0.1 equiv), and DMA (0.1 mL, 1 M) at –10 °C for 16 h following General Procedure G. The crude residue was purified by column chromatography (silica, 20% PhMe/hexanes) to afford **143** (13 mg, 38% yield) as a colorless oil.

^{1}H NMR ($CDCl_3$, 400 MHz): δ 6.32 (s, 2H), 5.96 – 5.85 (m, 1H), 5.85 – 5.74 (m, 1H), 5.43 (dqd, *J* = 15.2, 6.4, 1.0 Hz, 1H), 5.01 (dq, *J* = 17.1, 1.7 Hz, 1H), 4.94 (ddt, *J* = 10.2, 2.3, 1.3 Hz, 1H), 3.86 (q, *J* = 8.0 Hz, 1H), 3.78 (s, 6H), 2.59 (dd, *J* = 13.4, 6.1 Hz, 1H), 2.31 (dd, *J* = 13.4, 8.2 Hz, 1H), 2.23 – 2.11 (m, 1H), 2.11 – 1.99 (m, 1H), 1.82 – 1.66 (m,

3H), 1.63 (dd, J = 6.4, 1.6 Hz, 3H), 1.53 – 1.42 (m, 1H), 1.38 – 1.16 (m, 4H), 1.16 – 1.01 (m, 1H), 0.88 (d, J = 6.6 Hz, 2H), 0.85 (t, J = 7.2 Hz, 2H).

$^{13}C\{^{1}H\}$ NMR ($CDCl_3$, 101 MHz): δ 158.1, 158.1, 140.4, 139.3, 134.7, 124.0, 119.3, 114.3, 105.9, 56.0, 44.2, 39.0, 36.0, 34.5, 33.6, 31.6, 30.6, 22.9, 19.6, 18.1, 14.3.

FTIR (ATR, cm^{-1}): 2927, 1579, 1454, 1419, 1233, 1138, 1118, 969.

$\boxed{[\alpha]_D^{23} =}$ –7 (c = 0.7, $CHCl_3$).

(2*S*,3*E*,10*S*,11*E*)-2,10-dibutyl-12,16,93,95-tetramethoxy-1,9(1,4)-dibenzenacyclohexadecaphane-3,11-diene (113)

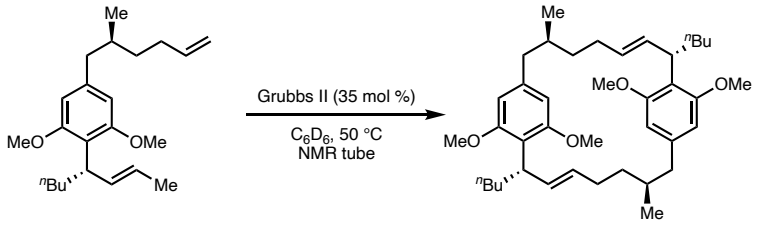

General Procedure H was followed with **112** (1.8 mg, 0.0052 mmol, 1 equiv), C_6D_6 (261 µL, 0.02 M), Grubbs second generation catalyst (1.6 mg, 0.0019 mmol, 0.36 equiv), and 2,3,4,5-tetrachloronitrobenzene (2.1 mg, 0.008 mmol, 1.54 equiv).

(*S*,*E*)-1-(hex-5-en-1-yl)-4-(oct-2-en-4-yl)benzene (144)

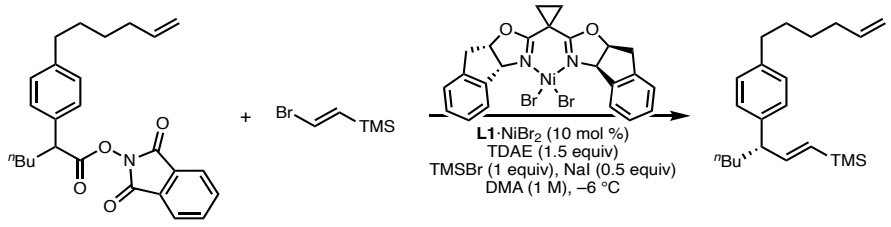

Prepared from NHP ester **106** (44 mg, 0.1 mmol, 1 equiv), (*E*)-(2-bromovinyl)trimethylsilane (16 µL, 0.1 mmol, 1 equiv), TDAE (35 µL, 0.15 mmol, 1.5

equiv), TMSBr (13 μL, 0.1 mmol, 1 equiv), NaI (7.5 mg, 0.05 mmol, 0.5 equiv), **L1**·$NiBr_2$ (5.8 mg, 0.01 mmol, 0.1 equiv), and DMA (0.1 mL, 1 M) at –6 °C for 12 h following General Procedure G. The crude residue was purified by preparative thin layer chromatography (silica, hexanes) to afford **144** (27 mg, 83% yield) as a colorless oil.

^{1}H NMR ($CDCl_3$, 400 MHz): δ 7.14 – 7.04 (m, 4H), 6.10 (dd, *J* = 18.6, 7.1 Hz, 1H), 5.81 (ddt, *J* = 16.9, 10.2, 6.7 Hz, 1H), 5.63 (dt, *J* = 18.5, 0.9 Hz, 1H), 5.06 – 4.96 (m, 1H), 4.94 (ddt, *J* = 10.2, 2.2, 1.2 Hz, 1H), 3.33 – 3.14 (m, 1H), 2.63 – 2.54 (m, 2H), 2.14 – 2.04 (m, 2H), 1.75 – 1.56 (m, 4H), 1.50 – 1.39 (m, 2H), 1.36 – 1.24 (m, 3H), 1.24 – 1.09 (m, 1H), 0.86 (t, *J* = 7.1 Hz, 3H), 0.04 (d, *J* = 0.7 Hz, 9H).

^{13}C{^{1}H} NMR ($CDCl_3$, 101 MHz): δ 150.4, 142.1, 140.4, 139.1, 128.8, 128.5, 127.7, 114.5, 52.2, 35.6, 35.4, 33.8, 31.1, 29.9, 28.8, 22.8, 14.2, -1.0.

FTIR (ATR, cm^{-1}): 1979, 1608, 1456, 1258, 988, 866, 835, 739.

HRMS (TOF-ESI, *m/z*): $[M + Na]^+$ calcd for $C_{22}H_{36}SiNa$: 351.2478; found: 351.1781.

HRMS (FD, *m/z*): $[M]^+$ calcd for $C_{22}H_{36}Si$: 328.2586; found: 328.2572.

$\boxed{[\alpha]_D^{23} =}$ +29 (c = 0.3, $CHCl_3$).

Chiral SFC: (OJ-H, 2.5 mL/min, 100% CO_2, λ = 210 nm); t_R (major) = 2.5 min, t_R (minor) = 2.4 min.

144: racemic

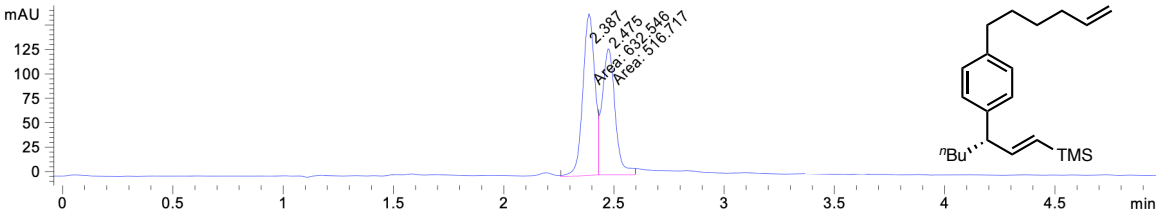

Signal 1: DAD1 A, Sig=210,16 Ref=370,60

Peak #	RetTime [min]	Type	Width [min]	Area [mAU*s]	Height [mAU]	Area %
1	2.387	MM	0.0635	632.54620	166.12740	55.0393
2	2.475	MM	0.0663	516.71655	129.80881	44.9607

(+)-144: enantioenriched (98% ee)

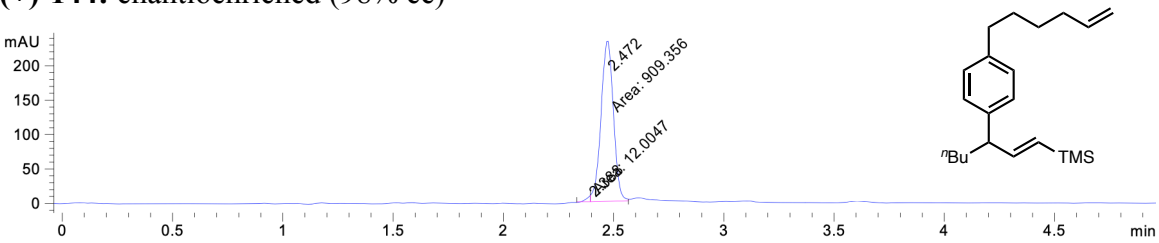

Signal 1: DAD1 A, Sig=210,16 Ref=370,60

Peak #	RetTime [min]	Type	Width [min]	Area [mAU*s]	Height [mAU]	Area %
1	2.388	MM	0.0273	12.00470	7.32126	1.3029
2	2.472	MM	0.0645	909.35565	235.09142	98.6971

(*S*,E)-(3-(4-(hex-5-en-1-yl)phenyl)hept-1-en-1-yl)trimethylsilane (119)

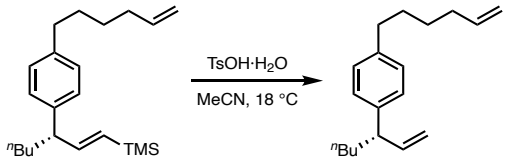

Prepared from alkenyl silane **144** (26 mg, 0.08 mmol, 1 equiv), *p*-toluenesulfonic acid monohydrate (30 mg, 0.16 mmol, 2 equiv), and MeCN (65 µL, 1.2 M) following a published procedure[160] to afford **119** (19 mg, 91% yield) as a colorless oil.

^{1}H NMR ($CDCl_3$, 400 MHz): δ 7.10 (d, *J* = 1.1 Hz, 4H), 5.93 (ddd, *J* = 17.1, 10.3, 7.7

Hz, 1H), 5.81 (ddt, J = 16.9, 10.2, 6.7 Hz, 1H), 5.09 – 4.99 (m, 2H), 4.98 (dd, J = 3.3, 2.1 Hz, 1H), 4.94 (ddt, J = 10.2, 2.4, 1.3 Hz, 1H), 3.19 (q, J = 7.5 Hz, 1H), 2.64 – 2.51 (m, 2H), 2.15 – 1.99 (m, 2H), 1.74 – 1.57 (m, 4H), 1.44 (p, J = 7.5 Hz, 2H), 1.37 – 1.23 (m, 3H), 1.23 – 1.08 (m, 1H), 0.87 (t, J = 7.1 Hz, 3H).

$^{13}C\{^1H\}$ NMR ($CDCl_3$, 101 MHz): δ 142.9, 142.1, 140.5, 139.1, 128.5, 127.5, 114.5, 113.8, 49.7, 35.5, 35.3, 33.8, 31.1, 29.9, 28.8, 22.8, 14.2.

FTIR (ATR, cm^{-1}): 2956, 2927 1638, 1511, 1413, 991, 909.

HRMS (FD, *m/z*): $[M]^+$ calcd for $C_{19}H_{28}$: 256.2191; found: 256.2196.

$\boxed{[\alpha]_D^{22} =}$ +31 (c = 1, $CHCl_3$).

Chiral SFC: (OJ-H, 2.5 mL/min, 100% CO_2, λ = 210 nm); t_R (major) = 6.1 min, t_R (minor) = 5.8 min.

119: racemic

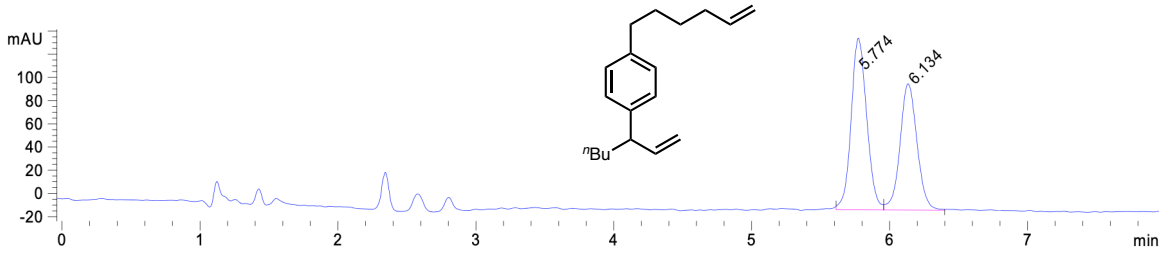


```
Signal 1: DAD1 A, Sig=210,16 Ref=370,60

Peak RetTime Type  Width     Area      Height     Area
  #   [min]        [min]   [mAU*s]     [mAU]       %
----|-------|----|-------|----------|----------|--------|
   1   5.774 BV    0.1238 1163.93909  147.89851  55.4695
   2   6.134 VB    0.1322  934.40240  108.80348  44.5305
```

(+)-119: enantioenriched (96% ee)

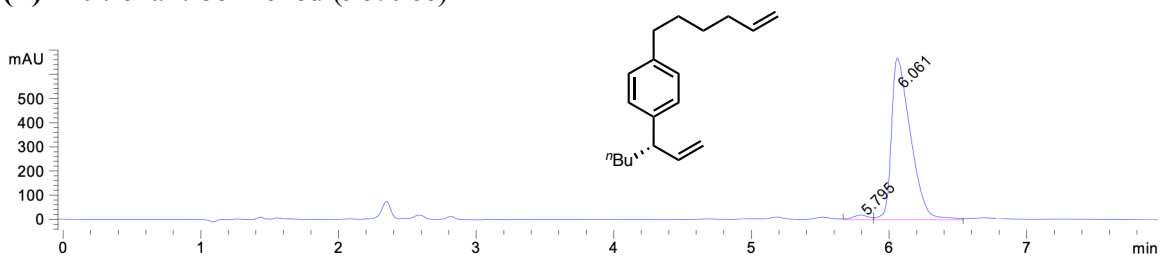

Signal 1: DAD1 A, Sig=210,16 Ref=370,60

Peak #	RetTime [min]	Type	Width [min]	Area [mAU*s]	Height [mAU]	Area %
1	5.795	VV	0.1152	151.72513	19.85121	2.2963
2	6.061	VV	0.1448	6455.74609	667.99994	97.7037

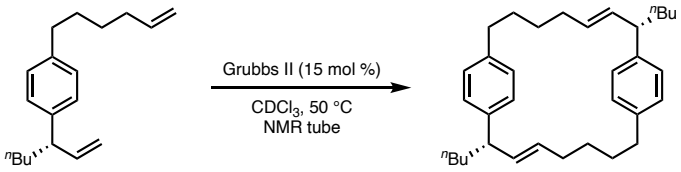

General Procedure H was followed with **119** (3.7 mg, 0.014 mmol, 1 equiv), C_6D_6 (0.83 mL, 0.017 M), Grubbs second generation catalyst (1.7 mg, 0.002 mmol, 0.14 equiv), and 2,3,4,5-tetrachloronitrobenzene (9.4 mg, 0.036 mmol, 2.5 equiv).

1,3-dimethoxy-5-((*S*)-2-methylhex-5-en-1-yl)-2-((*E*)-oct-2-en-4-yl)benzene (145)

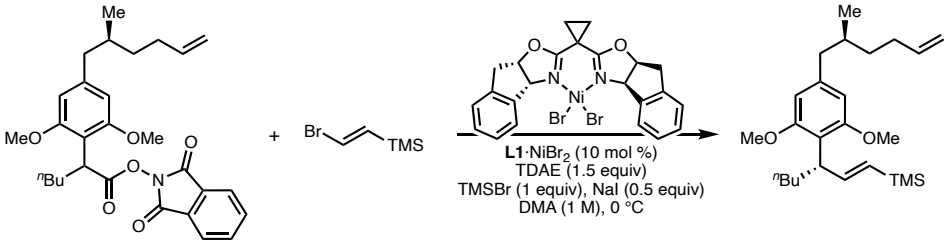

Prepared from NHP ester **111** (44 mg, 0.09 mmol, 1 equiv), (*E*)-(2-bromovinyl)trimethylsilane (16 µL, 0.1 mmol, 1 equiv), TDAE (35 µL, 0.15 mmol, 1.5 equiv), TMSBr (13 µL, 0.1 mmol, 1 equiv), NaI (7.5 mg, 0.05 mmol, 0.5 equiv),

L1·$NiBr_2$ (5.8 mg, 0.01 mmol, 0.1 equiv), and DMA (0.1 mL, 1 M) at 0 °C for 12 h following General Procedure G. The crude residue was purified by column chromatography (silica, 0 to 1% Et_2O/hexanes) to afford **145** (24 mg, 66% yield) as a colorless oil.

^{1}H NMR ($CDCl_3$, 400 MHz): δ 6.40 (dd, *J* = 18.7, 6.8 Hz, 1H), 6.32 (d, *J* = 3.7 Hz, 2H), 5.81 (ddt, *J* = 16.9, 10.1, 6.7 Hz, 1H), 5.60 – 5.45 (m, 1H), 5.00 (dq, *J* = 17.1, 1.7 Hz, 1H), 4.97 – 4.91 (m, 1H), 3.91 (q, *J* = 7.2 Hz, 1H), 3.75 (s, 6H), 2.60 (dd, *J* = 13.4, 6.0 Hz, 1H), 2.31 (dd, *J* = 13.4, 8.0 Hz, 1H), 2.21 – 1.98 (m, 1H), 1.87 – 1.68 (m, 3H), 1.47 (tt, *J* = 11.5, 4.9 Hz, 1H), 1.25 (tq, *J* = 17.9, 8.5, 7.6 Hz, 5H), 1.13 – 1.01 (m, 1H), 0.93 – 0.86 (m, 3H), 0.83 (t, *J* = 7.1 Hz, 3H), 0.01 (s, 9H).

^{13}C{^{1}H} NMR ($CDCl_3$, 101 MHz): δ 158.3, 150.6, 140.6, 139.3, 127.4, 119.0, 114.3, 106.0, 56.0, 44.2, 42.1, 36.1, 34.5, 33.0, 31.5, 30.4, 22.9, 19.6, 14.3, -0.8.

FTIR (ATR, cm^{-1}): 2953, 2856, 1608, 1580, 1454, 1418, 1245, 121, 867, 836.

HRMS (FD, *m/z*): $[M]^+$ calcd for $C_{25}H_{42}O_2Si$: 402.2954; found: 402.2949.

$\boxed{[\alpha]_D^{22} =}$ –1 (c = 1.0, $CHCl_3$).

2-((*S*)-hept-1-en-3-yl)-1,3-dimethoxy-5-((*S*)-2-methylhex-5-en-1-yl)benzene (120)

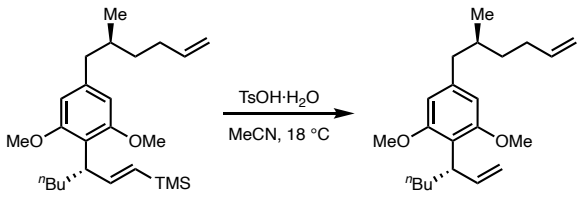

Prepared from alkenyl silane **145** (22 mg, 0.05 mmol, 1 equiv), *p*-toluenesulfonic acid monohydrate (21 mg, 0.1 mmol, 2 equiv), and MeCN (45 µL, 1.2 M) following a published procedure[160] to afford **120** (16 mg, 89% yield) as a colorless oil.

^{1}H NMR ($CDCl_3$, 400 MHz): δ 6.32 (s, 2H), 6.30 – 6.20 (m, 1H), 5.80 (ddt, *J* = 16.9, 10.2, 6.6 Hz, 1H), 5.04 – 4.84 (m, 4H), 3.91 (q, *J* = 7.8 Hz, 1H), 3.77 (s, 6H), 2.58 (dd, *J* = 13.4, 6.1 Hz, 1H), 2.35 – 2.22 (m, 1H), 2.21 – 2.10 (m, 1H), 2.10 – 1.98 (m, 1H), 1.75 (dtdt, *J* = 9.8, 5.9, 3.7, 2.0 Hz, 3H), 1.47 (dddd, *J* = 13.4, 9.7, 6.2, 5.2 Hz, 1H), 1.36 – 1.16 (m, 4H), 1.15 – 1.03 (m, 1H), 0.85 (dd, *J* = 14.7, 7.0 Hz, 6H).

^{13}C{^{1}H} NMR ($CDCl_3$, 101 MHz): δ 158.2, 142.4, 140.7, 139.3, 118.6, 114.3, 113.2, 105.8, 56.0, 44.2, 40.0, 36.0, 34.5, 33.0, 31.5, 30.5, 22.9, 19.6, 14.3.

FTIR (ATR, cm^{-1}): 2954, 2926, 2360, 1580, 1454, 1418, 1232, 1143, 1117, 909, 739.

HRMS (FI, *m/z*): $[M]^+$ calcd for $C_{22}H_{34}O_2$: 330.2559; found: 330.2569.

$\boxed{[\alpha]_D^{22} =}$ +16 (c = 0.4, $CHCl_3$).

((*R*,*E*)-3-(2,6-dimethoxy-4-((*S*)-2-methylhex-5-en-1-yl)phenyl)hept-1-en-1-yl)trimethylsilane (146)

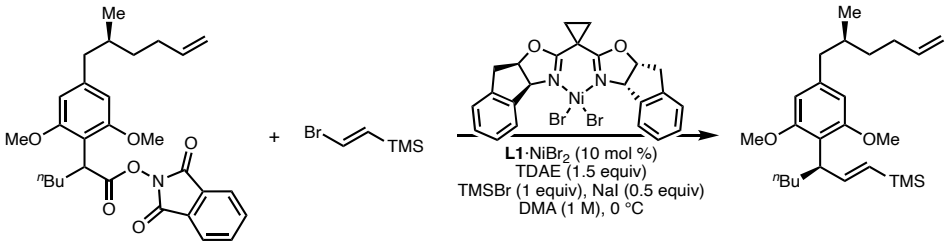

Prepared from NHP ester **111** (42 mg, 0.09 mmol, 1 equiv), (*E*)-(2-bromovinyl)trimethylsilane (16 μL, 0.1 mmol, 1 equiv), TDAE (35 μL, 0.15 mmol, 1.5 equiv), TMSBr (13 μL, 0.1 mmol, 1 equiv), NaI (7.5 mg, 0.05 mmol, 0.5 equiv), **L1**·$NiBr_2$ (5.8 mg, 0.01 mmol, 0.1 equiv), and DMA (0.1 mL, 1 M) at 0 °C for 12 h following General Procedure G. The crude residue was purified by column chromatography (silica, 0 to 1% Et_2O/hexanes) to afford **146** (20 mg, 57% yield) as a

colorless oil.

^{1}H NMR ($CDCl_3$, 400 MHz): δ 6.41 (ddd, *J* = 18.7, 6.8, 0.9 Hz, 1H), 6.33 (s, 2H), 5.81 (ddtd, *J* = 16.9, 10.1, 6.7, 0.9 Hz, 1H), 5.55 (dt, *J* = 18.6, 1.2 Hz, 1H), 5.06 – 4.97 (m, 1H), 4.94 (ddq, *J* = 10.1, 2.2, 1.1 Hz, 1H), 3.92 (q, *J* = 7.4 Hz, 1H), 3.76 (d, *J* = 0.9 Hz, 6H), 2.60 (dd, *J* = 13.4, 6.1 Hz, 1H), 2.32 (dd, *J* = 13.3, 8.2 Hz, 1H), 2.23 – 1.99 (m, 2H), 1.83 – 1.69 (m, 3H), 1.56 – 1.41 (m, 1H), 1.39 – 1.13 (m, 4H), 1.08 (dddd, *J* = 15.4, 13.2, 9.2, 6.4 Hz, 1H), 0.92 – 0.87 (m, 3H), 0.87 – 0.77 (m, 3H), 0.02 (d, *J* = 0.9 Hz, 9H).

^{13}C{^{1}H} NMR ($CDCl_3$, 101 MHz): δ 158.3, 150.6, 140.6, 139.3, 127.4, 119.0, 114.3, 106.0, 56.0, 44.2, 42.1, 36.1, 34.5, 33.0, 31.6, 30.4, 22.9, 19.6, 14.3, -0.8.

FTIR (ATR, cm^{-1}): 2953, 1360, 1608, 1580, 1454, 1245, 1122, 867, 836.

$\boxed{[\alpha]_D^{22} =}$ –10 (c = 0.8, $CHCl_3$).

2-((*R*)-hept-1-en-3-yl)-1,3-dimethoxy-5-((*S*)-2-methylhex-5-en-1-yl)benzene (147)

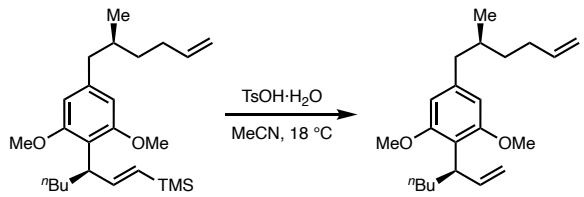

Prepared from alkenyl silane **146** (16 mg, 0.04 mmol, 1 equiv), *p*-toluenesulfonic acid monohydrate (15 mg, 0.08 mmol, 2 equiv), and MeCN (33 µL, 1.2 M) following a published procedure[160] to afford **147** (8 mg, 58% yield) as a colorless oil.

^{1}H NMR ($CDCl_3$, 400 MHz): δ 6.32 (s, 2H), 6.30 – 6.20 (m, 1H), 5.81 (ddt, *J* = 16.9, 10.2, 6.6 Hz, 1H), 5.06 – 4.86 (m, 4H), 3.97 – 3.87 (m, 1H), 3.78 (s, 6H), 2.59 (dd, *J* = 13.3, 6.1 Hz, 1H), 2.31 (dd, *J* = 13.4, 8.2 Hz, 1H), 2.23 – 1.99 (m, 2H), 1.81 – 1.71 (m, 3H), 1.48 (dddd, *J* = 13.5, 9.8, 6.2, 5.2 Hz, 1H), 1.39 – 1.15 (m, 4H), 1.17 – 1.03 (m, 1H),

0.86 (dd, *J* = 14.5, 7.1 Hz, 6H).

$^{13}C\{^{1}H\}$ NMR ($CDCl_3$, 101 MHz): δ 158.2, 142.4, 140.7, 139.3, 118.6, 114.3, 113.2, 105.8, 56.0, 44.2, 40.0, 36.0, 34.5, 33.0, 31.6, 30.5, 22.9, 19.6, 14.3.

FTIR (ATR, cm^{-1}): 2926, 1606, 1580, 1454, 1416, 1232, 1142, 1117, 907.

$\boxed{[\alpha]_D^{22} =}$ –33 (c = 0.5, $CHCl_3$).

((*E*)-3-(2,6-dimethoxy-4-((*S*)-2-methylhex-5-en-1-yl)phenyl)hept-1-en-1-yl)trimethylsilane (148)

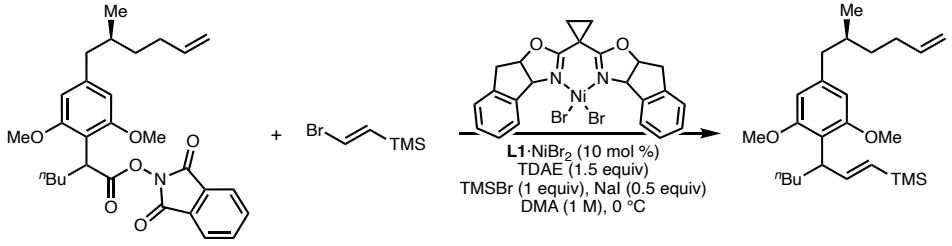

Prepared from NHP ester **111** (42 mg, 0.09 mmol, 1 equiv), TDAE (35 μL, 0.15 mmol, 1.5 equiv), TMSBr (13 μL, 0.1 mmol, 1 equiv), (*E*)-(2-bromovinyl)trimethylsilane (16 μL, 0.1 mmol, 1 equiv), NaI (7.5 mg, 0.05 mmol, 0.5 equiv), racemic **L1**·$NiBr_2$ (5.8 mg, 0.01 mmol, 0.1 equiv), and DMA (0.1 mL, 1 M) at 0 °C for 12 h following General Procedure G. The crude residue was purified by column chromatography (silica, 0 to 1% Et_2O/hexanes) to afford **148** (21 mg, 61% yield) as a colorless oil.

^{1}H NMR ($CDCl_3$, 400 MHz): δ 6.41 (ddd, *J* = 18.6, 6.9, 1.9 Hz, 1H), 6.33 (d, *J* = 1.9 Hz, 2H), 5.89 – 5.73 (m, 1H), 5.55 (dt, *J* = 18.6, 1.8 Hz, 1H), 5.01 (dt, *J* = 17.1, 1.9 Hz, 1H), 4.95 (dtt, *J* = 10.2, 2.3, 1.2 Hz, 1H), 3.97 – 3.87 (m, 1H), 3.76 (d, *J* = 2.0 Hz, 6H), 2.61 (ddd, *J* = 13.3, 6.1, 1.9 Hz, 1H), 2.32 (dd, *J* = 13.4, 8.1 Hz, 1H), 2.26 – 2.00 (m, 2H), 1.81 – 1.70 (m, 3H), 1.48 (dtd, *J* = 11.9, 6.9, 6.4, 3.0 Hz, 1H), 1.27 (qt, *J* = 7.9, 4.1 Hz,

4H), 1.09 (dddd, *J* = 13.0, 10.3, 4.8, 2.9 Hz, 1H), 0.89 (dd, *J* = 6.6, 1.9 Hz, 3H), 0.84 (t, *J* = 8.1 Hz, 3H), 0.03 (d, *J* = 2.1 Hz, 9H).

$^{13}C\{^{1}H\}$ NMR ($CDCl_3$, 101 MHz): δ 158.3, 150.6, 140.6, 139.3, 127.3, 119.0, 114.3, 106.0, 56.0, 44.2, 42.1, 36.1, 34.5, 33.0, 31.5, 30.4, 22.9, 19.6, 14.3, -0.8.

FTIR (ATR, cm^{-1}): 2928, 1608, 1580, 1454, 1245, 1121, 868, 836.

$\boxed{[\alpha]_D^{22} =}$ –3 (c = 0.8, $CHCl_3$).

2-(hept-1-en-3-yl)-1,3-dimethoxy-5-((*S*)-2-methylhex-5-en-1-yl)benzene (149)

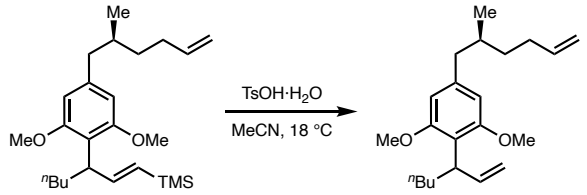

Prepared from alkenyl silane **148** (13 mg, 0.03 mmol, 1 equiv), *p*-toluenesulfonic acid monohydrate (12 mg, 0.6 mmol, 2 equiv), and MeCN (26 µL, 1.2 M) following a published procedure[160] to afford **149** (7 mg, 64% yield) as a colorless oil.

^{1}H NMR ($CDCl_3$, 400 MHz): δ 6.32 (s, 2H), 6.31 – 6.20 (m, 1H), 5.81 (ddt, *J* = 16.9, 10.2, 6.6 Hz, 1H), 4.95 (dddd, *J* = 30.4, 17.3, 10.3, 2.2 Hz, 4H), 3.92 (q, *J* = 8.0 Hz, 1H), 3.77 (s, 6H), 2.59 (dd, *J* = 13.3, 6.1 Hz, 1H), 2.31 (dd, *J* = 13.4, 8.1 Hz, 1H), 2.23 – 1.96 (m, 2H), 1.76 (td, *J* = 13.8, 9.9, 4.1 Hz, 3H), 1.50 – 1.41 (m, 1H), 1.26 (tt, *J* = 17.8, 5.5 Hz, 4H), 1.10 (tt, *J* = 11.6, 6.6 Hz, 1H), 0.94 – 0.73 (m, 6H).

$^{13}C\{^{1}H\}$ NMR ($CDCl_3$, 101 MHz): δ 770.4, 754.6, 752.9, 751.5, 730.8, 726.5, 725.4, 718.0, 668.1, 656.4, 652.1, 648.1, 646.6, 645.1, 643.7, 642.6, 635.0, 631.7, 626.4.

FTIR (ATR, cm^{-1}): 2926, 1606, 1579, 1454, 1416, 1232, 1142, 1117, 908.

$\boxed{[\alpha]_D^{22} =}$ +3 (c = 0.3, $CHCl_3$).

5.9 REFERENCES

(1) Wang, X.; Dai, Y.; Gong, H. Nickel-Catalyzed Reductive Couplings. *Top. Curr. Chem. (Z)* **2016**, *374* (4), 43.

(2) Poremba, K. E.; Dibrell, S. E.; Reisman, S. E. Nickel-Catalyzed Enantioselective Reductive Cross-Coupling Reactions. *ACS Catal.* **2020**, *10* (15), 8237–8246.

(3) Zhou, Z.; Xu, S.; Zhang, J.; Kong, W. Nickel-Catalyzed Enantioselective Electroreductive Cross-Couplings. *Org. Chem. Front.* **2020**, *7* (20), 3262–3265.

(4) Weix, D. J. Methods and Mechanisms for Cross-Electrophile Coupling of Csp^2 Halides with Alkyl Electrophiles. *Acc. Chem. Res.* **2015**, *48* (6), 1767–1775.

(5) J. DeLano, T.; E. Dibrell, S.; R. Lacker, C.; R. Pancoast, A.; E. Poremba, K.; Cleary, L.; S. Sigman, M.; E. Reisman, S. Nickel-Catalyzed Asymmetric Reductive Cross-Coupling of α-Chloroesters with (Hetero)Aryl Iodides. *Chemical Science* **2021**, *12* (22), 7758–7762.

(6) Beutner, G. L.; Simmons, E. M.; Ayers, S.; Bemis, C. Y.; Goldfogel, M. J.; Joe, C. L.; Marshall, J.; Wisniewski, S. R. A Process Chemistry Benchmark for Sp^2–Sp^3 Cross Couplings. *J. Org. Chem.* **2021**, *86* (15), 10380–10396.

(7) Kutchukian, P. S.; Dropinski, J. F.; Dykstra, K. D.; Li, B.; DiRocco, D. A.; Streckfuss, E. C.; Campeau, L.-C.; Cernak, T.; Vachal, P.; Davies, I. W.; Krska, S. W.; Dreher, S. D. Chemistry Informer Libraries: A Chemoinformatics Enabled Approach to Evaluate and Advance Synthetic Methods. *Chem. Sci.* **2016**, *7* (4), 2604–2613.

(8) Mennie, K. M.; Vara, B. A.; Levi, S. M. Reductive Sp^3–Sp^2 Coupling Reactions Enable Late-Stage Modification of Pharmaceuticals. *Org. Lett.* **2020**, *22* (2), 556–559.

(9) Nimmagadda, S. K.; Korapati, S.; Dasgupta, D.; Malik, N. A.; Vinodini, A.; Gangu, A. S.; Kalidindi, S.; Maity, P.; Bondigela, S. S.; Venu, A.; Gallagher, W. P.; Aytar, S.; González-Bobes, F.; Vaidyanathan, R. Development and Execution of an Ni(II)-Catalyzed Reductive Cross-Coupling of Substituted 2-Chloropyridine and Ethyl 3-Chloropropanoate. *Org. Process Res. Dev.* **2020**, *24* (6), 1141–1148.

(10) Yi, L.; Ji, T.; Chen, K.-Q.; Chen, X.-Y.; Rueping, M. Nickel-Catalyzed Reductive Cross-Couplings: New Opportunities for Carbon–Carbon Bond Formations through Photochemistry and Electrochemistry. *CCS Chem* **2021**, 3005–3026.

(11) Peng, Y.; Xiao, J.; Xu, X.-B.; Duan, S.-M.; Ren, L.; Shao, Y.-L.; Wang, Y.-W. Stereospecific Synthesis of Tetrahydronaphtho[2,3-b]Furans Enabled by a Nickel-Promoted Tandem Reductive Cyclization. *Org. Lett.* **2016**, *18* (19), 5170–5173.

(12) Wang, K.; Ding, Z.; Zhou, Z.; Kong, W. Ni-Catalyzed Enantioselective Reductive Diarylation of Activated Alkenes by Domino Cyclization/Cross-Coupling. *J. Am. Chem. Soc.* **2018**, *140* (39), 12364–12368.

(13) Tollefson, E. J.; Erickson, L. W.; Jarvo, E. R. Stereospecific Intramolecular Reductive Cross-Electrophile Coupling Reactions for Cyclopropane Synthesis. *J. Am. Chem. Soc.* **2015**, *137* (31), 9760–9763.

(14) Xue, W.; Xu, H.; Liang, Z.; Qian, Q.; Gong, H. Nickel-Catalyzed Reductive Cyclization of Alkyl Dihalides. *Org. Lett.* **2014**, *16* (19), 4984–4987.

(15) Standley, E. A.; Tasker, S. Z.; Jensen, K. L.; Jamison, T. F. Nickel Catalysis:

Synergy between Method Development and Total Synthesis. *Acc. Chem. Res.* **2015**, *48* (5), 1503–1514.

(16) Dale, J. Conformational Aspects of Many-Membered Rings. *Angew. Chem. Int. Ed.* **1966**, *5* (12), 1000–1021.

(17) Saridakis, I.; Kaiser, D.; Maulide, N. Unconventional Macrocyclizations in Natural Product Synthesis. *ACS Cent. Sci.* **2020**, *6* (11), 1869–1889.

(18) Berthold, D.; Breit, B. Total Syntheses of Cylindrocyclophanes Exemplifying the Power of Transition-Metal Catalysis in Natural-Product Synthesis. *Synlett* **2021**, *32* (5), 436–446.

(19) Martins, T. P.; Rouger, C.; Glasser, N. R.; Freitas, S.; Fraissinette, N. B. de; Balskus, E. P.; Tasdemir, D.; Leão, P. N. Chemistry, Bioactivity and Biosynthesis of Cyanobacterial Alkylresorcinols. *Nat. Prod. Rep.* **2019**, *36* (10), 1437–1461.

(20) Moore, B. S.; Chen, J. L.; Patterson, G. M. L.; Moore, R. E.; Brinen, L. S.; Kato, Y.; Clardy, J. [7.7]Paracyclophanes from Blue-Green Algae. *J. Am. Chem. Soc.* **1990**, *112* (10), 4061–4063.

(21) Moore, B. S.; Chen, J.-L.; Patterson, G. M. L.; Moore, R. E. Structures of Cylindrocyphanes A-f. *Tetrahedron* **1992**, *48* (15), 3001–3006.

(22) Dai, J.; Philbin, C. S.; Wakano, C.; Yoshida, W. Y.; Williams, P. G. New Nostocyclophanes from Nostoc Linckia. *Marine Drugs* **2023**, *21* (2), 101.

(23) Chlipala, G. E.; Sturdy, M.; Krunic, A.; Lantvit, D. D.; Shen, Q.; Porter, K.; Swanson, S. M.; Orjala, J. Cylindrocyclophanes with Proteasome Inhibitory Activity from the Cyanobacterium Nostoc Sp. *J. Nat. Prod.* **2010**, *73* (9), 1529–1537.

(24) Bui, H. T. N.; Jansen, R.; Pham, H. T. L.; Mundt, S. Carbamidocyclophanes A−E, Chlorinated Paracyclophanes with Cytotoxic and Antibiotic Activity from the Vietnamese Cyanobacterium Nostoc Sp. *J. Nat. Prod.* **2007**, *70* (4), 499–503.

(25) Luo, S.; Kang, H.-S.; Krunic, A.; Chlipala, G. E.; Cai, G.; Chen, W.-L.; Franzblau, S. G.; Swanson, S. M.; Orjala, J. Carbamidocyclophanes F and G with Anti-Mycobacterium Tuberculosis Activity from the Cultured Freshwater Cyanobacterium Nostoc Sp. *Tetrahedron Lett.* **2014**, *55* (3), 686–689.

(26) Preisitsch, M.; Harmrolfs, K.; Pham, H. T.; Heiden, S. E.; Füssel, A.; Wiesner, C.; Pretsch, A.; Swiatecka-Hagenbruch, M.; Niedermeyer, T. H.; Müller, R. Anti-MRSA-Acting Carbamidocyclophanes H–L from the Vietnamese Cyanobacterium Nostoc Sp. CAVN2. *J. Antiobiot.* **2015**, *68* (3), 165–177.

(27) Preisitsch, M.; Heiden, S. E.; Beerbaum, M.; Niedermeyer, T. H.; Schneefeld, M.; Herrmann, J.; Kumpfmüller, J.; Thürmer, A.; Neidhardt, I.; Wiesner, C. Effects of Halide Ions on the Carbamidocyclophane Biosynthesis in Nostoc Sp. CAVN2. *Marine Drugs* **2016**, *14* (1), 21.

(28) Kang, H.-S.; Santarsiero, B. D.; Kim, H.; Krunic, A.; Shen, Q.; Swanson, S. M.; Chai, H.; Kinghorn, A. D.; Orjala, J. Merocyclophanes A and B, Antiproliferative Cyclophanes from the Cultured Terrestrial Cyanobacterium Nostoc Sp. *Phytochemistry* **2012**, *79*, 109–115.

(29) May, D. S.; Chen, W.-L.; Lantvit, D. D.; Zhang, X.; Krunic, A.; Burdette, J. E.; Eustaquio, A.; Orjala, J. Merocyclophanes C and D from the Cultured Freshwater Cyanobacterium Nostoc Sp. (UIC 10110). *J. Nat. Prod.* **2017**, *80* (4), 1073–1080.

(30) Chen, J. L.; Moore, R. E.; Patterson, G. M. Structures of Nostocyclophanes AD. *J.*

Org. Chem. **1991**, *56* (14), 4360–4364.

(31) Bobzin, S. C.; Moore, R. E. Biosynthetic Origin of [7.7]Paracyclophanes from Cyanobacteria. *Tetrahedron* **1993**, *49* (35), 7615–7626.

(32) Mascal, M.; Kerdelhué, J.-L.; S. Batsanov, A.; J. Begley, M. Conformational Study of the Higher [n.n]Paracylophanes: Evaluation as Potential Hosts for Molecular Halogens and Benzenes. *J. Chem. Soc., Perkin Trans. 1* **1996**, *0* (11), 1141–1151.

(33) Nakamura, H.; Hamer, H. A.; Sirasani, G.; Balskus, E. P. Cylindrocyclophane Biosynthesis Involves Functionalization of an Unactivated Carbon Center. *J. Amr. Chem. Soc.* **2012**, *134* (45), 18518–18521.

(34) Nakamura, H.; Wang, J. X.; Balskus, E. P. Assembly Line Termination in Cylindrocyclophane Biosynthesis: Discovery of an Editing Type II Thioesterase Domain in a Type I Polyketide Synthase. *Chem. Sci.* **2015**, *6* (7), 3816–3822.

(35) Nakamura, H.; Schultz, E. E.; Balskus, E. P. A New Strategy for Aromatic Ring Alkylation in Cylindrocyclophane Biosynthesis. *Nat. Chem. Bio.* **2017**, *13* (8), 916–921.

(36) Wang, H.-Q.; Mou, S.-B.; Xiao, W.; Zhou, H.; Hou, X.-D.; Wang, S.-J.; Wang, Q.; Gao, J.; Wei, Z.; Liu, L.; Xiang, Z. Structural Basis for the Friedel–Crafts Alkylation in Cylindrocyclophane Biosynthesis. *ACS Catal.* **2022**, *12* (3), 2108–2117.

(37) May, D. S.; Kang, H.-S.; Santarsiero, B. D.; Krunic, A.; Shen, Q.; Burdette, J. E.; Swanson, S. M.; Orjala, J. Ribocyclophanes A–E, Glycosylated Cyclophanes with Antiproliferative Activity from Two Cultured Terrestrial Cyanobacteria. *J. Nat. Prod.* **2018**, *81* (3), 572–578.

(38) Thanh, N. V.; Thao, N. P.; Phong, N. V.; Cuong, N. X.; Nam, N. H.; Minh, C. V. A New [7.7]Paracyclophane from Vietnamese Marine Snail Planaxis Sulcatus (Born, 1780). *Nat. Prod. Res.* **2020**, *34* (2), 261–268.

(39) Thuan, N. H.; An, T. T.; Shrestha, A.; Canh, N. X.; Sohng, J. K.; Dhakal, D. Recent Advances in Exploration and Biotechnological Production of Bioactive Compounds in Three Cyanobacterial Genera: Nostoc, Lyngbya, and Microcystis. *Front. Chem.* **2019**, *7*.

(40) Yamakoshi, H.; Ikarashi, F.; Minami, M.; Shibuya, M.; Sugahara, T.; Kanoh, N.; Ohori, H.; Shibata, H.; Iwabuchi, Y. Syntheses of Naturally Occurring Cytotoxic [7.7]Paracyclophanes, (−)-Cylindrocyclophane A and Its Enantiomer, and Implications for Biological Activity. *Org. Biomol. Chem.* **2009**, *7* (18), 3772.

(41) Preisitsch, M.; Niedermeyer, T. H. J.; Heiden, S. E.; Neidhardt, I.; Kumpfmüller, J.; Wurster, M.; Harmrolfs, K.; Wiesner, C.; Enke, H.; Müller, R.; Mundt, S. Cylindrofridins A–C, Linear Cylindrocyclophane-Related Alkylresorcinols from the Cyanobacterium Cylindrospermum Stagnale. *J. Nat. Prod.* **2016**, *79* (1), 106–115.

(42) Freudenreich, J. J.; Bartlett, S.; Robertson, N. S.; Kidd, S. L.; Forrest, S.; Sore, H. F.; Galloway, W. R. J. D.; Welch, M.; Spring, D. R. Divergent Synthesis of Novel Cylindrocyclophanes That Inhibit Methicillin-Resistant Staphylococcus Aureus (MRSA). *ChemMedChem* **2020**, *15* (14), 1289–1293.

(43) Cram, D. J.; Steinberg, H. Macro Rings. I. Preparation and Spectra of the Paracyclophanes. *J. Am. Chem. Soc.* **1951**, *73* (12), 5691–5704.

(44) E. Gibson, S.; D. Knight, J. [2.2]Paracyclophane Derivatives in Asymmetric

Catalysis. *Org. Biomol. Chem.* **2003**, *1* (8), 1256–1269.

(45) Teyssandier, J.; De Feyter, S.; Mali, K. S. Host–Guest Chemistry in Two-Dimensional Supramolecular Networks. *Chem. Commun.* **2016**, *52* (77), 11465–11487.

(46) Collins, M. S.; Carnes, M. E.; Nell, B. P.; Zakharov, L. N.; Johnson, D. W. A Facile Route to Old and New Cyclophanes via Self-Assembly and Capture. *Nature Commun.* **2016**, *7* (1), 11052.

(47) Friščić, T.; Macgillivray, L. R. Cyclophanes and Ladderanes: Molecular Targets for Supramolecular Chemists. *Supramol. Chem.* **2005**, *17* (1–2), 47–51.

(48) Bachrach, S. M. DFT Study of [2.2]-, [3.3]-, and [4.4]Paracyclophanes: Strain Energy, Conformations, and Rotational Barriers. *J. Phys. Chem. A* **2011**, *115* (11), 2396–2401.

(49) Zauer, E. A. Cyclophanes: Simulation of the Formation Enthalpy by Quantum-Chemical Methods. *Russ. J. Gen. Chem.* **2017**, *87* (5), 918–922.

(50) Castillo, F.; Faúndez, R.; Tapia, J.; Verdugo, C.; Preite, M.; Chávez, I.; Manuel-Manriquez, J.; D. Ortiz, P.; Zarate, X.; Schott, E. Revisiting Cyclophanes: Experimental Characterization and Theoretical Elucidation of the Chain Length Influence on Their Structure and Reactivity. *New J. Chem.* **2022**, *46* (14), 6609–6621.

(51) Szymański, S.; Dodziuk, H.; Pietrzak, M.; Jaźwiński, J.; Demissie, T. B.; Hopf, H. Dynamics of [n.3]Paracyclophanes (n = 2 – 4) as Studied by NMR. Obtaining Separate Arrhenius Parameters for Two Dynamic Processes in [4.3]Paracyclophane. *J. Phys. Org. Chem.* **2013**, *26* (7), 596–600.

(52) Demissie, T. B.; Dodziuk, H.; Waluk, J.; Ruud, K.; Pietrzak, M.; Vetokhina, V.; Szymański, S.; Jaźwiński, J.; Hopf, H. Structure, NMR and Electronic Spectra of [*m.n*]Paracyclophanes with Varying Bridges Lengths (*m, n* = 2–4). *J. Phys. Chem. A* **2016**, *120* (5), 724–736.

(53) Hassan, Z.; Spuling, E.; Knoll, D. M.; Bräse, S. Regioselective Functionalization of [2.2]Paracyclophanes: Recent Synthetic Progress and Perspectives. *Angew. Chem. Int. Ed.* **2020**, *59* (6), 2156–2170.

(54) Gulder, T.; Baran, P. S. Strained Cyclophane Natural Products: Macrocyclization at Its Limits. *Nat. Prod. Rep.* **2012**, *29* (8), 899–934.

(55) Kotha, S.; Shirbhate, M. E.; Waghule, G. T. Selected Synthetic Strategies to Cyclophanes. *Beilstein J. Org. Chem.* **2015**, *11* (1), 1274–1331.

(56) Longone, D. T.; Kusefoglu, S. H.; Gladysz, J. A. A Convenient Synthesis of [3.3]Paracyclophane. *J. Org. Chem.* **1977**, *42* (16), 2787–2788.

(57) Pechlivanidis, Z.; Hopf, H.; Ernst, L. Paracyclophanes: Extending the Bridges. Synthesis. *Eur. J. Org. Chem.* **2009**, *2009* (2), 223–237.

(58) Staab, H. A.; Matzke, G.; Krieger, C. 9, 12, 22, 25-Tetramethoxy [7.7] Paracyclophan-4,17-dion: Synthese Und Molekülstruktur. *Chem. Ber.* **1987**, *120* (1), 89–91.

(59) Schubert, W. M.; Sweeney, W. A.; Latourette, H. K. Spectroscopic and Other Properties of Large Ring Mono- and Dimeric Benzocyclanones Prepared by a High-Dilution Friedel-Crafts Reaction. *J. Am. Chem. Soc.* **1954**, *76* (21), 5462–5466.

(60) Abell, J.; Cram, D. J. Macro Rings. VI. The Preparation of Three New

Paracyclophanes. *J. Am. Chem. Soc.* **1954**, *76* (17), 4406–4412.

(61) Nishimura, J.; Hashimoto, K.; Okuda, T.; Hayami, H.; Mukai, Y.; Oku, A. Cationic Cyclocodimerization. 1. Novel Synthesis of [3.3]Paracyclophane Skeleton from 1,3-Bis(p-Vinylphenyl)Propane. *J. Am. Chem. Soc.* **1983**, *105* (14), 4758–4767.

(62) Martin, V. A. Ph.D. dissertation. Wayne State University, **1992**.

(63) Liu, W.; Ren, Z.; Bosse, A. T.; Liao, K.; Goldstein, E. L.; Bacsa, J.; Musaev, D. G.; Stoltz, B. M.; Davies, H. M. L. Catalyst-Controlled Selective Functionalization of Unactivated C–H Bonds in the Presence of Electronically Activated C–H Bonds. *J. Am. Chem. Soc.* **2018**, *140* (38), 12247–12255.

(64) Davies, H.; Bosse, A.; Boni, Y. Catalyst-Controlled Site-Selective and Enantioselective C-H Functionalization. Presented at the National Meeting of the American Chemical Society, **2021**.

(65) Smith, A. B.; Kozmin, S. A.; Paone, D. V. Total Synthesis of (−)-Cylindrocyclophane F. *J. Am. Chem. Soc.* **1999**, *121* (32), 7423–7424.

(66) Schnaderbeck, M. Ph.D. dissertation. Stanford University, **1988**.

(67) Goodwin, N. C. Total Syntheses of the Spiculisporic Acids, Progress Towards the Total Synthesis of Cylindrocyclophane F, and Formal Synthesis of Cylindrocyclophane A. Ph.D. dissertation. California Institute of Technology, **2007**.

(68) Hoye, T. R.; Humpal, P. E.; Moon, B. Total Synthesis of (−)-Cylindrocyclophane A via a Double Horner-Emmons Macrocyclic Dimerization Event. *J. Am. Chem. Soc.* **2000**, *122* (20), 4982–4983.

(69) Nicolaou, K. C.; Sun, Y.-P.; Korman, H.; Sarlah, D. Asymmetric Total Synthesis of Cylindrocyclophanes A and F through Cyclodimerization and a Ramberg–Bäcklund Reaction. *Angew. Chem. Int. Ed.* **2010**, *49* (34), 5875–5878.

(70) Smith, A. B.; Adams, C. M.; Kozmin, S. A.; Paone, D. V. Total Synthesis of (−)-Cylindrocyclophanes A and F Exploiting the Reversible Nature of the Olefin Cross Metathesis Reaction. *J. Am. Chem. Soc.* **2001**, *123* (25), 5925–5937.

(71) Fürstner, A.; Langemann, K. Conformationally Unbiased Macrocyclization Reactions by Ring Closing Metathesis. *J. Org. Chem.* **1996**, *61* (12), 3942–3943.

(72) Smith, A. B.; Kozmin, S. A.; Adams, C. M.; Paone, D. V. Assembly of (−)-Cylindrocyclophanes A and F via Remarkable Olefin Metathesis Dimerizations. *J. Am. Chem. Soc.* **2000**, *122* (20), 4984–4985.

(73) Berthold, D.; Breit, B. Total Synthesis of (−)-Cylindrocyclophane F: A Yardstick for Probing New Catalytic C−C Bond-Forming Methodologies. *Chem. Eur. J.* **2018**, *24* (63), 16770–16773.

(74) Harned, A. M. From Determination of Enantiopurity to the Construction of Complex Molecules: The Horeau Principle and Its Application in Synthesis. *Tetrahedron* **2018**, *74* (28), 3797–3841.

(75) Suzuki, N.; Hofstra, J. L.; Poremba, K. E.; Reisman, S. E. Nickel-Catalyzed Enantioselective Cross-Coupling of *N*-Hydroxyphthalimide Esters with Vinyl Bromides. *Org. Lett.* **2017**, *19* (8), 2150–2153.

(76) Sandfort, F.; O'Neill, M. J.; Cornella, J.; Wimmer, L.; Baran, P. S. Alkyl−(Hetero)Aryl Bond Formation via Decarboxylative Cross-Coupling: A Systematic Analysis. *Angew. Chem. Int. Ed.* **2017**, *56* (12), 3319–3323.

(77) Ge, Y.; Wang, H.; Wang, H.-N.; Yu, S.-S.; Yang, R.; Chen, X.; Zhao, Q.; Chen, G. Biomimetic Total Syntheses of Ergot Alkaloids via Decarboxylative Giese Coupling. *Org. Lett.* **2021**, *23* (2), 370–375.

(78) Guo, R.; Witherspoon, B. P.; Brown, M. K. Evolution of a Strategy for the Enantioselective Synthesis of (−)-Cajanusine. *J. Am. Chem. Soc.* **2020**, *142* (11), 5002–5006.

(79) Schultz, E. E.; Braffman, N. R.; Luescher, M. U.; Hager, H. H.; Balskus, E. P. Biocatalytic Friedel-Crafts Alkylation Using a Promiscuous Biosynthetic Enzyme. *Angew. Chem. Int. Ed.* **2019**, *58* (10), 3151–3155.

(80) Poremba, K. E. Development of Nickel-Catalyzed Asymmetric Reductive Cross-Coupling Reactions. Ph.D. dissertation. California Institute of Technology, **2019**.

(81) Ju, L.; Lin, Q.; LiBretto, N. J.; Wagner, C. L.; Hu, C. T.; Miller, J. T.; Diao, T. Reactivity of (Bi-Oxazoline)Organonickel Complexes and Revision of a Catalytic Mechanism. *J. Am. Chem. Soc.* **2021**, *143* (36), 14458–14463.

(82) Zuo, Z.; Kim, R. S.; Watson, D. A. Synthesis of Axially Chiral 2,2′-Bisphosphobiarenes via a Nickel-Catalyzed Asymmetric Ullmann Coupling: General Access to Privileged Chiral Ligands without Optical Resolution. *J. Am. Chem. Soc.* **2021**, *143* (3), 1328–1333. https://doi.org/10.1021/jacs.0c12843.

(83) Tsou, T. T.; Kochi, J. K. Mechanism of Biaryl Synthesis with Nickel Complexes. *J. Am. Chem. Soc.* **1979**, *101* (25), 7547–7560.

(84) Charboneau, D. J.; Barth, E. L.; Hazari, N.; Uehling, M. R.; Zultanski, S. L. A Widely Applicable Dual Catalytic System for Cross-Electrophile Coupling Enabled by Mechanistic Studies. *ACS Catal.* **2020**, *10* (21), 12642–12656.

(85) Everson, D. A.; Weix, D. J. Cross-Electrophile Coupling: Principles of Reactivity and Selectivity. *J. Org. Chem.* **2014**, *79* (11), 4793–4798.

(86) Kim, S.; Goldfogel, M. J.; Gilbert, M. M.; Weix, D. J. Nickel-Catalyzed Cross-Electrophile Coupling of Aryl Chlorides with Primary Alkyl Chlorides. *J. Am. Chem. Soc.* **2020**, *142* (22), 9902–9907.

(87) Hofstra, J. L.; Poremba, K. E.; Shimozono, A. M.; Reisman, S. E. Nickel-Catalyzed Conversion of Enol Triflates into Alkenyl Halides. *Angew. Chem. Int. Ed.* **2019**, *58* (42), 14901–14905.

(88) Salgueiro, D. C.; Chi, B. K.; Guzei, I. A.; García-Reynaga, P.; Weix, D. J. Control of Redox-Active Ester Reactivity Enables a General Cross-Electrophile Approach to Access Arylated Strained Rings**. *Angew. Chem. Int. Ed.* **2022**, *61* (33), e202205673.

(89) Huihui, K. M. M.; Caputo, J. A.; Melchor, Z.; Olivares, A. M.; Spiewak, A. M.; Johnson, K. A.; DiBenedetto, T. A.; Kim, S.; Ackerman, L. K. G.; Weix, D. J. Decarboxylative Cross-Electrophile Coupling of *N*-Hydroxyphthalimide Esters with Aryl Iodides. *J. Am. Chem. Soc.* **2016**, *138* (15), 5016–5019.

(90) Cornella, J.; Edwards, J. T.; Qin, T.; Kawamura, S.; Wang, J.; Pan, C.-M.; Gianatassio, R.; Schmidt, M.; Eastgate, M. D.; Baran, P. S. Practical Ni-Catalyzed Aryl–Alkyl Cross-Coupling of Secondary Redox-Active Esters. *J. Am. Chem. Soc.* **2016**, *138* (7), 2174–2177.

(91) Huang, L.; Olivares, A. M.; Weix, D. J. Reductive Decarboxylative Alkynylation of *N*-Hydroxyphthalimide Esters with Bromoalkynes. *Angew. Chem. Int. Ed.* **2017**, *56* (39), 11901–11905.

(92) Zhang, B.; Gao, Y.; Hioki, Y.; Oderinde, M. S.; Qiao, J. X.; Rodriguez, K. X.; Zhang, H.-J.; Kawamata, Y.; Baran, P. S. Ni-Electrocatalytic Csp^3–Csp^3 Doubly Decarboxylative Coupling. *Nature* **2022**, *606* (7913), 313–318.

(93) Jiang, W.-T.; Yang, S.; Xu, M.-Y.; Xie, X.-Y.; Xiao, B. Zn-Mediated Decarboxylative Carbagermatranation of Aliphatic *N*-Hydroxyphthalimide Esters: Evidence for an Alkylzinc Intermediate. *Chem. Sci.* **2020**, *11* (2), 488–493.

(94) Jin, S.; Haug, G. C.; Nguyen, V. T.; Flores-Hansen, C.; Arman, H. D.; Larionov, O. V. Decarboxylative Phosphine Synthesis: Insights into the Catalytic, Autocatalytic, and Inhibitory Roles of Additives and Intermediates. *ACS Cat.* **2019**, *9* (11), 9764–9774.

(95) Charboneau, D. J.; Hazari, N.; Huang, H.; Uehling, M. R.; Zultanski, S. L. Homogeneous Organic Electron Donors in Nickel-Catalyzed Reductive Transformations. *J. Org. Chem.* **2022**, *87* (12), 7589–7609.

(96) Broggi, J.; Terme, T.; Vanelle, P. Organic Electron Donors as Powerful Single-Electron Transfer Reducing Agents in Organic Synthesis. *Angew. Chem. Int. Ed.* **2014**, *53* (2), 384–413.

(97) Jørgensen, M.; Lee, S.; Liu, X.; Wolkowski, J. P.; Hartwig, J. F. Efficient Synthesis of α-Aryl Esters by Room-Temperature Palladium-Catalyzed Coupling of Aryl Halides with Ester Enolates. *J. Am. Chem. Soc.* **2002**, *124* (42), 12557–12565.

(98) Murphy, J. M.; Liao, X.; Hartwig, J. F. Meta Halogenation of 1,3-Disubstituted Arenes via Iridium-Catalyzed Arene Borylation. *J. Am. Chem. Soc.* **2007**, *129* (50), 15434–15435.

(99) Preshlock, S. M.; Ghaffari, B.; Maligres, P. E.; Krska, S. W.; Maleczka, R. E.; Smith, M. R. High-Throughput Optimization of Ir-Catalyzed C–H Borylation: A Tutorial for Practical Applications. *J. Am. Chem. Soc.* **2013**, *135* (20), 7572–7582.

(100) Neumann, H.; Seebach, D. Stereospecific Preparation of Terminal Vinyllithium Derivatives by Br/Li-Exchange with t-Butyllithium. *Tetrahedron Lett.* **1976**, *17* (52), 4839–4842.

(101) Myers, A. G.; Yang, B. H.; Chen, H.; Gleason, J. L. Use of Pseudoephedrine as a Practical Chiral Auxiliary for Asymmetric Synthesis. *J. Am. Chem. Soc.* **1994**, *116* (20), 9361–9362.

(102) Trost, B. M.; Lehr, K.; Michaelis, D. J.; Xu, J.; Buckl, A. K. Palladium-Catalyzed Asymmetric Allylic Alkylation of 2-Acylimidazoles as Ester Enolate Equivalents. *J. Am. Chem. Soc.* **2010**, *132* (26), 8915–8917.

(103) Cha, J. Y.; Yeoman, J. T. S.; Reisman, S. E. A Concise Total Synthesis of (−)-Maoecrystal Z. *J. Am. Chem. Soc.* **2011**, *133* (38), 14964–14967.

(104) Beak, Peter.; Musick, T. J.; Chen, C. Wen. Does Formal Intramolecular Transfer of an Acidic Deuterium to a Site of Halogen-Lithium Exchange Show That Lithium-Halogen Exchange Is Faster than Loss of the Acidic Deuterium? Evidence in Favor of an Alternative Mechanism. *J. Am. Chem. Soc.* **1988**, *110* (11), 3538–3542.

(105) Narasimhan, N. S.; Sunder, N. M.; Ammanamanchi, R.; Bonde, B. D. Evidence in Favor of Lithium-Halogen Exchange Being Faster than Lithium-Acidic Hydrogen (Deuterium) Exchange. *J. Am. Chem. Soc.* **1990**, *112* (11), 4431–4435.

(106) Yamamoto, Y.; Maeda, K.; Tomimoto, K.; Mase, T. Lithiation of Aryl Bromides

Possessing α-Proton of Carbonyl Groups. *Synlett* **2002**, *2002* (4), 561–564.

(107) Kondo, Y.; Asai, M.; Miura, T.; Uchiyama, M.; Sakamoto, T. Mesityllithium as a Reagent for Chemoselective Halogen−Lithium Exchange Reaction. *Org. Lett.* **2001**, *3* (1), 13–15.

(108) Manolikakes, G.; Muñoz Hernandez, C.; Schade, M. A.; Metzger, A.; Knochel, P. Palladium- and Nickel-Catalyzed Cross-Couplings of Unsaturated Halides Bearing Relatively Acidic Protons with Organozinc Reagents. *J. Org. Chem.* **2008**, *73* (21), 8422–8436.

(109) Yang, C.-T.; Zhang, Z.-Q.; Liu, Y.-C.; Liu, L. Copper-Catalyzed Cross-Coupling Reaction of Organoboron Compounds with Primary Alkyl Halides and Pseudohalides. *Angew. Chem. Int. Ed.* **2011**, *50* (17), 3904–3907.

(110) Robbins, D. W.; Hartwig, J. F. Sterically Controlled Alkylation of Arenes through Iridium-Catalyzed C–H Borylation. *Angew. Chem. Int. Ed.* **2013**, *52* (3), 933–937.

(111) Everson, D. A.; Jones, B. A.; Weix, D. J. Replacing Conventional Carbon Nucleophiles with Electrophiles: Nickel-Catalyzed Reductive Alkylation of Aryl Bromides and Chlorides. *J. Am. Chem. Soc.* **2012**, *134* (14), 6146–6159.

(112) Girvin, Z. C.; Andrews, M. K.; Liu, X.; Gellman, S. H. Foldamer-Templated Catalysis of Macrocycle Formation. *Science* **2019**, *366* (6472), 1528–1531.

(113) Zhao, Y.; Weix, D. J. Nickel-Catalyzed Regiodivergent Opening of Epoxides with Aryl Halides: Co-Catalysis Controls Regioselectivity. *J. Am. Chem. Soc.* **2014**, *136* (1), 48–51.

(114) Schaus, S. E.; Brandes, B. D.; Larrow, J. F.; Tokunaga, M.; Hansen, K. B.; Gould, A. E.; Furrow, M. E.; Jacobsen, E. N. Highly Selective Hydrolytic Kinetic

Resolution of Terminal Epoxides Catalyzed by Chiral (Salen)Co^{III} Complexes. Practical Synthesis of Enantioenriched Terminal Epoxides and 1,2-Diols. *J. Am. Chem. Soc.* **2002**, *124* (7), 1307–1315.

(115) Johnson, C. R.; Dutra, G. A. Reactions of Lithium Diorganocuprates(I) with Tosylates. I. Synthetic Aspects. *J. Am. Chem. Soc.* **1973**, *95* (23), 7777–7782.

(116) Johnson, C. R.; Dutra, G. A. Reactions of Lithium Diorganocuprates(I) with Tosylates. II. Stereochemical, Kinetic, and Mechanistic Aspects. *J. Am. Chem. Soc.* **1973**, *95* (23), 7783–7788.

(117) Bloemendal, V. R. L. J.; Sondag, D.; Elferink, H.; Boltje, T. J.; van Hest, Jan. C. M.; Rutjes, F. P. J. T. A Revised Modular Approach to (–)-Trans-Δ8-THC and Derivatives Through Late-Stage Suzuki–Miyaura Cross-Coupling Reactions. *Eur. J. Org. Chem.* **2019**, *2019* (12), 2289–2296.

(118) Bajo, S.; Laidlaw, G.; Kennedy, A. R.; Sproules, S.; Nelson, D. J. Oxidative Addition of Aryl Electrophiles to a Prototypical Nickel(0) Complex: Mechanism and Structure/Reactivity Relationships. *Organometallics* **2017**, *36* (8), 1662–1672.

(119) Tsou, T. T.; Kochi, J. K. Mechanism of Oxidative Addition. Reaction of Nickel(0) Complexes with Aromatic Halides. *J. Am. Chem. Soc.* **1979**, *101* (21), 6319–6332.

(120) Massera, C.; Frenking, G. Energy Partitioning Analysis of the Bonding in L2TM−C2H2 and L2TM−C2H4 (TM = Ni, Pd, Pt; L2 = (PH3)2, (PMe3)2, H2PCH2PH2, H2P(CH2)2PH2). *Organometallics* **2003**, *22* (13), 2758–2765.

(121) Fürstner, A.; Seidel, G. Shortcut Syntheses of Naturally Occurring 5-Alkylresorcinols with DNA-Cleaving Properties. *J. Org. Chem.* **1997**, *62* (8), 2332–2336.

(122) Fürstner, A.; Leitner, A.; Méndez, M.; Krause, H. Iron-Catalyzed Cross-Coupling Reactions. *J. Am. Chem. Soc.* **2002**, *124* (46), 13856–13863.

(123) Corral-Bautista, F.; Klier, L.; Knochel, P.; Mayr, H. From Carbanions to Organometallic Compounds: Quantification of Metal Ion Effects on Nucleophilic Reactivities. *Angew. Chem. Int. Ed.* **2015**, *54* (42), 12497–12500.

(124) Pietruszka, J.; Witt, A. Synthesis of the Bestmann-Ohira Reagent. *Synthesis* **2006**, *2006* (24), 4266–4268.

(125) Hoye, T. R.; Suriano, J. A. A [W(CO)5·THF]-Mediated Pauson-Khand Reaction: Cyclizations of 1,6-Enynes via a Batch-Catalytic Protocol. *J. Am. Chem. Soc.* **1993**, *115* (3), 1154–1156.

(126) E. Greaves, M.; Humphrey, E. L. B. J.; J. Nelson, D. Reactions of Nickel(0) with Organochlorides, Organobromides, and Organoiodides: Mechanisms and Structure/Reactivity Relationships. *Cat. Sci. Tech.* **2021**, *11* (9), 2980–2996.

(127) Sontag, S. K.; Bilbrey, J. A.; Huddleston, N. E.; Sheppard, G. R.; Allen, W. D.; Locklin, J. π-Complexation in Nickel-Catalyzed Cross-Coupling Reactions. *J. Org. Chem.* **2014**, *79* (4), 1836–1841.

(128) Miyakoshi, R.; Yokoyama, A.; Yokozawa, T. Catalyst-Transfer Polycondensation. Mechanism of Ni-Catalyzed Chain-Growth Polymerization Leading to Well-Defined Poly(3-Hexylthiophene). *J. Am. Chem. Soc.* **2005**, *127* (49), 17542–17547.

(129) Bilbrey, J. A.; Bootsma, A. N.; Bartlett, M. A.; Locklin, J.; Wheeler, S. E.; Allen, W. D. Ring-Walking of Zerovalent Nickel on Aryl Halides. *J. Chem. Theory Comp.* **2017**, *13* (4), 1706–1711.

(130) Wu, S.; Sun, Y.; Huang, L.; Wang, J.; Zhou, Y.; Geng, Y. Grignard Metathesis Chain-Growth Polymerization for Poly (Bithienylmethylene) s: Ni Catalyst Can Transfer across the Nonconjugated Monomer. *Macromolecules (Print)* **2010**, *43* (10), 4438–4440.

(131) Rao, V. P.; Zimmt, M. B.; Turro, N. J. Photoproduction of Remarkably Stable Benzylic Radicals in Cyclodextrin Inclusion Complexes. *J. Photochem. Photobiol. A* **1991**, *60* (3), 355–360.

(132) Martí-Centelles, V.; Pandey, M. D.; Burguete, M. I.; Luis, S. V. Macrocyclization Reactions: The Importance of Conformational, Configurational, and Template-Induced Preorganization. *Chem. Rev.* **2015**, *115* (16), 8736–8834.

(133) Commeureuc, A. G. J.; Murphy, J. A.; Dewis, M. L. Synthesis of Muscothiazoles A and B: Critical Role of Methyl Group Substitution in RCM-Based Syntheses of Macrocycles. *Org. Lett.* **2003**, *5* (16), 2785–2788.

(134) Layton, M. E.; Morales, C. A.; Shair, M. D. Biomimetic Synthesis of (−)-Longithorone A. *J. Am. Chem. Soc.* **2002**, *124* (5), 773–775.

(135) Bressy, C.; Piva, O. Synthetic Approach to Pondaplin and Highly Strained Ansa Macrolides: The Dramatic Influence of a Fluorine Atom on the Efficiency of Ring-Closing Metathesis. *Synlett* **2003**, *2003* (1), 87–90.

(136) Yang, L.; Song, L.; Huang, C.; Huang, M.; Liu, B. Exploiting Ortho -Substitution Effect on Formation of Oxygen-Containing [10]Paracyclophane through Ring-Closing Metathesis. *Org. Chem. Front.* **2016**, *3* (3), 319–323.

(137) Mori, K.; Ohmori, K.; Suzuki, K. Hydrogen-Bond Control in Axially Chiral Styrenes: Selective Synthesis of Enantiomerically Pure C2-Symmetric

Paracyclophanes. *Angew. Chem. Int. Ed.* **2009**, *48* (31), 5638–5641.

(138) Esteve, F.; Altava, B.; Bolte, M.; Burguete, M. I.; García-Verdugo, E.; Luis, S. V. Highly Selective Anion Template Effect in the Synthesis of Constrained Pseudopeptidic Macrocyclic Cyclophanes. *J. Org. Chem.* **2020**, *85* (2), 1138–1145.

(139) Demircan, Ç. A.; Bozkaya, U. Transition Metal Cation−π Interactions: Complexes Formed by Fe^{2+}, Co^{2+}, Ni^{2+}, Cu^{2+}, and Zn^{2+} Binding with Benzene Molecules. *J. Phys. Chem. A* **2017**, *121* (34), 6500–6509.

(140) Schulz, J.; Vögtle, F. Transition Metal Complexes of (Strained) Cyclophanes. In *Cyclophanes*; Weber, E., Ed.; Topics in Current Chemistry; Springer-Verlag: Berlin/Heidelberg, 1994; Vol. 172, pp 41–86.

(141) Diederich, F. Complexation of Neutral Molecules by Cyclophane Hosts. *Angew. Chem. Int. Ed.* **1988**, *27* (3), 362–386.

(142) El-azizi, Y.; Schmitzer, A.; Collins, S. K. Exploitation of Perfluorophenyl–Phenyl Interactions for Achieving Difficult Macrocyclizations by Using Ring-Closing Metathesis. *Angew. Chem. Int. Ed.* **2006**, *45* (6), 968–973.

(143) Bolduc, P.; Jacques, A.; Collins, S. K. Efficient Macrocyclization Achieved via Conformational Control Using Intermolecular Noncovalent π-Cation/Arene Interactions. *J. Am. Chem. Soc.* **2010**, *132* (37), 12790–12791.

(144) Diederich, F. Molecular Recognition Studies with Cyclophane Receptors in Aqueous Solutions. In *Modern Cyclophane Chemistry*; Gleiter, R., Hopf, H., Eds.; Wiley-VCH Verlag GmbH & Co. KGaA: Weinheim, FRG, 2005; pp 519–546.

(145) Kandiyal, P. S.; Kim, J. Y.; Fortunati, D. L.; Mok, K. H. Size Determination of Protein Oligomers/Aggregates Using Diffusion NMR Spectroscopy. *Protein Self-Assembly: Methods and Protocols*; Humana: New York, NY, 2019; pp 173–183.

(146) Pracht, P.; Bohle, F.; Grimme, S. Automated Exploration of the Low-Energy Chemical Space with Fast Quantum Chemical Methods. *Phys. Chem. Chem. Phys.* **2020**, *22* (14), 7169–7192.

(147) Galli, C.; Mandolini, L. The Role of Ring Strain on the Ease of Ring Closure of Bifunctional Chain Molecules. *Eur. J. Org. Chem.* **2000**, *2000* (18), 3117–3125.

(148) Jawiczuk, M.; Marczyk, A.; Trzaskowski, B. Decomposition of Ruthenium Olefin Metathesis Catalyst. *Catalysts* **2020**, *10* (8), 887.

(149) Hoye, T. R.; Jeffrey, C. S.; Shao, F. Mosher Ester Analysis for the Determination of Absolute Configuration of Stereogenic (Chiral) Carbinol Carbons. *Nat. Protoc.* **2007**, *2* (10), 2451–2458.

(150) Coates, G. W.; Getzler, Y. D. Y. L. Chemical Recycling to Monomer for an Ideal, Circular Polymer Economy. *Nat. Rev. Mater.* **2020**, *5* (7), 501–516.

(151) Cherney, A. H.; Reisman, S. E. Nickel-Catalyzed Asymmetric Reductive Cross-Coupling Between Vinyl and Benzyl Electrophiles. *J. Am. Chem. Soc.* **2014**, *136* (41), 14365–14368.

(152) Kinoshita, H.; Kizu, R.; Horikoshi, M.; Inoue, G.; Fujimoto, M.; Saito, M.; Ichikawa, J.; Hosomi, A.; Miura, K. Regioselective Allylation of Carbon Electrophiles with Alkenyl-silanes under Dual Catalysis by Cationic Platinum(II) Species. *Synthesis* **2016**, *48* (4), 520–534.

(153) van Delft, M. F.; Chappaz, S.; Khakham, Y.; Bui, C. T.; Debrincat, M. A.; Lowes,

K. N.; Brouwer, J. M.; Grohmann, C.; Sharp, P. P.; Dagley, L. F.; Li, L.; McArthur, K.; Luo, M.-X.; Chin, H. S.; Fairlie, W. D.; Lee, E. F.; Segal, D.; Duflocq, S.; Lessene, R.; Bernard, S.; Peilleron, L.; Nguyen, T.; Miles, C.; Wan, S. S.; Lane, R. M.; Wardak, A.; Lackovic, K.; Colman, P. M.; Sandow, J. J.; Webb, A. I.; Czabotar, P. E.; Dewson, G.; Watson, K. G.; Huang, D. C. S.; Lessene, G.; Kile, B. T. A Small Molecule Interacts with VDAC2 to Block Mouse BAK-Driven Apoptosis. *Nat. Chem. Biol.* **2019**, *15* (11), 1057–1066.

(154) Meyer, C.; Marek, I.; Courtemanche, G.; Normant, J.-F. Intramolecular Metallo-Ene-Allene Reactions. A New Carbocycles Synthesis. *J. Org. Chem.* **1995**, *60* (4), 863–871.

(155) Jiang, X.-R.; Wang, P.; Smith, C. L.; Zhu, B. T. Synthesis of Novel Estrogen Receptor Antagonists Using Metal-Catalyzed Coupling Reactions and Characterization of Their Biological Activity. *J. Med. Chem.* **2013**, *56* (7), 2779–2790.

(156) Hofstra, J. L.; Cherney, A. H.; Ordner, C. M.; Reisman, S. E. Synthesis of Enantioenriched Allylic Silanes via Nickel-Catalyzed Reductive Cross-Coupling. *J. Am. Chem. Soc.* **2018**, *140* (1), 139–142.

(157) Bräse, S.; Wertal (nee Nüske), H.; Frank, D.; Vidović, D.; de Meijere, A. Intramolecular Heck Couplings and Cycloisomerizations of Bromodienes and Enynes with 1′,1′-Disubstituted Methylenecyclopropane Terminators: Efficient Syntheses of [3]Dendralenes. *Eur. J. Org. Chem.* **2005**, *2005* (19), 4167–4178.

(158) Rodier, F.; Rajzmann, M.; Parrain, J.-L.; Chouraqui, G.; Commeiras, L. Diastereoselective Access to Polyoxygenated Polycyclic Spirolactones through a

Rhodium-Catalyzed [3+2] Cycloaddition Reaction: Experimental and Theoretical Studies. *Chem. Eur. J.* **2013**, *19* (7), 2467–2477.

(159) Schäckermann, J.-N.; Lindel, T. Synthesis and Photooxidation of the Trisubstituted Oxazole Fragment of the Marine Natural Product Salarin C. *Org. Lett.* **2017**, *19* (9), 2306–2309.

(160) Meyer, C.; Marek, I.; Courtemanche, G.; Normant, J.-F. Intramolecular Carbometallation of Organozinc Reagents. *Tetrahedron* **1994**, *50* (40), 11665–11692.